

Quantum Error Correction and Simulation in Open Bosonic Systems

Présentée le 31 mai 2024

Faculté des sciences de base
Laboratoire de physique théorique des nanosystèmes
Programme doctoral en physique

pour l'obtention du grade de Docteur ès Sciences

par

David SCHLEGEL

Acceptée sur proposition du jury

Prof. J. H. Dil, président du jury
Prof. V. Savona, directeur de thèse
Dr J. Guillaud, rapporteur
Dr C. Sánchez Muñoz, rapporteur
Dr A. Grimm, rapporteur

*The world is not magic –
and that's the most magical
thing about it.*

— SEAN M. CAROLL,
Preposterous Universe

To Marie

Acknowledgements

This thesis presents the culmination of a time that I will never forget. It is the conclusion of a dynamic part of my life. It was filled with a multitude of emotions: Enthusiasm, excitement, curiosity, isolation, and self-doubt, to name just a few. Just after I had started as a doctoral student, the COVID-19 pandemic drastically changed almost every aspect of my life, some positive, some negative, and I am grateful to many individuals who helped me navigate not only through this challenging time but also through my time as a doctoral student at EPFL. Another unforeseen interruption came suddenly with a traffic accident that deeply impacted my work capabilities and I am truly grateful for everyone who supported me during these difficult times.

First, I want to thank my supervisor, Vincenzo Savona, for his continued support. His insights and discussions were precious and contributed to the success of this thesis. He supported me not only scientifically but also in many other ways, in particular by encouraging me to pursue my goals. His incredible experience and understanding were extremely important for the fruition of this work.

I am grateful to Alexander Grimm, Carlos Sánchez Muñoz, and Jérémie Guillaud for being part of the jury in the defense of this thesis.

I want to extend my gratitude to Fabrizio Minganti, who was extensively involved in all the scientific collaborations. His discussions were always constructive. He gave a unique angle at the scientific problems and challenges that arose in between. Also, it was just great hanging out with him and discussing physics or how to make the best Bolognese.

I also want to thank all the members of the Laboratory of Theoretical Physics of Nanosystems for their support and discussions. Especially, I want to thank Sara Santos and Debbie Eeltink with whom I shared lots of common ground. Thanks also go to all the members of the group: Filippo, Alberto, Luca, Lorenzo, Kilian, Riccardo, and Juan, for their enriching atmosphere.

I am also highly grateful to Stefano Barison and Gian Gentinetta for the many moments of interaction around the coffee machine in the office and for enduring my noisy keyboard all this time. There are too many people in the Computational Quantum Science Lab and the Laboratory of Quantum Information and Compu-


tation to name here for the great times we had together. I had the opportunity to see the corridor grow in the number of members, and with that came the joy of getting to know so many awesome people.

I want to thank all the people in the PolyPhys Association, an EPFL student association dedicated to connecting Ph.D. students in physics, for which I was happy to be an active part. Organizing the events for PolyPhys was always extremely enjoyable, and I am genuinely thankful for getting to know so many lovely people there.

I also thank all my friends from the *CaPhy* scientists with whom I have shared a lot of uplifting online coffee breaks that kept me going during the pandemic.

I want to express my heartfelt gratitude to my family, who have always supported me unconditionally.

Last but most importantly, I want to thank Marie. It is difficult to put into words how thankful I am to know you and for being part of my life. You are always supportive everywhere and have helped me navigate in extremely dark times by being the anchor in the storm. You got me up, when I was unable to. You always believed in me and convinced me to believe in myself, and you still continue to do so. I cannot say how much I respect you for giving up your previous life and for deciding to move to Lausanne. Without you, this work wouldn't have been possible.

A handwritten signature in black ink, reading "David Elger". The signature is written in a cursive, flowing style with a large initial 'D' and 'E'.

Abstract

Quantum computers have the potential to surpass conventional computing, but they are hindered by noise which induces errors that ultimately lead to the loss of quantum information. This necessitates the development of quantum error correction strategies for large-scale quantum information processors. Bosonic quantum codes offer a promising solution, enabling quantum error correction on redundantly encoded information in a quantum harmonic oscillator. Two of the main sources of errors encountered in bosonic systems are *photon loss* and *dephasing*. Multiple bosonic quantum codes have been proposed and experimentally realized in the recent past.

However, devising hardware-efficient bosonic quantum codes that are able to correct photon loss *and* dephasing to consistently enhance the life-time of logical quantum information beyond break-even, is a pressing problem in the scientific community. The cat code is a promising candidate as a *biased-noise* qubit, being able to correct well against dephasing errors, but it suffers from loss errors.

In this thesis, we propose the *squeezed cat code* as way to simultaneously correct for photon loss and dephasing errors. We provide a full numerical and analytical analysis of the squeezed cat code, including protocols for encoding, quantum gates, error characterization, and an optimized recovery procedure suitable for implementation on current quantum hardware platforms. Through numerical simulations using realistic parameters, we demonstrate that even moderate squeezing enables the squeezed cat code to significantly outperform the conventional cat code in correcting particle loss errors. Notably, the squeezed cat code improves resilience to dephasing errors at the same time, enhancing the noise bias of logical error errors. Our main motivation lies in the fact that as squeezing is a Gaussian operation, the generation and manipulation of the squeezed cat code can be achieved through quadratic operations, without the need to introduce higher-order processes.

To simulate the dynamics of driven-dissipative bosonic systems accurately and efficiently, with bosonic codes in mind specifically, new numerical methods need to be developed. For bosonic codes, tailored numerical methods can enable the

study of leakage out of the code space, effects of time-dependent and noisy gate operations, or dissipative phase transitions.

The second part of this thesis addresses this problem by focusing on a new variational approach for efficiently simulating the dynamics of open interacting many-boson quantum systems. The method uses an ansatz for the density matrix expanded in a basis of photon-added coherent states. This makes it well-suited for driven-dissipative systems where the state exhibits quantum fluctuations on top of a displaced field, enabling the simulation of multiple coupled modes with large occupation numbers that pose a challenge for Fock-space methods. Several example simulations are provided that validate the method and illustrate its potential for predictively modeling interacting bosonic systems. We further extend this method to include the rotational symmetry of cat qubits and showcase the efficient simulation of cat qubit dynamics.

Taken together, this thesis presents important theoretical and computational advancements towards realizing and simulating hardware-efficient bosonic quantum codes required for scalable and fault-tolerant quantum information processing.

Keywords: open quantum systems, quantum error correction, bosonic quantum codes, quantum harmonic oscillator, loss, dephasing, squeezed cat code, coherent-state ladder, cat-state ladder, variational time-dependent principle, coherent states

Résumé

Bien que les ordinateurs quantiques aient le potentiel de surpasser l'informatique conventionnelle, cela est rendu difficile en raison du bruit. En effet, il induit des erreurs qui conduisent à terme à la perte d'information quantique. Pour cela, la réalisation de processeurs d'information quantique à grande échelle nécessite le développement de stratégies de correction d'erreurs quantiques. Les codes quantiques bosoniques offrent une solution prometteuse permettant la correction d'erreurs quantiques sur l'information codée de manière redondante dans un oscillateur harmonique quantique. Les principales sources d'erreurs rencontrées dans les systèmes bosoniques sont la *perte de photons* et le *déphasage*. Plusieurs codes quantiques bosoniques ont récemment été proposés et réalisés expérimentalement.

Cependant, la conception de codes quantiques bosoniques efficaces sur le plan matériel, capables de corriger la perte de photons *et* le déphasage afin d'améliorer systématiquement la durée de vie de l'information quantique logique en pratique, constitue un problème urgent dans la communauté scientifique. Le *cat code* est un candidat prometteur en tant que qubit *biased-noise*, étant capable de efficacement corriger les erreurs de déphasage, bien que sensible aux erreurs de perte.

Dans cette thèse, nous proposons le *squeezed cat code* comme un moyen de corriger simultanément la perte de photons et les erreurs de déphasage. Nous fournissons une analyse numérique et analytique complète du *squeezed cat code*, y compris des protocoles d'encodage, des portes quantiques, la caractérisation des erreurs ainsi qu'une procédure de correction optimisée adaptée à sa mise en œuvre sur les plates-formes quantiques actuelles. Grâce à des simulations numériques utilisant des paramètres réalistes, nous démontrons que même un *squeezing* modéré permet au *squeezed cat code* de surpasser considérablement le *cat code* conventionnel en matière de correction des erreurs induites par les pertes de particules. En outre, le *squeezed cat code* améliore la résilience aux erreurs de déphasage, renforçant ainsi le *noise bias* des erreurs logiques. Notre principale motivation réside dans le fait que, étant donné que le *squeezing* est une opération gaussienne, la génération et la manipulation du *squeezed cat code* peuvent être réalisées par

des opérations quadratiques, sans qu'il soit nécessaire d'introduire des processus d'ordre supérieur.

Afin de simuler avec précision et efficacité la dynamique des systèmes bosoniques forcés et dissipatifs, en gardant spécifiquement à l'esprit les codes bosoniques, de nouvelles méthodes numériques doivent être développées. De telles méthodes numériques peuvent permettre l'étude des fuites hors de l'espace du code, de l'effet de portes bruitées et dépendantes du temps, ou des transitions de phase dissipatives.

La deuxième partie de cette thèse aborde ce problème en se concentrant sur une nouvelle approche variationnelle pour simuler efficacement la dynamique des systèmes quantiques ouverts constitués de multiples bosons en interaction. La méthode utilise un ansatz pour la matrice de densité exprimée dans une base d'états dits *photon-added coherent states*. Cela le rend adapté aux systèmes forcés et dissipatifs dont l'état présente des fluctuations quantiques sur un champ déplacé, permettant la simulation de plusieurs modes couplés avec de grandes populations photoniques, qui constituent un défi pour les approches dans l'espace de Fock. Plusieurs exemples de simulations sont fournis, qui valident la méthode et illustrent son potentiel pour la modélisation prédictive de systèmes bosoniques en interaction. Nous étendons cette méthode afin d'inclure la symétrie de rotation des cat qubits et présentons des simulations efficaces de leur dynamique.

Dans l'ensemble, cette thèse présente d'importantes avancées théoriques et numériques visant à la réalisation et la simulation de codes quantiques bosoniques efficaces sur le plan matériel, un préalable au traitement tolérant aux erreurs de l'information quantique à grande échelle.

Mots-clés : systèmes quantiques ouverts, correction d'erreur quantique, codes quantiques bosoniques, oscillateur harmonique quantique, pertes photoniques, déphasage, squeezed cat code, états cohérents, principe variationnel dépendant du temps

Zusammenfassung

Quantencomputer haben das Potenzial, herkömmliche Computer zu übertreffen, werden jedoch durch Rauschen behindert, welches Fehler verursacht die letztendlich zum Verlust von Quanteninformation führen. Dies erfordert die Entwicklung von Quantenfehlerkorrekturstrategien für große Quanteninformationsprozessoren. Bosonische Quantencodes bieten eine vielversprechende Lösung und ermöglichen eine Quantenfehlerkorrektur an redundant codierter Information in einem harmonischen Quantenoszillator. Eine der Hauptfehlerquellen in bosonischen Systemen sind *Photonenverlust* und *Dephasierung*. In der jüngeren Vergangenheit wurden mehrere bosonische Quantencodes vorgeschlagen und experimentell realisiert.

Allerdings ist die Entwicklung hardwareeffizienter bosonischer Quantencodes, die in der Lage sind, Photonenverlust *und* Dephasierung zu korrigieren, um die Lebensdauer logischer Quanteninformation über die Gewinnschwelle hinaus kontinuierlich zu verlängern, ein dringendes Problem in der wissenschaftlichen Gemeinschaft. Der Cat-Code ist ein vielversprechender Kandidat als *biased-noise*-Qubit, da er Dephasierungsfehler gut korrigieren kann, aber unter Fehlern durch Photonenverlust leidet.

In dieser Arbeit schlagen wir den *komprimierten Cat-Code* (Squeezed Cat-Code) als Möglichkeit vor, gleichzeitig Photonenverlust und Dephasierungsfehler zu korrigieren. Wir stellen eine vollständige numerische und analytische Analyse des komprimierten Cat-Codes vor, einschließlich Protokollen zur Kodierung, Quantengatter, Fehlercharakterisierung und einem optimierten Wiederherstellungsverfahren, das für die Implementierung auf aktuellen Quanten-Hardwareplattformen geeignet ist. Durch numerische Simulationen mit realistischen Parametern zeigen wir, dass der komprimierte Cat-Code selbst durch moderates Squeezing den herkömmlichen Cat-Code bei der Korrektur von Partikelverlustfehlern deutlich übertrifft. Insbesondere verbessert der komprimierte Cat-Code gleichzeitig die Widerstandsfähigkeit gegenüber Dephasierungsfehlern und erhöht so die Rauschverzerrung logischer Fehler. Unsere Hauptmotivation liegt in der Tatsache, dass das Komprimieren/Squeezing eine Gaussische Operation darstellt und die Generierung und Manipulation des komprimierten Cat-Codes durch quadratische Operationen

erreicht werden kann, ohne dass Prozesse höherer Ordnung eingeführt werden müssen.

Um die Dynamik getrieben-dissipativer bosonischer Systeme genau und effizient zu simulieren, insbesondere unter Berücksichtigung bosonischer Codes, bedarf es der Entwicklung neuer numerische Methoden. Für bosonische Codes können maßgeschneiderte numerische Methoden die Untersuchung von Leckagen aus dem Coderaum, Auswirkungen zeitabhängiger und verrauschter Gatter oder dissipativer Phasenübergänge ermöglichen.

Der zweite Teil dieser Arbeit befasst sich mit diesem Problem, indem er sich auf einen neuen Variationsansatz zur effizienten Simulation der Dynamik offen wechselwirkender Quantensysteme mit mehreren Bosonen konzentriert. Die Methode verwendet einen Ansatz für die Dichtematrix, der auf der Basis photonennaddierter kohärenter Zustände erweitert wird. Dadurch eignet sie sich gut für getrieben-dissipative Systeme, bei denen der Zustand Quantenfluktuationen über einem kohärenten Feld aufweist, was die Simulation mehrerer gekoppelter Moden mit großen Besetzungszahlen ermöglicht, die eine Herausforderung für herkömmliche Fock-Raum-Methoden darstellen. Es werden mehrere Beispielsimulationen vorgestellt, die die Methode validieren und ihr Potenzial für die prädiktive Modellierung interagierender bosonischer Systeme veranschaulichen. Wir erweitern diese Methode weiter, um die Rotationssymmetrie von Cat-Qubits einzubeziehen, und demonstrieren deren effiziente Simulation der Dynamik.

Zusammengenommen stellt diese Arbeit wichtige theoretische und numerische Fortschritte bei der Realisierung und Simulation hardwareeffizienter bosonischer Quantencodes dar, die für eine skalierbare und fehlertolerante Quanteninformatonsverarbeitung erforderlich sind.

Stichwörter: offene Quantensysteme, Quantenfehlerkorrektur, bosonische Quantencodes, harmonischer Quantenoszillator, Photonenverlust, Dephasierung, komprimierter Cat-Code, kohärente Zustandsleiter, Cat-zustandsleiter, Variationszeitabhängiges Prinzip, kohärente Zustände

Publications

The works of scientific and technical nature produced in the course of this thesis are listed below. The present manuscript is structured around the results reported in the works $[\alpha, \beta]$.

- [α] D. S. Schlegel, F. Minganti, V. Savona,
Quantum error correction using squeezed Schrödinger cat states,
[Physical Review A **106**, 022431 \(2022\)](#).
- [β] D. S. Schlegel, F. Minganti, V. Savona,
Coherent-State Ladder Time-Dependent Variational Principle for Open Quantum Systems,
[arXiv: 2306.13708 \(2023\)](#).
- [γ] D. S. Schlegel, S. Kehrein,
Measurement-induced Clock in a Lattice Ring of Non-interacting Electrons,
[arXiv: 2312.17672 \(2023\)](#).

Notation and Abbreviations

We could, of course, use any notation we want; do not laugh at notations; invent them, they are powerful. In fact, mathematics is, to a large extent, invention of better notations.

— RICHARD FEYNMAN, *The Feynman Lectures on Physics Vol 1*

In the following work, we set $\hbar = 1$ for notational convenience. We use the following definitions and abbreviations if not explicitly stated otherwise in the main text. We avoid an excessive use of acronyms and abbreviations in this thesis, but nevertheless use some of them occasionally throughout this work. We advise the reader to use common-sense reasoning should the notation be ambiguous in some parts of the manuscript.

Abbreviations

| | |
|---------------|--|
| GPE | Gross-Pitaevskii equation |
| TDVP | time-dependent variational principle |
| QEC | quantum error correction |
| BQC | bosonic quantum code |
| SDP | semidefinite program |
| CPTP | completely positive and trace-preserving |
| ATS | asymmetrically-threaded SQUID |
| GKP code | Gottesman-Kitaev-Preskill code |
| KL conditions | Knill-Laflamme conditions |

Symbols and Notations

We use the following symbols and notations.

Chapter 2

| | |
|--------------------------|---|
| \mathcal{L} | Liouvillian superoperator |
| $\mathcal{D}[\hat{A}]$ | dissipator with jump operator (Lindblad operator) \hat{A} |
| $\text{Op}(\mathcal{H})$ | operator space ($\mathcal{H} \otimes \mathcal{H}$) of the Hilbert space \mathcal{H} |

Chapter 3

| | |
|-----------------------------|--|
| \mathcal{E} | noise channel |
| \mathcal{R} | recovery channel |
| \mathcal{S} | qubit-bosonic mapping |
| \mathcal{Q} | combined quantum channel $\mathcal{Q} = \mathcal{S}^{-1} \circ \mathcal{R} \circ \mathcal{E} \circ \mathcal{S}$ |
| $M_{[i,k],[j,k']}$ | Knill-Laflamme tensor $M_{[i,k],[j,k']} \equiv \langle \psi_i \hat{E}_k^\dagger \hat{E}_{k'} \psi_j \rangle$ |
| $\mathcal{N}_L[\gamma]$ | loss channel |
| $\mathcal{N}_D[\gamma\phi]$ | dephasing channel |
| \mathcal{F} | channel fidelity |
| \mathcal{F}_e | entanglement fidelity |
| $\hat{\Pi}$ | parity operator $\hat{\Pi} = e^{i\pi\hat{a}^\dagger\hat{a}}$ |

Chapter 4

| | |
|--|-----------------------|
| $\hat{D}(\alpha)$ | displacement operator |
| $\hat{S}(\xi)$ | squeezing operator |
| $ \mathcal{C}_{\alpha,\xi}^\pm\rangle$ | squeezed cat states |

Chapter 5

| | |
|--|--|
| $\mathcal{S}, \mathcal{S}_N$ | coherent-state ladder basis (of order N) |
| $\mathcal{S}_{\text{cat}}, \mathcal{S}_{\text{cat},N}$ | cat-state ladder basis (of order N and total number of $2N$ basis states) |
| \mathbf{O} | matrix representation of operator \hat{O} in a given basis |
| \mathbf{S} | overlap matrix with matrix elements $S_{i,j} = \langle \varphi_i \varphi_j \rangle$ |
| \mathbf{C}_0 | quantum-geometric tensor with elements $[\mathbf{C}_0]_{bc}^{kl} = \langle \partial_{\theta_k} \varphi_b [\hat{\mathbf{1}} - \hat{P}_{\mathcal{S}}] \partial_{\theta_l} \varphi_c \rangle$ |
| \mathbf{Y}_0 | projection of the Liouvillian action on the tangent space of the basis $[\mathbf{Y}_0]_{ba}^k = \langle \partial_{\theta_k} \varphi_b [\hat{\mathbf{1}} - \hat{P}_{\mathcal{S}}] \mathcal{L}[\hat{\rho}] \varphi_a \rangle$ |
| \mathbf{L} | Liouvillian action on $\hat{\rho}$ in a given basis with $L_{i,j} = \langle \varphi_i \mathcal{L}[\hat{\rho}] \varphi_j \rangle$ |
| \mathbf{O}^{\rightarrow} | right derivative of an operator \hat{O} with respect to α |
| \mathbf{O}^{\leftarrow} | left derivative of an operator \hat{O} with respect to α |
| $\mathbf{O}^{\leftrightarrow}$ | left-right derivative of an operator \hat{O} with respect to α |
| $\hat{P}_{\mathcal{S}}$ | projector onto subspace \mathcal{S} |

Contents

| | |
|---|--------------|
| Acknowledgements | i |
| Abstract (English/Français/Deutsch) | iv |
| Publications | xi |
| Notation and Abbreviations | xiii |
| List of Figures | xxii |
| List of Tables | xxiii |
| List of Algorithms | xxiii |
| General Introduction | 1 |
| 2 Theory of Open Quantum Systems | 13 |
| I Density Matrix Formalism | 13 |
| I.1 The Density Matrix | 13 |
| I.2 Time-Evolution in a Closed Quantum System | 14 |
| I.3 Measurement Process | 15 |
| II Lindblad Master Equation | 16 |
| II.1 Quantum Markov Processes | 17 |
| II.2 Quantum Dynamical Semigroups | 18 |
| II.3 Spectral Properties | 22 |
| III Bosonic quantum systems | 24 |
| III.1 The quantum harmonic oscillator | 24 |
| III.2 Coherent states | 26 |
| III.3 Wigner representation | 28 |
| IV Numerical methods for open quantum systems | 29 |
| IV.1 Monte Carlo Wave Function method | 30 |
| IV.2 Coherent mean-field approximation | 34 |

| | | |
|----------|---|-----------|
| IV.3 | Phase-space methods | 35 |
| IV.4 | Other numerical methods | 36 |
| 3 | Bosonic Quantum Error Correction | 39 |
| I | Introduction | 40 |
| II | Quantum error correction codes | 42 |
| II.1 | Knill-Laflamme conditions | 45 |
| III | Bosonic quantum codes | 48 |
| IV | Modeling noise on bosonic systems | 50 |
| IV.1 | Photon Loss | 50 |
| IV.2 | Dephasing | 53 |
| IV.3 | Joint loss and dephasing | 54 |
| V | Channel Fidelity | 54 |
| V.1 | Continuous errors | 54 |
| V.2 | Definition of channel fidelity | 55 |
| V.3 | Approximate Knill-Laflamme conditions | 57 |
| V.4 | Convex Optimization of the Channel Fidelity | 58 |
| V.5 | Correcting a finite set of errors | 60 |
| VI | The cat code | 61 |
| VI.1 | Subsystem decomposition and Shifted-Fock method | 64 |
| VI.2 | Dissipation Engineering | 65 |
| VI.3 | Hamiltonian confinement | 70 |
| VII | Other bosonic codes | 72 |
| 4 | Quantum Error Correction with the Squeezed Cat Code | 77 |
| I | Squeezed Schrödinger Cat States | 78 |
| I.1 | Motivation | 78 |
| I.2 | Squeezed states | 79 |
| I.3 | The Squeezed cat code | 82 |
| I.4 | Asymptotic discrete translation invariance | 83 |
| I.5 | Code generation and gates | 84 |
| II | Quantum error correction conditions | 85 |
| II.1 | Intuitive picture | 85 |
| II.2 | Knill-Laflamme conditions for the squeezed cat code | 85 |
| II.3 | Correction of multiple errors | 88 |
| III | Approximate quantum error correction | 88 |
| III.1 | Channel fidelity | 90 |
| III.2 | Error correction in the quantum trajectory picture | 96 |

| | | |
|----------|--|------------|
| III.3 | Comparison between the squeezed cat code and the GKP code | 98 |
| IV | Approaches to Experimental Realization | 99 |
| IV.1 | Dissipative stabilization of squeezed cat states | 99 |
| IV.2 | Physical implementation | 101 |
| IV.3 | Dissipation Engineering with bit-flip suppression | 103 |
| V | Discussion and Outlook | 104 |
| 5 | Variational Simulation of Bosonic Open Quantum Systems | 107 |
| I | Variational Principles for Open Quantum Systems | 108 |
| II | Time-dependent Basis | 110 |
| II.1 | Parametrization of the Density Matrix | 113 |
| II.2 | TDVP Equations of Motion | 113 |
| II.3 | Remarks | 116 |
| III | Coherent-state Ladder Time-dependent Variational Principle | 117 |
| III.1 | Motivation | 117 |
| III.2 | Bargmann States and the Coherent-State Ladder | 119 |
| IV | Coherent-state Ladder Equations of Motion | 122 |
| V | Numerical implementation | 123 |
| V.1 | Quantum-geometric tensor \mathbf{C}_0 | 124 |
| V.2 | Calculation of \mathbf{L} and \mathbf{Y}_0 | 124 |
| V.3 | Numerical Regularization | 126 |
| V.4 | Sketch of the Implementation | 128 |
| VI | Fidelity and Wigner function | 129 |
| VII | Applications | 130 |
| VIII | Cat-state Ladder | 134 |
| IX | Applications | 138 |
| X | Beyond coherent-state and cat-state ladder TDVP | 142 |
| XI | Discussion and Outlook | 145 |
| | General Conclusion and Outlook | 147 |
| | Appendix A Analytical Knill-Laflamme matrix elements for the cat code and squeezed cat code | 152 |
| | Appendix B Expressions in the coherent- and cat-state ladder | 157 |
| I | Operators in the coherent-state ladder | 157 |
| II | Operators in the cat-state ladder | 158 |
| | Curriculum Vitae | 189 |

List of Figures

| | | |
|------|--|-----|
| 1 | Comparison between a classical bit and a quantum bit | 5 |
| 2.1 | Schematic representation of an open quantum system | 16 |
| 2.2 | Time-evolution of the density matrix using the dynamical map . . . | 17 |
| 2.3 | Eigenvalue structure of the Liouvillian | 23 |
| 2.4 | The coherent state | 27 |
| 2.5 | Unraveling of the master equation | 30 |
| 2.6 | Quantum trajectory method | 32 |
| 3.1 | Comparison between two-level and bosonic quantum error correction | 41 |
| 3.2 | Encoding and measurement circuit for the 3-qubit repetition code . | 43 |
| 3.3 | Conditions for quantum error correction | 46 |
| 3.4 | Effect of noise on points in the Wigner function | 52 |
| 3.5 | Combined error correction quantum channel | 55 |
| 3.6 | Bloch sphere and Wigner functions of the cat code | 62 |
| 3.7 | Subsystem decomposition | 65 |
| 3.8 | Dissipative stabilization of the cat-qubit manifold | 68 |
| 3.9 | The Kerr-cat qubit | 71 |
| 3.10 | The GKP code | 72 |
| 4.1 | Displaced squeezed state | 79 |
| 4.2 | Bloch sphere and Wigner functions of the squeezed cat code | 83 |
| 4.3 | Effect of loss and dephasing on squeezed cat states | 86 |
| 4.4 | Optimized channel fidelity for the squeezed cat code | 93 |
| 4.5 | Optimized displacement and squeezing for the squeezed cat code . . | 95 |
| 4.6 | Error correction in quantum trajectories of the squeezed cat code . | 97 |
| 4.7 | Circuit QED implementation for the dissipative stabilization of the squeezed cat code | 101 |
| 5.1 | Concept of the variational principle | 108 |
| 5.2 | The coherent-state ladder | 117 |

| | | |
|-----|--|-----|
| 5.3 | Performance analysis of the coherent-state ladder using a dissipative Kerr resonator | 132 |
| 5.4 | Simulation of an asymmetrically driven non-linear photonic dimer . | 133 |
| 5.5 | Steady-state simulation in a Bose-Hubbard chain | 134 |
| 5.6 | Dynamics of cat-deformations in the cat-state ladder | 138 |
| 5.7 | Simulation of non-adiabatic Zeno dynamics in a cat-qubit | 139 |
| 5.8 | Simulation of two interacting cat qubits using the cat-state ladder . | 141 |
| 5.9 | Simulation of three interacting cat-qubits using the cat-state ladder | 142 |

List of Tables

| | | |
|-----|--|-----|
| 5.1 | Comparison of different variational basis parametrizations | 144 |
| A.1 | Knill-Laflamme matrix elements for the cat states $ \mathcal{C}_\alpha^\pm\rangle$ | 153 |
| A.2 | Non-trivial Knill-Laflamme matrix elements for the squeezed cat code of the form $\langle \mathcal{C}_{\alpha,\xi}^\pm \hat{E}_l^\dagger \hat{E}_{l'} \mathcal{C}_{\alpha,\xi}^\pm \rangle$ | 155 |
| A.3 | Non-trivial Knill-Laflamme matrix elements for the squeezed cat code of the form $\langle \mathcal{C}_{\alpha,\xi}^\pm \hat{E}_l^\dagger \hat{E}_{l'} \mathcal{C}_{\alpha,\xi}^\mp \rangle$ | 156 |

List of Algorithms

| | | |
|---|--|-----|
| 1 | Semi-definite program for the recovery optimization | 91 |
| 2 | Computation of the derivatives $\dot{\alpha}$ and $\dot{\mathbf{B}}$ | 128 |
| 3 | Integration of the equations of motion | 129 |

General Introduction

The revolutions of quantum mechanics

The path of science is marked by several revolutions of discoveries that drastically changed our description of reality. No single discovery has arguably changed our understanding of the fabric of our universe as much as that of quantum mechanics. From the first discoveries by the great minds in the beginning of the 20th century, quantum mechanics has come a long way, solidifying its central position in the physical sciences and sparking the conception of new technologies that were unthinkable just a few decades ago. It has since emerged as one of the most precisely experimentally verified theories to date, revealing that the universe is fundamentally quantum, with all its striking phenomena that are hard to comprehend with our simple human capabilities.

The first revolution of quantum mechanics, emerging in the early 20th century, marked a paradigm shift in the understanding of the physical world. This revolution began with the groundbreaking work of Max Planck in the Year 1900, who introduced the concept of quantization to explain the radiation emitted from a *black body* [1]. At the time, Planck believed this to be a purely heuristic effect [2], but shortly after, Albert Einstein's explanation of the photoelectric effect, utilizing the concept of light quanta (photons), further substantiated the quantum theory [3]. Einstein was the first to coin the term *quantization*, characterizing that the energy of light is not distributed continuously but that light consists of a finite number of *energy quanta* that are localized in space, which can be absorbed or generated only as a whole [3]. Ernest Rutherford and Niels Bohr realized that the quantization of energy also applies to matter, giving rise to the first quantum model of the atom [4–7] that could explain the discrete emission spectrum observed in hydrogen.

Later in the 1920s, Werner Heisenberg [8], Erwin Schrödinger [9, 10], and Paul Dirac [11, 12], among others, laid the foundational pillars of modern quantum mechanics. These scientists radically changed our description of the atomic and subatomic levels, demonstrating that at the quantum scale, particles like electrons behave in ways that defy classical physics' predictability.

After the foundational work on the building blocks of quantum mechanics in the first half of the 20th century came a second, more gradual revolution. The revolution of quantum technologies. With technological advances, the quantum mechanical nature of our universe could be experimentally verified. From the double-slit experiment [13, 14], proving the striking duality of particle and wave, and the destructive role of measurement, to the experimental verification of *quantum entanglement* [15], proving the intrinsic non-local nature of light and matter that necessitates a joint description of spatially separated systems.

Not only did the quantum mechanical nature of light and matter become experimentally testable to an unprecedented degree, but technological advances such as nano-fabrication and cryogenics allowed the development of quantum technologies to go beyond the usefulness in science laboratories. Devices that use the fundamental principles of quantum mechanics have led to a plethora of useful applications. They allow for enhanced sensing devices [16] such as atomic clocks, superconducting interference devices for geology, magnetic resonance imaging devices for medical applications, or high-resolution spectrometers. Also quantum dots have found their way into displays for electronic devices, providing screens with lower energy consumption.

The dawn of quantum computing

Another quantum revolution, currently in full swing, involves manipulating the information of quantum systems. Classical computers, with their binary system of bits represented by either 0s or 1s, have been the backbone of technological advancement, transforming every aspect of our lives. As information is *always* physical [17], one might wonder what the information in quantum systems is and how it can be manipulated to perform computations. In the early 1980s, a new computational paradigm began to emerge. Paul Benioff and Yuri Manin were among the first to conceptualize a quantum mechanical model of a computer that performed operations, showing that a Turing machine could be implemented using quantum devices [18–20]. At a famous talk held at MIT in 1981, Richard Feynman clearly articulated the need for a quantum mechanical simulation device to simulate physical processes:

Nature isn't classical, dammit, and if you want to make a simulation of nature, you'd better make it quantum mechanical, and by golly it's a wonderful problem, because it doesn't look so easy. (Feynman, (1982) [21])

He realized that digital computers are not adequate machines for efficiently simulating quantum systems. One of the arguments is that the state space of quantum

mechanical systems needed to fully describe any arbitrary quantum space grows exponentially with the system's size, whereas in classical systems, it grows only linearly. Hence, to simulate another physical system for which quantum mechanical effects cannot be neglected, this has to be done on an intrinsically quantum device. Turning the problem around, one might wonder what kind of simulations or computations a quantum device could perform to solve certain problems that are otherwise classically intractable. Only shortly after Feynman, David Deutsch formulated and described the first *universal quantum computer* [22], a device capable of simulating any other quantum device efficiently.

During the 90s, algorithms were discovered that could be performed on a quantum computer operating on quantum bits instead of classical bits, performing some well-defined computational tasks more efficiently than any classical computer [22–26]. These radical ideas were met with criticism by some leading physicists, such as Landauer [27], Unruh [28], and Haroche [29], as they doubted whether such quantum machines could be practically implemented for the algorithms to work effectively.

Others were more hopeful and around the same time, different quantum hardware platforms were proposed and studied that would allow for universal control and measurements to perform quantum computational tasks, such as the semiconductor spin-qubits [30], quantum optics [31, 32], trapped ions [33], and superconducting circuits [34–36].

Fast-forwarding until today, we see a flourishing field of *quantum computing*, with the development of many different hardware platforms trying to implement a universal quantum computer that can tackle *useful* applications that are beyond reach for classical computers. Notable experiments have demonstrated (somewhat artificial) tasks that can be performed in a very short time with few physical resources on a quantum computer that would take decades or even centuries for its classical counterpart [37]. As it stands, researchers from both academic institutions and industry are making tremendous efforts to engineer large-scale *reliable* quantum computing devices that can run *practically useful* quantum algorithms.

Noise and the need for quantum error correction

Roughly 40 years since the inception of the theory of quantum computing, we find ourselves in a challenging yet hopeful situation. Quantum technologies have made remarkable progress in the last two decades, enabling the coherent control of multiple *qubits* to a degree that allows for the entanglement of many physical constituents. Yet, contrary to what one might expect, scaling up the qubit count in the hardware does not seem to easily increase the computational power of the quantum device in the same way.

At the heart of this problem lies *noise* that ultimately corrupts the information stored in the quantum states of a physical system. Any quantum system inevitably interacts – in some way or the other – with its surrounding environment, thereby generating entanglement with a larger system. As such any quantum system must be considered an *open quantum system* that couples to some kind of external degrees of freedom. At room temperature, many quantum effects are very quickly washed out due to the large kinetic thermal fluctuations within the system compared to the discrete quantized energy levels of the quantum system. Summarized under the term *decoherence*, these unwanted interactions are – to a large extent – one of the main reasons why many quantum phenomena are not observed in our daily lives. As a result, quantum devices often need to be cryogenically cooled to prevent as much unwanted interaction as possible with their surroundings in order to control the system accurately and for a long enough time. Otherwise, the environment will quickly introduce irreversible errors that will corrupt all information. However, for quantum devices with many physically coupled constituents, this seems to be not enough. Ever so slight interactions can quickly propagate through the entire quantum system, detrimentally affecting subsequent computations [38, 39].

The current hardware limitations of increasing the coherence times of physical qubits have sparked interest in the question of whether quantum information can be encoded redundantly to detect and correct errors along the way, preserving the information for a longer duration and enabling the implementation of deep quantum circuits.

Already in the 1940s, Shannon [40] explored ways to encode classical information to protect it from noise redundantly. Today, *classical error correction* protocols are used in everyday devices and communication channels, such as internet communication, deep-space telecommunication, satellite broadcasting, or data storage devices.

Early on in the history of quantum computing, many researchers wondered whether the information in quantum systems could be corrected in a similar way to classical error correction, which was a naturally more mature field at the time. Asher Peres [41], Peter Shor [42], Andrew Steane [43], and Alexei Kitaev [44], among others, recognized the importance of errors in quantum computing and proposed ways to correct them. Knill and Laflamme notably formulated mathematically precise conditions under which errors can be exactly correctable [45]. It is important to recognize that errors on quantum devices can manifest themselves in different ways compared to classical digital information, where the only possible error can be the flip of a logical bit. A quantum bit, on the other hand, can be in a *superposition* of quantum states, which can be characterized as a point on

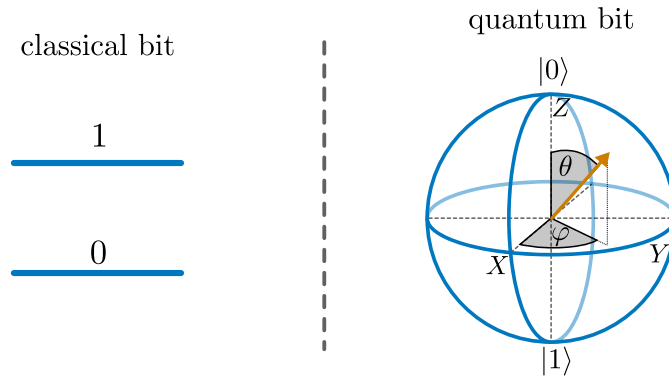


Figure 1: Schematic comparison between a classical bit (left) and a quantum bit (right). While a classical bit can be either in the state (0) or (1) , a quantum bit can be in a complex linear superposition of the basis states $|0\rangle$ and $|1\rangle$, described by a point on the unit sphere, called Bloch sphere, that is parametrized by the two angles θ and φ .

the unit sphere, called the Bloch sphere, shown in Fig. 1. As such, the complex *phase* of the superposition represents an additional dimension of information that needs to be protected from noise processes. Hence, a quantum bit can be prone to a bit flip error *and* a phase flip error (and a combination of both). Furthermore, simple approaches from classical error correction techniques that are based on copying information are not available for quantum states. Due to the linearity of quantum mechanical operations, the *no-cloning* theorem makes the copying of arbitrary superpositions of quantum states impossible [46, 47]. Different quantum error correction schemes have been developed to redundantly encode a logical quantum bit into multiple physical qubits. Such approaches have already been recently experimentally implemented [48] as a first proof of principle. It should be noted that all such approaches make a trade-off: Increasing the lifetime of the logical qubit at the expense of larger hardware overhead in the number of physical constituents. It is expected that in a realistic fully error-corrected quantum circuit, the vast majority of the resources are spent on error correction [42, 43, 49–52]. Therefore, scaling to large error-corrected quantum devices is limited by the hardware constraints of connecting and coherently controlling many physical qubits.

A pressing question, therefore, is:

How can we efficiently encode quantum information redundantly with a low hardware overhead?

This is one of the central guiding questions addressed in this thesis.

Bosonic quantum error correction

So far, qubit-based quantum error correction encoding and gate operations on the encoded qubits at a large scale beyond the quantum error correction threshold – the point where increasing the number of qubits that participate in the error correction scheme actually improves the lifetime of the encoded logical information – still remain elusive [53].

A promising solution to these challenges is offered by a different quantum computing approach: *Continuous variable* or *bosonic* quantum computing. In this approach to quantum computing, information is stored in the state space of quantum harmonic oscillators. These systems provide a much larger accessible Hilbert space for the manipulation and encoding of quantum information. A single bosonic mode can provide an (in principle) infinitely large Hilbert space, which allows the use of quantum error correction schemes by redundantly encoding information in the excitations of a quantum resonator while keeping the noise channels fixed [53]. At the same time, bosonic modes are hardware-scalable, as they can be realized with multiple degrees of freedom in, e.g., space, time, or frequency [53]. They are able to transfer information from one mode to another and can interact with other physical systems, such as two-level systems, and thus can reliably serve as elements in quantum networks.

For these reasons, bosonic systems have been widely studied for quantum sensing [54, 55], quantum communication [56, 57], quantum simulation [58–60], and quantum computing [61–64].

Different platforms for bosonic systems have been explored, such as trapped ions [65–67], photonics [66, 68–70], and perhaps most importantly, superconducting quantum circuits [53, 62, 71–75]. First experiments have showcased the viability of bosonic quantum error correction [61, 72, 76–78], in some cases even extending the logical lifetime of quantum information [76, 78].

Correcting quantum errors on bosonic systems, therefore, offer a promising building block toward large-scale fault-tolerant quantum information processing.

The cat qubit

One notable bosonic qubit that encodes information in a subspace of the full Hilbert space of a bosonic mode is the so-called *cat qubit* [79–81]. In this thesis, we will discuss the cat qubit in more detail and analyze its properties, including ways to improve it.

Two of the most important noise processes encountered in bosonic systems are *photon loss* and *dephasing*. Photon loss can be understood as an uncontrolled random emission of excitations (photons) into the environment, whereas dephasing

can be viewed as random fluctuations of the oscillator’s energy resulting in a loss of phase-coherence. Correcting these two sources of errors is one of the grand challenges in bosonic quantum error correction. But correcting errors from both noise channels equally well is a challenging task and represents an active area of research.

The cat qubit uses even and odd superpositions of two (classical) coherent states of opposite direction in phase space – characterized by position and momentum – as their logical code words. These superpositions are intrinsically non-classical quantum states that admit a specific rotational symmetry in phase space. This rotational symmetry results in the code-words consisting only of even and odd photon number superpositions respectively, and hence the states can be distinguished by measuring their photon number parity.

It has been shown that the cat qubit provides a way to correct for dephasing errors efficiently. Strikingly, bosonic codes can be stabilized through a carefully engineered dissipation [81] that autonomously drives the quantum state back to the manifold of the bosonic code. For the cat code, an autonomous stabilization scheme can be realized by engineering an effective two-photon exchange interaction [72, 81–83]. Furthermore, a setting to confine the code-space manifold through a Kerr-nonlinear Hamiltonian has been proposed and experimentally realized [84–86].

The cat code presents a type of *biased-noise* qubit in which some kind of *logical* errors are drastically suppressed compared to other errors [81], which makes it favorable for higher-level quantum error correction schemes for the correction of the remaining errors [87–89].

The need for a better cat qubit

However, the cat code suffers from photon loss, a dominant source of errors in many quantum hardware platforms. Due to their photon number parity, upon the loss of a single photon, the parity is flipped which represents an intrinsically unrecoverable error. It has been an active question of research whether by keeping the rotational symmetry of the cat qubit, photon loss error can be – at least approximately – be corrected. This is one of the driving questions in this work. Precisely, we ask the question:

Can the cat code be improved in its robustness against loss and dephasing errors?

Making headway in answering this question is of tremendous relevance in the field of quantum error correction, and in this thesis, we attempt to provide at least one affirmative answer, by using an essential ingredient: *Squeezing*.

Squeezed states of light have already been successfully employed for enhancing the sensitivity in certain measurement setups, an important example being the LIGO gravitational wave detector [90, 91]. Using squeezed states of light allows to go beyond the *standard quantum limit* in quantum metrology [92, 93] and suggests the usefulness in bosonic quantum error correction. This is our main motivation for the proposal of the *squeezed cat code*, an extension of the cat code that uses squeezing to drastically enhance the correctability of dephasing errors, while at the same time enabling the correction of photon loss errors by compressing the cat state in phase space. In this thesis, we thoroughly analyze the squeezed cat code and prove analytically and numerically that it can outperform the cat code in physically relevant regimes. Our findings presented in this thesis were already corroborated by first experiments that have showcased viability of this approach in practical implementations [94]. Importantly, by using squeezing as a resource, the experimental demands for an implementation require only quadratic operations, just like for the standard cat qubit, and autonomous stabilization schemes can be employed in a similar way.

Numerically simulating these bosonic codes, the application of time-dependent quantum gates, and leakage processes outside of the quantum code proves to be extremely challenging in many scenarios, which leads us to the second focus in this thesis.

The need for efficient simulations

As the Hilbert space of bosonic systems is in principle infinite dimensional, the need for efficient numerical methods are very apparent. Most realistic bosonic quantum states are constrained to a narrow corner or subspace of the Hilbert space due to the dissipation and Hamiltonian interactions present in the system. Conventional methods, dating back to second quantization by Vladimir Fock [95], construct the Hilbert space from excitations of the vacuum. This approach can however be inefficient when the average photon number in the system grows large. In many physically relevant scenarios, the dynamics of a quantum state of a driven-dissipative system can be well-described by a coherent state and its excitations that are evolving in phase space. In particular, non-Gaussian effects frequently occur in non-linear driven-dissipative oscillators, that are difficult to capture using Gaussian phase-space representations. But describing quantum fluctuations accurately is often crucial to make correct predictions of dynamical systems. Semi-classical methods that are based on the assumption of a coherent-

state descriptions throughout the entirety during the time-evolution do not capture quantum fluctuations. Other methods, such as the corner-space renormalization group [96] or the truncated Wigner approximation [97–99], are challenged by a dynamically changing phase-space structure or large quantum fluctuations.

As a result, we clearly identify the need to efficiently describe the dynamics of *coherent-state-like* states. Much progress has been made in describing the *dynamics* of quantum two-level systems by parametrizing the quantum state with some variational parameters and time-evolving the parameters according to variational principles [100]. So far, however, the application of variational methods to open bosonic systems has obtained little attention, despite its successful use in other areas. Motivated by this, we thus we pose the question in the second half of this thesis:

How can we efficiently simulate the dynamics of open bosonic quantum systems that are coherent-state-like?

By *coherent-state-like*, we mean states that can be described well in a basis of quantum fluctuations on top of coherent states. To answer this question, we propose the *coherent-state ladder time-dependent variational principle*, a variational approach based on a basis of photon-added unnormalized coherent states. This allows us to use a variational principle to describe dynamical changes in the *basis* as well as in the density matrix which describes the quantum states in the co-evolving basis. We showcase our method on various examples, and demonstrate its wide range of applicability.

Circling back to bosonic error correction, we might wonder whether we can incorporate rotational symmetries in such a variational approach. This would directly enable the simulation of the dynamics of cat qubits and other rotation-symmetric bosonic codes in a more efficient basis. Hence, we aim to answer the question:

How can we efficiently simulate the dynamics of cat qubits?

In the last part of the thesis, we illuminate this question by extending the previous variational approach to rotational symmetries. Although analytical expressions can no longer be easily obtained, we find that the symmetric extension of the coherent-state ladder to a *cat-state ladder* basis is surprisingly straightforward. The *cat-state variational principle* developed in this thesis provides an efficient numerical approach to simulate the dynamics of cat qubits. This allows to study many different phenomena in bosonic error correction with cat qubits, such as the leakage outside of the code-space due to noise, the effect of time-dependent and even noisy gates, and the interaction of multiple interacting cat qubits.

Overall, this thesis aims to address pressing problems in the field of bosonic quantum error correction, with particular focus of cat qubits and their simulation in an open quantum system setting.

Structure of the manuscript

In Chapter 2, we give an overview of the theory of open quantum systems, an essential foundation for the work presented in this thesis. We introduce bosonic systems and consider notable numerical simulation methods. In Chapter 3, we delve into quantum error correction, with a particular focus on bosonic quantum systems. There we present precise conditions under which errors can be exactly corrected and how to assess codes that can only approximately correct errors. As a special bosonic quantum error correction code, we review the two-component cat code. In Chapter 4, we present the *squeezed cat code*, a bosonic quantum error correction code capable of correcting dephasing and loss errors partially, outperforming the standard cat code. This chapter is based on the results presented in Ref. [α]. Finally, in Chapter 5, we present a method of simulating the dynamics of dissipative bosonic systems efficiently for coherent-state-like systems using a time-dependent variational principle. We extend our method to the simulation of cat states, allowing for an efficient simulation of the dynamics of cat states and other rotation-symmetric systems. This chapter is largely based on results presented in Ref. [β].

2

Theory of Open Quantum Systems

In this chapter, we outline the theory of open quantum systems. Using the density matrix formalism (Sec. I) describing statistical mixtures of quantum states, an open system can be described by the Lindblad Master equation (Sec. II). If the system is assumed to be Markovian, one can express the dynamics of the system by a quantum dynamical semigroup. We describe how the Lindblad master equation can be derived from general approximations and by using the Kraus representation theorem. Bosonic systems – which are fundamental in this work – are introduced in Sec. III. Finally we outline numerical methods for the treatment of open quantum systems in Sec. IV.

I Density Matrix Formalism

Quantum mechanical systems must be regarded as open quantum systems on a fundamental level to fully understand their behavior [101]. This is due to the fact that, just like in classical physics, any *realistic* system is inevitably – if ever so slightly – coupled to an uncontrollable environment that influences it in a way that can not be neglected.

In the treatment of open quantum systems, a quantum state representation in terms of pure states is not sufficient since the interaction with an environment requires a description of statistical mixtures of quantum states. In this section, we will, therefore, introduce the density matrix formalism, fully describing a quantum system of a statistical ensemble.

I.1 The Density Matrix

When describing an ensemble of quantum states and in the case where the state of a quantum system is not exactly known, it is convenient to represent its state by the density matrix. Let $\{|\psi_i\rangle\}$ be the set of possible states that build a basis

of the Hilbert space \mathcal{H} of the system. We can define the density matrix $\hat{\rho}$ by

$$\hat{\rho} \equiv \sum_i p_i |\psi_i\rangle\langle\psi_i|, \quad (2.1)$$

where $0 \leq p_i \leq 1$ is the probability for the system to be in state $|\psi_i\rangle$, with $\sum_i p_i = 1$. The density matrix obeys the following properties:

- Positive definiteness: $\langle\phi|\hat{\rho}|\phi\rangle > 0$ for all states $|\phi\rangle$,
- convex linearity: if $\hat{\rho}_1$, and $\hat{\rho}_2$ are in the set of all density matrices $\mathcal{S}(\mathcal{H})$, then any linear combination $\rho = \alpha\hat{\rho}_1 + (1 - \alpha)\hat{\rho}_2$ is also in $\mathcal{S}(\mathcal{H})$,
- normalization: $\text{Tr}\{\hat{\rho}\} = \sum_{ij} p_i \langle\psi_j|\psi_i\rangle \langle\psi_i|\psi_j\rangle = 1$.

The density matrix formalism facilitates the treatment of a statistical ensemble of states and is thereby essential for the treatment of open quantum systems.

I.2 Time-Evolution in a Closed Quantum System

The time-evolution for any quantum state of a closed system is governed by the Schrödinger equation

$$\frac{d}{dt} |\psi(t)\rangle = -i\hat{H} |\psi(t)\rangle. \quad (2.2)$$

If the Hamiltonian \hat{H} is time-independent, the time evolution of an initial state $|\psi(0)\rangle$ to the time-evolved state at time t is given by $|\psi(t)\rangle = U(t) |\psi(0)\rangle$, where $\hat{U}(t)$ is the time-evolution operator. The formal solution for the time-evolution operator $\hat{U}(t)$ is given by the operator equation $\partial_t \hat{U}(t) = -i\hat{H}\hat{U}(t)$ with the unique solution $\hat{U}(t) = e^{-i\hat{H}t}$. In terms of the density matrix of a pure state $\hat{\rho} = |\psi\rangle\langle\psi|$ the generator which governs the dynamics is likewise given by the von Neumann equation:

$$\frac{d\hat{\rho}}{dt} = -i[\hat{H}, \hat{\rho}(t)], \quad (2.3)$$

with the formal solution $\hat{\rho}(t) = \hat{U}(t)\hat{\rho}(0)\hat{U}^\dagger(t)$. Hence, for pure states the time-evolved density matrix remains pure for a closed system and the dynamics evolves according to the Schrödinger equation. Likewise, for a general density matrix $\hat{\rho} = \sum_i p_i |\psi_i\rangle\langle\psi_i|$ the time-evolution is given by

$$\hat{\rho}(t) = \sum_i p_i \hat{U}(t) |\psi_i\rangle\langle\psi_i| \hat{U}^\dagger(t). \quad (2.4)$$

As a consequence, transitions between any time-dependent states $|\psi_i(t)\rangle = \hat{U}(t)|\psi_i(0)\rangle$ are impossible under unitary time-evolution. The solution to the von Neumann equation (2.3) yields the same dynamics as an ensemble average over solutions to the Schrödinger equation for each of the states $|\psi_i\rangle$.

I.3 Measurement Process

The measurement process is central in quantum mechanics and plays an essential role in open quantum systems, as one can often regard the external environment as probing the system via some form of (a sometimes uncontrollable) measurement apparatus.

The measurement process can be generalized from a pure state description to the density matrix formulation. Taking a set $\{\hat{M}_m\}$ of measurement operators satisfying the *completeness relation* $\sum_m \hat{M}_m^\dagger \hat{M}_m = \hat{\mathbb{1}}$ in which each of the operators \hat{M}_m corresponds to a specific measurement outcome m , the probability of obtaining result m is given by

$$P_m = \|\hat{M}_m |\psi\rangle\|^2 = \langle\psi|\hat{M}_m^\dagger \hat{M}_m|\psi\rangle. \quad (2.5)$$

After observing measurement outcome m , the quantum state *collapses* into

$$|\psi\rangle \xrightarrow{m} |\psi'\rangle = \frac{\hat{M}_m |\psi\rangle}{\|\hat{M}_m |\psi\rangle\|} = \frac{\hat{M}_m |\psi\rangle}{\sqrt{\langle\psi|\hat{M}_m^\dagger \hat{M}_m|\psi\rangle}}. \quad (2.6)$$

The most general type of measurement is the *positive operator-valued measure*, or POVM, which is concerned only with the statistics of the measurement. In general, POVM operators are not necessarily orthogonal or commutative [102]. Importantly, the number of POVM operators is not restricted by the dimension of the Hilbert space whereas for projective operators $\hat{M}_m = |m\rangle\langle m|$ the number of operators is always equal to the dimension of the Hilbert space.

In terms of the density matrix notation, the probability of obtaining result m is given by

$$P_m = \text{Tr}\{\hat{M}_m \hat{\rho} \hat{M}_m^\dagger\} > 0. \quad (2.7)$$

The corresponding new state upon measuring outcome m is

$$\hat{\rho} \xrightarrow{m} \hat{\rho}' = \frac{\hat{M}_m \hat{\rho} \hat{M}_m^\dagger}{\text{Tr}\{\hat{M}_m^\dagger \hat{M}_m \hat{\rho}\}}. \quad (2.8)$$

As will be seen in Sec. II, a close connection can be made between the dynamics of open quantum systems and probing the system by means of continuous local measurements.

II Lindblad Master Equation

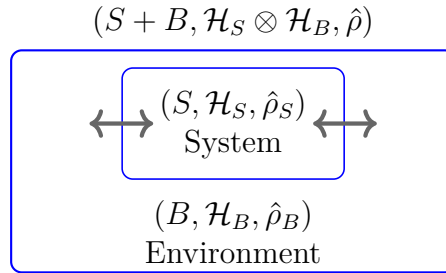


Figure 2.1: Schematic representation of an open quantum system.

We now transition to open quantum systems of a general kind. In this regard we couple the quantum system S that we are interested in to an environment B . Here we assume the combined system $S + B$ to be closed, such that for the entire system the von Neumann equation (2.3) holds and the entire system is thus following Hamiltonian dynamics. However, we can not expect that the system S follows Hamiltonian dynamics as its internal dynamics depends on the interaction with the environment. Alongside literature (see e.g. [101, 103]), the system S is often referred to as the *reduced system*, reflecting that the considered dynamics is reduced to the system described by the density matrix $\hat{\rho}_S$. In some cases, the environment itself is affected by internal processes of the reduced system, e.g., photon emission in atomic, molecular, and optical systems with light-matter interaction. These correlations with the environment will not be considered in this work and we will restrict ourselves solely to Markovian processes, detailed in Sec. II.1.

As schematically illustrated in Fig. 2.1, the total Hilbert space is spanned by the tensor product space $\mathcal{H} = \mathcal{H}_S \otimes \mathcal{H}_B$ on which the Hamiltonian may be defined as

$$\hat{H} = \hat{H}_S \otimes \hat{\mathbb{1}}_B + \hat{\mathbb{1}}_S \otimes \hat{H}_B + \hat{H}_I, \quad (2.9)$$

where \hat{H}_S defines the dynamics governing the reduced system, \hat{H}_B is the free Hamiltonian of the environment, and \hat{H}_I describes the interaction between the system and the environment.

The environment is generally assumed to have an infinite number of degrees of freedom, such that the frequencies of the environment form a continuum. Further-

$$\begin{array}{ccc}
 \hat{\rho}(0) = \hat{\rho}_S(0) \otimes \hat{\rho}_B & \xrightarrow{\text{unitary evolution}} & \hat{\rho}(t) = \hat{U}(t) [\hat{\rho}_S(0) \otimes \hat{\rho}_B] \hat{U}^\dagger(t) \\
 \text{Tr}_B \downarrow & & \downarrow \text{Tr}_B \\
 \hat{\rho}_S(0) & \xrightarrow{\text{dynamical map}} & \hat{\rho}_S(t) = V(t)\hat{\rho}_S(0)
 \end{array}$$

Figure 2.2: Diagram showing the time-evolution of the density matrix of the reduced system $\hat{\rho}_S$ using the dynamical map. Instead of evolving the density matrix of the closed system $\hat{\rho}$ and tracing out the environment (top and right path), the dynamics of the reduced system can be obtained by the action of the dynamical map $V(t)$ incorporating the interaction with the environment (left and bottom path).

more in many cases it is assumed that the environment is in thermal equilibrium, often referred to as a *thermal bath*. To obtain the density matrix of the reduced system one can trace out the environmental degrees of freedom,

$$\text{Tr}_B\{\hat{\rho}\} = \text{Tr}_B\{\hat{\rho}_S \otimes \hat{\rho}_B\} = \hat{\rho}_S \text{Tr}_B\{\hat{\rho}_B\} = \hat{\rho}_S, \quad (2.10)$$

where $\text{Tr}_B\{\bullet\}$ denotes the trace over the degrees of freedom of B . Since the entire system evolves unitarily under Hamiltonian dynamics governed by the von Neumann equation, the formal solution for the dynamics of the reduced system can be written as

$$\hat{\rho}_S(t) = \text{Tr}_B\{\hat{U}(t)\hat{\rho}(0)\hat{U}^\dagger(t)\}, \quad (2.11)$$

where $\hat{U}(t)$ is the time-evolution operator for the entire system $\hat{\rho}$.

II.1 Quantum Markov Processes

In general, directly obtaining the time-evolution of the reduced density matrix from Eq. (2.11) is often unfeasible. This is because calculating the time-evolution operator $\hat{U}(t)$ acting on the entire system is often impractical or impossible due to the infinite amount of degrees of freedom of the environment. Therefore, one seeks a treatment of the reduced system dynamics by incorporating the interaction with the environment, defining a dynamical equation on the Hilbert space for the reduced system only. The time-evolution is then given by a *dynamical map*. Here, we will introduce the notion of *quantum dynamical semigroups* to arrive at a master equation for the reduced density matrix.

If one neglects memory effects of the environment due to induced correlations by the interaction with the reduced system, one may treat the environmental

state as some reference state $\hat{\rho}_B$ that is in (thermal) equilibrium with no time-dependence. The reduced system's dynamics can then be described by a *quantum Markov process*, in which the time-evolution of the reduced system only depends on its current state and *not* on its history. This assumption of the system and environment being uncorrelated is justified if the systems can be prepared separately. The initial state of the entire system can then be written as a product state $\hat{\rho}(0) = \hat{\rho}_S(0) \otimes \hat{\rho}_B$. The time-evolution of the reduced system is then given by a dynamical map $V(t)$, defined by

$$\hat{\rho}_S(t) = V(t)\hat{\rho}_S(0) \equiv \text{Tr}_B \left\{ \hat{U}(t) [\hat{\rho}_S(0) \otimes \hat{\rho}_B] \hat{U}^\dagger(t) \right\}. \quad (2.12)$$

The dynamical map is thus solely defined on the Hilbert space of the reduced system \mathcal{H}_S and can be characterized by operators that are only acting on the reduced system.

II.2 Quantum Dynamical Semigroups

In this section, we introduce quantum dynamical semigroups and give a derivation of the Lindblad master equation, describing the time evolution of the density matrix. We approach the Lindblad equation from general assumptions and employ the Kraus representation theorem. The Lindblad master equation can also be derived microscopically from the underlying Hamiltonian dynamics of the total system [101] in the *weak coupling limit*, which will not be considered here. The Lindblad master equation can also be derived from other assumptions, leading, e.g., to the quantum-optical master equation [101].

Kraus Representation Theorem

Motivated by seeking an expression for the dynamical map $V(t)$, given a density matrix $\hat{\rho}$, one can ask for the most general form of a super-operator acting on $\hat{\rho}$ that preserves all relevant properties of $\hat{\rho}$, namely complete-positivity, trace-preservation, and convex-linearity. The *Kraus representation theorem* states that any super-operator V preserving these properties of $\hat{\rho}$, can be written in the Kraus representation given by [104, 105]

$$V[\hat{\rho}] = \sum_{\alpha} \hat{K}_{\alpha} \hat{\rho} \hat{K}_{\alpha}^{\dagger}, \quad \text{with} \quad \sum_{\alpha} \hat{K}_{\alpha}^{\dagger} \hat{K}_{\alpha} = \hat{\mathbb{1}}, \quad (2.13)$$

where \hat{K}_{α} are the so-called *Kraus operators* that form a countable set of operators.

To see that the dynamical map can be represented by operators acting only on the system's Hilbert space, we might take a spectral decomposition of the density matrix describing the environment $\hat{\rho}_B$:

$$\hat{\rho}_B = \sum_{\alpha} \lambda_{\alpha} |\phi_{\alpha}\rangle\langle\phi_{\alpha}|, \quad (2.14)$$

where $|\phi_{\alpha}\rangle$ form an orthonormal basis of \mathcal{H}_B . We can then rewrite Eq. (2.12):

$$V(t)\hat{\rho}_S = \sum_{\alpha,\beta} \lambda_{\alpha} \langle\phi_{\beta}|\hat{U}(t)|\phi_{\alpha}\rangle \hat{\rho}_S \langle\phi_{\alpha}|\hat{U}^{\dagger}(t)|\phi_{\beta}\rangle \quad (2.15)$$

$$= \sum_{\alpha,\beta} \hat{K}_{\alpha\beta}(t) \hat{\rho}_S \hat{K}_{\alpha\beta}^{\dagger}, \quad (2.16)$$

with $\hat{K}_{\alpha\beta}(t) \equiv \sqrt{\lambda_{\alpha}} \langle\phi_{\beta}|\hat{U}(t)|\phi_{\alpha}\rangle$. Since $\sum_{\alpha,\beta} \hat{K}_{\alpha\beta}^{\dagger} \hat{K}_{\alpha\beta} = \hat{\mathbb{1}}$, it is clear that the dynamical map $V(t)$ preserves the trace of the reduced density matrix $\hat{\rho}_S$. Hence, the dynamical map $V(t)$ defines a convex-linear, completely positive and trace-preserving quantum operation on the reduced density matrix $\hat{\rho}$ [106]. For varying t , the set $\{V(t)|t \geq 0\}$ defines a one-parameter family with $V(0) = \mathbb{1}$ being the identity map.

Memory effects of the environment induced by the interaction with the system can often be neglected if the time scales with associated correlation functions induced by the coupling between system and environment are much smaller in comparison to the characteristic time scale of the system dynamics itself [101]. This simple, yet important, assumption is well justified when the correlation time in the environment τ_B induced by the interaction with S is much shorter than the relaxation time scale τ_R over which the state of the system varies, induced by the action of the environment on the system, i.e., $\tau_B \ll \tau_R$. If this assumption holds, the dynamical map obeys the *semigroup property*:

$$V(t_1)V(t_2) = V(t_1 + t_2), \quad t_1, t_2 \geq 0. \quad (2.17)$$

The semigroup property guarantees that the dynamics of the reduced system is Markovian, such that the dynamics can be expressed as a differential equation in which the time derivative of the reduced density matrix depends only on the current state of the system.

Lindblad's Theorem

Given that a dynamical map satisfies the semigroup property and that it is convex-linear, completely positive, and trace preserving (CPTP), one can ask for a general

form of the generator \mathcal{L} of the semigroup:

$$\boxed{\frac{d}{dt}\hat{\rho}_S = \mathcal{L}[\hat{\rho}_S].} \quad (2.18)$$

\mathcal{L} is also called the *Liouvillian* superoperator that describes the effective equation of motion for $\hat{\rho}_S$. Remarkably, with the assumptions above, a specific form of the above equation can be derived. If the dynamical map satisfies the semigroup property and employing the Kraus representation theorem, the evolution of the density matrix over an infinitesimal timestep δt can be written as

$$\hat{\rho}_S(t + \delta t) = \sum_{\alpha} \hat{K}_{\alpha}(\delta t)\hat{\rho}_S(t)\hat{K}_{\alpha}^{\dagger}(\delta t), \quad (2.19)$$

where the Kraus operators $\hat{K}_{\alpha}(\delta t)$ do not depend on the current time t , as required by the semigroup property. To get a specific form for the Kraus operators, we may write

$$\hat{\rho}_S(t + \delta t) = \hat{\rho}_S(t) + \mathcal{O}(\delta t). \quad (2.20)$$

To obtain the first order correction, we demand $\hat{K}_{\alpha}(\delta t) = \sqrt{\delta t}\hat{A}_{\alpha}$, with some time-independent operator \hat{A}_{α} , since $\hat{K}_{\alpha}(\delta t)\hat{\rho}_S(t)\hat{K}_{\alpha}^{\dagger}(\delta t) = \delta t\hat{A}_{\alpha}\hat{\rho}_S(t)\hat{A}_{\alpha}^{\dagger} \sim \delta t$. To achieve that for $\delta t = 0$ we obtain the identity in Eq. (2.20), and to ensure the normalization of the Kraus operators, $\sum_{\alpha} \hat{K}_{\alpha}^{\dagger}(\delta t)\hat{K}_{\alpha}(\delta t) = \hat{\mathbb{1}}$, we need one Kraus operator to be different from the others:

$$\hat{K}_0 = \hat{\mathbb{1}} + \hat{G}\delta t \quad (2.21)$$

Computing the normalization of the Kraus operator, we find:

$$\sum_{\alpha} \hat{K}_{\alpha}^{\dagger}(\delta t)\hat{K}_{\alpha}(\delta t) = (\hat{\mathbb{1}} + \delta t\hat{G}^{\dagger})(\hat{\mathbb{1}} + \delta t\hat{G}) + \delta t \sum_{\alpha \neq 0} \hat{A}_{\alpha}^{\dagger}\hat{A}_{\alpha} \quad (2.22)$$

$$= \hat{\mathbb{1}} + \delta t(\hat{G}^{\dagger} + \hat{G}) + \delta t \sum_{\alpha \neq 0} \hat{A}_{\alpha}^{\dagger}\hat{A}_{\alpha} + \mathcal{O}(\delta t^2). \quad (2.23)$$

Since the operator \hat{G} is arbitrary, we can parameterize it as

$$\hat{G} = \hat{B} - i\hat{H}, \quad (2.24)$$

where \hat{B} and \hat{H} are both Hermitian. Then, we see that \hat{B} can be fixed by the normalization of the Kraus operators:

$$\hat{B} = -\frac{1}{2} \sum_{k \neq 0} \hat{A}_k^\dagger \hat{A}_k. \quad (2.25)$$

Substituting into Eq. (2.19), we obtain:

$$\hat{\rho}_S(t + \delta t) = \hat{\rho}_S(t) - i\delta t[\hat{H}, \hat{\rho}_S] + \delta t \sum_{\alpha \neq 0} \left(\hat{A}_\alpha \hat{\rho}_S \hat{A}_\alpha^\dagger - \frac{1}{2} \{ \hat{A}_\alpha^\dagger \hat{A}_\alpha, \hat{\rho}_S \} \right). \quad (2.26)$$

Here, $\{\bullet, \bullet\}$ denotes the anti-commutator. Taking the limit $\delta t \rightarrow 0$, substituting $\hat{A}_\alpha \rightarrow \hat{A}_\alpha \sqrt{\gamma_\alpha}$, with $\gamma_\alpha \in \mathbb{R}$, and relabeling the sum, we obtain the so-called *master equation in Lindblad form* [107]:

$$\frac{d}{dt} \hat{\rho}_S = \mathcal{L}[\hat{\rho}_S] \equiv -i[\hat{H}, \hat{\rho}_S] + \sum_{\alpha} \gamma_{\alpha} \mathcal{D}[\hat{A}_{\alpha}](\hat{\rho}_S), \quad \text{with} \quad (2.27)$$

$$\mathcal{D}[\hat{A}_{\alpha}](\hat{\rho}_S) = \hat{A}_{\alpha} \hat{\rho}_S \hat{A}_{\alpha}^{\dagger} - \frac{1}{2} \{ \hat{A}_{\alpha}^{\dagger} \hat{A}_{\alpha}, \hat{\rho}_S \} \quad (2.28)$$

Up to this point, no specific type for the operators \hat{H} and \hat{A}_{α} is assumed, it is however clear that the above equation resembles the Von Neumann equation if the operators \hat{A}_{α} vanish. It thus seems natural to interpret \hat{H} as an effective Hamiltonian. When deriving the Lindblad master equation from a microscopic model, the effective Hamiltonian might differ from the system Hamiltonian, demonstrating that the interaction with a reservoir can also change the unitary part of the time-evolution [108].

The right-most term of the above equation is called the dissipator $\mathcal{D}[\hat{A}_{\alpha}](\hat{\rho}_S)$, taking into account the interaction with the environment that leads to non-unitary, dissipative dynamics. Yet, no particular form for the Lindblad operators \hat{A}_{α} have been presupposed, but comparing the structure of the dissipator with Eq. (2.8) shows that it represents a set of generalized quantum measurements. In this context, one can interpret each $\hat{A}_{\alpha} \hat{\rho}_S \hat{A}_{\alpha}^{\dagger}$ term as a continuous quantum measurement of the system $\hat{\rho}_S$ with an observable \hat{A}_{α} . The other term in the dissipator then ensures the preservation of the trace. The real-valued amplitudes γ_{α} are often called dissipation amplitudes or dissipation rates as they play the role of relaxation rates for different decay channels, specified by the operators \hat{A}_{α} and determine the relaxation time scale of the system.

It is important to note that the Lindblad operators are not unique since the Lindblad master equation remains invariant under unitary transformations of the Lindblad operators \hat{A}_α [101]:

$$\hat{A}_\alpha \rightarrow \hat{A}'_\alpha = \sum_{\beta} \hat{U}_{\alpha\beta} \hat{A}_\beta \quad (2.29)$$

Hence, unitary transformations of the Lindblad operators will induce non-diagonal matrix elements in the Dissipator \mathcal{D} . Additionally, the Lindblad master equation remains invariant under inhomogeneous transformations of the Lindblad operators:

$$\begin{aligned} \hat{A}_\alpha &\rightarrow \hat{A}'_\alpha = \hat{A}_\alpha + c_\alpha, \\ \hat{H} &\rightarrow \hat{H}' = \hat{H} - \frac{i}{2} \sum_{\alpha} \gamma_{\alpha} \left(c_{\alpha}^* \hat{A}_{\alpha} - c_{\alpha} \hat{A}_{\alpha}^{\dagger} \right), \end{aligned} \quad (2.30)$$

with a constant shift $c_\alpha \in \mathbb{C}$.

From Eq. (2.27) it directly follows that the dynamics of $\hat{\rho}_S$ is no longer unitary. The formal solution of the master equation (2.27) is given by:

$$\hat{\rho}_S(t) = e^{\mathcal{L}t} \hat{\rho}_S(0). \quad (2.31)$$

We review numerical methods to solve the Lindblad master equation in Sec. IV

Choi-representation

It can be numerically advantageous to re-express the super-operator \mathcal{L} acting on the density matrix $\hat{\rho}_S$ as a matrix-vector product employing the *Choi-isomorphism* [104, 109], requiring the density matrix of dimension $N \times N$ to be cast into a N^2 -dimensional vector [110]. The Lindblad super-operator is then a $N^2 \times N^2$ matrix acting on the vectorized density matrix $\hat{\rho}_S$. In general, explicit schemes of discretizing Eq. (2.18) are simpler to be implemented than implicit schemes, but can be numerically unstable, requiring an adaptive stepsize [111].

II.3 Spectral Properties

To better understand the dynamics of the Lindblad master equation, a spectral analysis of the Liouvillian superoperator \mathcal{L} gives important insights. Analyzing the stability of the Lindblad master equation's solution, we can find eigenmatrices $\hat{\rho}^{(n)}$ and eigenvalues λ_n according to the eigenvalue equation:

$$\sum_{k,l} \mathcal{L}_{ijkl} \rho_{kl}^{(n)} = \lambda_n \rho_{ij}^{(n)}, \quad (2.32)$$

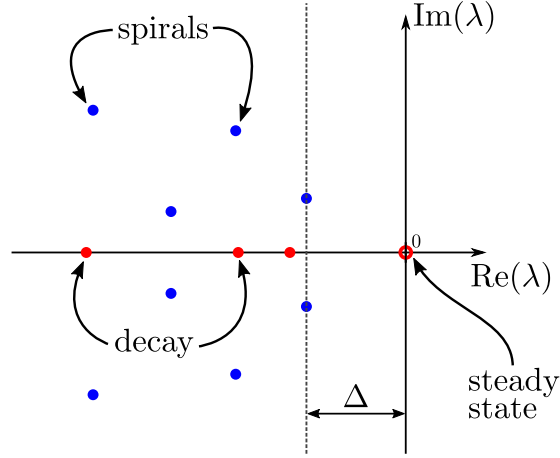


Figure 2.3: Schematic representation of the Eigenvalues λ_n of a general Liouvillian \mathcal{L} in the complex plane. Eigenvalues with non-zero imaginary part come in conjugate pairs (blue) and represent damped oscillations of the corresponding eigen-matrices $\hat{\rho}^{(n)}$. For zero imaginary part (red), $\hat{\rho}^{(n)}$ are exponentially decaying. The $\lambda = 0$ eigenvalue corresponds to the steady state (red circle). The smallest non-zero eigenvalue defines the dissipative gap Δ , characterizing the slowest decay rate of the system.

for a density matrix of the form $\hat{\rho} = \sum_{ij} \rho_{ij} |\psi_i\rangle\langle\psi_j|$. Here λ_n are the eigenvalues of \mathcal{L} . In general, the eigenmatrices are not orthogonal, $\text{Tr}\{\hat{\rho}^{(n)}\hat{\rho}^{(m)}\} \neq 0$, since \mathcal{L} is not Hermitian. If the Liouvillian can be diagonalized, one can use the eigenstates of \mathcal{L} as a basis of the Liouville space [112] and for any operator \hat{A} , there exists a unique decomposition into eigenstates of \mathcal{L} :

$$\hat{A} = \sum_n c_n \hat{\rho}^{(n)}, \quad (2.33)$$

with complex coefficients c_n .

The eigenvalues of the Liouvillian have the following properties [112]:

- (i) The eigenvalues of \mathcal{L} are either real or come in conjugate pairs.
- (ii) Positivity of \mathcal{L} requires the eigenvalues to have a negative real part, $\text{Re}(\lambda_n) \leq 0$.
- (iii) For any \mathcal{L} , there is at least one eigenvalue with $\lambda_0 = 0$. The corresponding eigenstate is referred to as the *steady state*, $\hat{\rho}_{ss} \equiv \hat{\rho}^{(0)}$. If the zero eigenvalue is degenerate with multiplicity n , there exist n multiple steady states towards which the system can evolve, depending on the initial conditions.
- (iv) $\text{Tr}[\rho^{(n)}] = 0$ if $\text{Re}(\lambda_n) \neq 0$. Hence, apart from the steady-state eigenmatrix $\hat{\rho}_{ss}$ the other eigenmatrices cannot be understood as density matrices, but rather as excitations of the steady-state density matrix.

For a time-independent Liouvillian with a finite Hilbert space dimension, the steady state is unique under quite general conditions [113, 114]. We can then decompose the time-evolved density matrix by eigenstates of \mathcal{L} [112]

$$\hat{\rho}(t) = \frac{\hat{\rho}_{\text{ss}}}{\text{Tr}[\hat{\rho}_{\text{ss}}]} + \sum_{n \neq 0} c_n(t) \hat{\rho}^{(n)} = \frac{\hat{\rho}_{\text{ss}}}{\text{Tr}[\hat{\rho}_{\text{ss}}]} + \sum_{n \neq 0} c_n(0) e^{\lambda_n t} \hat{\rho}^{(n)}, \quad (2.34)$$

with the overlap between the initial state and the n -th eigenstate $c_n(0) = \text{Tr}[\hat{\rho}(0) \hat{\rho}^{(n)}]$.

Another relevant quantity, characterizing the relaxation behavior of the system is the *dissipation gap*, or asymptotic decay rate [115], defined by $\Delta \equiv \min_n \{|\text{Re}(\lambda_n)| : n \neq 0\}$. The dissipation gap characterizes the slowest time scale with which the system relaxes to the steady state, given by $\tau \sim 1/\Delta$. A schematic representation of the structure of the eigenvalues of a general Liouvillian \mathcal{L} is shown in Fig. 2.3.

III Bosonic quantum systems

In this work, we are primarily interested in bosonic systems. Such systems are ubiquitously encountered in quantum mechanics and can be found on a wide range of platforms, such as photonics, optomechanical systems, and electromagnetic resonators in superconducting devices.

III.1 The quantum harmonic oscillator

Classical harmonic oscillator: An illustrative and insightful example is provided by the model of the *quantum harmonic oscillator* [116, 117]. However, let us first look at the *classical* one-dimensional harmonic oscillator, which is described by an angular oscillation frequency ω and a mass m , such that its Hamiltonian reads

$$H = \frac{p^2}{2m} + \frac{1}{2} m \omega^2 x^2. \quad (2.35)$$

Here, x and p describe the position and momentum of the massive particle, respectively. The dynamics of the harmonic oscillator is given by the Hamiltonian equations

$$\begin{aligned} \frac{d}{dt} p(t) &= \frac{\partial H}{\partial p} = -m\omega^2 x(t), \\ \frac{d}{dt} x(t) &= \frac{\partial H}{\partial x} = \frac{p(t)}{m}. \end{aligned} \quad (2.36)$$

We can solve the set of coupled differential equations above by introducing the complex dimensionless variable

$$\alpha(t) = \sqrt{\frac{m\omega}{2}} \left(x(t) + \frac{i}{m\omega} p(t) \right). \quad (2.37)$$

Then, the set of differential equations above is reduced to a single complex-valued equation

$$\frac{d}{dt}\alpha(t) = -i\omega\alpha(t), \quad (2.38)$$

which has a simple oscillating solution

$$\alpha(t) = \alpha_0 e^{-i\omega t}. \quad (2.39)$$

The evolution of x and p are given by the relations

$$\begin{aligned} x &= \frac{1}{\sqrt{2m\omega}}(\alpha + \alpha^*) = \sqrt{\frac{2}{m\omega}}\text{Re}(\alpha) \\ p &= -i\sqrt{\frac{m\omega}{2}}(\alpha - \alpha^*) = \sqrt{2m\omega}\text{Im}(\alpha) \end{aligned} \quad (2.40)$$

The energy of the system is then simply $H = \omega|\alpha_0|^2$. The interpretation of this that x and p represent conjugate variables that can be represented as real and imaginary parts of a complex variable α . The dynamics of the system then describes a point that is moving in a circle around the origin of the complex plain.

Quantum harmonic oscillator: Let us now look on the quantum version of the harmonic oscillator. Similar to the classical case, the Hamiltonian of the system takes the form

$$\hat{H} = \frac{\hat{p}^2}{2m} + \frac{1}{2}m\omega\hat{x}^2. \quad (2.41)$$

Note that here, the position and momentum variables are operators, obeying $[\hat{x}, \hat{p}] = i$. Similarly, we can introduce the *creation* and *annihilation* operators

$$\begin{aligned} \hat{a} &= \sqrt{\frac{m\omega}{2}} \left(\hat{x} + \frac{i}{m\omega}\hat{p} \right), \\ \hat{a}^\dagger &= \sqrt{\frac{m\omega}{2}} \left(\hat{x} - \frac{i}{m\omega}\hat{p} \right). \end{aligned} \quad (2.42)$$

It is straightforward to check that \hat{a} and \hat{a}^\dagger obey

$$[\hat{a}, \hat{a}^\dagger] = \hat{1}. \quad (2.43)$$

We can re-express \hat{x} and \hat{p} in terms of the creation and annihilation operators as

$$\begin{aligned}\hat{x} &= \sqrt{\frac{1}{2m\omega}} (\hat{a}^\dagger + \hat{a}), \\ \hat{p} &= i\sqrt{\frac{m\omega}{2}} (\hat{a}^\dagger - \hat{a}).\end{aligned}\tag{2.44}$$

Inserting the above expression, the Hamiltonian has the form

$$\hat{H} = \omega \left(\hat{a}^\dagger \hat{a} + \frac{1}{2} \right).\tag{2.45}$$

We can conveniently define the photon number operator $\hat{n} \equiv \hat{a}^\dagger \hat{a}$ whose eigenstates are the eigenstates of the Hamiltonian \hat{H} . For eigenstates $|n\rangle$, the action of the operators \hat{a} , \hat{a}^\dagger and \hat{n} are given by

$$\begin{aligned}\hat{a}^\dagger |n\rangle &= \sqrt{n+1} |n+1\rangle, \\ \hat{a} |n\rangle &= \sqrt{n} |n-1\rangle, \\ \hat{n} |n\rangle &= n |n\rangle.\end{aligned}\tag{2.46}$$

The states $|n\rangle$ of \hat{H} are often referred to as Fock states. In the above expression, the naming of \hat{a} and \hat{a}^\dagger as annihilation and creation operators becomes apparent as the annihilate and create excitations, whereas the number operator counts the number of excitations of the quantum harmonic oscillator. Formally, the Fock-states are given by

$$|n\rangle = \frac{\hat{a}^{\dagger n}}{\sqrt{n!}} |0\rangle,\tag{2.47}$$

where $|0\rangle$ is the ground state of the quantum harmonic oscillator.

III.2 Coherent states

We might wonder whether there are states that have a similar analogy to the oscillating solutions for the classical harmonic oscillator. The eigenstates $|n\rangle$ have always zero expectation value for \hat{x} and \hat{p} and are non-oscillating. As in the classical picture, where the solution is simply given by the complex amplitude $\alpha(t)$ in phase space, we might define an analogous state for the quantum harmonic oscillator by displacing the vacuum. Then, the resulting state is a unique *eigenstate* of the annihilation operator, defined by the relation

$$\hat{a} |\alpha\rangle = \alpha |\alpha\rangle,\tag{2.48}$$

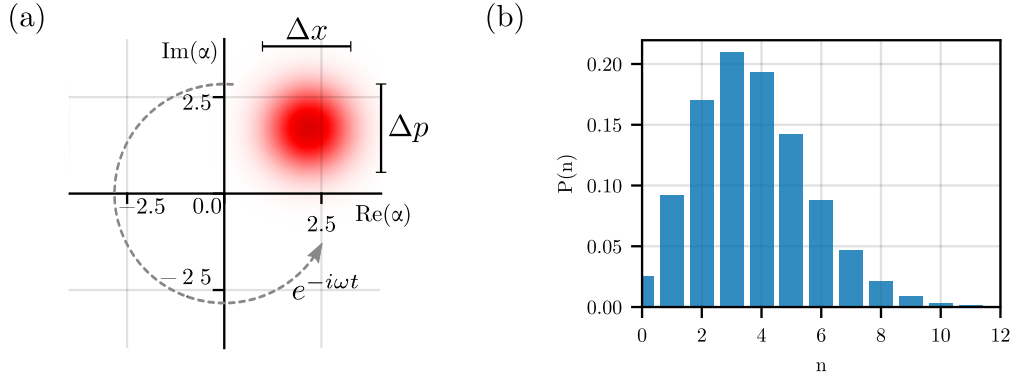


Figure 2.4: (a) Quasi-probability representation of a coherent state $|\alpha\rangle$ in phase space. (b) The photon number distribution $P(n) = |\langle n|\alpha\rangle|^2$ follows a Poissonian distribution.

with complex eigenvalue α . Using the definition of the annihilation operator, we can check that the above eigenvalue equation is satisfied when

$$|\alpha\rangle = e^{-\frac{|\alpha|^2}{2}} \sum_{n=0}^{\infty} \frac{\alpha^n}{\sqrt{n!}} |n\rangle. \quad (2.49)$$

We can obtain a coherent state by displacing it from the vacuum:

$$|\alpha\rangle = \hat{D}(\alpha) |0\rangle, \quad (2.50)$$

with

$$\hat{D}(\alpha) \equiv e^{\alpha \hat{a}^\dagger - \alpha^* \hat{a}} = e^{-\frac{|\alpha|^2}{2}} e^{\alpha \hat{a}^\dagger} e^{-\alpha^* \hat{a}}. \quad (2.51)$$

We can verify that the above definition of the displacement operator $\hat{D}(\alpha)$ satisfies the relation in Eq. (2.48).

By calculating the expectation values for the operators \hat{x} and \hat{p} for the state $|\alpha\rangle$, the analogy to the classical harmonic oscillator becomes very clear:

$$\begin{aligned} \langle \hat{x} \rangle &= \sqrt{\frac{2}{m\omega}} \operatorname{Re}(\alpha), \\ \langle \hat{p} \rangle &= \sqrt{2m\omega} \operatorname{Im}(\alpha). \end{aligned} \quad (2.52)$$

These relations are *exactly* identical to the classical harmonic oscillator in Eq. (2.40), which is why the coherent states are often referred to as *semi-classical* states.

One important difference with respect to the classical picture is that the state $|\alpha\rangle$ saturates the Heisenberg uncertainty principle with equal uncertainty in the \hat{x} and \hat{p} quadratures:

$$\Delta x = \Delta p, \quad \text{with} \quad \Delta x \Delta p = \frac{1}{2}, \quad (2.53)$$

with $(\Delta A)^2 \equiv \langle \hat{A}^2 \rangle - \langle \hat{A} \rangle^2$. As such, the state $|\alpha\rangle$ represents a wave-packet of minimum Heisenberg uncertainty in \hat{x} and \hat{p} , as depicted in Fig. 2.4.

III.3 Wigner representation

One can fully represent a continuous-variable quantum system in phase space using quasi-probability distributions. This provides a powerful tool to describe pure and mixed bosonic quantum states. One such approach, which we briefly detail here, is the *Wigner function* representation of a density matrix $\hat{\rho}$. The idea to represent bosonic states in phase space is intrinsically inspired from classical mechanics, for which a state can be described by a point in phase space that moves through it according to the governing equations of motion. For a quantum state, such an approach is more subtle due to the fundamentally probabilistic nature of quantum mechanics. Nonetheless, we can define a close analogy of a *quantum* state representation in phase space. The uncertainty relation does not allow us to represent a quantum state as a single point in phase space, but we can represent in terms of a quasi-probability $W(q, p)$, such that

$$\int_{-\infty}^{+\infty} W(q, p) dp = \langle q | \hat{\rho} | q \rangle, \quad \int_{-\infty}^{+\infty} W(q, p) dq = \langle p | \hat{\rho} | p \rangle, \quad (2.54)$$

where $|q\rangle$ and $|p\rangle$ are eigenstates of the position operator \hat{x} and momentum operator \hat{p} , respectively.

For this, we define the Wigner *characteristic function*

$$\chi(u, v) = \chi(\eta) \equiv \text{Tr} [\hat{\rho} \hat{D}(\eta)], \quad (2.55)$$

with u, v being the real and imaginary part of η .

The Wigner function can be defined by the Fourier transform of the characteristic function [97, 99, 118] as

$$W(\alpha, \alpha^*) \equiv \frac{1}{\pi} \int_{-\infty}^{\infty} d^2\eta \chi(\eta) e^{\eta^* \alpha - \eta \alpha^*} \quad (2.56)$$

Here, α and α^* act as two independent orthogonal variables, representing the two quadratures in phase space, and can alternatively be represented by the real-valued variables $q = \text{Re}(\alpha)$ and $p = \text{Im}(\alpha)$.

An alternative representation of the Wigner function can be given in terms of the parity operator $\hat{\Pi} \equiv e^{i\pi \hat{a}^\dagger \hat{a}}$ [119–121]:

$$W(\alpha, \alpha^*) = 2 \text{Tr} \{ \hat{D}^\dagger(\alpha) \hat{\rho} \hat{D}(\alpha) \hat{\Pi} \}. \quad (2.57)$$

By integrating over q or p , (or α , α^* equivalently) we obtain the non-negative marginal distributions in Eq. (2.54) that can be interpreted as probability distributions.

The Wigner function obeys the following important properties:

- The Wigner function is properly normalized: $\frac{1}{\pi} \int_{-\infty}^{\infty} W(\alpha, \alpha^*) d^2\alpha = 1$.
- $W(\alpha, \alpha^*)$ is a real-valued function. Regions of negativity characterize non-classical quantum states [116, 122, 123]. For non-negativity of the Wigner function for pure states, $W(\alpha, \alpha^*)$ is required to be Gaussian (See also Chap. 4).
- The Wigner function is unique for any density matrix $\hat{\rho}$ and represents a one-to-one mapping, i.e. the density matrix can be uniquely determined from its Wigner representation. Hence, the Wigner function contains all information about $\hat{\rho}$.

Interestingly, the action of operators on the density matrix $\hat{\rho}$ corresponds to derivatives in the Wigner function [97]:

$$\begin{aligned}
 \hat{a}\hat{\rho} &\longrightarrow \left(\alpha + \frac{1}{2} \frac{\partial}{\partial \alpha^*} \right) W(\alpha, \alpha^*) \\
 \hat{a}^\dagger\hat{\rho} &\longrightarrow \left(\alpha^* - \frac{1}{2} \frac{\partial}{\partial \alpha} \right) W(\alpha, \alpha^*) \\
 \hat{\rho}\hat{a}^\dagger &\longrightarrow \left(\alpha^* + \frac{1}{2} \frac{\partial}{\partial \alpha} \right) W(\alpha, \alpha^*) \\
 \hat{\rho}\hat{a} &\longrightarrow \left(\alpha - \frac{1}{2} \frac{\partial}{\partial \alpha^*} \right) W(\alpha, \alpha^*)
 \end{aligned} \tag{2.58}$$

This correspondence between action of creation and annihilation operator on the density matrix and derivatives in the Wigner function can be used to devise numerical methods of simulating the dynamics of the quantum state in phase space.

IV Numerical methods for open quantum systems

Several numerical methods have been proposed for the treatment of open quantum systems. We will detail a selection of numerical methods that are relevant to this work here. For a general overview, see, e.g., Ref. [124].

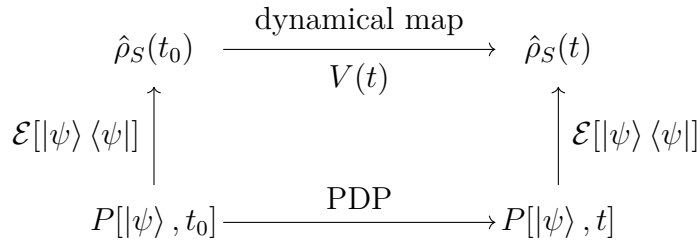


Figure 2.5: Unraveling of the master equation as a commutative diagram. Instead of time-evolving the density matrix $\hat{\rho}_S$ by applying the dynamical map $V(t)$, one can time-evolve single quantum states drawn from an initial probability distribution $P[|\psi\rangle, t_0]$ using a piecewise deterministic process to approximate the final probability distribution $P[|\psi\rangle, t]$. The density matrix is then given by calculating the stochastic average of the covariance matrix corresponding to state $|\psi(t)\rangle$.

IV.1 Monte Carlo Wave Function method

Numerically solving the Lindblad master equation requires to store N^2 matrix elements of the density matrix for a Hilbert space of dimension N . Even taking Hermiticity into account – reducing the number of matrix elements to $N^2/2$ – storing the matrix elements fully describing the system requires substantial memory and computation power when N is large. Thus, for larger system sizes, solving the Lindblad master equation becomes impracticable, also due to the limited possibilities to parallelize the time-evolution, since the Lindblad master equation is usually a set of highly coupled differential equations, requiring a sequential numerical integration. If it is possible to store at least N complex-valued amplitudes, one can implement a stochastic process whose ensemble average resembles the Lindblad master equation. This allows an *unraveling* of the Lindblad master equation to *piece-wise deterministic processes* (PDPs), often referred to as *quantum trajectories*, which evolve in time as pure states. Note that the respective *unraveling* is not unique, and other approaches have been developed, giving rise to, e.g., a *Wiener process*, sometimes referred to as *quantum diffusion* [101], which will not be considered here. Unlike using the Lindblad equation, where the full density matrix has to be propagated in time, here, only single state vectors are time-evolved in the quantum trajectory method, posing a substantial advantage of this technique. This, however, necessitates stochastic sampling of multiple quantum trajectories to achieve a significantly high accuracy. Therefore, the quantum trajectory method is only superior to the classical Lindblad approach if the number of samples is well below the dimension of the Hilbert space [125].

The simplest approach of *unraveling* the Lindblad equation as a piece-wise deterministic process was first proposed by Dalibard et al. [126, 127] and Dum

et al. [128] in optical settings for laser cooling and continuous measurements. In these works, the Lindblad equation is expanded in first order of the timestep δt .

To arrive at a stochastic equation that resembles the Lindblad master equation in the statistic limit, we can rewrite Eq. (2.27) as:

$$\frac{d}{dt}\hat{\rho}_S = -i(\hat{H}_{\text{eff}}\hat{\rho}_S - \hat{\rho}_S\hat{H}_{\text{eff}}^\dagger) + \sum_{\alpha} \gamma_{\alpha}\hat{A}_{\alpha}\hat{\rho}_S\hat{A}_{\alpha}^\dagger, \quad (2.59)$$

where \hat{H}_{eff} is the *effective Hamiltonian* given by

$$\hat{H}_{\text{eff}} = \hat{H} - \frac{i}{2} \sum_{\alpha} \gamma_{\alpha} \hat{A}_{\alpha}^\dagger \hat{A}_{\alpha}. \quad (2.60)$$

It is important to note that \hat{H}_{eff} is not Hermitian. Following Ref. [125], as an intuitive stochastic approach to Eq. (2.59), we can take an initial pure state $|\psi(t)\rangle$ for which a candidate for a new state at time $t + \delta t$ in first order is

$$|\psi^{(1)}(t + \delta t)\rangle \approx (1 - i\hat{H}_{\text{eff}}\delta t) |\psi\rangle. \quad (2.61)$$

The norm of the resulting state is less than one due to the dissipative term in the effective Hamiltonian:

$$\langle \psi^{(1)}(t + \delta t) | \psi^{(1)}(t + \delta t) \rangle = \langle \psi(t) | (1 + i\hat{H}_{\text{eff}}^\dagger\delta t)(1 - i\hat{H}_{\text{eff}}\delta t) | \psi(t) \rangle = 1 - \delta p, \quad (2.62)$$

where the loss δp is due to possible decay channels corresponding to the action of different Lindblad operators \hat{A}_{α} :

$$\begin{aligned} \delta p &\equiv \delta t \langle \psi(t) | i(\hat{H}_{\text{eff}} - \hat{H}_{\text{eff}}^\dagger) | \psi(t) \rangle \\ &= \delta t \sum_{\alpha} \gamma_{\alpha} \langle \psi(t) | \hat{A}_{\alpha}^\dagger \hat{A}_{\alpha} | \psi(t) \rangle \equiv \sum_{\alpha} \delta p_{\alpha}. \end{aligned} \quad (2.63)$$

Intuitively, one can interpret δp_{α} as the probability that the action by the Lindblad operator \hat{A}_{α} occurs during the given timestep. With the definition (2.63), we can now construct a simple stochastic process in which we choose the propagated state stochastically according to the following rule:

- **no jump**: with probability $1 - \delta p$

$$|\psi(t + \delta t)\rangle = \frac{|\psi^{(1)}(t + \delta t)\rangle}{\sqrt{1 - \delta p}} \quad (2.64)$$

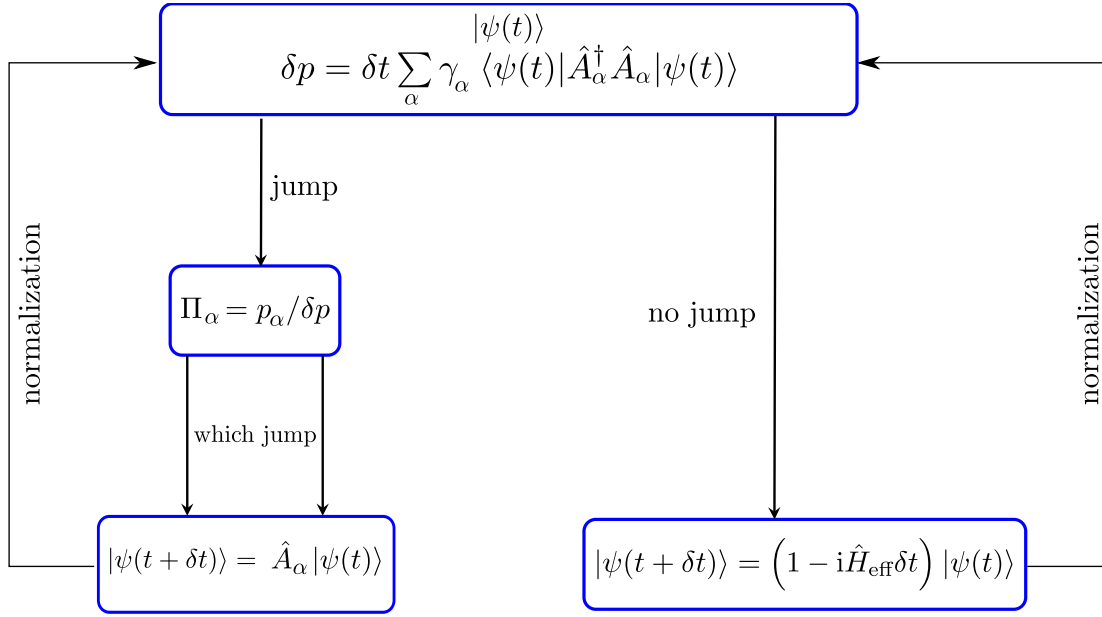


Figure 2.6: Schematic representation of the quantum trajectory method. With the initial state, the jump probability for time-step δt is calculated. If a jump occurs, a particular Lindblad operator \hat{A}_{α} is applied to the state with probability Π_{α} . If no jump occurs, the state evolves under the effective Hamiltonian \hat{H}_{eff} .

- **jump**: with probability δp

$$|\psi(t + \delta t)\rangle = \frac{\sqrt{\gamma_{\alpha}} \hat{A}_{\alpha} |\psi(t)\rangle}{\sqrt{\delta p_{\alpha} / \delta t}} \quad (2.65)$$

where the particular Lindblad operator \hat{A}_{α} is chosen out of all possible Lindblad operators with probability $\Pi_{\alpha} = \delta p_{\alpha} / \delta p$.

If the initial state of the density matrix is not a pure state, the initial states for the quantum trajectory approach can be sampled from a distribution to match the initial mixed state of the density matrix.

It is important to show that the stated method resembles the Lindblad master equation in the stochastic average. We therefore consider the density matrix of a pure state:

$$\hat{\rho}(t) = |\psi(t)\rangle \langle \psi(t)| \quad (2.66)$$

Then, the statistical average of the density matrix after a timestep δt is given by

$$\begin{aligned} \mathcal{E}[\hat{\rho}(t + \delta t)] &= (1 - \delta p) \frac{|\psi^{(1)}(t + \delta t)\rangle \langle \psi^{(1)}(t + \delta t)|}{\sqrt{(1 - \delta p)}} \frac{1}{\sqrt{1 - \delta p}} \\ &+ \delta p \sum_{\alpha} \Pi_{\alpha} \frac{\sqrt{\gamma_{\alpha}} \hat{A}_{\alpha} |\psi(t)\rangle \langle \psi(t)| \sqrt{\gamma_{\alpha}} \hat{A}_{\alpha}^{\dagger}}{\sqrt{\delta p_{\alpha} \delta t}} \frac{1}{\sqrt{\delta p_{\alpha} \delta t}} \end{aligned} \quad (2.67)$$

This simplifies to:

$$\begin{aligned} \mathcal{E}[\hat{\rho}(t + \delta t)] &= (1 - i\delta t \hat{H}_{\text{eff}}) |\psi(t)\rangle \langle \psi(t)| (1 + i\delta t \hat{H}_{\text{eff}}^{\dagger}) + \delta t \sum_{\alpha} \gamma_{\alpha} \hat{A}_{\alpha} |\psi(t)\rangle \langle \psi(t)| \hat{A}_{\alpha}^{\dagger} \\ &= \hat{\rho}(t) - i\delta t (\hat{H}_{\text{eff}} \hat{\rho}(t) - \hat{\rho}(t) \hat{H}_{\text{eff}}^{\dagger}) + \delta t \sum_{\alpha} \gamma_{\alpha} \hat{A}_{\alpha} \hat{\rho}(t) \hat{A}_{\alpha}^{\dagger}. \end{aligned} \quad (2.68)$$

Thus, for arbitrary small timesteps δt , this yields Eq. (2.59):

$$\frac{d}{dt} \hat{\rho} = -i(\hat{H}_{\text{eff}} \hat{\rho} - \hat{\rho} \hat{H}_{\text{eff}}^{\dagger}) + \sum_{\alpha} \gamma_{\alpha} \hat{A}_{\alpha} \hat{\rho} \hat{A}_{\alpha}^{\dagger}. \quad (2.69)$$

It is important to note that the above equation holds regardless of whether the corresponding state of $\hat{\rho}(t)$ is pure or mixed.

Stochastic Schrödinger Equation: More formally, we can cast the above procedure of a piecewise deterministic process into a stochastic differential equation. The Lindblad master equation can be effectively modeled by the stochastic equation [101, 129]:

$$|d\psi\rangle = \left[-i\hat{H}_{\text{eff}} + \frac{1}{2} \sum_{\alpha} \gamma_{\alpha} \langle \psi | \hat{A}_{\alpha}^{\dagger} \hat{A}_{\alpha} | \psi \rangle \right] |\psi\rangle dt + \sum_{\alpha} \left(\frac{\hat{A}_{\alpha} |\psi\rangle}{\|\hat{A}_{\alpha} |\psi\rangle\|} - |\psi\rangle \right) dN_{\alpha}, \quad (2.70)$$

where the stochastic Poisson increments dN_{α} have the expectation value

$$\mathcal{E}[dN_{\alpha}] = \gamma_{\alpha} \langle \psi | \hat{A}_{\alpha}^{\dagger} \hat{A}_{\alpha} | \psi \rangle dt, \quad (2.71)$$

with $dN_{\alpha} dN_{\beta} = \delta_{\alpha\beta} dN_{\alpha}$, such that only one quantum jump can occur at once. The above equation (2.70) is a piecewise deterministic process with stochastic quantum jumps that collapses the quantum state, indicated by the right-most term. In this framework, the process $|\psi(t)\rangle$ encompasses the random change of the state conditioned on the outcomes of continuous monitoring of certain environmental observables, represented by the operators \hat{A}_{α} .

Physical interpretation: It is insightful to treat the quantum trajectory approach to dissipative systems not only as a technical tool for efficiently calculating expectation values through stochastic averaging. Rather, it also gives an intriguing physical interpretation of *how* the system and the reservoir are interacting. In the described process, the system undergoes the evolution of a non-Hermitian effective Hamiltonian \hat{H}_{eff} which is interrupted by *quantum jumps* that act like a generalized quantum measurement. Hence, we can view the interaction between the system and its environment as a measurement collapsing the wave function at stochastically chosen times.

It is also clear that we gain information about the system: If we *measure* outcome α , we know that a quantum jump corresponding to the operator \hat{A}_α occurred. Even if no jump occurs, we know that the system evolves according to the effective Hamiltonian \hat{H}_{eff} , from which we can infer its state after the previous quantum jump. We can, therefore, interpret each of the individual quantum trajectories in terms of an experimental setup in which information about the system is gained by probing it via measurement-like observables. This interpretation is only possible if there exists an appropriate set of Lindblad operators for the modeled dynamics that can be interpreted as or transformed into measurement-like operators. To this regard, it is important to note that the Lindblad equation remains invariant under unitary transformation of the Lindblad operators (See Eq. (2.29)). Therefore, the same effective dynamics can be achieved with different operators that might correspond to different types of measurements. Hence, if one seeks a physical interpretation in terms of a local measurement, one has to choose the Lindblad operators accordingly.

IV.2 Coherent mean-field approximation

In quantum-optical systems, a central method to describe the dynamics of an open and interacting system is the *semi-classical* mean-field approximation.

A common approach for the numerical treatment of open quantum systems consists of assuming the density matrix to be in a product state of subsystem density matrices $\hat{\rho}_i$ [130], such that

$$\hat{\rho} = \bigotimes_i \hat{\rho}_i. \quad (2.72)$$

In quantum optical systems [131], a versatile method is the *Gross-Pitaevskii mean-field approximation* [132, 133] (initially used for the description of cold Bose gases). The central assumption in this *semi-classical* approximation is that the density matrix of a single mode $\hat{\rho}$ is described by a single coherent state with complex

field amplitude α at all times:

$$\hat{\rho}(t) = |\alpha(t)\rangle\langle\alpha(t)|. \quad (2.73)$$

This approximation is justified when no or only weak correlations or quantum fluctuations are induced throughout the system's time evolution. In this approximation, expectation values take the simple form

$$\langle \hat{a}^{\dagger m} \hat{a}^n \rangle (t) = \alpha^{*m}(t) \alpha^n(t). \quad (2.74)$$

We can obtain an equation of motion for $\alpha(t)$ through

$$\frac{\partial \alpha}{\partial t} = \frac{\partial}{\partial t} \langle \hat{a} \rangle = \text{Tr} \left\{ \hat{a} \frac{\partial \hat{\rho}}{\partial t} \right\} = \text{Tr} \left\{ \frac{\partial \hat{a}}{\partial t} \hat{\rho}(t) \right\}. \quad (2.75)$$

We can thus obtain the right-hand side by projecting the Liouvillian from Eq. (2.27) onto the coherent state $|\alpha(t)\rangle$:

$$\frac{\partial \alpha}{\partial t} = -i \langle \alpha(t) | [\hat{a}, \hat{H}] | \alpha(t) \rangle + \sum_{\beta} \gamma_{\beta} \langle \alpha(t) | \hat{A}_{\beta}^{\dagger} \hat{a} \hat{A}_{\beta} - \frac{1}{2} \{ \hat{A}_{\beta}^{\dagger} \hat{A}_{\beta}, \hat{a} \} | \alpha(t) \rangle \quad (2.76)$$

The terms involved on the right-hand side can typically be expressed in terms of polynomial combinations of \hat{a} and \hat{a}^{\dagger} .

For interacting bosonic systems, the product ansatz in Eq. (2.72) can be used,

$$\hat{\rho}(t) = \bigotimes_i |\alpha_i(t)\rangle\langle\alpha_i(t)|. \quad (2.77)$$

The equation of motion for the fields α_i will, in general, be coupled, yielding a set of first-order non-linear ordinary differential equations.

Often, analytical treatments are possible when the right-hand side of Eq. (2.76) is a low-order polynomial in α and α^* . Additionally, calculating fixed points in this semi-classical approximation can give valuable insights about dissipative phase transitions in driven-dissipative systems [112].

IV.3 Phase-space methods

An important example of phase-space methods using the Wigner function is the *truncated Wigner approximation* [131, 134, 135]. From Sec. III.3, we have seen that the action of operators on the density matrix corresponds to first-order derivatives in the Wigner function. Non-linear terms in the Hamiltonian or dissipator will thus correspond to derivatives of order higher than two in the Wigner function.

The truncated Wigner approximation consists in dropping third and higher order derivatives, which is justified if the originating interaction or dissipation strength is sufficiently small.

In doing so, the differential equation for the Wigner function represents a *Fokker-Planck equation* under general assumptions [131, 136], so that the differential equation for $W(\alpha, \alpha^*)$ reads

$$\begin{aligned} \frac{\partial W(\alpha, \alpha^*)}{\partial t} &\approx \hat{L}(\alpha, \alpha^*)W(\alpha, \alpha^*), \quad \text{with} \\ \hat{L}(\alpha, \alpha^*) &= \frac{\partial}{\partial \alpha} A(\alpha, \alpha^*) + \frac{1}{2} \frac{\partial^2}{\partial \alpha \partial \alpha^*} D(\alpha, \alpha^*), \end{aligned} \quad (2.78)$$

with *drift* term $A(\alpha, \alpha^*)$ and *diffusion* term $D(\alpha, \alpha^*)$, which depend on the Hamiltonian and dissipators of the system.

We can associate a *stochastic Langevin* equation to the Fokker-Planck equation:

$$d\alpha = A(\alpha, \alpha^*)dt + B(\alpha, \alpha^*)d\chi(t), \quad (2.79)$$

with $|B(\alpha, \alpha^*)|^2 = D(\alpha, \alpha^*)$ and normalized random complex Gaussian noise $\chi(t)$, such that $\langle \chi(t)\chi(t') \rangle = 0$ and $\langle \chi(t)\chi^*(t') \rangle = \delta(t - t')$.

Integrating the above equation drastically reduces the computational complexity of the problem: Instead of time-evolving the entire Wigner function, we evolve only stochastic trajectories $\alpha(t)$ in the complex plane. By ensemble-averaging over many trajectories, we recover the Fokker-Planck equation in Eq. (2.78). Simulating an N -boson system, we therefore only need to simulate a coupled stochastic N -dimensional trajectory $\vec{\alpha}(t)$.

One disadvantage of this method is that by the nature of the truncation of higher-order derivatives, only classical correlations can be induced in the system. While preparing a non-classical initial state by carefully selecting appropriately distributed initial values α_0 is possible, this method limits the simulation of cases of long-living or even increasing quantum fluctuations.

Other phase-space methods have been developed over the past for the simulation of open bosonic quantum systems [137, 138], in particular with approaches to simulate the evolution of the Wigner function directly using Gaussian wavefunction approaches [139, 140].

IV.4 Other numerical methods

Let us mention some other notable numerical methods for the treatment of open quantum systems

Corner-space renormalization. In most systems, the density matrix has support on a finite subspace of the Hilbert space. Describing the system in this most relevant subspace in an exponentially growing Hilbert space has led to an efficient representation of open quantum systems using the *corner-space renormalization* method [96, 141]. In this method, the individual subsystem density matrices are diagonalized from a product ansatz. By taking only the most dominant eigenvalues to capture only the relevant *corners*, one can obtain a truncated basis of the Hilbert space by joining the two bases together. Iteratively increasing this *corner-space* basis has shown to be effective in many scenarios, in particular for steady-state calculations [96, 141].

Tensor networks. One can describe a pure state of a system consisting of N one-dimensional subsystems of Hilbert space dimensions d using an N -dimensional coefficient tensor:

$$|\psi\rangle = \sum_{\sigma_1, \dots, \sigma_N=1}^d c_{\sigma_1, \dots, \sigma_N} |\sigma_1, \sigma_2, \dots, \sigma_N\rangle \quad (2.80)$$

However, we can decompose the tensor \mathbf{c} in terms of singular-value decompositions as

$$c_{\sigma_1, \dots, \sigma_N} = A^{(\sigma_1)} A^{(\sigma_2)} \dots A^{(\sigma_N)} \quad (2.81)$$

Such a decomposition is referred to as a *matrix product state*. If the entanglement between the subsystems is sufficiently bounded (satisfying an area-law entanglement growth), the matrices $A^{(\sigma_i)}$ can be reduced to incorporate only the non-negligible singular value components, thereby drastically reducing the memory needed to represent the state [142–144]. Contracting the matrices $A^{(\sigma_i)}$ can be done exactly and efficiently [145]. This approach has been very successful in ground-state calculations for systems with area-law bounded entanglement [146].

The matrix product state framework has been extended to density matrices, yielding a *matrix product operator* decomposition [144, 147–149].

Variational approaches. Variational approaches by parametrizing the density matrix with a set of *variational parameters* have been explored in various settings [100, 124, 131, 140, 150–153], and we will revisit variational principles for open quantum systems in detail in Chap. 5. All these principles have in common to restrict the representation of the density matrix to a *variational manifold* that best describes the system at any given time. By employing a variational principle, equations of motion for the variational parameters can be obtained that govern the evolution of the parameters on the variational manifold.

3

Bosonic Quantum Error Correction

Quantum errors are nasty, unforgiving things. If you don't know what you are doing, a single misstep can result in the destruction of irreplaceable quantum information.

— DANIEL GOTTESMAN, *Surviving as a Quantum Computer in a Classical World*

In this chapter, we introduce the field of quantum error correction with a particular focus on bosonic quantum codes. In Sec. II, we define quantum error correction codes and give provide an intuitive example of how errors can be corrected using the 3-qubit repetition code. Furthermore, we introduce the Knill-Laflamme conditions for the correctability of errors. In Sec. III, we illustrate bosonic quantum error correction using the example of the *kitten-code*. We characterize the most common noise process encountered on bosonic platforms: *loss* and *dephasing* in terms of quantum channels in Se. IV. In Sec. V, we define a robust measure to gauge the performance of bosonic codes in terms of *channel fidelity* and discuss ways of numerically calculating it using convex optimization methods. We then consider the *cat code* in Sec. VI, an important bosonic *biased-noise* qubit in bosonic error correction and detail its error correction properties, logical gates, and stabilization methods. Finally, we briefly consider other notable bosonic codes, such as the GKP, binomial, and multi-component cat code in Sec. VII.

I Introduction

Quantum computers have the potential to surpass conventional computing by leveraging the quantum nature of light and matter. Various platforms of using the discrete energy levels of physical systems, such as Rydberg atoms [154–162], trapped ions [163–174], superconducting circuits [71, 175–183], photonics [69, 70, 184–197], optomechanical systems [198–203], to name only the most prominent platforms, can be used to encode information and to manipulate it to execute computational tasks. Controlling quantum devices, however, can be extremely challenging due to *decoherence* effects [204–209] that lead to the loss of information and errors in the computational task. This is due to the fact that quantum systems constantly interact with their surrounding environment, thereby generating entanglement between system and environment, such that the information is no longer stored by the considered system alone. Protecting physical systems from unwanted interaction, therefore, is one of the greatest current challenges in designing and engineering quantum devices to carry out large-scale computational tasks. Reducing the amount of thermal interactions by reducing the temperature of the environment, such that the energy level separation between the logical qubits is much larger than the energy scale of the thermal fluctuations, is but one of the main requirements to be able to coherently control quantum bits to carry out quantum computations. There are, however, physical and engineering limits to the degree of isolation between the system and the surrounding environment, setting bounds to the lifetime of quantum information, even for a single quantum bit. Performing quantum computations on the physical qubits on state-of-the-art quantum hardware is still limited by the decoherence effects of the physical systems, presenting a roadblock towards useful quantum computations.

To overcome these challenges, one can redundantly encode quantum information in a way that allows for the detection and correction of some errors. In the last three decades, this field of *quantum error correction* has been intensively studied [42, 47, 210–215], leading to various proofs of principles in device setups [48, 216–220]. In these schemes, a logical qubit is redundantly encoded in multiple physical two-level systems.

An alternative approach that has attracted recent interest in quantum error correction is to encode quantum information in the state space of a quantum harmonic oscillator. These so-called bosonic quantum codes (BQCs) offer a hardware-efficient approach to quantum error correction on redundantly encoded quantum information. Due to the principally infinite-dimensional Hilbert space, a much larger state space is available to encode logical qubits in a single physical system, making BQCs promising candidates for fault-tolerant quantum computing.

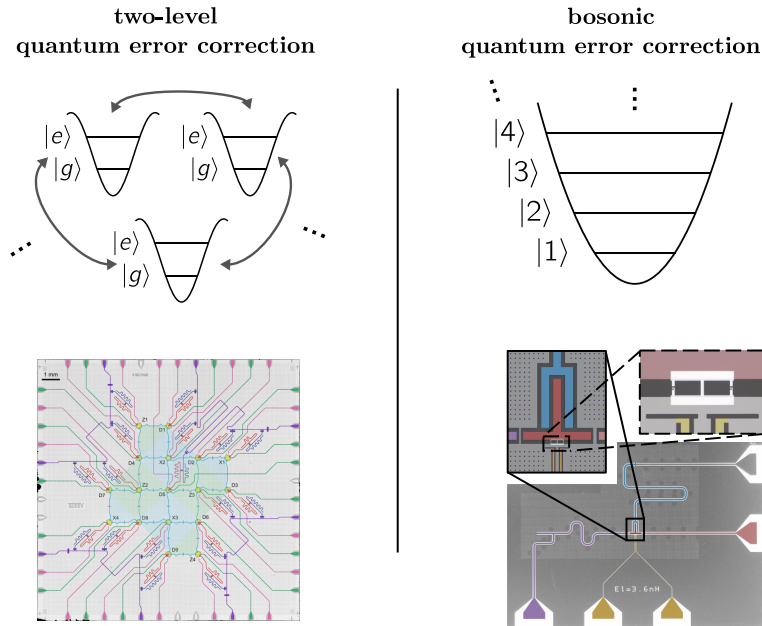


Figure 3.1: Schematic comparison between two-level quantum error correction (QEC) and bosonic quantum error correction. In two-level QEC, quantum information is redundantly encoded in multiple two-level systems. As an example, we show on the bottom left a false-color image of a distance-3 surface code from Ref. [48] using 17 physical qubits. Here, a logical qubit is encoded in nine superconducting transmons, with eight auxiliary qubits for detection and correction of errors. In bosonic quantum error correction, shown on the right, quantum information is encoded in the state-space of a quantum harmonic oscillator. As an example, an optical micrograph, adapted from Ref. [242], of a superconducting circuit implementing a cat-qubit is shown at the bottom right. Here, the blue colored line represents the memory mode of the system storing the quantum information, while other connections are used for coherent control and readout. Note that while the distance-3 surface code in Ref. [48] is able to correct single-qubit bit-flip and phase-flip errors, the cat-qubit in Ref. [242] suppresses only one type of errors (bit- or phase-flip, depending on the choice of basis), such that the remaining error type needs to be addressed in a higher-level error-correction scheme.

Bosonic quantum codes have been proposed theoretically [32, 79, 80, 221–238], and we have recently seen first experimental realizations [64, 77, 86, 239–242], even extending the life-time of the qubit [76, 78] over the physical constituent. Being able to store quantum information redundantly in a system with low hardware overhead is crucial for scaling quantum devices towards useful applications, and hence bosonic quantum codes are intensively studied to reduce hardware demands while reaching logical qubit life times long enough to carry out quantum algorithms with industry use cases.

II Quantum error correction codes

In the following, we define and outline quantum error correction codes and give a few examples.

In the classical world, the theory of error correction has been widely studied since the 1940s [40, 243–247], leading to many applications in signal-processing with everyday use to protect against noise. In the quantum world, however, the theory of classical error correction cannot be straightforwardly extended due to the intrinsically different structure of quantum information. Most importantly, contrary to classical information, it is impossible to copy arbitrary quantum states, $|\psi\rangle \rightarrow |\psi\rangle \otimes |\psi\rangle$, due to the no-cloning theorem [248], and hence error correction schemes based on copying arbitrary quantum information are unavailable. Furthermore, measuring a quantum system changes our description of it. One of the most important questions in quantum error corrections is, therefore, how can we measure a quantum system without destroying the quantum information we aim to protect? Lastly, in the classical world, the state-space of classical bits is the point set $\{0, 1\}$ and can be described using a Boolean algebra. The only possible error can be a bit-flip. On the other hand, the state-space of a quantum bit is \mathbb{C}^2 , described by two phases on a Bloch-sphere describing a superposition of the basis states $|0\rangle$ and $|1\rangle$. Here, in addition to a bit-flip, described by the change of one of the phases, we have an additional phase-flip to deal with that has no counterpart in the classical world.

In quantum error correction, rather than *copying* quantum information, which is only available for classical information, we can *encode* quantum information into a *sub-space* of the available Hilbert space.

Intuitive example: The repetition code

An intuitive example to correct some errors is the *3-qubit repetition code*, which we use to showcase the power of error correction codes. To this end, consider n qubits, with a Hilbert space of $\dim(\mathcal{H}) = 2^n$. We can define an error channel acting on the density matrix $\hat{\rho} \in \text{Op}(\mathcal{H})$:

$$\mathcal{E}(\hat{\rho}) = \sum_{\hat{P}} p_P \hat{P} \hat{\rho} \hat{P}, \quad (3.1)$$

where the sum is taken over \hat{P} which are tensor products of Pauli-group operators $\hat{\mathbb{I}}$, \hat{X} , \hat{Y} , and \hat{Z} . This channel is often referred to as a *Pauli channel*. We can interpret p_P as the probability of the occurrence of an error with operator \hat{P} .

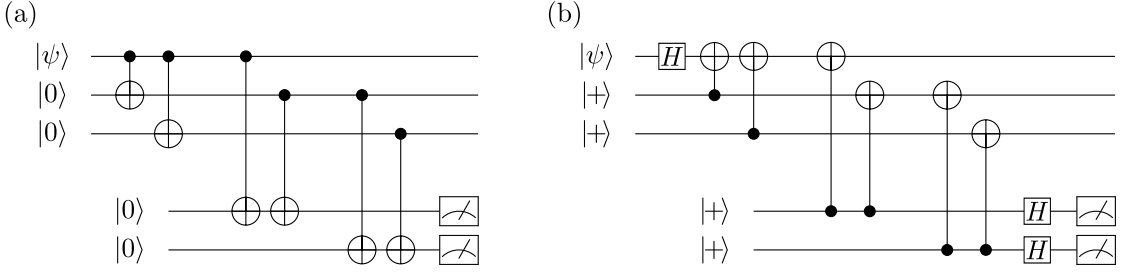


Figure 3.2: Encoding and syndrome measurement quantum circuit for the 3-qubit repetition code correcting single-qubit bit flips (a) and single-qubit phase flips (b).

As an example, we can consider 3 qubits, with the Pauli channel $\mathcal{E}(\hat{\rho}) = \sum_{n=1}^3 p \hat{X}_n \hat{\rho} \hat{X}_n^\dagger + (1 - 3p) \hat{\rho}$, that is the occurrence of the operator \hat{X}_n – corresponding to a bit-flip of the n -th qubit – takes place with probability p . A simple error correction code using 3 qubits consists in extending the classical repetition code to the repetition of basis states:

$$|\psi_0\rangle = |000\rangle, \quad |\psi_1\rangle = |111\rangle. \quad (3.2)$$

Note that the no-cloning theorem only prohibits us from copying *superpositions* of quantum states, but not from copying basis states, so the above 3-qubit repetition code is a valid encoding of quantum information. We can observe how this code can correct for a single bit-flip error. Suppose we act with operator \hat{X}_2 on a linear superposition of the code-words:

$$\hat{X}_2(\alpha |000\rangle + \beta |111\rangle) = \alpha |010\rangle + \beta |101\rangle. \quad (3.3)$$

Here, under the considered error channel, we can identify *unambiguously* that the error \hat{X}_2 acted upon the code by identifying that the middle qubit was flipped. Importantly, the superposition-carrying parameters α and β remain unperturbed, and the resulting state is orthogonal to the original code-space. It is thus possible to measure the fact that the respective qubit is different from the others without gaining information about α or β , which would destroy the superposition. We can hence measure the error without measuring the information that we are trying to protect.

A possible quantum circuit to encode and measure the error syndromes of the 3-qubit repetition code is given in Fig. 3.2(a). In the first part, we start with an unencoded state $|\psi\rangle = \alpha |0\rangle + \beta |1\rangle$ and add two additional qubits using CNOT operations. The resulting encoded state is an *entangled* state. By making two pairwise comparisons of the *parity* of neighboring qubits, using two ancillary qubits, we can exactly identify on which qubit an error has occurred. It is important to

note that this strategy only works if we know that the error channel \mathcal{E} entails only single-qubit bit-flip errors. For example the weight-2 error $\hat{X}_1\hat{X}_2$ would flip the first two bits, and in our scheme we would mistake it for a bit-flip in the third qubit.

Furthermore, we can check that *phase-flips* of the form \hat{Z}_n also remain uncorrected with this code, as for example

$$\hat{Z}_2(\alpha|000\rangle + \beta|111\rangle) = \alpha|000\rangle - \beta|111\rangle. \quad (3.4)$$

We see that, here, the resulting state remains within the code space, changing $\beta \rightarrow -\beta$, thus changing the initial superposition, resulting in an uncorrectable error. Note, however, that in a change of basis from $|0/1\rangle \leftrightarrow |\pm\rangle = \frac{1}{\sqrt{2}}(|0\rangle + |1\rangle)$ (which can be carried out using a Hadamard rotation), any single qubit phase flip acts as a bit flip in the new basis:

$$\hat{Z}_2(\alpha|+++ \rangle + \beta|--- \rangle) = \alpha|+-+ \rangle + \beta|-+- \rangle. \quad (3.5)$$

Hence, we can devise a very similar encoding scheme to protect against single-qubit phase flip errors by rotating states into the $|\pm\rangle$ basis as shown in Fig. 3.2(b). Note that the CNOT gate used for code-state preparation is reversed compared to the bit-flip repetition code due to the Hadamard transform.

We can thus straightforwardly design two repetition codes that correct single-qubit bit-flip errors and single-qubit phase-flip errors, respectively, but not both independently. To do this, we can *stack* the two codes together to form a 9-qubit code, also called *Shor's code* [42], with the code-words:

$$\begin{aligned} |\psi_0\rangle &= |+\text{bit-flip}\rangle |+\text{bit-flip}\rangle |+\text{bit-flip}\rangle \\ &= \frac{1}{2\sqrt{2}}(|000\rangle + |111\rangle)(|000\rangle + |111\rangle)(|000\rangle + |111\rangle) \\ |\psi_1\rangle &= |-\text{bit-flip}\rangle |-\text{bit-flip}\rangle |-\text{bit-flip}\rangle \\ &= \frac{1}{2\sqrt{2}}(|000\rangle - |111\rangle)(|000\rangle - |111\rangle)(|000\rangle - |111\rangle), \end{aligned} \quad (3.6)$$

with rotated code-words of the bit-flip code:

$$|\pm\text{bit-flip}\rangle = \frac{1}{\sqrt{2}}(|000\rangle \pm |111\rangle) \quad (3.7)$$

We see that we can group the qubits together in three groups of three qubits, respectively. If we now have a single \hat{X}_n error on one of the nine qubits, we can identify this error by a change of parity in one of the groups. If, however, we have

a single \hat{Z}_n error, one of the groups will flip a sign from $|+\text{bit-flip}\rangle \rightarrow |-\text{bit-flip}\rangle$, and we can identify this change by comparing to the other two groups. We also see that the effect of single-qubit bit flips and phase flips manifests itself in two different ways, making the identification of both of these errors independently possible. By realizing that $\hat{X}_n\hat{Z}_n = -i\hat{Y}_n$, we can see that also individual \hat{Y}_n errors are correctable in the Shor code. Because of the independence of these errors, any linear combination of an error $\hat{E}_n = c_{1,n}\hat{1} + c_{2,n}\hat{X}_n + c_{3,n}\hat{Y}_n + c_{4,n}\hat{Z}_n$ acting on a single-qubit can be corrected [47].

II.1 Knill-Laflamme conditions

We now define an error correction code and give conditions for the correction of errors.

Given a Hilbert space \mathcal{H} , we define a logical qubit, with density matrix $\hat{\rho}_L$ in a sub-space of the Hilbert space, such that $\hat{\rho} \in \text{Op}(\mathcal{H}_C) \subset \text{Op}(\mathcal{H})$. The sub-space \mathcal{H}_C is called the *code-space*, defining the sub-space of \mathcal{H} in which the quantum information of the qubit is encoded.

A central question in quantum error correction is: Can we find a recovery channel \mathcal{R} that reverses the errors caused by some noise channel \mathcal{E} , such that

$$(\mathcal{R} \circ \mathcal{E})(\hat{\rho}_L) = \hat{\rho}_L \quad (3.8)$$

Here, $(g \circ f)(x) = g(f(x))$. As a result, $\mathcal{R} \circ \mathcal{E}$ would act as the identity on the code-space.

The Knill-Laflamme error correction conditions

We now give one of the most central theorems in QEC theory that addresses exactly this question by providing a necessary and sufficient condition for the correctability of errors for a quantum code. Let $\{\hat{E}_k\}$ be a set of Kraus-operators associated to the noise channel \mathcal{E} that we here refer to as errors. Furthermore, let $\hat{P}_C = |\psi_0\rangle\langle\psi_0| + |\psi_1\rangle\langle\psi_1|$ be the projector onto the code-space, with the logical qubit states $|\psi_0\rangle, |\psi_1\rangle \in \mathcal{H}_C$. Then, there exists a recovery \mathcal{R} for the noise channel \mathcal{E} if and only if

$$\hat{P}_C \hat{E}_k^\dagger \hat{E}_{k'} \hat{P}_C = \alpha_{k,k'} \hat{P}_C, \quad (3.9)$$

with a Hermitian matrix $\alpha_{k,k'}$ that is independent of the code-words. This condition was found and named after Knill and Laflamme [45] and independently found by Bennet et al. [249]. If this condition is fulfilled for the set $\{\hat{E}_k\}$ of errors, we

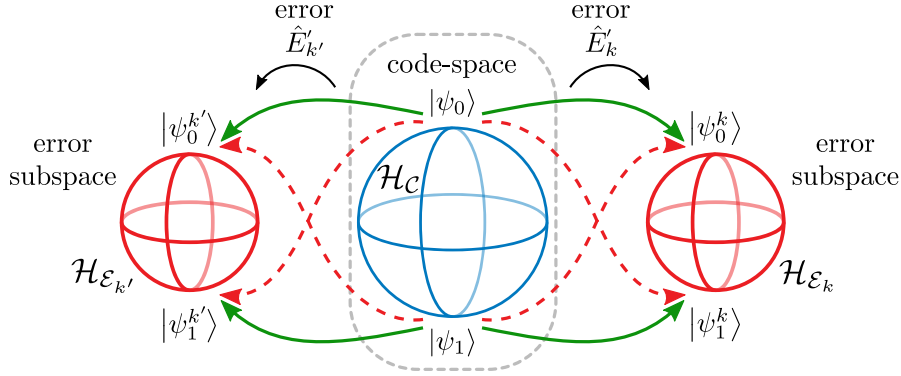


Figure 3.3: Schematic illustration of the conditions for quantum error correction. The quantum information is encoded in a two-level sub-space \mathcal{H}_C of the full Hilbert space, shown as the blue Bloch sphere with orthonormal code-words $|\psi_0\rangle$ and $|\psi_1\rangle$. Upon the action of errors \hat{E}_k and $\hat{E}_{k'}$, the code-space is in general mapped to mutually orthogonal error sub-spaces, shown as red Bloch spheres, with corresponding error sub-spaces $\mathcal{H}_{\mathcal{E}_k}$ and $\mathcal{H}_{\mathcal{E}_{k'}}$. To preserve superpositions of the original quantum information in the code-space errors must act in the same way on the code-words $|\psi_0\rangle$ and $|\psi_1\rangle$, mapping a qubit in the code-space to a qubit into the respective error sub-space. As an example, upon the action of an error \hat{E}_k , $|\psi_0\rangle$ is mapped onto a state $|\psi_0^k\rangle$ in the associated error sub-space (green arrow). Likewise, $|\psi_1\rangle \rightarrow |\psi_1^k\rangle$ in the same way. Transitions mapping $|\psi_{0,1}\rangle \rightarrow |\psi_{1,0}^k\rangle$ (red arrows) would allow to gain information about the original state and are therefore not allowed.

refer to them as correctable errors for a code-space \mathcal{H}_C . As a first remark, it is interesting to observe that the condition above does not contain information of *how* an actual recovery operation \mathcal{R} can be constructed, it only shows that such an operation exists.

By sandwiching Eq. (3.9) with a basis state $\langle\psi_i|$ on the left and another $|\psi_j\rangle$ on the right, we obtain the matrix elements for the KL-conditions,

$$M_{[i,k],[j,k']} \equiv \langle\psi_i|\hat{E}_k^\dagger\hat{E}_{k'}|\psi_j\rangle = \delta_{i,j}\alpha_{k,k'}, \quad (3.10)$$

with the KL tensor $M_{[i,k],[j,k']}$ specifying the overlap between the two states $\hat{E}_k|\psi_i\rangle$ and $\hat{E}_{k'}|\psi_j\rangle$.

Let us provide an intuitive picture of the KL conditions. If the condition above is satisfied, α is a Hermitian matrix, and we can always decompose it into $\alpha = udu^\dagger$ with a diagonal matrix d and a unitary matrix u . When rotating the error operators \hat{E}_k by the unitary matrix u , such that $\hat{E}'_k = \sum_\ell u_{k,\ell}\hat{E}_\ell$, it is

straightforward to show that we cast the KL conditions to a simpler form,

$$\hat{P}_C \hat{E}'_k \hat{E}'_{k'} \hat{P}_C = \delta_{k,k'} d_k \hat{P}_C. \quad (3.11)$$

Expressing this condition in terms of orthonormal basis states of the logical qubits $|\psi_0\rangle$ and $|\psi_1\rangle$, we have

$$\langle \psi_i | \hat{E}'_k \hat{E}'_{k'} | \psi_j \rangle = \delta_{i,j} \delta_{k,k'} d_k, \quad (3.12)$$

with $\sum_k d_k = 1$ and $d_k > 0$.

Distinguishing errors. For $k \neq k'$, we directly have $\langle \psi_i | \hat{E}'_k \hat{E}'_{k'} | \psi_j \rangle = 0$ as a consequence of the diagonalization of α . This means that the error sub-spaces $\mathcal{H}_{\mathcal{E}_k}$ and $\mathcal{H}_{\mathcal{E}_{k'}}$ associated to the errors \hat{E}'_k and $\hat{E}'_{k'}$ are mutually orthogonal to each other, so that the two distinct errors can be distinguished from one another. Measuring a set of commuting observables probing the error sub-spaces $\mathcal{H}_{\mathcal{E}_k}$ and $\mathcal{H}_{\mathcal{E}_{k'}}$, these errors can be unambiguously identified.

Mapping of a qubit to another qubit. However, ensuring that distinct errors are mapped to orthogonal sub-spaces is not sufficient for error correction. For the same error sub-space, $k = k'$, we must also ensure that when we make a measurement to probe the error sub-space we don't learn anything about the original state of the code-space. Otherwise, superpositions would be disturbed. Through the relation $\langle \psi_i | \hat{E}'_k \hat{E}'_k | \psi_j \rangle = \delta_{i,j} d_k$, we make sure that \hat{E}'_k rotates the logical code-words to an orthogonal basis in $\mathcal{H}_{\mathcal{E}_k}$, thereby mapping the qubit in the code-space to a qubit in the error sub-space. This ensures that upon detection of an error \hat{E}'_k , we can apply a unitary operation that reverses the action of the error.

More concretely, we can set $\hat{E}'_k = \sqrt{d_k} \hat{U}_k$, such that the projector on to $\mathcal{H}_{\mathcal{E}_k}$ is given by $\hat{\Pi}_{\mathcal{E}_k} = \hat{U}_k \hat{P}_C \hat{U}_k^\dagger$. We can thus construct recovery operators $\hat{R}_k = \hat{U}_k^\dagger \hat{\Pi}_{\mathcal{E}_k} = \hat{P}_C \hat{U}_k^\dagger$ that rotate states in $\mathcal{H}_{\mathcal{E}_k}$ back to the code-space. We can verify this by computing

$$(\mathcal{R} \circ \mathcal{E})(\hat{\rho}_L) = \sum_{k,\ell} \hat{R}_\ell \hat{E}'_k \hat{\rho}_L \hat{E}'_k^\dagger \hat{R}_\ell^\dagger \quad (3.13)$$

$$= \sum_{k,\ell} d_k \hat{P}_C \hat{U}_\ell^\dagger \hat{U}_k \hat{\rho}_L \hat{U}_k^\dagger \hat{U}_\ell \hat{P}_C = \hat{\rho}_L, \quad (3.14)$$

where in the last line we have used that $\hat{U}_\ell^\dagger \hat{U}_k = \delta_{\ell,k} \hat{\mathbb{1}}$ as the unitaries \hat{U}_k and \hat{U}_ℓ act on mutually orthogonal sub-spaces. Furthermore, we have used that $\sum_k d_k = 1$.

If the error correction conditions in Eq. (3.9) are not exactly satisfied, there will, in general, be a contribution of Pauli-errors induced on the code-space. As the space of 2-by-2 matrices can always be decomposed in terms of the Pauli-group [236], we can write the projection of an error pair $\hat{E}_\ell^\dagger \hat{E}_{\ell'}$ as:

$$\hat{P}_C \hat{E}_\ell^\dagger \hat{E}_{\ell'} \hat{P}_C = c_{\ell,\ell'} \hat{\mathbf{1}}_L + x_{\ell,\ell'} \hat{X}_L + y_{\ell,\ell'} \hat{Y}_L + z_{\ell,\ell'} \hat{Z}_L. \quad (3.15)$$

Examining the different contributions from the error-inducing components $x_{\ell,\ell'}$, $y_{\ell,\ell'}$, and $z_{\ell,\ell'}$ can give valuable information in what *logical* errors are produced as the effect of the error $\hat{E}_\ell^\dagger \hat{E}_{\ell'}$. Here again, comparing the above equation with the Knill-Laflamme error correction condition in Eq. (3.9), we see that we have perfect error correction when $x_{\ell,\ell'} = y_{\ell,\ell'} = z_{\ell,\ell'} = 0$.

III Bosonic quantum codes

Here, we define and characterize bosonic quantum codes, study their hardware realizations, and provide a few examples, focusing on the cat code.

We can use the infinite dimensional Hilbert space of a quantum harmonic oscillator to redundantly encode quantum information, just like we can encode quantum information in multiple connected physical two-level systems. Encoding quantum information in the state-space of a quantum harmonic oscillator can have various advantages: First, we already have an infinite Hilbert space available to encode quantum information instead of a finite Hilbert space for two-level error correction codes. Practically, this does not mean that we can perfectly encode information, as the noise channels are intrinsically different from the noise processes for two-level systems. As an example, one of the most prominent decay processes in microwave cavities is photon damping for which excitations decay with a rate proportional to their excitation number, and so encoding information in highly excited states becomes unfeasible. Another advantage is the resources needed for coherent quantum control: In general, we can universally control a quantum harmonic oscillator using a single non-linear element [250–253]. We can thus perform operations, such as error correction cycles or gates, with a much lower hardware footprint compared to multiple physical two-level systems, which are individually addressed.

A main difference between two-level and bosonic quantum error correction codes are the different noise channels that are typically encountered. While two-level systems often suffer from noise processes, such as depolarization, dephasing, and amplitude damping, typically involving only two energy levels. For bosonic systems, however, we often deal with noise processes, such as photon loss, dephas-

ing, photon gain, or thermal noise, and correcting for these types of errors in a single bosonic mode can be challenging.

Illustrative Example: The Kitten code

We demonstrate how to encode and correct errors in a bosonic mode by using the illustrative example of the so-called *Kitten code*, a bosonic code in the class of *binomial codes* [232]. For this example, let us assume a discrete set of errors $\{\hat{1}, \hat{a}\}$. Note that we include the identity operation here to be able to distinguish whether nothing happened or whether we lost a photon. The main idea is to encode the logical code-words $|\psi_0\rangle$ and $|\psi_1\rangle$, in such a way that, upon the action of \hat{a} , a state in the code-space is brought to a state orthogonal to the code-space, without the possibility of gaining information about superpositions between basis states.

We now define the two code-words of the Kitten code,

$$|\psi_0\rangle = \frac{1}{\sqrt{2}}(|0\rangle + |4\rangle), \quad |\psi_1\rangle = |2\rangle. \quad (3.16)$$

We immediately observe that both these states involve only superpositions of even Fock states and have therefore an even photon number parity. Hence, a single photon loss event maps an even parity state $|\psi_L\rangle = \alpha|\psi_0\rangle + \beta|\psi_1\rangle$ to an odd parity state $\hat{a}|\psi_L\rangle = \sqrt{2}(\alpha|3\rangle + \beta|1\rangle)$ and is therefore orthogonal to $|\psi_L\rangle$ [74]. We could therefore detect whether a single-photon loss event occurred by measuring the photon number parity $\hat{\Pi} = e^{i\pi\hat{n}}$. Importantly, in order to learn nothing about superpositions, the states have the property:

$$\langle\psi_0|\hat{a}^\dagger\hat{a}|\psi_0\rangle = \langle\psi_1|\hat{a}^\dagger\hat{a}|\psi_1\rangle = 2. \quad (3.17)$$

We see that we have chosen the code-words in Eq. (3.16) in such a way as to have the same average photon number, so that a single-photon loss event does not distort the information that is encoded in the state $|\psi_L\rangle$ [74]. We can think of this in terms of information that can be extracted from the error sub-space: If we are able to gain partial information from probing the error sub-space as to whether $|\psi_L\rangle$ was in $|\psi_0\rangle$ or in $|\psi_1\rangle$, we would change the superposition of the initial state.

As a recovery of the error \hat{a} , we can simply measure the photon number parity $\hat{\Pi}$, and in case of odd measured parity apply a recovery to the state:

$$|\psi_L\rangle \xrightarrow{\hat{a}} \hat{a}|\psi_L\rangle = \sqrt{2}(\alpha|3\rangle + \beta|1\rangle) \xrightarrow{\text{recovery}} \hat{R}(\hat{a}|\psi_L\rangle) = \alpha|\psi_0\rangle + \beta|\psi_1\rangle = |\psi_L\rangle, \quad (3.18)$$

with the recovery $\hat{R} = [(|0\rangle + |4\rangle)\langle 3| + |2\rangle\langle 1|]/\sqrt{2}$. Intuitively, instead of applying the recovery operator \hat{R} , we might be tempted to just add a photon back to the

state by applying \hat{a}^\dagger , but it is easy to check that this approach does not yield the correct initial state $|\psi_L\rangle$. We can systematically check that for the set of errors $\{\mathbb{1}, \hat{a}\}$ the KL conditions in Eq. (3.9) are satisfied for the Kitten code. More general codes can be designed to correct for arbitrary discrete errors (See Sec. VII). In order to correct more errors of the form $\{\hat{\mathbb{1}}, \hat{a}, \hat{a}^2, \dots, \hat{a}^K, \hat{a}^\dagger, \dots, \hat{a}^{\dagger M}, \hat{n}, \dots, \hat{n}^D\}$ for some integer values of K , M and D , code-words in the class of *binomial codes* exactly satisfy the KL conditions [232]. While the Kitten code has been demonstrated experimentally [64, 239], it remains challenging to experimentally construct bosonic codes correcting higher-order errors in this way, as the Fock-state coefficients have to be precisely engineered.

IV Modeling noise on bosonic systems

Here, we focus on different noise models of bosonic systems that typically arise in superconducting circuit platforms but are also prominent on other hardware platforms. In particular, we explore photon loss and dephasing below.

IV.1 Photon Loss

Photon loss often represents a dominant error channel in bosonic platforms [74, 232, 236], where the rate of photon loss is determined by the internal quality factor of the superconducting cavity. Furthermore, the pure-loss channel is also an accurate model in broadband-line and free-space communication [254]. We define the pure-loss channel in terms of the Lindblad master equation

$$\frac{d\hat{\rho}}{dt} = \kappa \mathcal{D}[\hat{a}](\hat{\rho}). \quad (3.19)$$

It is useful to define the dimensionless quantity $\gamma \equiv 1 - e^{-\kappa t} \in [0, 1]$. Integrating Eq. (3.19) over time defines the channel

$$\mathcal{N}_L[\gamma](\hat{\rho}(0)) \equiv \kappa \int_0^t \mathcal{D}[\hat{a}](\hat{\rho}(\tau)) d\tau \quad (3.20)$$

By applying the loss channel to a Fock-space coherence $|n\rangle\langle m|$, we have [255]

$$\mathcal{N}_L[\gamma](|n\rangle\langle m|) = \sum_{\ell=0}^{\min\{n,m\}} \sqrt{\binom{n}{\ell} \binom{m}{\ell}} \gamma^\ell (1-\gamma)^{\frac{n+m}{2}-\ell} |n-\ell\rangle\langle m-\ell|. \quad (3.21)$$

We see that the loss channel introduces transitions towards lower excitation numbers.

We can think of the loss channel as an unwanted *coherent* beam-splitter coupling with an auxiliary system B. This purification of a channel – called *Stinespring dilation* – can be described by the unitary [256]

$$\hat{U} = \exp\left(\sin^{-1}(\sqrt{\gamma})(\hat{a}\hat{b}^\dagger - \hat{a}^\dagger\hat{b})\right), \quad (3.22)$$

where \hat{b} describes the auxiliary system B. By tracing out the degrees of freedom of the auxiliary mode, we are left with

$$\text{Tr}_B\{\hat{U}(\hat{\rho} \otimes |0\rangle\langle 0|_B)\hat{U}^\dagger\} = \mathcal{N}_L[\gamma](\hat{\rho}). \quad (3.23)$$

We can represent the loss channel in an operator-sum representation as:

$$\mathcal{N}_L[\gamma] = \sum_{n=0}^{\infty} \hat{L}_n \bullet \hat{L}_n^\dagger, \quad \text{with} \quad \hat{L}_n = \sqrt{\frac{\gamma^n}{n!}}(1 - \gamma)^{\frac{n}{2}} \hat{a}^n. \quad (3.24)$$

Here, the Kraus operators are ordered in powers of dimensionless rate γ .

As the operators \hat{L}_k are trace-class, we can expand them in terms of displacements. In particular, we have [236]

$$\hat{L}_k^\dagger \hat{L}_{k'} = \int \frac{d^2\alpha}{\pi} e^{-\frac{1}{2}(1-\gamma)|\alpha|^2} \langle k|\hat{D}(\alpha^*)|k'\rangle \hat{D}(\sqrt{\gamma}\alpha). \quad (3.25)$$

The first two Kraus operators in leading order of γ are given by:

$$\hat{L}_0 = \hat{\mathbb{1}} - \frac{\gamma}{2}\hat{a}^\dagger\hat{a}, \quad \hat{L}_1 = \sqrt{\gamma}\hat{a}. \quad (3.26)$$

We see that this channel does not contain the identity in the Kraus-operator for $\gamma \neq 0$, due to the *back-action* of the damping term $(1 - \gamma)^{\hat{n}/2}$ in Eq. (3.24). This is due to the fact that during the time intervals where no losses are recorded, information is gained about what state the system is in, causing a redistribution of probabilities by \hat{L}_0 .

It proves insightful to look at how states in phase space are transformed under the loss channel. The loss channel gives rise to the equation of motion for the Wigner function $W(q, p)$ [122]:

$$\frac{\partial W(q, p)}{\partial t} = \frac{\kappa}{2} \left(\frac{\partial q W}{\partial q} + \frac{\partial p W}{\partial p} \right) + \frac{\kappa}{4} \left(\frac{\partial^2 W}{\partial q^2} + \frac{\partial^2 W}{\partial p^2} \right) \quad (3.27)$$

The above equation is a *Fockker-Planck equation* for the Wigner function under the loss channel [257]. The first term is a drift term, describing the loss of amplitude, while the second term is a diffusion term, accounting for the loss-induced noise. We

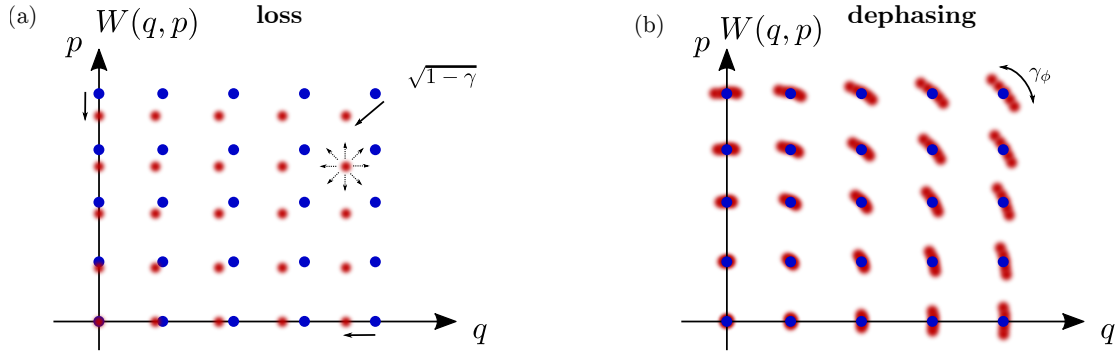


Figure 3.4: Schematic illustration of the effect of noise on points in the Wigner function. (a) For the pure loss channel $\mathcal{N}_L[\gamma]$, initial points (blue) are re-scaled towards the origin with a rate of $\sqrt{1-\gamma}$ and smoothed with a Gaussian function. (b) For the pure dephasing channel $\mathcal{N}_D[\gamma_\phi]$, initial points get smeared out tangentially.

can straightforwardly solve the Fock-Planck equation through a Fourier transformation. Let $\tilde{W}(u, v)$ be the Fourier transformation of $W(q, p)$, called *characteristic function*. Then, $\tilde{W}(u, v)$ has a simple form:

$$\frac{\partial \tilde{W}(u, v)}{\partial t} = -\frac{\kappa}{2} \left(u \frac{\partial \tilde{W}}{\partial u} + v \frac{\partial \tilde{W}}{\partial v} \right) - \frac{\kappa}{4} (u^2 + v^2) \tilde{W}. \quad (3.28)$$

With $\frac{\partial \tilde{W}}{\partial t}$ containing only first-order derivatives, we can obtain a solution by integration, yielding:

$$\tilde{W}(u, v, t) = \tilde{W}(\sqrt{1-\gamma}u, \sqrt{1-\gamma}v, t=0) \exp\left(-\gamma \frac{u^2 + v^2}{4}\right), \quad (3.29)$$

We observe that the characteristic function \tilde{W} gets point-wise rescaled under the action of loss from low frequencies to higher frequencies and multiplied with a Gaussian function with variance of $1/(2\gamma)$. This multiplication with a Gaussian acts as a low-pass filter that dampens higher-frequency components. We can also obtain the structure of the regular time-evolved Wigner function $W(q, p)$ by an inverse-Fourier transformation, yielding [122]:

$$W(q, p, t) = \frac{1}{\gamma\pi} W\left(\frac{q}{\sqrt{1-\gamma}}, \frac{p}{\sqrt{1-\gamma}}, t=0\right) * \exp\left(-\frac{q^2 + p^2}{\gamma}\right), \quad (3.30)$$

where $f * g \equiv \int_{-\infty}^{\infty} f(u, v)g(x-u, y-v)dudv$ is a convolution. Here, we see a similar effect of a point-wise re-scaling towards the origin $(q, p) = (0, 0)$ and Gaussian smoothing.

In Fig. 3.4(a), we schematically depict the action of the loss function for points in phase space. From Eq. (3.30), we can straightforwardly see that Gaussian states remain Gaussian under the application of the loss channel. Hence, the loss channel is in the class of Gaussian quantum channels.

IV.2 Dephasing

Temperature fluctuations [258], Kerr non-linearities [259], and other phenomena [260, 261] can lead to decoherence effects that can be jointly described by noise model of *pure dephasing*. In superconducting circuits, the dephasing channel often arises through an unwanted dispersive coupling to an auxiliary system [74].

We define the pure-dephasing channel by the Lindblad master equation:

$$\frac{d\hat{\rho}}{dt} = \kappa_\phi \mathcal{D}[\hat{a}^\dagger \hat{a}](\hat{\rho}). \quad (3.31)$$

We introduce the dimensionless parameter $\gamma_\phi \equiv \kappa_\phi t \geq 0$. In Fock-space, the dephasing channel can be described by

$$\mathcal{N}_D[\gamma_\phi](\hat{\rho}) = \sum_{m,n=0}^{\infty} e^{-\frac{\gamma_\phi}{2}(m-n)^2} |m\rangle\langle m| \hat{\rho} |n\rangle\langle n|. \quad (3.32)$$

We see that the dephasing channel has the effect of dampening Fock-space coherences in the density matrix, but does not introduce transitions as compared to the loss channel. The dephasing channel can be expressed in an operator-sum representation [256],

$$\mathcal{N}_D[\gamma_\phi] = \sum_{k=0}^{\infty} \hat{L}_k \bullet \hat{L}_k^\dagger, \quad \text{with} \quad \hat{L}_k = \sqrt{\frac{\gamma_\phi^k}{k!}} e^{-\frac{\gamma_\phi}{2} \hat{n}^2} \hat{n}^k. \quad (3.33)$$

Similar to the pure loss channel, we can look at the Kraus operators in leading order of γ_ϕ :

$$\hat{L}_0 = \hat{\mathbb{1}} - \frac{\gamma_\phi}{2} \hat{n}^2, \quad \hat{L}_1 = \sqrt{\gamma_\phi} \hat{n} \quad (3.34)$$

Similar to the loss channel, the dephasing channel can be dilated with a dispersive – or *longitudinal* – coherent interaction [262–264]:

$$\hat{U} = \exp\left(-i\sqrt{\gamma_\phi}(\hat{a}^\dagger \hat{a})(\hat{b} + \hat{b}^\dagger)\right), \quad (3.35)$$

such that

$$\text{Tr}_B\{\hat{U}(\hat{\rho} \otimes |0\rangle\langle 0|_B)\hat{U}^\dagger\} = \mathcal{N}_D[\gamma_\phi](\hat{\rho}). \quad (3.36)$$

To better understand the effect of the pure dephasing channel, we can decompose it in terms of phase space rotations [262]:

$$\mathcal{N}_D[\gamma_\phi](\hat{\rho}) = \int_{-\infty}^{\infty} p(\phi) e^{-i\phi\hat{a}^\dagger\hat{a}} \hat{\rho} e^{i\phi\hat{a}^\dagger\hat{a}} d\phi, \quad \text{with} \quad p(\phi) = \sqrt{\frac{\gamma_\phi}{2\pi}} e^{-\frac{1}{2}\gamma_\phi\phi^2}. \quad (3.37)$$

The channel $\mathcal{N}_D[\gamma_\phi]$ is thus a convex combination of phase space rotations with $\hat{\rho} \rightarrow e^{-i\phi\hat{a}^\dagger\hat{a}} \hat{\rho} e^{i\phi\hat{a}^\dagger\hat{a}}$, where the variable ϕ is a Gaussian distribution with variance $1/\gamma_\phi$. As a result, the density matrix $\hat{\rho}$ is tangentially *smeared out* in phase space according to the Gaussian envelope $p(\phi)$, schematically depicted in Fig. 3.4(b). It is important to note that the dephasing channel is a non-Gaussian channel, mapping Gaussian states to non-Gaussian states, as can be seen from Eq. (3.37).

IV.3 Joint loss and dephasing

In a realistic scenario, a quantum system can be subjected to *both* loss and dephasing. We can define the joint-loss dephasing channel $\mathcal{N}_{LD}[\gamma, \gamma_\phi]$ through the Lindblad master equation:

$$\mathcal{N}_{LD}[\gamma, \gamma_\phi](\hat{\rho}(0)) = \hat{\rho}(t), \quad \text{with} \quad \frac{d\hat{\rho}}{dt} = \kappa\mathcal{D}[\hat{a}](\hat{\rho}) + \kappa_\phi\mathcal{D}[\hat{a}^\dagger\hat{a}](\hat{\rho}). \quad (3.38)$$

Because the dissipators $\mathcal{D}[\hat{a}]$ and $\mathcal{D}[\hat{a}^\dagger\hat{a}]$ commute, the loss-dephasing channel is also commutative:

$$\mathcal{N}_{LD}[\gamma, \gamma_\phi] = \mathcal{N}_L[\gamma] \circ \mathcal{N}_D[\gamma_\phi] = \mathcal{N}_D[\gamma_\phi] \circ \mathcal{N}_L[\gamma]. \quad (3.39)$$

In a setting where γ and γ_ϕ differ significantly from each other, such as in a noise-biased environment, in order to simulate the dynamics using a finite number of Kraus operators for $\mathcal{N}_{LD}[\gamma, \gamma_\phi]$, one should choose a truncation of Kraus-operators carefully.

V Channel Fidelity

V.1 Continuous errors

The KL conditions determine if a given set of discrete errors can be *exactly* corrected. However most noise acting on a quantum system induces errors in a continuous way. Typically, a noise channel \mathcal{E} can be expressed in terms of a Lindblad master equation evolution acting for some duration τ until we measure the system for possible errors or for reading out the state of the system. For such a channel, we have $\mathcal{E} = \exp\{\mathcal{L}\tau\}$, with Liouvillian \mathcal{L} as defined in Eq (2.18). In general, for

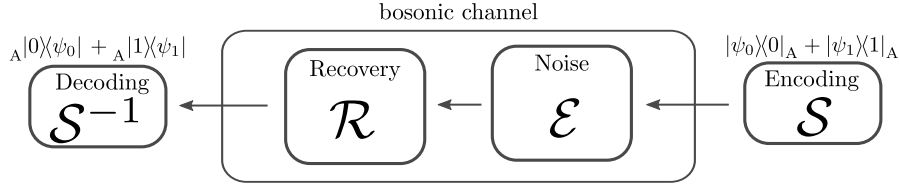


Figure 3.5: Combined quantum channel \mathcal{Q} , consisting of an encoding \mathcal{S} of a qubit into a bosonic mode, a bosonic noise channel \mathcal{E} , a subsequent recovery channel \mathcal{R} , and finally a decoding \mathcal{S}^{-1} back to the qubit space A .

the infinite-dimensional Hilbert space of a bosonic system, \mathcal{E} has infinitely many Kraus-operators in its operator-sum representation, generating an infinite set of discrete errors. Instead of trying to know which of these errors can be corrected, we might want to ask instead: Given a bosonic code and a noise channel \mathcal{E} , what information can still be extracted from the system after performing a recovery operation \mathcal{R} after time τ ?

V.2 Definition of channel fidelity

To answer this question, we resort to the concept of *channel fidelity* [236, 265]. We define a perfect *encoding channel* \mathcal{S} , with $\mathcal{S}(\hat{\rho}) \equiv \hat{S}\hat{\rho}\hat{S}^\dagger$ and $\hat{S} = |\psi_0\rangle\langle 0|_A + |\psi_1\rangle\langle 1|_A$ that maps the basis states $|0/1\rangle_A$ of a qubit to the logical code-words $|\psi_{0/1}\rangle$ in a bosonic mode, satisfying $\hat{S}\hat{S}^{-1} = \hat{P}_C$, and $\hat{S}^{-1}\hat{S} = \hat{P}_A$. Let \mathcal{E} be a noise channel, and \mathcal{R} a recovery channel trying to correct the channel \mathcal{E} . Then, we define a combined quantum channel \mathcal{Q} , mapping a qubit density matrix again to a qubit density matrix .

$$\mathcal{Q} \equiv \mathcal{S}^{-1} \circ \mathcal{R} \circ \mathcal{E} \circ \mathcal{S} \quad (3.40)$$

While the combined channel \mathcal{Q} is a mapping between a density matrices in a two-level basis, the channels \mathcal{R} and \mathcal{E} are mappings between density matrices in the bosonic Hilbert space, as depicted in Fig. 3.5. We can therefore always express \mathcal{Q} in terms of only four distinct operators in the Pauli group,

$$\mathcal{Q} = \sum_{\alpha,\beta} Q_{\alpha,\beta} \hat{\sigma}_\alpha \bullet \hat{\sigma}_\beta^\dagger = \sum_i \hat{Q}_i \bullet \hat{Q}_i^\dagger, \quad (3.41)$$

with $\hat{\sigma}_{\alpha,\beta} \in \{\hat{1}, \hat{\sigma}_x, \hat{\sigma}_y, \hat{\sigma}_z\}$. The matrix elements $Q_{\alpha,\beta}$ can be computed as

$$Q_{\alpha,\beta} = \text{Tr}\{\hat{\sigma}_\alpha \mathcal{Q}(\hat{\sigma}_\beta)\}. \quad (3.42)$$

The operators \hat{Q}_i can be found by diagonalizing the matrix above. Let A be the system acted upon with the channel \mathcal{Q} and let B be a reference system. We can define an entanglement fidelity [236, 265–267] for a mixed state in A in terms

of a *purification* to the reference system B . If $|\Psi\rangle \in \mathcal{H}_A \otimes \mathcal{H}_B$ is a purification of $\hat{\rho}_A$, then $\hat{\rho}_A$ can be obtained by tracing out the degrees of freedom in B , i.e. $\hat{\rho}_A = \text{Tr}_B\{|\Psi\rangle\langle\Psi|\}$, and $|\Psi\rangle$, therefore, captures all information about $\hat{\rho}_A$. In general, $|\Psi\rangle$ contains entanglement between the systems A and B .

The channel fidelity is a measure of how much the channel \mathcal{Q} preserves the state $|\Psi\rangle$. It is therefore a measure how well \mathcal{Q} preserves the entanglement with its reference system B :

$$\mathcal{F}_e(\hat{\rho}_A, \mathcal{Q}) \equiv \langle\Psi|(\mathcal{Q} \otimes \mathcal{I})(|\Psi\rangle\langle\Psi|)|\Psi\rangle \quad (3.43)$$

The *entanglement* fidelity \mathcal{F}_e is linear in \mathcal{Q} for any input state $\hat{\rho}_A$. This is particularly useful for quantum error correction that is adapted to the specific channel \mathcal{Q} and enables the application of convex optimization problems called *semidefinite programs* to optimize e.g. a bosonic encoding \mathcal{S} and/or the respective recovery \mathcal{R} .

Computing the entanglement fidelity using the definition in Eq. (3.43) directly does not seem straightforward. Interestingly, however, we can express \mathcal{F}_e in terms of the channel \mathcal{Q} and the density matrix $\hat{\rho}_A$ alone:

$$\mathcal{F}_e(\hat{\rho}_A, \mathcal{Q}) = \sum_{i=1}^4 \langle\Psi|(\hat{Q}_i \otimes \hat{\mathbb{1}})|\Psi\rangle \langle\Psi|(\hat{Q}_i \otimes \hat{\mathbb{1}})^\dagger|\Psi\rangle \quad (3.44)$$

$$= \sum_{i=1}^4 \text{Tr}\{\hat{\rho}_A \hat{Q}_i\} \text{Tr}\{\hat{\rho}_A \hat{Q}_i^\dagger\} = \sum_{i=1}^4 |\text{Tr}\{\hat{\rho}_A \hat{Q}_i\}|^2, \quad (3.45)$$

with the Kraus operators \hat{Q}_i corresponding to the channel \mathcal{Q} . It is often more insightful to consider a strict fidelity condition for a state $\hat{\rho}_A$, which is the case for a fully mixed state $\hat{\rho}_A = \hat{\mathbb{1}}/2$. In this case, the purification with subsystem B produces a maximally entangled state $|\Psi\rangle = (|0_A 0_B\rangle + |1_A 1_B\rangle)/\sqrt{2}$. We thus obtain the *average channel fidelity*

$$\mathcal{F} \equiv \mathcal{F}_e(\hat{\mathbb{1}}/2, \mathcal{Q}) = \frac{1}{4} \sum_{i=1}^4 |\text{Tr}\{\hat{Q}_i\}|^2 \quad (3.46)$$

We can also express \mathcal{F} in terms of the matrix elements $Q_{\alpha,\beta}$ in the basis spanned by the Pauli group $\sigma_\alpha \in \{\hat{\mathbb{1}}, \hat{\sigma}_x, \hat{\sigma}_y, \hat{\sigma}_z\}$ of orthogonal operators,

$$\mathcal{F} = \frac{1}{4} \text{Tr}\{\mathcal{Q}\} = \frac{1}{4} \sum_{\alpha=1}^4 \text{Tr}\{\sigma_\alpha \mathcal{Q}(\sigma_\alpha)\} = \frac{1}{4} \text{Tr}\{\mathcal{Q}\}, \quad (3.47)$$

where $\text{Tr}\{\mathcal{Q}\}$ is the matrix trace of the matrix-representation of \mathcal{Q} in the basis of the Pauli group, given in Eq. (3.41), with matrix elements $Q_{\alpha,\beta}$. The channel

fidelity \mathcal{F} now is a quantity depending only on the channel \mathcal{Q} and can be computed from an operator-sum representation.

\mathcal{F} gives an intuitive measure on how much entanglement can be preserved when the system of interest is purified to a reference system. It, therefore, gives a better insight into the correctability of errors for a specific error correction code and for a specific noise channel when the KL conditions are not exactly satisfied.

In the scenario of dissipative stabilization of the code-space manifold, detailed in Sec. VI.2, no active recovery is applied to the system and the system evolves in time entirely with the channel $\mathcal{E}' = e^{\mathcal{L}'\tau}$, where \mathcal{L}' includes both the natural dissipation and the engineered dissipation. The channel fidelity in Eq. (3.47) then reduces to

$$\mathcal{F} = \frac{1}{4} \sum_{\alpha=1}^4 \text{Tr}\{\hat{\sigma}_\alpha \mathcal{E}'(\hat{\sigma}_\alpha)\} = \frac{1}{4} \sum_{\alpha=1}^4 \text{Tr}\{\hat{\sigma}_\alpha \hat{\sigma}_\alpha(\tau)\}, \quad (3.48)$$

where $\hat{\sigma}_\alpha(\tau)$ is the evolution of the the code-space Pauli operator $\hat{\sigma}_\alpha$ under the dissipator \mathcal{L}' .

V.3 Approximate Knill-Laflamme conditions

Note that contrary to the KL conditions, which only pose the existence of a recovery map for a given set of correctable errors, in the expression of the channel fidelity, a recovery operation has to be explicitly specified (See Eq. (3.40)). To be able to compare the channel fidelity to the KL conditions, we would therefore need to find an optimal recovery operation

$$F^{\text{opt}}(\mathcal{E}, \mathcal{S}) = \max_{\mathcal{R}} \mathcal{F}(\mathcal{E}, \mathcal{S}, \mathcal{R}), \quad (3.49)$$

which can be found using convex optimization techniques, detailed in the next section.

We can relate the recovery-optimized fidelity \mathcal{F}^{opt} to the KL conditions [268], by considering the near-optimal fidelity, \mathcal{F}_{KL}

$$\mathcal{F}_{\text{KL}} \equiv \frac{1}{4} \left\| \text{Tr}_L \{ \sqrt{\mathbf{M}} \} \right\|_{\text{F}}, \quad (3.50)$$

with $\text{Tr}_L \{ \mathbf{A} \}_{\ell, \ell'} = \sum_i A_{[i, \ell], [i, \ell']}$ and the Frobenius norm $\| \mathbf{A} \|_{\text{F}} = \sqrt{\text{Tr}[\mathbf{A}^\dagger \mathbf{A}]}$. Here, \mathbf{M} is the KL-tensor with matrix elements $M_{[i, \ell], [i, \ell']}$, introduced in Sec. II.1, Eq. (3.10). \mathcal{F}_{KL} gives an upper *and* lower bound to the optimal channel fidelity [268] \mathcal{F}^{opt} :

$$\frac{1}{2} (1 - \mathcal{F}_{\text{KL}}) \leq 1 - \mathcal{F}^{\text{opt}} \leq 1 - \mathcal{F}_{\text{KL}}. \quad (3.51)$$

A more straightforward measure for the violation of some discrete set of errors $\{\hat{E}_k\}$ can be given in terms of the cost function [236, 269]

$$C_{\text{KL}} \equiv \sum_{\ell, \ell'} |M_{[0, \ell], [0, \ell']} - M_{[1, \ell], [1, \ell']}|^2 + |M_{[0, \ell], [1, \ell']}|^2 \quad (3.52)$$

The above cost function is exactly zero only if the Knill-Laflamme conditions for the given set of errors are exactly satisfied, as can be straightforwardly checked from the definition of the Knill-Laflamme tensor in Eq. (3.10).

V.4 Convex Optimization of the Channel Fidelity

In the expression of the channel fidelity \mathcal{F} defined in Eq. (3.46), the recovery operation \mathcal{R} has to be explicitly specified. Rather than specifying a recovery \mathcal{R} inspired by physical intuition or experimental constraints, we might want to know the *optimal* recovery that maximizes the amount of quantum information that can be sent through the noisy channel \mathcal{Q} .

Let us call the \mathcal{R}^{opt} the optimal recovery resulting from optimizing over all possible recoveries \mathcal{R} :

$$\mathcal{R}^{\text{opt}} = \operatorname{argmax}_{\mathcal{R}} \mathcal{F}(\mathcal{Q}). \quad (3.53)$$

Let $\mathcal{R} = \sum_i \hat{R}_i \bullet \hat{R}_i^\dagger$ an operator-sum representation of the recovery map in diagonal form. Let $\{\hat{B}_r \in \mathcal{H}_c \otimes \mathcal{H}_b \subset \operatorname{Op}(\mathcal{H}_b)\}$ be a set of basis operators, taking states in the bosonic Hilbert space \mathcal{H}_b back to states in the code-space manifold \mathcal{H}_c . Following the quantum process tomography method [47, 270], we can expand the operators \hat{R}_r in terms of the basis operators \hat{B}_i :

$$\hat{R}_r = \sum_i x_{r,i} \hat{B}_i, \quad (3.54)$$

with complex scalars $\{x_{r,i}\}$. We can now define a *process matrix*, describing the noise-channel matrix elements, when inserting the map $\mathcal{R}_{i,j} \equiv \hat{B}_i \bullet \hat{B}_j^\dagger$ for the recovery [271]:

$$F_{\mathcal{R}}(\mathcal{E}, \mathcal{S})_{i,j} \equiv \frac{1}{4} \operatorname{Tr}\{\mathcal{S}^{-1} \circ \mathcal{R}_{i,j} \circ \mathcal{E} \circ \mathcal{S}\} \quad (3.55)$$

$$= \sum_{k,l,m} \operatorname{Tr}\{\hat{S}_m^{-1} \hat{B}_i \hat{E}_k \hat{S}_l\} \operatorname{Tr}\{\hat{S}_m^{-1} \hat{B}_j \hat{E}_k \hat{S}_l\}^* \quad (3.56)$$

$$= \frac{1}{4} \sum_k \operatorname{Tr}\{\hat{B}_i \hat{E}_k\} \operatorname{Tr}\{\hat{B}_j \hat{E}_k\}^*. \quad (3.57)$$

If the noise channel \mathcal{E} is expressed in terms of a Liouvillian time evolution, $\mathcal{E} = \exp(\mathcal{L}\tau)$, the process matrix can be written in the form

$$F_{\mathcal{R}}(\mathcal{E}, \mathcal{S})_{i,j} = \frac{1}{4} \text{Tr}\{(\hat{B}_i \otimes \hat{B}_j^\dagger) \exp(\mathcal{L}\tau)\} = \frac{1}{4} \sum_{k=1}^4 \text{Tr}\{\hat{A}_k^\dagger \hat{B}_i \hat{A}_k(\tau) \hat{B}_j^\dagger\}, \quad (3.58)$$

where $\hat{A}_k \in \text{Op}(\mathcal{H}_C)$ are orthonormal basis operators in the code-space. Here, we have time-evolved a basis operator $\hat{A}_k(\tau) = e^{\mathcal{L}\tau} \hat{A}_k$.

Due to the linearity of the operators \hat{R}_r in the basis operators \hat{B}_i (See Eq. (3.54)), we can write the average channel fidelity \mathcal{F} as

$$\mathcal{F} = \sum_{i,j} [\mathbf{X}_{\mathcal{R}}]_{i,j} [\mathbf{F}_{\mathcal{R}}]_{i,j} = \text{Tr}\{\mathbf{X}_{\mathcal{R}} \mathbf{F}_{\mathcal{R}}\}. \quad (3.59)$$

Here, we have defined the *recovery matrix*

$$[\mathbf{X}_{\mathcal{R}}]_{i,j} \equiv \sum_r x_{r,i} x_{r,j}^* \quad (3.60)$$

Trace-preservation of the channel \mathcal{R} demands

$$\sum_{i,j} (X_{\mathcal{R}})_{i,j} \hat{B}_i^\dagger \hat{B}_j = \hat{\mathbf{1}}_b. \quad (3.61)$$

We note that the process matrix $\mathbf{F}_{\mathcal{R}}$ is a positive semidefinite matrix [104, 271, 272], due to the fact that the combined channel \mathcal{Q} is a CPTP map.

We can now define an optimization over \mathcal{R} in terms of $\mathbf{X}_{\mathcal{R}}$ and $\mathbf{F}_{\mathcal{R}}$:

$$\begin{aligned} & \text{maximize} && \mathcal{F}(\mathcal{Q}) = \text{Tr}\{\mathbf{X}_{\mathcal{R}} \mathbf{F}_{\mathcal{R}}\} \\ & \text{subject to} && \sum_{i,j} (X_{\mathcal{R}})_{i,j} \hat{B}_i^\dagger \hat{B}_j = \hat{\mathbf{1}}_b, \\ & && (X_{\mathcal{R}})_{i,j} \equiv \sum_r x_{r,i} x_{r,j}^* \end{aligned} \quad (3.62)$$

We observe that the equality constraints in the optimization in Eq. (3.62) are quadratic in $x_{r,i}$, and therefore, do not form a convex set [271]. We can however relax the above optimization to the following optimization that in which the optimization parameters form a convex set:

$$\begin{aligned} & \text{maximize} && \text{Tr}\{\mathbf{X}_{\mathcal{R}} \mathbf{F}_{\mathcal{R}}\} \\ & \text{subject to} && \mathbf{X}_{\mathcal{R}} \succcurlyeq 0 \\ & && \sum_{i,j} (X_{\mathcal{R}})_{i,j} \hat{B}_i^\dagger \hat{B}_j = \hat{\mathbf{1}}_b. \end{aligned} \quad (3.63)$$

In the optimization above, instead of optimizing over the parameters $x_{r,i}$, we directly optimize over the matrix elements of $\mathbf{X}_{\mathcal{R}}$, which we constrain to be positive semidefinite. A convex optimization as in Eqs. (3.63) with the optimization matrix $\mathbf{X}_{\mathcal{R}}$ being positive semidefinite is often referred to as a *semidefinite program* [273, 274] (SDP). There are various numerical methods to efficiently solve SDP problems [275–282].

Once a solution $\mathbf{X}_{\mathcal{R}}^{\text{near-opt}}$ to the SDP in Eqs. (3.63) is found, we can obtain an explicit form of the near-optimal channel $\mathcal{R}^{\text{near-opt}}$ by expressing $\mathbf{X}_{\mathcal{R}}^{\text{near-opt}}$ in its singular value decomposition,

$$\mathbf{X}_{\mathcal{R}}^{\text{near-opt}} = \mathbf{V}\mathbf{\Sigma}\mathbf{V}^\dagger \quad (3.64)$$

Then, the Kraus-operators $\hat{R}_r^{\text{near-opt}}$ of the near-optimal recovery $\mathcal{R}^{\text{near-opt}}$ are given by

$$\hat{R}_r^{\text{near-opt}} \equiv \sqrt{\sigma_r} \sum_i V_{i,r} \hat{B}_i, \quad (3.65)$$

where σ_r are the singular values of the diagonal matrix $\mathbf{\Sigma}$. We immediately see that $\sum_r \hat{R}_r^{\text{near-opt}\dagger} \hat{R}_r^{\text{near-opt}} = \hat{\mathbb{1}}_{\mathbf{b}}$, and hence $\mathcal{R}^{\text{near-opt}}$ is a CPTP map.

V.5 Correcting a finite set of errors

The complete set of basis operators $\{\hat{B}_i\}$ transforming states in the Hilbert space is often too large to be tractable numerically. We can, however, restrict the set of basis operators $\{\hat{B}_i\}$ to operations transforming states in certain error-subspaces back to the code-space. Let $\{\hat{E}_k\}$ be a discrete set of errors. We can, for example, obtain such a discrete set of errors by considering the Kraus-operators in the noise channel \mathcal{E} (See Eq. (3.40)) up to order $\mathcal{O}((\delta t)^n)$. We can construct mutually orthogonal sub-spaces $\mathcal{H}_{\mathcal{E}_{k'}}$ by first applying the operators in the finite error set $\{\hat{E}_k\}$ to the states $|\psi_0\rangle, |\psi_1\rangle$ in the code-space and subsequently orthonormalizing the states with respect to each other using, e.g. the Gram-Schmidt process [283], such that the sub-spaces $\mathcal{H}_{\mathcal{E}_{k'}} = \text{Span}\{|\psi_0^{(k')}\rangle, |\psi_1^{(k')}\rangle\} \subset \mathcal{H}_{\mathbf{b}}$ are mutually orthogonal two-dimensional error sub-spaces that are also orthogonal to the code space. We now define the Pauli operators $\hat{\sigma}_i^{(k')} : \mathcal{H}_{\mathcal{E}_{k'}} \rightarrow \mathcal{H}_{\mathcal{C}}$ mapping the states in $\mathcal{H}_{\mathcal{E}_{k'}}$ back to $\mathcal{H}_{\mathcal{C}}$:

$$\begin{aligned} \hat{\sigma}_1^{(k')} &= \hat{\mathbb{1}}_{\mathcal{H}_{\mathcal{E}_{k'}} \rightarrow \mathcal{H}_{\mathcal{C}}} = |\psi_0\rangle\langle\psi_0^{(k')}| + |\psi_1\rangle\langle\psi_1^{(k')}| \\ \hat{\sigma}_2^{(k')} &= \hat{X}_{\mathcal{H}_{\mathcal{E}_{k'}} \rightarrow \mathcal{H}_{\mathcal{C}}} = |\psi_0\rangle\langle\psi_1^{(k')}| + |\psi_1\rangle\langle\psi_0^{(k')}| \\ \hat{\sigma}_3^{(k')} &= \hat{Y}_{\mathcal{H}_{\mathcal{E}_{k'}} \rightarrow \mathcal{H}_{\mathcal{C}}} = i|\psi_0\rangle\langle\psi_1^{(k')}| - i|\psi_1\rangle\langle\psi_0^{(k')}| \\ \hat{\sigma}_4^{(k')} &= \hat{Z}_{\mathcal{H}_{\mathcal{E}_{k'}} \rightarrow \mathcal{H}_{\mathcal{C}}} = |\psi_0\rangle\langle\psi_0^{(k')}| - |\psi_1\rangle\langle\psi_1^{(k')}| \end{aligned} \quad (3.66)$$

The operators in Eqs. (3.66) define a basis of mutually orthogonal recovery operations, such that any arbitrary recovery operator $\hat{B}^{(k')} : \mathcal{H}_{\mathcal{E}_{k'}} \rightarrow \mathcal{H}_{\mathcal{C}}$ can be uniquely decomposed into the operators $\hat{\sigma}_i^{(k')}$. The operator set $\{\hat{B}_i\} = \{\hat{\sigma}_n^{(k')}, n = 1, \dots, 4, k' = 0, \dots, N\}$, with N the number of orthogonal error-sub-spaces, thus defines a basis of operators mapping all considered error-sub-spaces to the code-space. Considering, e.g., N error-sub-spaces, we have a number of $4(N + 1)$ basis operators $\{\hat{B}_I\}$ (The $N + 1$ originates from also considering rotations within the code-space). A critical remark is that, in general, the operators in Eq. (3.66) do *not* yield $\sum_i \hat{B}_i^\dagger \hat{B}_i = \hat{1}_b$, as long as error-operators $\{\hat{E}_k\}$ are not a generating set of \mathcal{E} .

VI The cat code

To address some of the noise discussed in the previous section that is typically encountered in bosonic systems, various bosonic quantum error correction codes have been proposed.

In this section, we will discuss the so-called two-component *cat code*, a prominent example of a bosonic quantum error correction code. It has gained recent interest as a *biased-noise* qubit [72, 86, 284–286], where a quantum system is engineered to have one type of error occur much more frequently than other types of errors, which can address the remaining errors in the next layer of quantum error correction efficiently [87, 88, 287, 288].

The cat code as an error correction code was first proposed by *Cochrane et al.* [79] and was further analyzed by *Ralph et al.* [289]. It has since regained more attraction [81, 86, 227, 233, 236] and led to experimental realizations [64, 72, 76, 82, 94, 242, 290, 291]. In the following, we will define the cat code, present its error-correcting properties, and their realization through dissipation engineering and Hamiltonian confinement.

To begin, we construct the code-words of the *two-component* cat code (we use the wording *two-component* to distinguish it from other cat codes but omit it hereafter) by taking even and odd superpositions of two coherent states with opposite displacement [79, 289]:

$$\begin{aligned} |\mathcal{C}_\alpha^+\rangle &\equiv \frac{1}{N^+} [\hat{D}(\alpha) + \hat{D}(-\alpha)] |0\rangle = \frac{1}{N^+} (|\alpha\rangle + |-\alpha\rangle) \\ |\mathcal{C}_\alpha^-\rangle &\equiv \frac{1}{N^-} [\hat{D}(\alpha) - \hat{D}(-\alpha)] |0\rangle = \frac{1}{N^-} (|\alpha\rangle - |-\alpha\rangle) \end{aligned} \quad (3.67)$$

Here, $N^\pm = \sqrt{2(1 \pm e^{-2|\alpha|^2})}$ is a normalization constant. We use the convention of defining $|\mathcal{C}_\alpha^+\rangle$ as the logical \hat{Z} eigenstate, with eigenvalue $+1$. Note that this choice

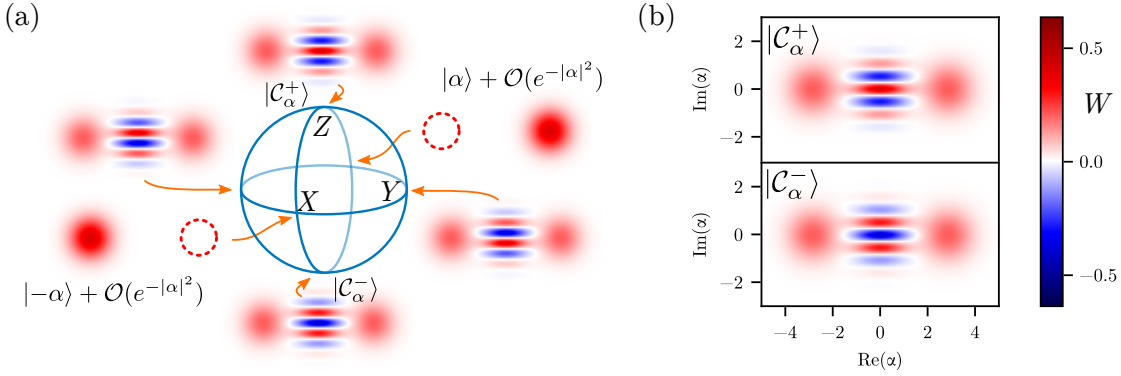


Figure 3.6: (a) Bloch sphere of the cat code. The states $|\mathcal{C}_\alpha^\pm\rangle$ are the logical \hat{Z} eigenstates. We also depict the \hat{X} and \hat{Y} eigenstates. (b) Wigner functions of the even and odd cat states for $\alpha_0 = 2$.

is arbitrary, and throughout the literature, different conventions can be found. We depict the Wigner functions of the logical \hat{X}_L , \hat{Y}_L , and \hat{Z}_L eigenstates in Fig. 3.6. Interestingly, the cat states $|\mathcal{C}_\alpha^+\rangle$ and $|\mathcal{C}_\alpha^-\rangle$ contain superpositions of only even and odd Fock-states, respectively:

$$\begin{aligned} |\mathcal{C}_\alpha^+\rangle &\propto \sum_{n=0}^{\infty} \frac{\alpha^{2n}}{\sqrt{(2n)!}} |2n\rangle \\ |\mathcal{C}_\alpha^-\rangle &\propto \sum_{n=0}^{\infty} \frac{\alpha^{2n+1}}{\sqrt{(2n+1)!}} |2n+1\rangle \end{aligned} \quad (3.68)$$

To see this more clearly, we define the rotation operator $\hat{R}(\theta)$, rotating a state at an angle θ around the origin in phase space,

$$\hat{R}(\theta) \equiv e^{i\theta\hat{a}^\dagger\hat{a}}. \quad (3.69)$$

For $\theta = \pi$, we have $\hat{R}(\theta = \pi) \equiv \hat{\Pi} = e^{i\pi\hat{a}^\dagger\hat{a}} = (-1)^{\hat{n}}$. $\hat{\Pi}$ is called the *photon number parity operator* and transforms \hat{a} , and \hat{a}^\dagger , as $\hat{\Pi}\hat{a}\hat{\Pi}^\dagger = -\hat{a}$, and $\hat{\Pi}\hat{a}^\dagger\hat{\Pi}^\dagger = -\hat{a}^\dagger$, as can be seen from applying the Baker-Campbell-Hausdorff formula [292, 293]. We can decompose $\hat{\Pi}$ in two parity sectors, $\hat{\Pi} = \hat{\Pi}_{\text{even}} - \hat{\Pi}_{\text{odd}} = \sum_{n=0}^{\infty} |2n\rangle\langle 2n| - |2n+1\rangle\langle 2n+1|$. We immediately see that the parity operator changes displacements from $\alpha \rightarrow -\alpha$,

$$\hat{\Pi}\hat{D}(\alpha)\hat{\Pi}^\dagger = \hat{D}(-\alpha). \quad (3.70)$$

As a result, taking the definition of the cat states in Eq. (3.67), we have

$$\begin{aligned}\hat{\Pi} [\hat{D}(\alpha) + \hat{D}(-\alpha)] \hat{\Pi}^\dagger &= +\mathbf{1} [\hat{D}(\alpha) + \hat{D}(-\alpha)] \\ \hat{\Pi} [\hat{D}(\alpha) - \hat{D}(-\alpha)] \hat{\Pi}^\dagger &= -\mathbf{1} [\hat{D}(\alpha) - \hat{D}(-\alpha)].\end{aligned}\quad (3.71)$$

From this, we can immediately deduce that the cat states $|\mathcal{C}_\alpha^\pm\rangle$ are eigenstates of the photon number parity, with eigenvalues ± 1 . $\hat{\Pi}$ therefore serves as the logical \hat{Z} operator of the cat states. We can also see that from Eq. (3.68), $|\mathcal{C}_\alpha^+\rangle$ and $|\mathcal{C}_\alpha^-\rangle$ are orthogonal for any value of α and therefore represent a valid qubit. Furthermore, we have the limiting behavior of $|\mathcal{C}_\alpha^+\rangle \rightarrow |0\rangle$ and $|\mathcal{C}_\alpha^-\rangle \rightarrow |1\rangle$ for $\alpha \rightarrow 0$.

The logical \hat{X} eigenstates are given by

$$\begin{aligned}|+\rangle_L &= \frac{1}{\sqrt{2}} (|\mathcal{C}_\alpha^+\rangle + |\mathcal{C}_\alpha^-\rangle) = |\alpha\rangle + \mathcal{O}(e^{-2|\alpha|^2}) \\ |-\rangle_L &= \frac{1}{\sqrt{2}} (|\mathcal{C}_\alpha^+\rangle - |\mathcal{C}_\alpha^-\rangle) = |-\alpha\rangle + \mathcal{O}(e^{-2|\alpha|^2})\end{aligned}\quad (3.72)$$

The deviation from coherent states $|\pm\alpha\rangle$ on the right-hand side is given by the overlap between opposite states:

$$\langle\alpha|-\alpha\rangle = e^{-2|\alpha|^2}\quad (3.73)$$

For large α , the states $|\pm\alpha\rangle$ thus represent the basis of a valid qubit in the conjugate basis.

A coherent state $|\alpha\rangle$ is an eigenstate of \hat{a} with eigenvalue α . For the cat code, it is straightforward to verify that \hat{a}^2 has the cat states $|\mathcal{C}_\alpha^\pm\rangle$ as their eigenstates with eigenvalue α^2 :

$$\hat{a}^2 |\mathcal{C}_\alpha^\pm\rangle = \alpha^2 |\mathcal{C}_\alpha^\pm\rangle\quad (3.74)$$

Error correction properties

Consider the set of errors $\{\hat{\mathbf{1}}, \hat{a}\}$, which is the generating set of errors of the loss channel to leading order of dissipation rate or equivalently the duration of the channel (See Sec. IV, Eq. (3.26)). A single-photon loss event \hat{a} flips the parity of the corresponding code-word, so we directly have $\langle\mathcal{C}_\alpha^\pm|\hat{a}|\mathcal{C}_\alpha^\pm\rangle = 0$. With the projector on the code space $\hat{P}_C = |\mathcal{C}_\alpha^+\rangle\langle\mathcal{C}_\alpha^+| + |\mathcal{C}_\alpha^-\rangle\langle\mathcal{C}_\alpha^-|$, we can compute the Knill-Laflamme matrix elements (See Eq. (3.9)). We compute in the asymptotic regime of large α , i.e. $\alpha \gg 1$:

$$\hat{P}_C \hat{a} \hat{P}_C = \alpha \begin{pmatrix} 0 & \frac{N_\alpha^-}{N_\alpha^+} \\ \frac{N_\alpha^+}{N_\alpha^-} & 0 \end{pmatrix} \stackrel{\alpha \gg 1}{\cong} \alpha(1 - e^{-2|\alpha|^2}) \hat{X}_L - i\alpha e^{-2|\alpha|^2} \hat{Y}_L\quad (3.75)$$

We see that in the limit of large α , a photon loss event *exactly* corresponds to a bit flip in the code-space – a fact noted very early by *Cochrane et al.* [79] (up to a re-scaling by α), where phase flip errors \hat{Y}_L are exponentially suppressed. Furthermore, we have

$$\hat{P}_C \hat{a}^\dagger \hat{a} \hat{P}_C = |\alpha|^2 \begin{pmatrix} \left(\frac{N_C^-}{N_C^+}\right)^2 & 0 \\ 0 & \left(\frac{N_C^+}{N_C^-}\right)^2 \end{pmatrix} \stackrel{\alpha \gg 1}{\approx} 2|\alpha|^2 (1 - e^{-2|\alpha|^2}) \hat{1}_L - 2|\alpha|^2 e^{-2|\alpha|^2} \hat{Z}_L \quad (3.76)$$

Here, we obtain the crucial result that a dephasing event $\hat{a}^\dagger \hat{a}$ becomes *correctable* as for large α the action on the code-space is proportional to the identity. It is thus unaffected by this error (up to a re-scaling by $2|\alpha|^2$). For a more detailed list of Knill-Laflamme matrix elements, see Appendix A.

From these two relations in Eq. (3.75) and Eq. (3.76), we can deduce that in the limit of large displacement α , a dephasing error $\hat{a}^\dagger \hat{a}$ induces an exponentially suppressed \hat{Z}_L error, while a photon loss \hat{a} only induced an \hat{X}_L error that scales linearly with α . We hence observe that the cat code presents a *biased-noise* qubit, as \hat{X}_L errors occur much more frequently than \hat{Z}_L or \hat{Y}_L errors. This noise bias has been shown to lead to high thresholds for the tolerable errors when multiple cat qubits are part of a higher-level error correction scheme [87, 238, 284–286, 288] and thus, the cat code represents a promising candidate for fault-tolerant quantum computation.

VI.1 Subsystem decomposition and Shifted-Fock method

A powerful method used to study the cat code is the so-called *Shifted Fock Basis*, first introduced in *Chamberland et al.* [238]. This makes use of a *subsystem decomposition* [294, 295], by breaking the Hilbert space of the bosonic mode into two sectors, which capture the encoded logical information in one sector and gauge information about the system in the other sector,

$$\mathcal{H} = \mathcal{H}_L \otimes \mathcal{H}_{\text{gauge}}, \quad (3.77)$$

as schematically illustrated in Fig. 3.7 in the case of a qubit decomposition with $\dim(\mathcal{H}_L) = 2$.

The shifted Fock basis provides an intuitive basis for studying logical errors on the cat qubit as well as leakage outside of the cat qubit manifold. We refer to Refs. [238, 296] for details and give an introduction here as this method proves to be very useful here and in Chap. 5. For the cat code, we have seen that the two basis states defining the cat code are characterized by symmetric and antisymmetric displacements, as in Eqs. (3.71). We can apply these to Fock-states to obtain the

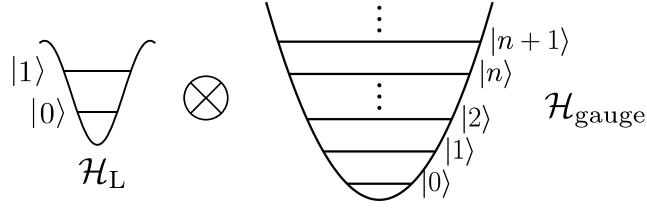


Figure 3.7: Schematic illustration of a subsystem decomposition [294, 295] of a single bosonic mode. Here the total Hilbert space of the bosonic mode \mathcal{H} is decomposed into a subsystem of a qubit \mathcal{H}_L and a gauge mode $\mathcal{H}_{\text{gauge}}$.

basis states

$$|0/1, n\rangle \equiv \frac{1}{\sqrt{2}} \left[\hat{D}(\alpha) \pm (-1)^n \hat{D}(-\alpha) \right] |n\rangle, \quad (3.78)$$

where 0 and 1 represent the even and odd parity of the state, respectively. For $n = 0$, we obtain the cat states $|0/1, 0\rangle \propto |\mathcal{C}_\alpha^\pm\rangle$. The space $\text{Span}\{|\mu, n\rangle\}_{\{\mu, n\}}$ covers the entire Hilbert space. However, the states $|\mu, n\rangle$ and $|\mu, m\rangle$ are not mutually orthogonal due to the fact that displaced number states have non-zero overlap [297, 298]. By Gram-Schmidt diagonalizing the individual two parity sectors, we can, however, obtain an orthogonal basis [238].

We can nicely represent combinations of creation and annihilation operators in the shifted Fock basis. For example, we have in the regime of $\alpha \gg 1$,

$$\begin{aligned} \hat{a} |0/1, n\rangle &= \sqrt{n} |1/0, n-1\rangle + \alpha |1/0, n\rangle \\ &= \hat{X}_L \otimes (\tilde{a} + \alpha) |0/1, n\rangle, \end{aligned} \quad (3.79)$$

with the operator \tilde{a} acting only on the gauge mode as $\tilde{a} |0/1, n\rangle = \sqrt{n} |0/1, n-1\rangle$. As a result, we map the annihilation operator to the shifted Fock basis, as

$$\hat{a} \sim \hat{X}_L \otimes (\tilde{a} + \alpha). \quad (3.80)$$

We can thus see that the annihilation operator acts as a logical \hat{X}_L on the code space, defined by the photon number parity, and as the annihilation operator displaced by α in the gauge mode. We can obtain similar expressions of other operators that facilitate the study of the action on the code-space.

VI.2 Dissipation Engineering

The cat code detailed above presents us with several more practical questions: (i) How can the code-words be generated efficiently? (ii) How can we efficiently perform a recovery operation for the correctable errors? (iii) How can we perform quantum gates that do not break the noise bias of the bosonic code? Here, we

will deal with questions (i) and (ii) in a broader context by introducing *dissipation engineering* and using the cat code as an intuitive example. We detail gates of the cat qubit subsequently.

In the last sections, we have assumed either the existence of an active recovery operation in the case of the Knill-Laflamme conditions or, in the case of channel fidelity, explicitly specified a recovery that measures and corrects errors of the bosonic code under study. This usually requires a classical adaptive control mechanism of measuring a non-demolition *error syndrome* that measures the respective error sub-spaces and subsequently maps the error sub-space back to the original code-space manifold. Although recent experimental demonstrations of bosonic quantum codes used classical adaptive control to surpass the break-even point [76, 78], the performance is often limited by readout errors [76, 239] or the decoherence from error syndrome measurement [61, 65]. Additionally, a classical feedback loop introduces time delays and additional heating of the system [77, 299], accompanied by significant computational and physical resources for the control pulses of the recovery protocol [300, 301].

We might alternatively try to implement a bosonic code *without* the need for an active recovery relying on classical adaptive control. We can think of errors in a QEC producing entropy, which active adaptive control schemes aim to reduce under additional energetic, computational, and hardware costs. Using an approach called autonomous quantum error correction, dissipation engineering, or dissipative stabilization, we can try to empty the entropy that is being produced by errors into the environment [302–305]. In recent experiments, autonomous QEC has efficiently suppressed dephasing errors [72, 83, 86] as well as single-photon loss errors [64] using the cat code. Autonomous QEC methods are, therefore, a promising candidate for realizing hardware-efficient QEC [81, 85, 87, 306, 307].

The general idea of autonomous quantum error correction is to add an engineered dissipation $\mathcal{L}_R(\hat{\rho}) = \sum_k \mathcal{D}[\hat{A}_{R,k}](\hat{\rho})$ to the present natural dissipation $\mathcal{L}_N(\hat{\rho}) = \sum_k \mathcal{D}[\hat{A}_{N,k}](\hat{\rho})$, such that the system $\hat{\rho}$ evolves under the master equation

$$\mathcal{L}(\hat{\rho}) = -i [\hat{H}, \hat{\rho}] + \lambda \mathcal{L}_R(\hat{\rho}) + \kappa \mathcal{L}_N(\hat{\rho}), \quad (3.81)$$

where \hat{H} is a control Hamiltonian for the realization of logical gates on the bosonic code. It has been shown that such an autonomous QEC scheme can improve the decoherence rate to $\mathcal{O}(\kappa^2/\lambda)$ at the logical level [302–305, 307].

Let us illustrate this dissipative stabilization technique for the two-component cat code. In Eq. (3.74), we have seen that cat states $|\mathcal{C}_\alpha^\pm\rangle$ are degenerate eigenstates of the operator \hat{a}^2 with eigenvalue α^2 . As a direct consequence, $|\mathcal{C}_\alpha^\pm\rangle$ are

annihilated by $\hat{L} = \hat{a}^2 - \alpha^2$. By taking the Liouvillian

$$\mathcal{L}(\hat{\rho}) = \kappa_2 \mathcal{D}[\hat{a}^2 - \alpha^2](\hat{\rho}), \quad (3.82)$$

we see that any coherence $\hat{\rho}_{\mu,\nu} = |\mathcal{C}_\alpha^\mu\rangle\langle\mathcal{C}_\alpha^\nu|$, with $\mu, \nu \in \{+, -\}$ is preserved under this evolution. In other words, the steady state is spanned by the density matrix

$$\hat{\rho}_{\text{ss}} = \sum_{\mu,\nu \in \{+,-\}} \rho_{\mu,\nu} |\mathcal{C}_\alpha^\mu\rangle\langle\mathcal{C}_\alpha^\nu|. \quad (3.83)$$

We can use the fact that the Lindblad master equation in Eq. (3.82) is invariant under inhomogeneous transformations (See Chap. 2, Sec. II), and cast it in the form

$$\mathcal{L}(\hat{\rho}) = -i \left[\frac{G}{2} \hat{a}^{2\dagger} + \frac{G^*}{2} \hat{a}^2, \hat{\rho} \right] + \kappa_2 \mathcal{D}[\hat{a}^2, \hat{\rho}](\hat{\rho}) \quad (3.84)$$

The coherent field amplitude α is then given by $\alpha = \sqrt{iG/\kappa_2}$. We now clearly see that the cat code can be stabilized with a two-photon drive and a two-photon loss process.

The Liouvillian \mathcal{L} in Eq. (3.84) possesses a *strong* \mathbb{Z}_2 symmetry [113, 308], and the Liouvillian can be block-diagonalized, corresponding to the four different parity sectors (including even-odd transitions). Due to the strong symmetry, the Liouvillian admits four distinct preserved quantities $\hat{J}_{\mu,\nu}$.

The density matrix coefficients $\rho_{\mu,\nu}$ are uniquely determined by [81, 113, 309]

$$\rho_{\mu,\nu} = \text{Tr}\{\hat{J}_{\mu,\nu}^\dagger \hat{\rho}(0)\}. \quad (3.85)$$

Here, $\hat{J}_{++} \equiv \hat{\Pi}_{\text{even}}$ and $\hat{J}_{--} \equiv \hat{\Pi}_{\text{odd}}$. The other conserved quantities are given by:

$$\hat{J}_{+-} \equiv \sqrt{\frac{2\alpha^2}{\sinh(2\alpha^2)}} \sum_{a=-\infty}^{\infty} \frac{(-1)^a}{2a+1} I_a(\alpha^2) \hat{J}_{+-}^{(a)}, \quad (3.86)$$

where I_a is the modified Bessel function of the first kind, and the operators $\hat{J}_{+-}^{(a)}$ are given by

$$\hat{J}_{+-}^{(a)} \equiv \begin{cases} \frac{(\hat{a}^\dagger \hat{a} - 1)!!}{(\hat{a}^\dagger \hat{a} + 2a)!!} \hat{J}_{++} \hat{a}^{2a+1} & a \geq 0 \\ \hat{J}_{++} \hat{a}^{\dagger(2|a|-1)} \frac{(\hat{a}^\dagger \hat{a})!!}{(\hat{a}^\dagger \hat{a} + 2|a|-1)!!} & a < 0 \end{cases}, \quad (3.87)$$

where $n!! = (n-2)!!n$ is the double factorial. Furthermore, $\hat{J}_{-+} = \hat{J}_{+-}^\dagger$. Physically, \hat{J}_{+-} represents how the environment distinguishes components of $\hat{\rho}$ [113]. These conserved quantities can be used to extract decay rates in the logical basis of cat states when other noise processes are present.

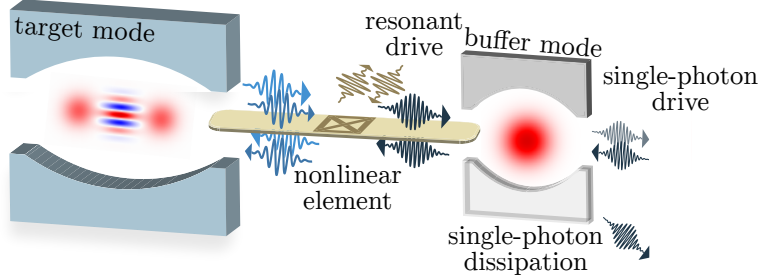


Figure 3.8: Schematic representation of a dissipative stabilization of the cat-qubit manifold. A lossy buffer mode is driven with a single-photon drive. Through a non-linear element that is resonantly driven with respect to an interaction causing an exchange of two photons in the target mode with a photon in the buffer mode, leading to an effective two-photon drive of the target mode. Figure adapted from Ref. [310] with slight modifications.

If we now subject the dissipatively stabilized cat code to the noise channel of pure dephasing with dissipator $\kappa_\phi \mathcal{D}[\hat{a}^\dagger \hat{a}]$, \hat{J}_{+-} no longer is a conserved quantity and we can use its decay rate to calculate the phase-flip rate [81]. For $\kappa_2 \gg \kappa_\phi$, we have the asymptotic behavior

$$\gamma_Z \simeq 2\kappa_\phi |\alpha|^2 e^{-|\alpha|^2}, \quad (3.88)$$

where we once again see the exponential suppression with the coherent-field amplitude α , already encountered for discrete dephasing errors in Eq. (3.76).

Reservoir engineering with an auxiliary mode

To engineer a two-photon dissipation and a two-photon drive to stabilize the cat-qubit manifold as in Eq. (3.84) in practice, we can make use of a two-mode system where the target mode \hat{a} for the bosonic qubit is coupled to a strongly damped auxiliary mode \hat{b} (or buffer mode). To this end, let us assume the Lindblad master equation for the joint system

$$\begin{aligned} \frac{d\hat{\rho}}{dt} &= -i[\hat{H}_{\text{int}}, \hat{\rho}] + \kappa_b \mathcal{D}[\hat{b}](\hat{\rho}), \quad \text{where} \\ \hat{H}_{\text{int}} &= g_2(\hat{a}^2 - \alpha^2)\hat{b} + \text{h.c.} \end{aligned} \quad (3.89)$$

The interaction Hamiltonian \hat{H}_{int} introduces exchanges of single photons in the auxiliary mode with photon pairs in the target mode. We can recast \hat{H}_{int} as

$$\hat{H}_{\text{int}} = g_2 \hat{a}^2 \hat{b}^\dagger + g_2^* \hat{a}^{2\dagger} \hat{b} + F_b \hat{b}^\dagger + F_b^* \hat{b}, \quad (3.90)$$

with the single-photon drive amplitude of the auxiliary mode $F_b = -\alpha^2 g_2$. In the limit of strong dissipation in the auxiliary mode compared to the exchange rate g_2 , i.e. $\kappa_b \gg g_2$, all processes in the auxiliary mode are decaying at a much faster time-scale than in the target mode, and we can adiabatically eliminate the degrees of freedom of the auxiliary mode to obtain an effective dynamics [311, 312] of only the target mode:

$$\frac{d\hat{\rho}_a}{dt} = \frac{4g_2^2}{\kappa_b} \mathcal{D}[\hat{a}^2 - \alpha^2](\hat{\rho}_a). \quad (3.91)$$

Such a process was experimentally realized by, e.g., *Leghtas et al.* [290] and *Lescanne et al.* [72] using superconducting circuits, where the interaction Hamiltonian was engineered using an asymmetrically threaded SQUID (ATS) [313, 314] that was driven resonant with respect to the target interaction Hamiltonian.

Logical gates

Let us briefly detail some notable quantum gates for the dissipatively stabilized cat code. See Refs. [81, 85, 87, 238] for a detailed analysis of gates for stabilized cat qubits.

\hat{X} -rotation. We can perform rotations around the logical \hat{X} -axis by using an *adiabatic* single-photon drive with Hamiltonian:

$$\hat{H}_X = F^* \hat{a} + F \hat{a}^\dagger \quad (3.92)$$

The coherent rotation around the logical \hat{X} -axis can be realized by adding \hat{H}_X to the master equation in Eq. (3.82) [81], with single-photon driving amplitude F . In the adiabatic limit $F \ll \kappa_2$, the logical code space remains the cat qubit manifold and the qubit is adiabatically rotated an angle $\varphi = \Omega_X t$ around the \hat{X} -axis, with Rabi frequency $\Omega_X = 2F|\alpha|$ [81], for real values of F and α . In Chap. 4, we will explore in-depth how non-adiabatic effects of this continuous rotation can be simulated efficiently.

\hat{Z} -gate. The \hat{X} -eigenstates of the cat qubit are approximately given by $|\pm\alpha\rangle$ (See also Eq. (3.72)), in the limit of large displacement field. Hence, the \hat{Z} -gate corresponds to interchanging the states $|+\rangle_L \approx |\alpha\rangle$ and $|-\rangle_L \approx |-\alpha\rangle$. Intuitively, this can be achieved by varying the phase of the effective two-photon drive G in Eq. (3.83), controlling the phase of α . In fact, detuning the resonator by an amount Δ with respect to the resonant frequency generates a continuous time-dependent rotation of the cat-qubit manifold:

$$\mathcal{L}(\hat{\rho}) = -i \left[\Delta \hat{a}^\dagger \hat{a} + \frac{G e^{-2i\Delta t}}{2} \hat{a}^{2\dagger} + \frac{G^* e^{2i\Delta t}}{2} \hat{a}^2 \right] + \kappa_2 \mathcal{D}[\hat{a}^2](\hat{\rho}) \quad (3.93)$$

A π -rotation from $\alpha \leftrightarrow -\alpha$ is achieved at $T = \pi/\Delta$. We can see that in a frame rotated by frequency 2Δ , the cat-qubit manifold is stationary.

CNOT-gate. For a universal gate set, we need at least one entangling gate. Here, we consider the CNOT-gate, consisting of a Pauli X gate on a target qubit conditioned on the state of a control qubit along the logical Z axis, or equivalently in the adjoint picture, a Pauli Z gate on a target qubit conditioned on the state of a control qubit along the X axis. For our choice of basis, we will consider the latter. As a result, we can combine the \hat{Z} -gate and \hat{X} -rotation, explained above to realize a CNOT gate. An engineered dissipator that realizes a \hat{Z} -gate conditioned on the state of the control mode can be formally given by the jump operator [238]

$$\hat{L}_2(t) = \hat{a}_2^2 - \alpha^2 + \frac{\alpha}{2}(e^{2i\Delta t} - 1)(\hat{a}_1 - \alpha). \quad (3.94)$$

When mode 1 is in the state $|-\rangle_L \approx |-\alpha\rangle$, the dissipator $\hat{L}_2(t)$ reduces (approximately) to the rotating dissipator for the \hat{Z} -gate on mode 2. On the other hand, when mode 1 is in the state $|+\rangle_L \approx |+\alpha\rangle$, $\hat{L}_2(t)$ reduces to the usual time-independent Lindblad operator $\hat{a}_1^2 - \alpha^2$ [238]. The control mode is always stabilized using the usual two-photon dissipation, with $\hat{L}_1 = \hat{a}_1^2 - \alpha^2$. Similar to the \hat{Z} -gate where the detuning term $\Delta\hat{a}^\dagger\hat{a}$ provides a compensating Hamiltonian for arbitrarily fast gates, we can apply a similar conditional Hamiltonian here to ensure that at any time, the two-mode system remains in the sub-space stabilized by the dissipators $\mathcal{D}[\hat{L}_1]$ and $\mathcal{D}[\hat{L}_2(t)]$. Such an *approximately* compensating Hamiltonian can be given by [87, 238]

$$\hat{H}_{\text{CX}} = \frac{\Delta}{4\alpha}(\hat{a}_1 + \hat{a}_1^\dagger - 2\alpha)(\hat{a}_2^\dagger\hat{a}_2 - \alpha^2). \quad (3.95)$$

We thus have the following master equation, realizing an CNOT gate:

$$\frac{d\hat{\rho}}{dt} = -i[\hat{H}_{\text{CX}}, \hat{\rho}] + \kappa_2\mathcal{D}[\hat{L}_1](\hat{\rho}) + \kappa_2\mathcal{D}[\hat{L}_2(t)](\hat{\rho}). \quad (3.96)$$

VI.3 Hamiltonian confinement

A different approach to engineering a stable cat qubit manifold is through Hamiltonian confinement instead of purely reservoir engineering approaches. This approach, first introduced by *Puri et al.* [84] and experimentally realized by *Grimm et al.* [86], uses a strong Kerr-nonlinearity to encode the cat qubit in the degenerate groundstate of the system Hamiltonian. In fact, the Kerr-cat Hamiltonian

$$\hat{H}_{\text{Kerr}} = -K(\hat{a}^{\dagger 2} - \alpha^{*2})(\hat{a}^2 - \alpha^2) \quad (3.97)$$

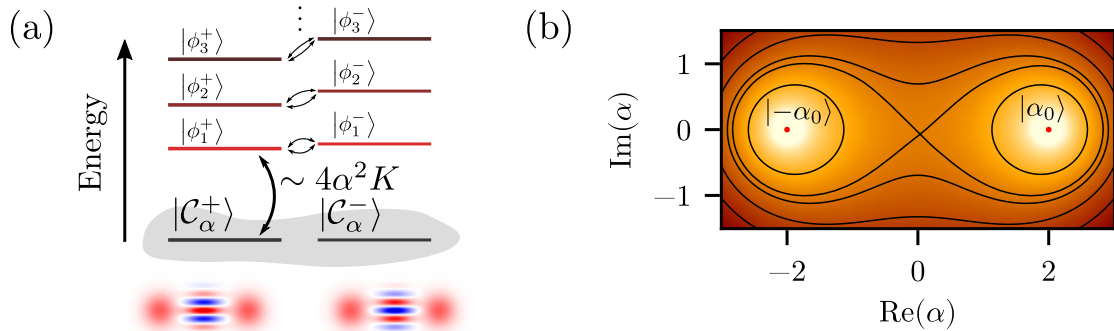


Figure 3.9: (a) Schematic representation of the eigenspectrum of the Kerr-cat. The groundstate is two-fold degenerate and hosts the cat-qubit manifold. The first excited states are gapped by an energy gap of $\Delta E_{\text{gap}} \sim 4\alpha^2 K$. (b) Semi-classical potential of the Kerr Hamiltonian, with the two fix points $-\alpha_0$ and α_0 .

has a two-fold degenerate sub-space of groundstates, spanned by coherent states $|\pm\alpha\rangle$. By diagonalizing the Hamiltonian \hat{H}_{Kerr} , we find that the groundstate sub-space is gapped to excited eigenstates by an energy of order $\Delta E_{\text{gap}} \sim 4\alpha^2 K$, and hence a large Kerr non-linearity protects the groundstate manifold from undesired leakage to excited states, as depicted in Fig. 3.9(a). Indeed, weak perturbations by spurious Hamiltonian terms to \hat{H}_{Kerr} will only produce exponentially small leakage outside of the groundstate manifold. In a semiclassical treatment, the dynamics has the two coherent states $|\pm\alpha\rangle$ as fix points of the semiclassical potential, shown in Fig. 3.9(b). We can rewrite \hat{H}_{Kerr} in Eq. (3.97) as

$$\hat{H}_{\text{Kerr}} = -K\hat{a}^{\dagger 2}\hat{a}^2 + \frac{G}{2}\hat{a}^{\dagger 2} + \frac{G^*}{2}\hat{a}^2, \quad (3.98)$$

with Kerr nonlinearity K and two-photon drive amplitude G , such that $\pm\alpha = \pm\sqrt{G/(2K)}$.

However, higher excited eigenstates split the degeneracy of the ground-state manifold [315]. By carefully detuning the Kerr resonator with respect to the resonant frequency, we can benefit from strong symmetries in the system, leading to multiple degeneracies in the spectrum of the Kerr Hamiltonian, causing the higher-excited eigenstates to be non-degenerate [316]. It should be noted that in this purely Hamiltonian confinement, there is no engineered process that ensures convergence back to the groundstate sub-space after leakage to higher excited eigenstates. It is, however, possible to combine Hamiltonian confinement using the Kerr-cat Hamiltonian and two-photon dissipative stabilization to confine the steady-state manifold to the groundstate manifold of the Kerr-cat Hamiltonian [310]. Furthermore, these *hybrid* confinement approaches have also been analyzed in the regime of non-zero detuning, making use of the first-order crit-

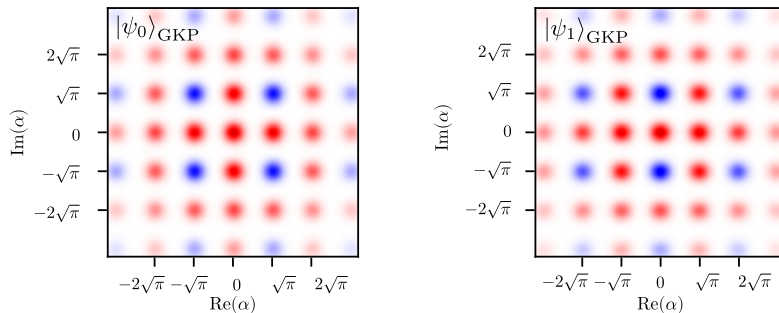


Figure 3.10: Schematic Wigner functions of the logical GKP code-words $|\psi_0\rangle$ and $|\psi_1\rangle$, according to Eq. (3.100) with an additional Gaussian envelope for finite-energy states.

ical phase transition of the driven-dissipative Kerr resonator [317] to reduce the phase-flip rate further under the loss-dephasing channel.

For gates on the Kerr-cat qubit, we refer to Ref. [85].

VII Other bosonic codes

Let us briefly illustrate two other notable single-mode bosonic codes, the *GKP* code and the binomial code, of which we already encountered one illustrative example in Sec. III. For a detailed review of single-mode bosonic codes, we refer to Refs. [53, 73, 74, 89, 236, 318].

Translation symmetric codes: The Gottesmann-Kitaev-Preskill code

The GKP code – named after *Gottesman, Kitaev, and Preskill* – is a bosonic encoding defined through two commuting displacement operators that act as translations in phase space [224]. This simplest version of it is the *square lattice* GKP, which encodes a bosonic qubit by the two commuting displacement operators:

$$\hat{S}_q \equiv e^{i2\sqrt{\pi}\hat{q}} = \hat{D}(i\sqrt{2\pi}), \quad \hat{S}_p \equiv e^{-i2\sqrt{\pi}\hat{p}} = \hat{D}(\sqrt{2\pi}), \quad (3.99)$$

where $\hat{q} = (\hat{a} + \hat{a}^\dagger)/\sqrt{2}$, and $\hat{p} = (\hat{a} - \hat{a}^\dagger)/(i\sqrt{2})$ are the position and momentum operators, respectively. Crucially, the two operators \hat{S}_q and \hat{S}_p commute, and hence can be simultaneously measured. Measuring \hat{S}_q and \hat{S}_p is equivalent as measuring \hat{q} and \hat{p} modulo $\sqrt{\pi}$. Being able to measure these operators modulo $\sqrt{\pi}$ importantly does not violate the Heisenberg uncertainty but rather shifts the uncertainty to which unit cell of a square lattice the measurement belongs. We

can define the code-words of the *square* GKP code as:

$$\begin{aligned} |\psi_0\rangle &\propto \sum_{n \in \mathbb{Z}} |\hat{q} = (2n)\sqrt{\pi}\rangle \propto \sum_{n \in \mathbb{Z}} |\hat{p} = n\sqrt{\pi}\rangle, \\ |\psi_1\rangle &\propto \sum_{n \in \mathbb{Z}} |\hat{q} = (2n+1)\sqrt{\pi}\rangle \propto \sum_{n \in \mathbb{Z}} (-1)^n |\hat{p} = n\sqrt{\pi}\rangle, \end{aligned} \quad (3.100)$$

As a result, any wave function in the code space has support on $q = k\sqrt{\pi}$ and $p = l\sqrt{\pi}$, with $k, l \in \mathbb{Z}$. We can obtain the structure of the code-words in Eq.(3.100) by applying the *stabilizer formalism* [214, 319], as the simultaneous +1 eigenspace of the operators \hat{S}_q and \hat{S}_p . The logical operators \hat{Z}_L , \hat{X}_L , and \hat{Y}_L are given by [73]

$$\hat{Z}_L = e^{i\sqrt{\pi}\hat{q}}, \quad \hat{X}_L = e^{-i\sqrt{\pi}\hat{p}}, \quad \text{and} \quad \hat{Y}_L = e^{i\sqrt{\pi}(\hat{q}-\hat{p})}, \quad (3.101)$$

The wave function of the state $|\psi_0\rangle$ is a sum of Dirac-delta functions in q at even multiple values of $\sqrt{\pi}$, whereas $|\psi_1\rangle$ has support in q at odd multiples of $\sqrt{\pi}$, as can be seen from Eq. (3.100). We can also conceptually understand the GKP code-words as a superposition of infinitely many and infinitely strong squeezed states, where each component is described by a Dirac delta function. As the states define a grid in phase space with $\sqrt{\pi}$ periodicity, the GKP admits an invariance under discrete translations by multiples of $\sqrt{\pi}$. This naturally means that any translations smaller than $\sqrt{\pi}/2$ result in a sub-space orthogonal to the code-space. Therefore, any errors of discrete displacements with $\{e^{iu\hat{p}}, e^{iv\hat{q}}; |u|, |v| \leq \sqrt{\pi}/2\}$ are correctable errors [73]. We can relate single-photon loss errors to displacements (See Sec. IV Eq. (3.25)) and verify that the GKP code can partially correct loss errors, making it an interesting bosonic code for the pure loss channel [224, 236, 320, 321].

It is important to note – and easy to verify from Eq. (3.100) – that the ideal GKP code-words have an infinite energy. We can regularize the GKP code by applying a Gaussian envelope [224, 320], equivalent to superpositions of finite-squeezed states. The two \hat{Z}_L eigenstates $|\psi_0\rangle$ and $|\psi_1\rangle$ code-words of the *approximate* GKP code are shown in Fig. 3.10 in phase space. However, the GKP suffers from dephasing as even small random rotations in phase space result in large displacement errors [320]. Different ways to realize approximate GKP code on several hardware platforms have been proposed [74, 224, 320, 322–335], as well as approaches to simulate the approximate states efficiently [73, 294, 336–339]. The GKP code has been experimentally realized in trapped ions [65, 336] and superconducting circuit QED platforms [78, 340], even reaching lifetimes beyond break-even [78].

Rotation-symmetric codes: Binomial codes and multi-component cat codes

The class of binomial codes is a class of rotation-symmetric bosonic codes [341] that uses precisely engineered superpositions of Fock-states to correct for a finite set of discrete errors [232]. Notably, it possesses a discrete \mathbb{Z}_N rotation symmetry with $\hat{R}(\theta = 2\pi/N) = e^{i2\pi/N\hat{a}^\dagger\hat{a}}$ (See also Eq. (3.69)). By construction of the rotational symmetry, rotation-symmetric codes are capable of detecting $N - 1$ photon loss events, as one can encode information in photon number parity subspaces that leak into orthogonal sub-spaces upon the loss of $N - 1$ photons. As we have seen in Sec. III, for exact *correctability* of a quantum code, we also have to ensure that the errors $\hat{E}_\ell^\dagger\hat{E}_{\ell'}$ act in the same way on both of the code-words in order to gain no information about superpositions in the encoded state. For example, in the *Kitten code*, detailed in Sec. III, that can correct single-photon loss errors, this amounts to the requirement of both code-words having the same average photon number. For higher-order discrete loss and dephasing errors, we can match precisely these requirements. To this end, consider the finite error set $\{\hat{\mathbb{1}}, \hat{a}, \hat{a}^2, \dots, \hat{a}^K, \hat{a}^\dagger, \dots, \hat{a}^{\dagger M}, \hat{n}, \dots, \hat{n}^D\}$ for some integer values of K , M and D . We define the code-words of the general *binomial code*:

$$|\psi_{0/1}\rangle \equiv \frac{1}{\sqrt{2^N}} \sum_{p \text{ even/odd}}^{[0, N+1]} \sqrt{\binom{N+1}{p}} |p(S+1)\rangle, \quad (3.102)$$

Here, $S = K + M$ is the Fock-space spacing, i.e., the rotational symmetry of the code, and $N = \max\{K, M, 2D\}$ is the maximum Fock-number in the code. We see that the Fock-number coefficients are binomially distributed. It can be checked that the binomial code, defined in Eq. (3.102) satisfies the Knill-Laflamme error correction conditions for the given set of errors. The Kitten code, the smallest binomial code with $K = 1$, $M = D = 0$, has been demonstrated experimentally [64, 239], but it remains challenging to experimentally construct bosonic codes correcting higher-order errors in this way, as the Fock-state coefficients have to be precisely engineered, and dissipatively stabilizing arbitrary superpositions of Fock-states requires very large nonlinearities, making the scaling towards higher-order binomial codes extremely challenging.

Lastly, we mention here that we can also construct higher rotation-symmetric codes of the cat code. In Sec. VI, we have analyzed the two-component cat code, which possesses a discrete \mathbb{Z}_2 symmetry. We can use arbitrary discrete rotational symmetries by taking superpositions of coherent states $|\alpha e^{i\phi}\rangle$ with the same magnitude $|\alpha|$, but with different phases. We can define the general multi-component

cat states by

$$|\mathcal{C}_{N,\alpha}^{(n)}\rangle \equiv \frac{1}{\sqrt{\mathcal{N}_{N,\alpha}^{(n)}}} \sum_{k=0}^{N-1} e^{-\frac{i2\pi nk}{N}} |\alpha e^{\frac{i2\pi k}{N}}\rangle. \quad (3.103)$$

Here $\mathcal{N}_{N,\alpha}^{(n)}$ is a normalization constant, given by

$$\mathcal{N}_{N,\alpha}^{(n)} = \sum_{k,k'=0}^{N-1} e^{\frac{2\pi in}{N}(k-k')} \langle \alpha e^{\frac{2\pi ik}{N}} | \alpha e^{\frac{2\pi ik'}{N}} \rangle. \quad (3.104)$$

Due to the discrete \hat{Z}_N -rotation symmetry of the states in Eq. (3.103), the states $\{|\mathcal{C}_{N,\alpha}^{(n)}\rangle, n = 0, \dots, N-1\}$ are all orthogonal to each other, as they contain superpositions of n Fock-states modulo N .

We have the freedom of choice to define the code space within this manifold, but by convention [81, 236, 341], we choose the logical basis:

$$|\psi_0\rangle \equiv |\mathcal{C}_{N,\alpha}^{(0)}\rangle, \quad |\psi_1\rangle \equiv |\mathcal{C}_{N,\alpha}^{(N/2)}\rangle \quad (3.105)$$

Upon the loss of k photons, we have in the limit of large α :

$$\hat{a}^k |\mathcal{C}_{N,\alpha}^{(n)}\rangle \propto |\mathcal{C}_{N,\alpha}^{(n-k \bmod N)}\rangle, \quad (3.106)$$

and hence a multi-component cat code of spacing N can correct $k = N/2 - 1$ photon losses.

As an example, the four-component cat code [81, 342, 343] with $N = 4$ consists of superpositions of the states $|\alpha\rangle$, $|- \alpha\rangle$, $|i\alpha\rangle$, and $|-i\alpha\rangle$. This code is capable of correcting single-photon loss errors and has been experimentally realized using adaptive classical control techniques in a superconducting resonator [76].

Autonomous stabilization of multi-component cat states using dissipation engineering requires engineering an effective N -photon interaction. Higher-order interactions are typically much weaker than, e.g., four-wave mixing interactions, and hence, it remains challenging to experimentally design a setup with a sizeable target interaction strength without introducing parasitic processes.

To summarize, we have seen in this chapter how to characterize bosonic quantum codes and how to assess their error correction capabilities. In particular, we have detailed the biased-noise cat qubit as a promising candidate for fault-tolerant quantum computing devices. Most importantly, we have seen that while dephasing errors are exponentially suppressed in the cat code, they are vulnerable to photon loss. Other codes, such as the GKP, binomial, and multi-component cat

code, have been proposed as a means to address photon loss errors. These codes, however, require strong non-linearities for preparation, stabilization, and error recovery. In the next chapter, we explore how we can extend the two-component cat code to address photon loss errors while further increasing the protection against dephasing errors, requiring only quadratic operations for state preparation and gates.

4

Quantum Error Correction with the Squeezed Cat Code

*A cat has nine lives.
For three he plays,
for three he strays,
and for the last three he stays.*

— ENGLISH PROVERB

We have seen in the previous chapter that the cat qubit, composed of even and odd superpositions of two opposite coherent states as their logical code-words, is a promising bosonic code that can be used to exponentially suppress errors induced by dephasing in a noise-biased environment by increasing the average photon number of the cat qubit and can thereby efficiently autonomously correct dephasing errors [74, 81, 236]. A single particle loss in the code-space, however, *exactly* maps the code-word with even photon number $|\mathcal{C}_\alpha^+\rangle$ to the code-word with odd photon number $|\mathcal{C}_\alpha^-\rangle$ and vice versa, thereby inducing a logical error in the code-space. Furthermore, a photon loss event does not map the code space into an associated error space but only introduces an unwanted rotation within the code space. We might, therefore, ask whether we can extend the cat qubit to a different bosonic code that inherits its protection against dephasing but makes it correctable also against photon loss.

In this chapter, we introduce the *squeezed cat code* $[\alpha]$ – a two-component cat code that relies on squeezed states – that is able to correct particle loss errors while at the same time drastically improving the correction of dephasing errors. We provide a comprehensive analysis of the squeezed cat code in terms of KL conditions as well as channel fidelity and discuss how the squeezed cat code can be implemented experimentally.

In Sec. I, we motivate the use of squeezing for quantum error correction, introduce squeezed states, analyze some important properties, and define and characterize squeezed cat states. We briefly outline how the code can be generated and how gates can be performed on the squeezed cat code. In Sec. II, we detail the error correction capabilities of the code and analyze the Knill-Laflamme error cor-

rection conditions for discrete errors arising from the loss-dephasing channel. We then analyze the performance of the squeezed cat code in Sec. III where we consider the full continuous-time loss-dephasing channel and optimize the code and recovery to reach the optimal channel fidelity. We finally briefly outline approaches towards experimental realizations in terms of dissipative stabilization techniques in Sec. IV. Sec. V concludes the chapter and gives a future outlook.

I Squeezed Schrödinger Cat States

I.1 Motivation

Let us motivate the proposal of the squeezed cat as a bosonic quantum code.

As a first motivation, it is well-known that squeezed states are not eigenstates of the annihilation operator \hat{a} [123]. An immediate consequence is that upon a single-photon loss event on a squeezed state, the resulting state will have a non-zero contribution orthogonal to the original state. This leakage carries information about the occurrence of a photon loss event and can be used in an error correction scheme to at least partially correct photon loss errors.

Notably, squeezed states of light have been studied in the context of quantum metrology for enhanced quantum sensing devices [90, 91, 93, 344–347], even beyond the standard quantum limit [92]. These results strongly suggest the use of squeezed states for enhanced bosonic quantum error correction, as a crucial task in bosonic error correction is the unambiguous identification of different kinds of errors. As squeezed states are non-classical states of light with reduced uncertainty in one phase-space quadrature and increased uncertainty in the conjugate quadrature [123], one might intuitively wish to exploit this to enhance the sensitivity with respect to certain errors.

Lastly, we might think of squeezing as compressing information in phase space [94]. Loss manifests itself in the Wigner function by deterministically rescaling the quadratures and applying a Gaussian smoothing [122] (See Chap. 3, Sec. IV for details), whereas dephasing is represented as a rotational smearing of the Wigner function. Fourier-transforming the Wigner function of a cat state, obtaining the *characteristic function*, the interference fringes between the opposite coherent states are mapped to coherent states with amplitudes $\pm\alpha$ in reciprocal space. Under the effect of loss, these large-frequency components diminish significantly as loss acts as a low-pass Gaussian filter. Compressing the cat state in phase space would result in a deterministic reshaping of the characteristic function, and therefore in principle allow to fit the high-frequency components that carry the non-classical superposition features within the low-pass filter [94]. As a result, we

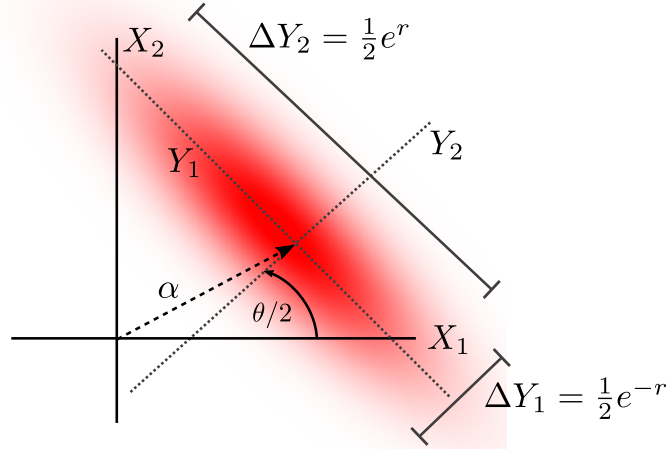


Figure 4.1: Schematic representation of a displaced squeezed state $|\alpha, \xi\rangle$ in phase space, with displacement α and squeezing $\xi = re^{i\theta}$. We show the quadratures $Y_{1,2}$ that are rotated by $\theta/2$, with respect to $X_{1,2}$ and highlight their respective uncertainties.

expect the decay of the interference features to be more protected from the Gaussian filtering caused by loss due to the compression of the characteristic function. In the Wigner function, this would result in a larger spacing between interference fringes, or equivalently, in lower-frequency components in the characteristic function, resulting in a slowing down of loss-induced quantum decoherence. [348–356]. In the following, we will analytically and numerically confirm that the squeezed cat code indeed possess stronger error correction properties than compared to the standard cat code.

I.2 Squeezed states

Here, we introduce the squeezed cat code and analyze some important properties. In quantum optical systems, squeezed states of light were first introduced to characterize minimum-uncertainty quantum states [357–366]. First, let us define a squeezed state in terms of its displacement α and squeezing parameter ξ [366] by first squeezing the vacuum and then displacing it:

$$|\alpha, \xi\rangle \equiv \hat{D}(\alpha)\hat{S}(\xi)|0\rangle. \quad (4.1)$$

In the above definition, $\hat{D}(\alpha)$ is the displacement operator (See also Chap. 2, Sec. III) and $\hat{S}(\xi)$ is the squeezing operator, defined by

$$\hat{D}(\alpha) \equiv \exp[\alpha\hat{a}^\dagger - \alpha^*\hat{a}], \quad (4.2)$$

$$\hat{S}(\xi) \equiv \exp\left[\frac{1}{2}(\xi^*\hat{a}^2 - \xi\hat{a}^{\dagger 2})\right]. \quad (4.3)$$

The phase-space representation of $|\alpha, \xi\rangle$ is schematically depicted in Fig. 4.1. In the following, we use the notation $\xi = re^{i\theta}$ with non-negative amplitude r and phase θ . We can rotate the canonical quadratures X_1 and X_2 (See also Chap. 2, Sec III, where we used the equivalent notation of x and p for the quadratures) by $\theta/2$ into new quadratures Y_1, Y_2 for which the uncertainties are increased and decreased with the squeezing amplitude r , respectively [123]:

$$\Delta Y_1 = \frac{1}{2}e^{-r}, \quad \Delta Y_2 = \frac{1}{2}e^r, \quad (4.4)$$

with $\Delta A \equiv \sqrt{\langle \hat{A}^2 \rangle - \langle \hat{A} \rangle^2}$. Some notable properties of the squeezed states are [366]:

$$\begin{aligned} \langle \hat{X}_1 + i\hat{X}_2 \rangle &= \langle \hat{Y}_1 + i\hat{Y}_2 \rangle e^{i\theta/2} = \alpha \\ \langle \hat{a}^\dagger \hat{a} \rangle &= |\alpha|^2 + \sinh^2(r) \\ \langle \hat{a}^2 \rangle &= \alpha^2 - e^{i\theta} \sinh(r) \cosh(r) \end{aligned} \quad (4.5)$$

Importantly, note that squeezed states maintain minimum Heisenberg uncertainty.

To analyze the effect of squeezing on operators, we can apply a similarity transform $\hat{S}(\xi)$ on the annihilation operator \hat{a} , yielding [123]

$$\hat{S}(\xi)\hat{a}\hat{S}^\dagger(\xi) = \hat{a} \cosh(r) + e^{i\theta}\hat{a}^\dagger \sinh(r), \quad (4.6)$$

From this relation, we can deduce that the order of the operators $\hat{D}(\alpha)$ and $\hat{S}(\xi)$ in Eq. (4.1) is important, as they obey the relations

$$\hat{D}(\alpha)\hat{S}(\xi) = \hat{S}(\xi)\hat{D}(\zeta), \quad (4.7)$$

with

$$\zeta = \alpha \cosh(r) - e^{i\theta}\alpha^* \sinh(r) \quad (4.8)$$

We can see from Eq. (4.7) that a squeezed state $|\alpha, \xi\rangle$ can be obtained by displacing first with a different complex amplitude ζ and then squeezing with the same parameter ξ . If both ξ and α are real, the squeezing is orthogonal to the displacement, and we simply have

$$\zeta = \alpha e^r. \quad (4.9)$$

Importantly, contrary to a coherent state $|\alpha\rangle$ which is an eigenstate of \hat{a} , a squeezed state no longer is an eigenstate of \hat{a} , since the squeezing similarity transform of the operator \hat{a} in Eq. (4.6) produces a non-zero contribution of \hat{a}^\dagger which cannot have a coherent state as an eigenstate. Analogous to coherent states, we

can find an operator \hat{b} that has $|\alpha, \xi\rangle$ as an eigenstate. We can show that a squeezed annihilation operator, with $\hat{b} \equiv \hat{S}(\xi)\hat{a}\hat{S}^\dagger(\xi)$, is in fact the operator with $|\alpha, \xi\rangle$ as an eigenstate:

$$\begin{aligned}\hat{b}|\alpha, \xi\rangle &= \hat{S}(\xi)\hat{a}\hat{S}^\dagger(\xi)|\alpha, \xi\rangle \\ &= \hat{S}(\xi)\hat{a}\hat{S}^\dagger(\xi)\hat{D}(\alpha)\hat{S}(\xi)|0\rangle \\ &= \hat{S}(\xi)\hat{a}\hat{D}(\zeta)|0\rangle \\ &= \hat{S}(\xi)\zeta|\zeta\rangle = \zeta|\alpha, \xi\rangle,\end{aligned}\tag{4.10}$$

where we have used the relation in Eq. (4.7).

We can decompose a squeezed state $|\alpha, \xi\rangle$ in its number state representation [123]

$$\begin{aligned}|\alpha, \xi\rangle &= \frac{1}{\sqrt{\cosh r}} \exp\left[-\frac{1}{2}|\alpha|^2 - \frac{1}{2}\alpha^{*2}e^{i\theta}\tanh r\right] \\ &\quad \times \sum_{n=0}^{\infty} \frac{\left[\frac{1}{2}e^{i\theta}\tanh r\right]^{n/2}}{\sqrt{n!}} H_n\left[\gamma\left(e^{i\theta}\sinh(2r)\right)^{-1/2}\right]|n\rangle.\end{aligned}\tag{4.11}$$

Here, $H_n(x)$ are Hermite polynomials of the second kind. We thus have the probability P_n of finding n photons in the state $|\alpha, \xi\rangle$

$$\begin{aligned}P_n &\equiv |\langle n | \alpha, \xi \rangle|^2 \\ &= \frac{\left(\frac{1}{2}\tanh r\right)^n}{n! \cosh r} \exp\left[-|\alpha|^2 - \frac{1}{2}\left(\alpha^{*2}e^{i\theta} + \alpha^2e^{-i\theta}\right)\tanh r\right] \\ &\quad \times \left|H_n\left[\gamma\left(e^{i\theta}\sinh(2r)\right)^{-1/2}\right]\right|^2.\end{aligned}\tag{4.12}$$

It is clear from the above expression that the distribution P_n depends both on the phase of $\alpha = |\alpha|e^{i\varphi}$ and of $\xi = re^{i\theta}$. For $\varphi - \theta/2 = 0$ for example, the distribution P_n is narrower than for a coherent state $|\alpha\rangle$ – also referred to as number squeezing [367] – for which the distribution is sub-Poissonian and is an unequivocally quantum effect. In this case, the photon number distribution can exhibit large scale oscillations [368–370]. On the other hand, in the case of $\varphi - \theta/2 = \pi/2$, the distribution is super-Poissonian, i.e. broader than for a coherent state, which is *not* a non-classical effect [123], as it can be generated classically.

From projecting a squeezed state $|\alpha, \xi\rangle$ onto coherent states, one can obtain the Wigner function representation (here, for $\theta = 0$ and $\alpha = 0$ for simplicity)

$$W(\beta) = \frac{2}{\pi} \exp\left[-\frac{1}{2}[\text{Re}(\beta)]^2 e^{-2r} - \frac{1}{2}[\text{Im}(\beta)]^2 e^{2r}\right].\tag{4.13}$$

From this expression, we can once again see a narrowing in one quadrature and an expansion in the conjugate quadrature as a function of squeezing amplitude r . A notable property of the squeezed state $|\alpha, \xi\rangle$ is that it is the most general *pure* quantum state with non-negative Wigner function [371].

I.3 The Squeezed cat code

Let us now define the code-words of the squeezed cat code:

$$|\mathcal{C}_{\alpha,\xi}^{\pm}\rangle \equiv \frac{1}{N_{\alpha,\xi}^{\pm}}(|\alpha, \xi\rangle \pm |-\alpha, \xi\rangle) \quad (4.14)$$

In close analogy to the cat code, we have taken even (+) and odd (-) superposition of squeezed states for the definition of the states $|\mathcal{C}_{\alpha,\xi}^{\pm}\rangle$. The connection to the cat code becomes even more apparent when we reverse the order of squeezing and displacement using Eq. (4.7):

$$|\mathcal{C}_{\alpha,\xi}^{\pm}\rangle = \hat{S}(\xi) \frac{1}{N_{\zeta}^{\pm}}(|\zeta\rangle \pm |-\zeta\rangle), \quad (4.15)$$

with ζ as defined in Eq. (4.8).

An important observation is that the squeezed cat states leave the photon number parity of the cat code intact. Since the squeezing operator, defined in Eq. (4.3), contains square powers of \hat{a} and \hat{a}^{\dagger} in the exponential, it is straightforward to check that $\hat{\Pi}\hat{S}(\xi)\hat{\Pi}^{\dagger} = \hat{S}(\xi)$. As a result, the states $|\mathcal{C}_{\alpha,\xi}^{+}\rangle$ ($|\mathcal{C}_{\alpha,\xi}^{-}\rangle$) maintain even(odd) photon number parity, respectively. The normalization constant in Eq. (4.15) is given by $N_{\alpha,\xi}^{\pm} = N_{\zeta}^{\pm} = \sqrt{2(1 \pm e^{-2|\zeta|^2})}$.

The squeezing phase θ determines the phase-space direction of the squeezing. In the following, we set the squeezing orthogonal to the direction of the displacement, that is, $\alpha = |\alpha|e^{2\theta}$. Without loss of generality, we set $\theta = 0$ for simplicity. This implies that $\alpha > 0$ is a positive real-valued parameter. In particular, with this choice, the overlap between squeezed states with opposite displacement becomes minimal,

$$\langle \alpha, \xi | -\alpha, \xi \rangle = \exp\left(-2|\alpha|^2 e^{2|\xi|}\right). \quad (4.16)$$

We notice that the overlap between these states is double-exponentially suppressed in the squeezing ξ and exponentially suppressed in the displacement α .

The code-words $|\mathcal{C}_{\alpha,\xi}^{\pm}\rangle$, defining the logical \hat{Z} -eigenstates, are depicted in Fig. 4.2(a) on the logical Bloch-sphere. Wigner functions of the even and odd squeezed cat states are shown in Fig. 4.2(b-c).

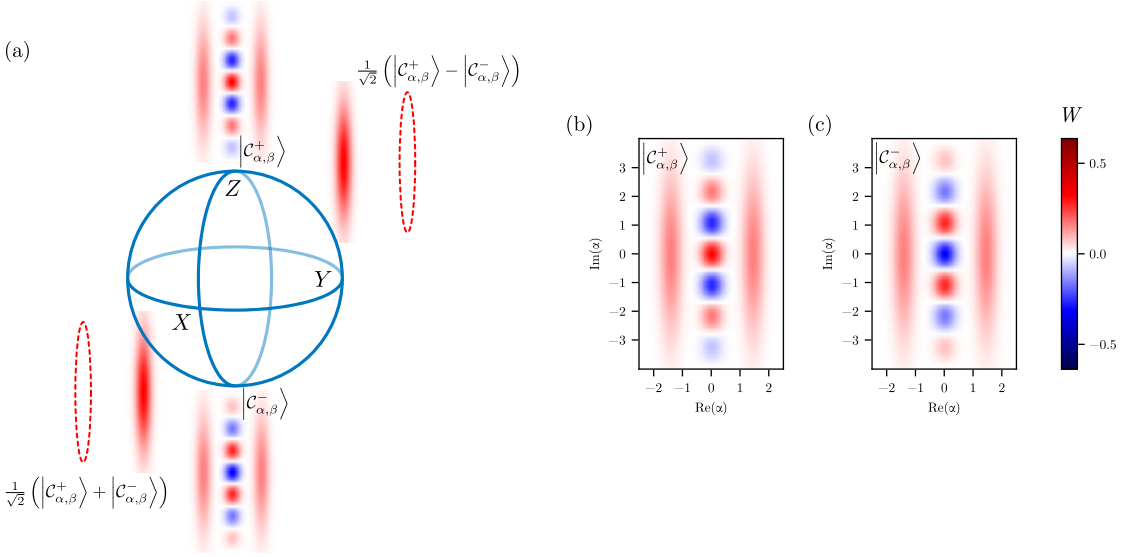


Figure 4.2: (a) Bloch sphere of the squeezed cat code. The states $|\mathcal{C}_{\alpha,\xi}^{\pm}\rangle$ are the logical \hat{Z} -eigenstates. We also depict the logical \hat{X} -eigenstates, i.e. the superpositions $\frac{1}{\sqrt{2}}(|\mathcal{C}_{\alpha,\xi}^{\pm}\rangle \pm |\mathcal{C}_{\alpha,\xi}^{\mp}\rangle)$. (b-c) Wigner functions $W(\alpha)$, of the even squeezed cat state $|\mathcal{C}_{\alpha}^{\pm}\rangle$ (b) and the odd squeezed cat state $|\mathcal{C}_{\alpha}^{\mp}\rangle$ (c). Parameters: $\alpha = 1$, $\xi = 1$.

I.4 Asymptotic discrete translation invariance

In addition to the \mathbb{Z}_2 -symmetry due to the even and odd superpositions of mirrored squeezed states, in the limit of large squeezing, the squeezed cat states become invariant under phase-space translations orthogonal to the displacement direction, connecting rotation-symmetric codes [341] to translation-invariant codes, such as the GKP code [224]. For a displacement $\hat{D}(\eta)$, with $\eta \perp \alpha$, we have

$$\langle \mathcal{C}_{\alpha,\xi}^+ | \hat{D}(\eta) | \mathcal{C}_{\alpha,\xi}^+ \rangle = \cos(|\alpha\eta|) \exp\left(-\frac{1}{2}e^{-2|\xi|}|\eta|^2\right) \quad (4.17)$$

In the limit $\xi \rightarrow \infty$, the exponential term vanishes and we have $\langle \mathcal{C}_{\alpha,\xi}^+ | \hat{D}(\eta) | \mathcal{C}_{\alpha,\xi}^+ \rangle = \cos(|\alpha\eta|)$. In this limit, we have for the odd squeezed cat state $\langle \mathcal{C}_{\alpha,\xi}^- | \hat{D}(\eta) | \mathcal{C}_{\alpha,\xi}^- \rangle = \sin(|\alpha\eta|)$. As a result, in the limit $\xi \rightarrow \infty$, the squeezed cat code becomes invariant under translation along *one* direction in phase space, with $|\eta| = n2\pi/|\alpha|$, with $n \in \mathbb{Z}$. Note that contrary to the ideal GKP code, which is invariant under discrete translations in two directions in phase space, the squeezed cat code is only invariant under discrete translations along a single direction in phase space in the infinite-squeezing limit. In the GKP, the discrete translation invariance can be related to the ability to partially correct for certain errors – including single-photon loss [74, 236, 237]. For finite squeezing, we therefore expect the capability of approximately correcting particle loss, similar to a finite-energy GKP code.

I.5 Code generation and gates

As seen in Eq. (4.15), we can obtain a squeezed cat state by squeezing a standard two-component cat state. Moreover, we can express any linear combination of squeezed states as

$$a|\alpha, \xi\rangle + b|-\alpha, \xi\rangle = \hat{S}(\xi)(a|\zeta\rangle + b|-\zeta\rangle). \quad (4.18)$$

As a result, the squeezed cat code can be potentially implemented on platforms where squeezing and coherent states can be generated. This includes, for example, superconducting circuits [372, 373], quantum optomechanics [198, 291], and photonics [348, 351, 374–378]. Through two-photon processes, squeezed cat states can be generated from squeezing two-component cat states [290, 379].

Furthermore, we can generate bright squeezed states $|\alpha, \xi\rangle$ by decomposing the displacement and squeezing into a series of smaller displacement and squeezing:

$$\hat{D}(\alpha)\hat{S}(\xi) = \prod_{k=1}^N \hat{D}(\alpha_k)\hat{S}(\xi_k), \quad (4.19)$$

with

$$\alpha_0 = \alpha/N, \quad \xi_k = \xi/N, \quad (4.20)$$

$$\alpha_k = \alpha_{k-1} \cosh(r) - \alpha_{k-1}^* e^{i\theta} \sinh(r). \quad (4.21)$$

Eq. (4.19) allows the use of pulsed schemes of small squeezing and displacement to generate bright squeezed states.

We can implement quantum gates with the squeezed cat code similar to the two-component cat code [81] by first de-squeezing to the two-component cat code manifold, performing the gate and then re-squeezing back to the squeezed cat code manifold. Formally, any gate $\hat{U}_{\mathcal{H}_{\text{SC}}}$ in the squeezed cat code can be expressed as

$$\hat{U}_{\mathcal{H}_{\text{SC}}} = \hat{S}(\xi)\hat{U}_{\mathcal{H}_{\text{cat}}}\hat{S}^\dagger(\xi), \quad (4.22)$$

with a gate $\hat{U}_{\mathcal{H}_{\text{cat}}}$ acting in the two-component cat-state manifold. Note that this procedure does, in general, not preserve the enhanced noise bias of the squeezed cat code.

Noise-bias preserving gates for the squeezed cat qubit can be straightforwardly extended from the standard two-component cat states, as the photon-parity structure of the code-words remain unaffected by squeezing. For a detailed set of bias-preserving gates, we refer to Ref. [83].

II Quantum error correction conditions

II.1 Intuitive picture

Let us give a first intuitive picture of the partial correctability of loss errors using the squeezed cat code. To highlight the difference with respect to the two-component cat code, let us recall that for the cat code, we have $\hat{a}|\mathcal{C}_\alpha^\pm\rangle \propto |\mathcal{C}_\alpha^\mp\rangle$. A single-photon loss event acting on the cat code remains entirely within the code space, generating a bit-flip error, and hence, there is no error syndrome that can detect if such an error occurred.

For the squeezed cat code, however, the action of \hat{a} results in a state that lies partially outside of the code-space:

$$\hat{a}|\mathcal{C}_{\alpha,\xi}^\pm\rangle = c_1|\mathcal{C}_{\alpha,\xi}^\mp\rangle + c_2|\tilde{\mathcal{C}}_{\alpha,\xi}^\mp\rangle, \quad (4.23)$$

where the states $|\tilde{\mathcal{C}}_{\alpha,\xi}^\mp\rangle$ lie in an error-sub-space orthogonal to the code-space. The states $|\tilde{\mathcal{C}}_{\alpha,\xi}^\mp\rangle$ remain orthogonal to each other, just like the original code-space and thus, the qubit information is (partially) contained in the error-sub-space. An appropriate non-demolition syndrome, probing the sub-space spanned by $|\tilde{\mathcal{C}}_{\alpha,\xi}^\mp\rangle$ will obtain information about the error and can be used to devise a recovery operation. We have an analogous picture for the action of dephasing with photon number operator \hat{n} .

In Fig 4.3(a), we show the phase space deformation of the logical code-words $|\mathcal{C}_{\alpha,\xi}^\pm\rangle$ upon the action of \hat{a} and $\hat{a}^\dagger\hat{a}$, respectively. Arguing from the phase-space deformations, a contribution outside of the original code-space manifold as in Eq. (4.23) becomes evident. First, it is important to note that for finite squeezing, the action of \hat{a} on a state in the code-space does not fully bring the state into an orthogonal error sub-space (See Eq. (4.23)). Therefore, there will be a finite uncorrectable part of the error. Second, when considering multiple errors, such as \hat{a} and $\hat{a}^\dagger\hat{a}$, the resulting error sub-spaces are not mutually orthogonal for finite squeezing, and hence, unambiguously identifying which error occurred is, in general not possible (See Fig. 4.3(b)). In the limiting case of infinite squeezing, however, the error sub-spaces associated with single-photon loss and dephasing errors become mutually orthogonal, and the KL conditions can be satisfied for discrete loss and dephasing errors.

II.2 Knill-Laflamme conditions for the squeezed cat code

We now analyze the correctability of discrete errors using the Knill-Laflamme error correction conditions (See Sec. II.1). To this end, let us consider the discrete set of

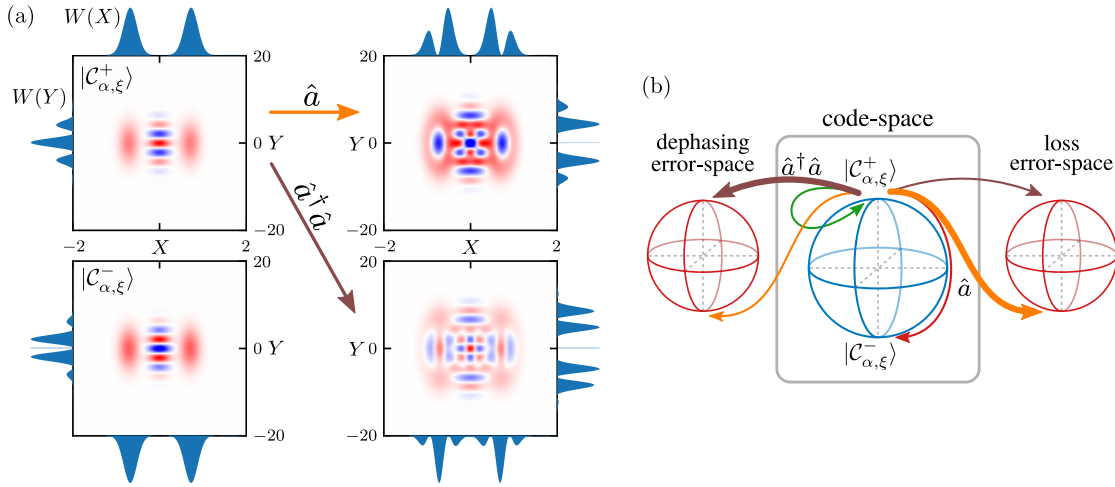


Figure 4.3: (a) Wigner quasi-probability distribution function $W(X, Y)$ of the squeezed cat code-words $|\mathcal{C}_{\alpha,\xi}^{\pm}\rangle$ for $\alpha = 0.5$ and $\xi = 1.5$. The arrows indicate the action of operators \hat{a} and $\hat{a}^{\dagger}\hat{a}$ on the state $|\mathcal{C}_{\alpha,\xi}^{\pm}\rangle$, respectively, notably deforming the initial phase space structure. Note the difference in scale between X and Y axis by one order of magnitude. On the sides of each subpanel, we show the integrated Wigner functions $W(X)$ and $W(Y)$. (b) Schematic illustration of the effect of single-photon loss and dephasing events on the code-space. For $|\mathcal{C}_{\alpha,\xi}^{\pm}\rangle$, we schematically depict the action of these errors for finite squeezing.

errors $\{\hat{1}, \hat{a}, \hat{a}^{\dagger}\hat{a}\}$. These are the generating set of errors up to order $\mathcal{O}(\tau)$ arising from the joint loss-dephasing channel (See Chap. 3, Sec. IV).

Here, we report and analyze the limiting cases of the Knill-Laflamme conditions for the squeezed cat code. For full analytical expressions, see Appendix A. First, we consider single-photon loss. In the limit of large squeezing, we have

$$\lim_{\xi \rightarrow \infty} \langle \mathcal{C}_{\alpha,\xi}^{\mp} | \hat{a} | \mathcal{C}_{\alpha,\xi}^{\pm} \rangle = \alpha. \quad (4.24)$$

This is similar to the cat code, where we have $\langle \mathcal{C}_{\alpha}^{\mp} | \hat{a} | \mathcal{C}_{\alpha}^{\pm} \rangle \propto \alpha$. Hence, in the limit of large displacement, both cat code and squeezed cat code are equally vulnerable to particle loss. The difference here with respect to the cat code is that in the squeezed cat code, we can reduce the displacement in favor of an increased squeezing to make the error \hat{a} increasingly correctable, such that Eq. (4.24) approaches zero, as for a fully correctable error. In this regime of small α and large ξ , the squeezed cat code is able to correct loss due to the small α , but also dephasing due to the large ξ , which we demonstrate below.

The KL conditions for the given set of errors require the code-words to have the same average photon number,

$$\langle \mathcal{C}_{\alpha,\xi}^+ | \hat{a}^\dagger \hat{a} | \mathcal{C}_{\alpha,\xi}^+ \rangle = \langle \mathcal{C}_{\alpha,\xi}^- | \hat{a}^\dagger \hat{a} | \mathcal{C}_{\alpha,\xi}^- \rangle. \quad (4.25)$$

This condition is fulfilled in the limit of either large displacement or large squeezing. We can show that in this limit, the difference between the left-hand side and right-hand side is given by

$$\langle \mathcal{C}_{\alpha,\xi}^+ | \hat{a}^\dagger \hat{a} | \mathcal{C}_{\alpha,\xi}^+ \rangle - \langle \mathcal{C}_{\alpha,\xi}^- | \hat{a}^\dagger \hat{a} | \mathcal{C}_{\alpha,\xi}^- \rangle \propto 2|\alpha|^2 \langle \alpha, \xi | -\alpha, \xi \rangle = 2|\alpha|^2 \exp(-2|\alpha|^2 e^{2|\xi|}), \quad (4.26)$$

where we have used the expression of the overlap $\langle \alpha, \xi | -\alpha, \xi \rangle$ in Eq. (4.16). From the above equation, we deduce an improved suppression of dephasing errors, generated by the operator $\hat{a}^\dagger \hat{a}$ due to the double-exponential decay of the overlap of opposite squeezed states with the squeezing ξ .

As detailed in Chap. 3, Sec. II.1, we can decompose discrete errors in logical operations, by projecting the errors on the code-space. We have, in particular:

$$\hat{P}_C \hat{a} \hat{P}_C = e^{-r} \zeta \frac{e^{2\zeta^2}}{\sqrt{e^{4\zeta^2} - 1}} \hat{X}_L - i e^r \zeta \frac{1}{\sqrt{e^{4\zeta^2} - 1}} \hat{Z}_L. \quad (4.27)$$

In the regime of large squeezing or displacement, $e^{-2\zeta^2} \ll 0$, the above expression reduced to

$$\hat{P}_C \hat{a} \hat{P}_C = \sqrt{\bar{n} - \sinh^2(\xi)} \hat{X}_L - i e^{\xi - 2\zeta^2} \zeta \hat{Z}_L, \quad (4.28)$$

where $\bar{n} \equiv \text{Tr}\{\hat{P}_C \hat{n}\}/2$ is the average photon number of the squeezed cat code. From the above expression, we see that phase flips, corresponding to \hat{Z}_L , are exponentially suppressed, while for $\xi \rightarrow \infty$, we recover the linear scaling of the logical \hat{X}_L error with α , as stated in Eq. (4.24). Furthermore, the projection of $\hat{a}^\dagger \hat{a}$ yields in the regime $e^{-2\zeta^2} \ll 0$

$$\hat{P}_C \hat{a}^\dagger \hat{a} \hat{P}_C = \bar{n} \hat{1}_L + 2|\alpha|^2 e^{-2\zeta^2} \hat{Z}_L, \quad (4.29)$$

from which the exponential suppression of phase-flip errors, equivalent to Eq. (4.26), becomes even more apparent.

For the remaining elements of the Knill-Laflamme tensor $M_{[i,\ell],[j,\ell']} = \langle \psi_i | \hat{E}^{\ell^\dagger} \hat{E}^{\ell'} | \psi_j \rangle$ for the considered error set (See Chap. 3, Sec. (II.1)), we can analytically verify that the Knill-Laflamme conditions are exactly verified in the considered limit. See Appendix A for the analytical expressions.

We can summarize the correction against loss and dephasing in the following intuitive picture: Due to the additional degree of freedom in the squeezing param-

eter ξ , we can increase the correctability against single-photon loss by lowering the displacement α , and compensate for the reduced correctability by increasing the squeezing parameter ξ , with code-words that are widely spread out in one direction of the phase space, reminiscent of squeezed comb states [380]. This is notably not the case in the GKP code, where the correctability against dephasing decreases with the squeezing (that defines the envelope of the grid states in phase space).

II.3 Correction of multiple errors

Although we focus on the correction of loss and dephasing errors in the remainder of this chapter, it is notable that the squeezed cat code is able to correct also other errors, such as photon gain or higher-order dephasing or particle loss errors. This stems from the fact that, in the regime of large displacement, or finite displacement and large squeezing, the operators \hat{a}^\dagger and \hat{a} have a similar effect when acted on the code-words (up to a complex phase). For example, we have in this limit

$$\langle \mathcal{C}_{\alpha,\xi}^\pm | \hat{a}^\dagger \hat{a} | \mathcal{C}_{\alpha,\xi}^\pm \rangle = - \langle \mathcal{C}_{\alpha,\xi}^\pm | \hat{a}^2 | \mathcal{C}_{\alpha,\xi}^\pm \rangle = \frac{e^{2|\xi|}}{4}. \quad (4.30)$$

Hence, the Knill-Laflamme conditions for \hat{a}^\dagger and \hat{a}^2 become identical up to a sign in this limit. As we have previously demonstrated that $\hat{a}^\dagger \hat{a}$ is a correctable error, so is \hat{a}^2 .

In this light, we can see that the squeezed cat code constitutes a degenerate bosonic quantum code, in which multiple errors – such as $\hat{a}^\dagger \hat{a}$ and \hat{a}^2 act identical on the code-space. This a crucial difference between the squeezed cat code and other bosonic quantum codes, such as the binomial code [232]. As a result, higher-order error correction schemes for the squeezed cat code might be devised beyond first-order single-photon loss and dephasing errors.

III Approximate quantum error correction

In a realistic scenario, squeezing is a limited resource in most experimental platforms, and as a result, the Knill-Laflamme conditions for the correction of loss and dephasing are not exactly satisfied. Nevertheless, the results above suggest that we can *approximately* correct errors arising from the loss-dephasing channel to some degree. We can, therefore, ask the question: How much information can the squeezed cat code preserve in an approximate error-correction recovery protocol where both displacement and squeezing are bounded? Naturally, due to the fact that different errors (e.g. \hat{a} and $\hat{a}^\dagger \hat{a}$) can not unambiguously be identified from

their respective error sub-spaces (See Fig. 4.3(b)), a recovery protocol aiming to correct these errors optimally depends on the nature of the noise channel and on the respective noise rates in particular.

Here, we assess the performance of the squeezed cat code in terms of channel fidelity, detailed in Chap. 3, Sec. V for the joint loss-dephasing channel. To this extent, let us consider the Lindblad master equation of the joint loss-dephasing channel (See Chap. 3, Sec. IV for details)

$$\mathcal{L}(\hat{\rho}) = \kappa_1 \mathcal{D}[\hat{a}](\hat{\rho}) + \kappa_2 \mathcal{D}[\hat{a}^\dagger \hat{a}](\hat{\rho}). \quad (4.31)$$

with single-photon loss rate κ_1 and dephasing rate κ_2 . We consider that the loss channel with Liouvillian \mathcal{L} acts for a time τ , after which we perform a recovery operation. To obtain a finite error set, we consider the Kraus operators in leading order of τ . We therefore consider the errors generated by the Kraus operators:

$$\begin{aligned} \hat{E}_0 &= \hat{\mathbb{1}} - \frac{\kappa_1 \tau}{2} \hat{a}^\dagger \hat{a} - \frac{\kappa_2 \tau}{2} (\hat{a}^\dagger \hat{a})^2, \\ \hat{E}_1 &= \sqrt{\kappa_1 \tau} \hat{a}, \quad \hat{E}_2 = \sqrt{\kappa_2 \tau} \hat{a}^\dagger \hat{a}. \end{aligned} \quad (4.32)$$

In a quantum-trajectory picture, the additional terms in the expression of \hat{E}_0 are due to the information back-action, for the case where no quantum jump with either operator \hat{E}_1 or \hat{E}_2 occurred. For the subsequent analysis, instead of considering the Kraus operators above, which explicitly depend on the decay rates $\kappa_{1,2}$ and time τ , we consider the equivalent generating set of errors:

$$\{\hat{E}_k\} = \{\hat{\mathbb{1}}, \hat{a}, \hat{a}^\dagger \hat{a}, (\hat{a}^\dagger \hat{a})^2\}. \quad (4.33)$$

We compute error sub-spaces associated to the operators in $\{\hat{E}_k\}$:

$$|\tilde{\psi}_i^\pm\rangle = \hat{E}_i |\mathcal{C}_{\alpha,\xi}^\pm\rangle, \quad \text{with } \hat{E}_i \in \{\hat{E}_k\} \quad (4.34)$$

Note that the states $|\tilde{\psi}_i^\pm\rangle$ are parity eigenstates as the operators in $\{\hat{E}_k\}$ do not mix parity sectors (although the action of \hat{a} flips the parity). Therefore, $\langle \tilde{\psi}_i^+ | \tilde{\psi}_i^- \rangle = 0$, for every state in the error-sub-spaces. Hence, the states within each error sub-space remain orthogonal. With the notation in Eq. (4.34), $|\tilde{\psi}_0^\pm\rangle = |\mathcal{C}_{\alpha,\xi}^\pm\rangle$ describes the states in the code-space.

Importantly, the spaces $\text{Span}\{|\tilde{\psi}_i^+\rangle, |\tilde{\psi}_i^-\rangle\}$ and $\text{Span}\{|\tilde{\psi}_j^+\rangle, |\tilde{\psi}_j^-\rangle\}$ for finite α and ξ are not mutually orthogonal to each other. As a direct consequence, the Knill-Laflamme conditions for the correction of the errors in Eq. (4.33) are not exactly satisfied. We can, however, obtain a set of orthonormal error sub-spaces by applying an orthonormalization procedure such as Gram-Schmidt or-

thonormalization. We thus obtain mutually orthogonal error subspaces $\mathcal{H}_{\mathcal{E}_j} = \text{Span}\{|\psi_j^+\rangle, |\psi_j^-\rangle\}$, with $\langle\psi_i^\mu|\psi_j^\nu\rangle = \delta_{i,j}$. Errors in the set $\{\hat{E}_k\}$ in Eq. (4.33) will, in general, leak into multiple error sub-spaces $\{\mathcal{H}_{\mathcal{E}_j}\}$, depending on the code-space parameters α and ξ , as well as on the noise parameters, namely the single-photon loss rate κ_1 and dephasing rate κ_2 .

To obtain a near-optimal recovery, attempting to correct the errors in $\{\hat{E}_k\}$, we construct a set of basis operators (See also Chap. 3, Sec. V, Eq. (3.66))

$$\begin{aligned}\hat{\sigma}_1^{(k)} &= \hat{\mathbb{I}}_{\mathcal{H}_{\mathcal{E}_k} \rightarrow \mathcal{H}_C} = |\mathcal{C}_{\alpha,\xi}^+\rangle\langle\psi_k^+| + |\mathcal{C}_{\alpha,\xi}^-\rangle\langle\psi_k^-|, \\ \hat{\sigma}_2^{(k)} &= \hat{X}_{\mathcal{H}_{\mathcal{E}_k} \rightarrow \mathcal{H}_C} = |\mathcal{C}_{\alpha,\xi}^+\rangle\langle\psi_k^-| + |\mathcal{C}_{\alpha,\xi}^-\rangle\langle\psi_k^+|, \\ \hat{\sigma}_3^{(k)} &= \hat{Y}_{\mathcal{H}_{\mathcal{E}_k} \rightarrow \mathcal{H}_C} = i|\mathcal{C}_{\alpha,\xi}^+\rangle\langle\psi_k^-| - i|\mathcal{C}_{\alpha,\xi}^-\rangle\langle\psi_k^+|, \\ \hat{\sigma}_4^{(k)} &= \hat{Z}_{\mathcal{H}_{\mathcal{E}_k} \rightarrow \mathcal{H}_C} = |\mathcal{C}_{\alpha,\xi}^+\rangle\langle\psi_k^+| - |\mathcal{C}_{\alpha,\xi}^-\rangle\langle\psi_k^-|.\end{aligned}\tag{4.35}$$

The Pauli-operators in Eq. (4.35) define a basis of a general quantum map that projects the error space $\mathcal{H}_{\mathcal{E}_k}$ to the code-space \mathcal{H}_C .

Using a *semidefinite program*, a convex optimization procedure, described in detail in Chap. 3, Sec. V, and using the basis operators defined in Eq. (4.35), we can numerically obtain a near-optimal recovery operation to gauge the performance of an approximate error correction protocol for the squeezed cat code. It is important to note that the recovery operation \mathcal{R} with basis operators $\{\hat{\sigma}_i^{(k)}, i = 1, \dots, 4, k = 1, \dots, 4\}$ is assumed to be noise-less and instantaneous and thus provides an upper bound on the achievable correctability of the set of errors, defined in Eq. (4.33). Furthermore, despite considering only the correction of a finite error set $\{\hat{E}_k\}$ that includes leading-order errors from the loss-dephasing channel to limit the numerical complexity of the problem, for the noise channel, we consider the full loss-dephasing channel to all orders. As a result, a recovery operation considering higher-order errors will, in general, yield a better performance. As a first benchmark, however, we will restrict ourselves to the correction of the errors $\{\hat{E}_k\}$ in Eq. (4.33).

III.1 Channel fidelity

In the following, for given values of the loss and dephasing rates $\kappa_{1,2}$, or equivalently for different times τ , we optimize the recovery operation for the error set $\{\hat{E}_k\}$ in Eq. (4.33) using a semidefinite program explained in Chap. 3, Sec. V to maximize the channel fidelity \mathcal{F} . The resulting near-optimal recovery \mathcal{R}^* yields an explicit form of its operator-sum representation with Kraus operators $\{\hat{R}_k^*\}$, such that actual hardware operations could be devised to construct the desired target operations using, for example, optimal-control techniques [381–385]. This

Algorithm 1 Schematic pseudocode for the optimization of the encoding parameters α , ξ and the recovery \mathcal{R} for a range of noise channel parameters $\kappa_1\tau$, $\kappa_2\tau$.

```

1: for  $\kappa_1\tau \in \text{range}(\kappa_1\tau)$  do           ▷ Loop over dimensionless single-photon loss
   parameter
2:   for  $\kappa_2\tau \in \text{range}(\kappa_2\tau)$  do   ▷ Loop over dimensionless dephasing parameter
3:     repeat
4:        $\mathcal{R}, \mathcal{F} \leftarrow \text{SDP}(\kappa_1\tau, \kappa_2\tau, \alpha, \xi)$   ▷ Perform SDP to obtain optimal  $\mathcal{R}$ 
5:        $\alpha, \xi \leftarrow \text{propose\_new}(\alpha, \xi, \mathcal{F})$       ▷ Propose new code-space
   parameters  $\alpha, \xi$ 
6:     until  $\mathcal{F}$  converged or break condition reached
7:     save  $\alpha^*, \xi^*, \mathcal{R}^*, \mathcal{F}$    ▷ Save optimal results for each value of  $\kappa_1\tau, \kappa_2\tau$ 
8:   end for
9: end for

```

is a significant advantage over measures for approximate error correction based on the Knill-Laflamme tensor alone (See Eq. (3.10)), which do not give an explicit expression for the recovery operation.

Note also that the optimal recovery operation \mathcal{R}^* is not conditional to the outcome of syndrome measurements, as it is usually the case for stabilizer-based quantum error correction protocols [214]. The overall quantum-error correction protocol for the squeezed cat code can therefore be considered *semi-autonomous*, in the sense that it requires periodic syndrome measurements but only an unconditional recovery operation, as the recovery operation does not depend on the state of the density matrix itself. A generalized procedure could, in principle, be developed for the squeezed cat code where the recovery is conditioned on the outcome of the syndrome measurement, probing the error sub-spaces. Although such an approach could further improve the error correction efficiency of the squeezed cat code, it is usually associated with additional resource costs in quantum hardware implementations.

It is important to note that the overall channel fidelity also depends on the displacement α and the squeezing ξ that define the code-words $|\mathcal{C}_{\alpha,\xi}\rangle$. An intuitive understanding of this can be given in terms of the probabilities of single-photon loss and dephasing events:

$$p_{\hat{a}} = \kappa_1\tau \langle \hat{a}^\dagger \hat{a} \rangle, \quad p_{\hat{a}^\dagger \hat{a}} = \kappa_2\tau \langle (\hat{a}^\dagger \hat{a})^2 \rangle. \quad (4.36)$$

Both single-photon loss probability $p_{\hat{a}}$ and dephasing probability $p_{\hat{a}^\dagger \hat{a}}$ grow with displacement α and squeezing ξ , therefore increasing the probability of these errors. At the same time, the capabilities of correcting these errors also increase.

As a result, depending on the dimensionless loss and dephasing rates $\kappa_1\tau$ and $\kappa_2\tau$, there exists optimal displacement α^* and squeezing parameters ξ^* , as well as an optimal recovery \mathcal{R}^* . Unfortunately, the encoding parameters α and ξ do not enter linearly in the definition of the code-words $|\mathcal{C}_{\alpha,\xi}^\pm\rangle$, and therefore a bi-convex optimization for both recovery *and* encoding is not possible [271]. We can, however, devise an iterative optimization scheme that globally optimizes the encoding parameters α and ξ in a restricted parameter regime, using derivative-free constrained optimization techniques [386, 387]. A sketch of the implementation is shown in Alg. 1, where we loop over a predefined regime of dimensionless noise parameters $\kappa_1\tau, \kappa_2\tau$ to obtain for each pair $[\kappa_1\tau, \kappa_2\tau]$ the optimized values of $\alpha^*, \xi^*, \mathcal{R}^*$ and its associated channel fidelity \mathcal{F} .

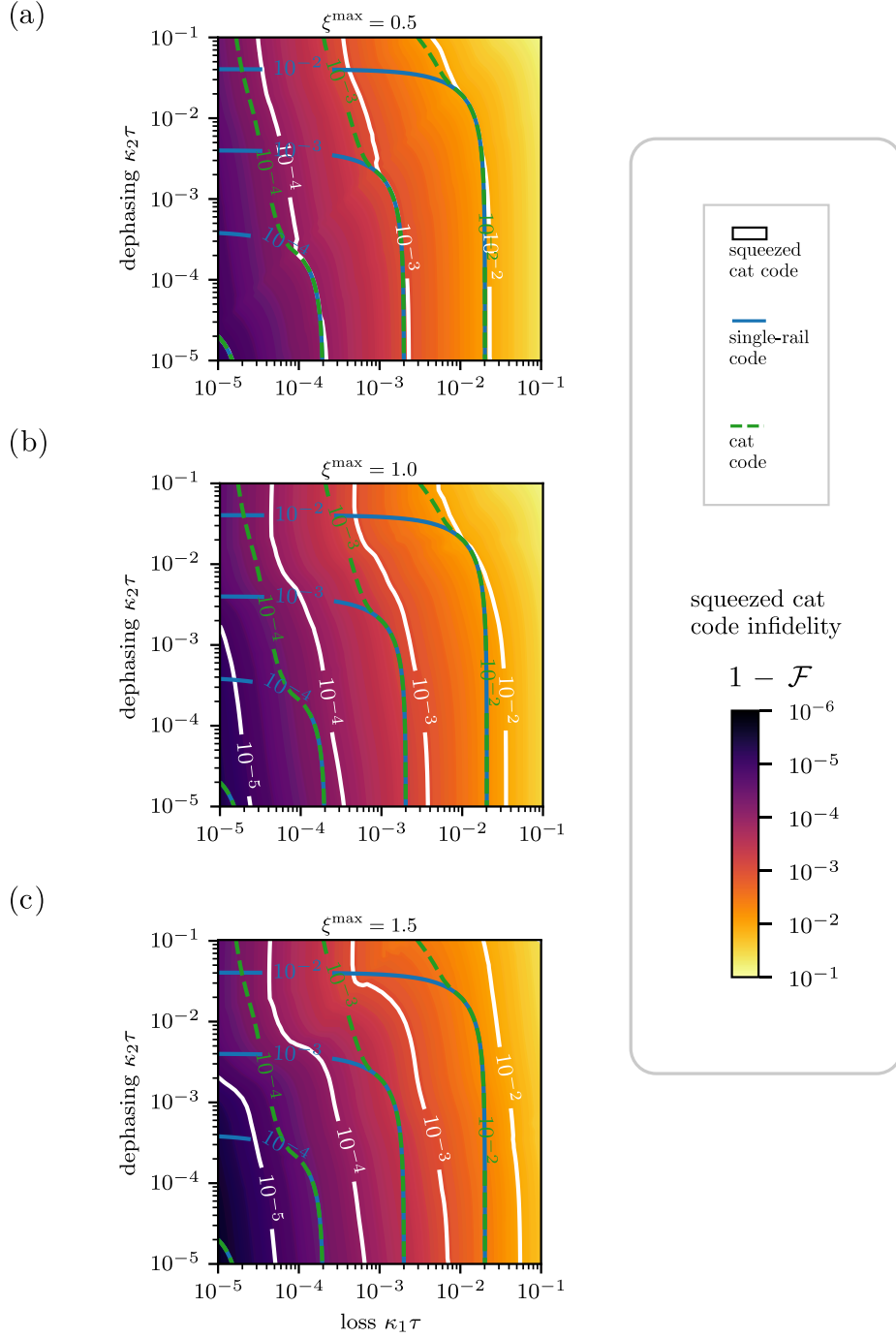


Figure 4.4: Optimal channel infidelity $1 - \mathcal{F}$ color map of the squeezed cat code for optimal encoding parameters α^* , ξ^* and recovery \mathcal{R}^* for the loss-dephasing channel as a function of dimensionless loss parameter $\kappa_1 \tau$ and dephasing parameter $\kappa_2 \tau$. We restrict the maximum squeezing to $\xi^{\max} = 0.5$ (a), 1.0 (b) and 1.5 (c). White contour lines represent channel infidelity isolines of the squeezed cat codes, while other isolines represent the channel infidelity for the single-rail code (blue) and the two-component cat code (green) with optimal recovery and encoding.

With the optimization procedure detailed above, we compute the optimal channel fidelity \mathcal{F} as a function of $\kappa_1\tau$ and $\kappa_2\tau$. As τ characterizes the duration of the noise channel or, equivalently, the time between two subsequent recoveries, a larger value of $\kappa_1\tau$ or $\kappa_2\tau$ either corresponds to stronger dissipation or longer intervals between two recoveries. In Fig. 4.4(a-c), we plot the channel infidelity $1 - \mathcal{F}$ as a function of $\kappa_1\tau$ and $\kappa_2\tau$, for three different values of maximal squeezing $\xi^{\max} = 0.5, 1.0,$ and 1.5 . White isolines highlight selected values of equal infidelity of the squeezed cat code.

We compare the squeezed cat code to two other bosonic codes that also admit a \mathbb{Z}_2 symmetry: First, the single-rail code, i.e., the encoding in the Fock states $|0\rangle$ and $|1\rangle$ for which the recovery operation is trivial, and second, the *optimal* two-component cat code for which we also optimize the recovery for the same set of errors $\{\hat{E}_k\}$ considered for the squeezed cat code as well as the displacement α .

An important reason for this choice of comparison is that all three bosonic codes are limiting cases of each other: The squeezed cat code entails the cat code (in the limit of vanishing squeezing), and the cat code entails the single-rail code (in the limit vanishing displacement). Hence, we have the general relation $\mathcal{F}^{\text{squeezed cat}} \geq \mathcal{F}^{\text{cat}} \geq \mathcal{F}^{\text{single-rail}}$. All three bosonic codes require at most quadratic operations for state-preparation and, therefore, are expected to require similar resources for experimental realizations.

We observe that for increasing the allowed maximum squeezing ξ^{\max} , the channel fidelity of the squeezed cat code increasingly improves upon the single-rail and the optimal cat code. We can identify three different regimes: (I) $\kappa_1 > \kappa_2$. In the regime where the channel is dominated by particle loss, the squeezed cat code slightly improves over the cat code for small squeezing (See Fig. 4.4(a)), but notably for larger squeezing (See Fig. 4.4(b-c)) due to the fact that the error-sub-spaces associated to single-photon loss become increasingly orthogonal to the code-space, demonstrating the partial correctability of single-photon loss errors. (II) $\kappa_1 < \kappa_2$. In the dephasing-dominated regime, the squeezed cat code outperforms the cat code, even for moderate squeezing of $\xi^{\max} = 0.5$, due to its double exponentially decreasing overlap $\langle \alpha, \xi | -\alpha, \xi \rangle$ with ξ , in agreement with recent experimental results [94, 352]. Also the cat code drastically outperforms the single-rail code in this regime due to the exponentially decreasing overlap $\langle \alpha | -\alpha \rangle$ with α . (III) $\kappa_1 \sim \kappa_2$. In the regime of comparable loss and dephasing rates – a relevant working regime for many quantum hardware platforms – the squeezed cat code also shows a significant improvement over the cat and single-rail codes for $\xi^{\max} > 0.5$.

In Fig. 4.5, we show the resulting optimal parameters for the code space as a function of $\kappa_1\tau$ and $\kappa_2\tau$. We observe that in most regimes, the optimal squeezing

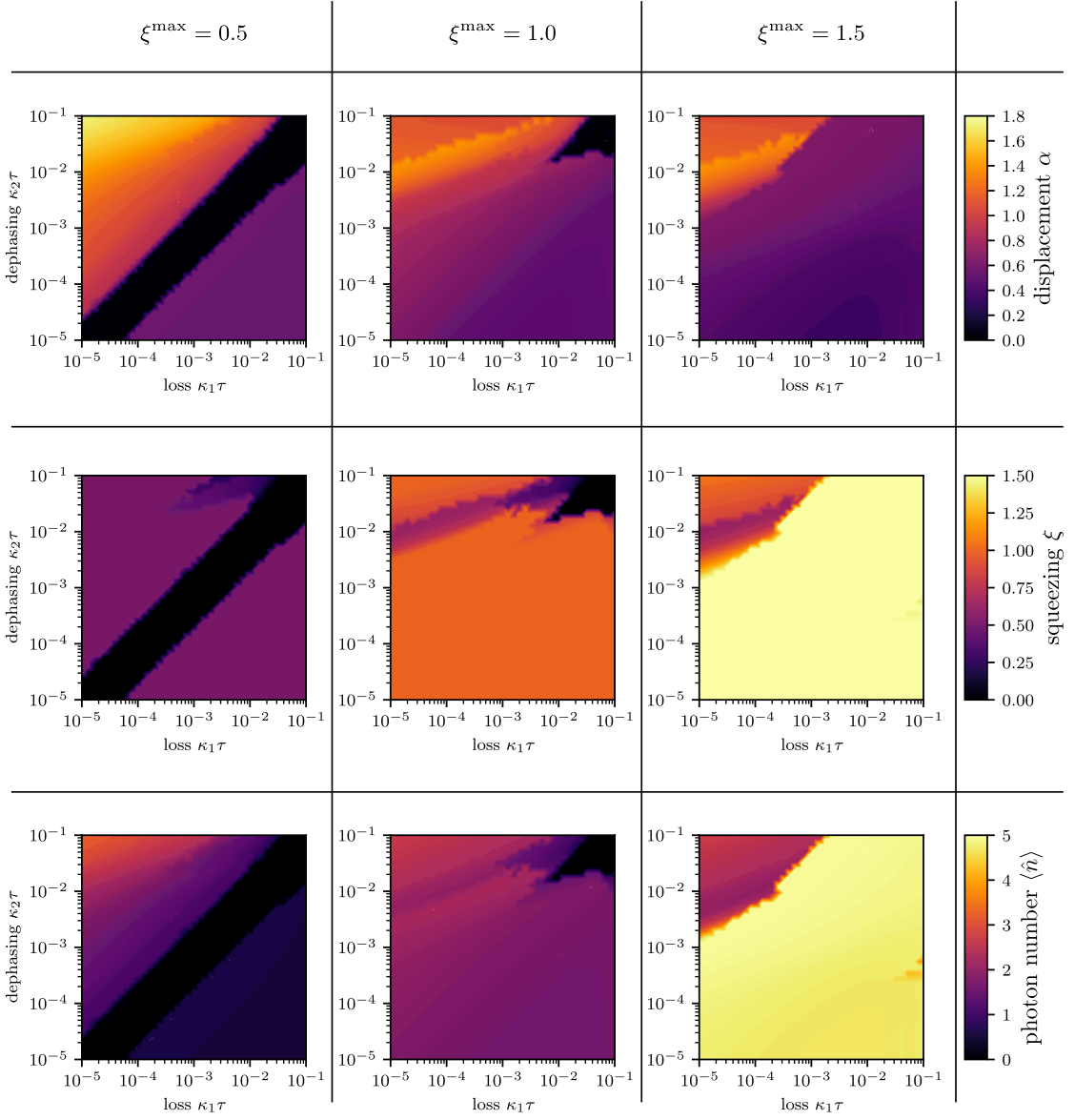


Figure 4.5: Optimized values of the displacement α (top row) and squeezing ξ (middle row) for different values of maximum squeezing $\xi^{\max} = 0.5$ (first column), 1.0 (second column), and 1.5 (third column) as a function of dimensionless loss rate $\kappa_1 \tau$ and dephasing rate $\kappa_2 \tau$. For comparison, we show the average photon number \hat{n} of the squeezed cat code in the last row.

saturates the maximum squeezing ξ^{\max} , while the displacement mostly grows with increasing dephasing rate $\kappa_2 \tau$. Especially we observe that in the loss-dominated regime, the displacement α is much smaller than the squeezing parameter ξ . Interestingly, we observe discontinuities for $\kappa_1 \sim \kappa_2$ and $\xi^{\max} = 0.5$, where the optimized parameters converged towards the single-rail encoding of $\xi = \alpha = 0$ (See Fig. 4.5). For $\xi^{\max} = 1.5$, we further observe a discontinuity in the dephasing-

dominated regime $\kappa_2 > \kappa_1$, for which the optimized encoding favors less squeezing, but large displacement and low average photon number compared to the other regimes.

III.2 Error correction in the quantum trajectory picture

We can illustrate the effect of the correction of photon loss in a recovery operation by considering the quantity

$$P(t) = 1 - \langle \mathcal{C}_{\alpha,\xi}^+ | \hat{\rho}(t) | \mathcal{C}_{\alpha,\xi}^+ \rangle, \quad (4.37)$$

which describes the difference in overlap between $\hat{\rho}(t)$ and the logical code-word $|\mathcal{C}_{\alpha,\xi}^+\rangle$. Let us assume an initial state $\hat{\rho}(0) = |\mathcal{C}_{\alpha,\xi}^+\rangle\langle\mathcal{C}_{\alpha,\xi}^+|$, for which $P(0) = 0$. In Fig. 4.6(a), we plot $P(t)$ as a function of time. We can sample individual quantum trajectories [101, 126, 128, 388, 389] from repeatedly applied channel $\mathcal{R} \circ e^{\mathcal{L}\tau}$, in close resemblance to a repeated recovery protocol, aiming to correct errors in the system. Note that in a quantum trajectory, due to information back-action, the system with initial state $|\psi(0)\rangle$ evolves according to the non-Hermitian effective Hamiltonian

$$\hat{H}_{\text{eff}} = -i\frac{\kappa_1}{2}\hat{a}^\dagger\hat{a} - i\frac{\kappa_2}{2}(\hat{a}^\dagger\hat{a})^2, \quad (4.38)$$

until a quantum jump with jump operators \hat{a} (for single-photon loss) or $\hat{a}^\dagger\hat{a}$ (for dephasing) occurs after a randomly chosen time-interval (See also Chap 2, Sec. IV). At multiples of the measurement time τ , the recovery operation acts on the time-evolved state $|\psi(t)\rangle$. We recover the Lindblad master equation of this quantum trajectory *unraveling* by averaging over the statistical ensemble of quantum trajectories. As individual quantum trajectories remain pure at all times, we have in this case

$$P(t) = 1 - |\langle \mathcal{C}_{\alpha,\xi}^+ | \psi(t) \rangle|^2, \quad (4.39)$$

with the initial state $|\psi(0)\rangle = |\mathcal{C}_{\alpha,\xi}^+\rangle$. In Fig. 4.6(a), we show three different sample trajectories in which (i) no error occurs, (ii) a loss event with operator \hat{a} occurs and is successfully corrected in the following recovery, and (iii) a loss event occurs, but is incorrectly identified and therefore not accurately corrected in the subsequent recovery. Note that even during intervals where no quantum jump occurs, the overlap with the initial state decreases due to the evolution under the non-Hermitian Hamiltonian in Eq. (4.38). In the absence of errors, the recovery operation reverses this non-Hermitian evolution by projecting the system back to the code space. In case (ii), in which a quantum jump with operator \hat{a} occurs and is accurately corrected, the projective syndrome measurement included in the recovery correctly identifies the error by projecting the error on the photon-

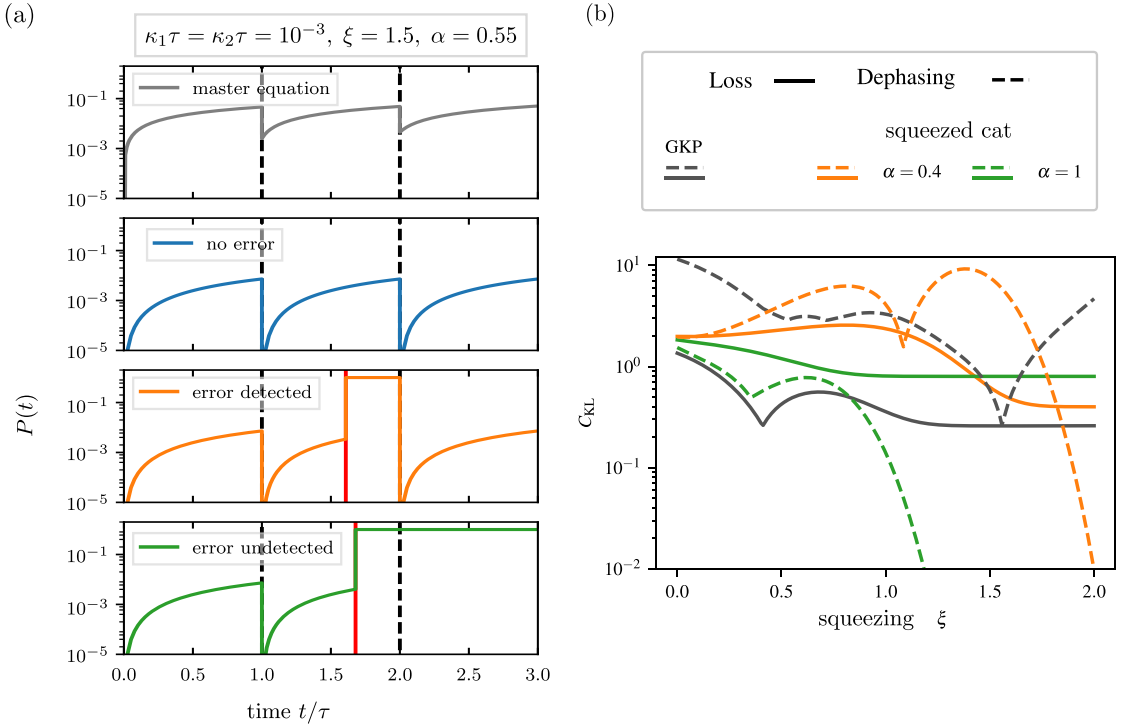


Figure 4.6: (a) $P(t)$ as defined in Eqs.(4.37) and (4.39) of a quantum state initially prepared in $|\mathcal{C}_{\alpha,\xi}^+\rangle$ as it evolves in time under the loss-dephasing channel and repeated recovery operation at multiples of time τ , shown as black dashed lines. In the first row, we show the full master equation evolution. In the second to last row, we show quantum trajectories in which no error occurs (second row), an error occurred (red line) and is correctly identified and corrected (third row), and an error occurred but is not correctly identified and, therefore uncorrected (last row). (b) Knill-Laflamme cost function C_{KL} , defined in Chap. 3, Sec. III, Eq. (3.52) as a function of squeezing parameter for the GKP code (grey), and the squeezed cat code for $\alpha = 0.4$ (orange) and $\alpha = 1$ (green) for the error set $\{\hat{1}, \hat{a}\}$ (loss, solid lines) and for the error set $\{\hat{1}, \hat{a}^\dagger \hat{a}\}$ (dephasing, dashed lines).

loss error sub-space (instead of another error sub-space). The recovery can be viewed as subsequently correcting the error by rotating the error sub-space and projecting the state back onto the code space. Immediately after the occurrence of the quantum jump, we have $P(t) = 1$, due to the fact that $|\psi(t)\rangle$ transforms into a state with opposite parity, and $P(t) = 0$, immediately after the successful recovery. For case (iii), the recovery operation is unsuccessful in correcting the error, as the syndrome measurement erroneously projects the system back onto the code space instead of the associated error sub-space due to their final overlap of sub-spaces. We can obtain the quantity $P(t)$, shown in the top panel of Fig. 4.6(a) obtained from integrating the full Lindblad master equation and applying the recovery map from ensemble-averaging over quantum trajectories. The analysis of individual

quantum trajectories, however, gives an intuitive picture of the recovery process and highlights the effectiveness of the error detection and correction procedure.

III.3 Comparison between the squeezed cat code and the GKP code

We can compare the error correction properties of the squeezed cat code with those of the finite-energy GKP code [341] (See Chap. 3, Sec. VII for details on the GKP code). Here, we assume a Gaussian envelope of the GKP code-words $|\mu\rangle$, with $\mu \in \{0, 1\}$

$$|\mu(\Delta)\rangle \propto e^{-\Delta^2 \hat{a}^\dagger \hat{a}} |\mu\rangle \quad (4.40)$$

The GKP code-words are in the ideal limit (See also Chap. 3, Sec. VII)

$$|\mu\rangle \propto \sum_{k,l=-\infty}^{\infty} e^{-i\pi(kl+\mu/2)} \hat{D}((2k+\mu)\alpha + l\beta) |0\rangle \quad (4.41)$$

To explicitly relate the GKP code to the squeezed cat code, we can express the finite-energy GKP code-words in terms of the squeezing operator as [236]

$$|\mu(\Delta)\rangle \propto \sum_{n \in \mathbb{Z}} e^{-\frac{\pi}{2} \Delta^2 (2n+\mu)^2} \hat{D}\left(\sqrt{\frac{\pi}{2}}(2n+\mu)\right) \hat{S}(-\ln \Delta) |0\rangle. \quad (4.42)$$

We can thus identify the squeezing parameter of the GKP due to its finite energy as $\xi = -\ln(\Delta)$. We can now compare the performance of the GKP code and the squeezed cat code for the same value of squeezing parameter ξ . As a metric, we use the Knill-Laflamme cost function $C_{\text{KL}}\{\hat{E}_k\}$, introduced in Chap. 3, Sec. V.3.

In Fig. 4.6(b), we show C_{KL} as a function of the squeezing parameter ξ for the squeezed cat code for two different values of α and for the GKP code. We consider the two error sets $\{\hat{\mathbb{1}}, \hat{a}\}$ for loss (solid lines) and $\{\hat{\mathbb{1}}, \hat{a}^\dagger \hat{a}\}$ for dephasing (dashed lines). We observe that the cost function C_{KL} for loss shows similar features for the GKP code and the squeezed cat code and saturates to a finite value for large squeezing that depend on the value of α in the case of the squeezed cat code. For dephasing, the Knill-Laflamme cost function rapidly approaches zero as α increases for the squeezed cat code. On the other hand, C_{KL} grows indefinitely for the GKP code in this case for large squeezing. This analysis clearly highlights the difference between the squeezed cat code and the GKP code with respect to their correctability of loss and dephasing errors, and shows how the squeezed cat code takes advantage of squeezing as a quantum error correction resource. This further corroborates results on the analysis of optimal bosonic codes for the loss-dephasing

channel [256], showing that the performance of GKP and squeezed cat code highly depends on the noise regime they are subjected to.

IV Approaches to Experimental Realization

Here, we discuss how the squeezed cat code can be implemented in experimental platforms.

Squeezed cat states have been experimentally realized in various ways in quantum optical setups [94, 348, 390] and trapped ion devices [352, 391], while their time dynamics and robustness against photon loss have only been experimentally probed using an optical parametric process [351]. Very recently, the increased protection of the non-Gaussian interference features of the squeezed cat has been experimentally verified in superconducting microwave 3D cavity designs [94]. The authors in Ref. [94] used conditional displacement operations, employing only the native cavity and transmon gates to generate superpositions of the states $|\alpha, \xi\rangle$ and $|- \alpha, \xi\rangle$, thereby overcoming previous obstacles of implementing fast non-linear controls for the state preparation without introducing excessive non-linear effects in the bosonic mode. This setup, however, did not implement the semi-autonomous recovery protocol to *actively* correct errors, but only makes use of the slowed decoherence due to squeezing that compress cat states in phase space.

IV.1 Dissipative stabilization of squeezed cat states

In the previous sections, we have assumed an active recovery operation \mathcal{R} that detects and corrects errors generated from a finite error set. It remains a challenging task to engineer these targeted optimized recovery operations in experimental setups as they generally require strong non-linearities.

We can, however, employ autonomous quantum error correction schemes through engineered dissipation that stabilizes the code manifold of squeezed cat states [392] (See Chap. 3, Sec. VI.2 for details on dissipation engineering), similar to the dissipative stabilization techniques used for the stabilization of regular cat qubits [81, 82, 290]. We here detail two dissipative stabilization approaches: The first is a straightforward extension of the cat qubit stabilization to squeezed modes. The second approach takes into account the autonomous correction of photon-loss errors using a conditional dissipator, explored in Ref. [83].

For the first approach, we recall from Eq. (4.10) that a squeezed state $|\alpha, \xi\rangle$ is an eigenstate of $\hat{s} = \hat{S}(\xi)\hat{a}\hat{S}^\dagger(\xi)$ with eigenvalue ζ , defined in Eq. (4.8). From this relation, it is straightforward to show that squeezed cat states are degenerate

eigenstates of \hat{s}^2 ,

$$\hat{s}^2 |\mathcal{C}_{\alpha,\xi}^\pm\rangle = \zeta^2 |\mathcal{C}_{\alpha,\xi}^\pm\rangle. \quad (4.43)$$

As a consequence, the squeezed cat code manifold can be dissipatively stabilized with the dissipator $\mathcal{D}[\hat{s}^2 - \zeta^2]$, such that

$$\kappa \mathcal{D}[\hat{s}^2 - \zeta^2] (|\mathcal{C}_{\alpha,\xi}^\mu\rangle\langle\mathcal{C}_{\alpha,\xi}^\nu|) = 0, \quad (4.44)$$

with $\mu, \nu \in \{+, -\}$, and dissipation rate κ . We can transform the purely dissipative process into the following Liouvillian [393]:

$$\mathcal{L}(\hat{\rho}) = -i[\Omega\hat{s}^{2\dagger} + \Omega^*\hat{s}^2, \hat{\rho}] + \kappa\mathcal{D}[\hat{s}^2](\hat{\rho}), \quad (4.45)$$

with $\zeta^2 = -2i\Omega/\kappa$. In Eq. (4.45), we can identify a coherent part with $\hat{H} = \Omega\hat{s}^{2\dagger} + \Omega^*\hat{s}^2$, corresponding to a two-photon drive of a squeezed mode, with drive amplitude Ω .

To further analyze the effect of errors, we can choose a subsystem decomposition for the squeezed cat qubit, explained in detail in Chap. 3, Sec. VI.1, by defining the states

$$|\mathcal{C}_{\alpha,\xi}^\pm\rangle_{\text{L}} \otimes |n\rangle_{\text{g}} \approx \frac{1}{N_\zeta^\pm} \hat{S}(\xi) [\hat{D}(\zeta) \pm (-1)^n \hat{D}(-\zeta)] |n\rangle, \quad (4.46)$$

where the approximate equality is due to the fact that the right-hand side should be orthonormalized within each parity sector. In this notation, $|\mathcal{C}_{\alpha,\xi}^\pm\rangle_{\text{L}} \otimes |n=0\rangle_{\text{g}} = |\mathcal{C}_{\alpha,\xi}^\pm\rangle$, i.e. the code-space is the two-dimensional manifold in which the gauge mode is in the ground state.

In this picture, the action of \hat{a} becomes more intuitive:

$$\hat{a} = \hat{X}_{\text{L}} \otimes (e^{-r}\zeta + \cosh(r)\tilde{a} - \sinh(r)\tilde{a}^\dagger) + \mathcal{O}(e^{-2\zeta^2}), \quad (4.47)$$

where we have used the notation $\tilde{a} = \sum_{n=0}^{\infty} \sqrt{n+1} |n\rangle_{\text{g}} \langle n+1|$ to represent the annihilation operator of the gauge mode.

For the dissipative stabilization of the squeezed cat code in Eq. (4.44), the jump operator $\hat{L}' \equiv \hat{s}^2 - \zeta^2$ is decomposed in the subsystem decomposition as follows,

$$\hat{L}' \equiv (\hat{s}^2 - \zeta^2) \approx \hat{\mathbf{1}}_{\text{L}} \otimes 2\zeta\tilde{a}, \quad (4.48)$$

where we neglected higher order terms, from which it becomes clear that the code space is acted upon with the identity operator. We see that although \hat{L}' in Eq. (4.48) drives states back to the original code space manifold, the induced

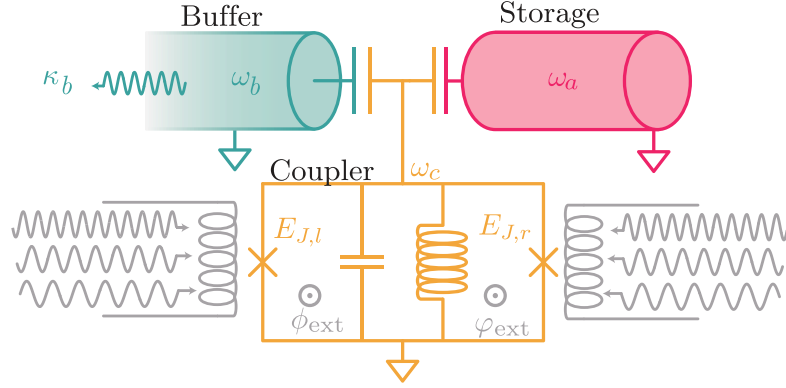


Figure 4.7: Schematic illustration of a circuit QED implementation autonomously stabilizing the squeezed cat qubit. The storage (target) mode (red) is coupled to a strongly dissipative buffer mode (turquoise) and an ATS coupler (orange). The coupler is flux-pumped with three tones to enable the targeted three-wave mixing interaction to realize an effective two-photon interaction of a squeezed storage mode. Figure adapted from Ref. [392] with slight modifications.

bit-flip of \hat{a} in Eq. (4.47), remains uncorrected. Nevertheless, we can make use of enhanced noise-bias of the logical errors, outperforming the cat-qubit.

IV.2 Physical implementation

It should be noted that experimentally stabilizing the squeezed cat code manifold is a matter of active research [83, 392]. Let us nonetheless give an approach to a realization on superconducting circuits, following Ref. [392]. Analogous to the cat code stabilization, the main goal is the generation of an interaction Hamiltonian that exchanges photons of a buffer mode \hat{b} with two-photons of a squeezed mode \hat{s} :

$$\begin{aligned} \hat{H} &= g\hat{s}^2\hat{b}^\dagger + \text{h.c.} \\ &= g\left(\cosh(r)\hat{a} - \sinh(r)\hat{a}^\dagger\right)^2\hat{b}^\dagger + \text{h.c.} \end{aligned} \quad (4.49)$$

In the limit of strong dissipation in the buffer mode, adiabatic elimination yields the targeted squeezed two-photon interaction and dissipation. Similar to the cat-qubit stabilization techniques on superconducting circuits [72], we can couple the buffer mode to the storage mode using a non-linear coupler, provided by an asymmetrically threaded SQUID (ATS), as schematically shown in Fig. 4.7. The microscopic Hamiltonian reads

$$\hat{H} = \omega_a\hat{a}^\dagger\hat{a} + \omega_b\hat{b}^\dagger\hat{b} + \omega_c\hat{c}^\dagger\hat{c} - 2E_J\varphi(t)\sin(\hat{\varphi}). \quad (4.50)$$

Here ω_a , ω_b , and ω_c represent the frequencies of the target mode, buffer mode, and coupler, respectively, and E_J is the Josephson energy. $\hat{\varphi}$ describes the hybridized mode in the non-linear coupler and is given by $\hat{\varphi} = (\varphi_a \hat{a} + \varphi_b \hat{b} + \varphi_c \hat{c} + \text{h.c.})$, with φ_a , φ_b , and φ_c being the respective participation ratios of the modes in the Josephson element that depend on microscopic circuit parameters. $\varphi(t)$ represents a modulation of the ATS flux bias. Expanding the above Hamiltonian of the ATS interaction up to third order yields

$$\hat{H} = \omega_a \hat{a}^\dagger \hat{a} + \omega_b \hat{b}^\dagger \hat{b} + \omega_c \hat{c}^\dagger \hat{c} - 2E_J \left[\varphi(t) \hat{\varphi} - \varphi(t) \frac{\hat{\varphi}^3}{6} \right] \quad (4.51)$$

We can apply a three-tone modulation of the flux bias, yielding

$$\varphi(t) = \epsilon_1 \cos(\omega_1 t) + \epsilon_2 \cos(\omega_2 t) + \epsilon_3 \sin(\omega_3 t). \quad (4.52)$$

We can enter a displaced frame [136], through the unitary

$$\hat{U}_D = \exp \left(\xi_a^* \hat{a} - \xi_a \hat{a}^\dagger + \xi_b^* \hat{b} - \xi_b \hat{b}^\dagger + \xi_c^* \hat{c} - \xi_c \hat{c}^\dagger \right), \quad (4.53)$$

with time-dependent parameters ξ_a , ξ_b , ξ_c . For the continuous wave drives in Eq. (4.52), the parameters ξ_x are the solution of the differential equations

$$\frac{d\xi_x}{dt} = - \left(\frac{\kappa_x}{2} + i\omega_x \right) \xi_x - iE_J \varphi(t), \quad \Rightarrow \quad \xi_x(t) = \sum_{k=1}^3 \frac{E_J \varphi_x e^{-i\omega_k t}}{i\kappa_x/2 - |\omega_k - \omega_x|}, \quad (4.54)$$

where κ_x is the decay rate of the respective mode. In this displaced frame, the linear term $\hat{\varphi}$ in \hat{H} is removed and the Hamiltonian reads

$$\hat{H} = \omega_a \hat{a}^\dagger \hat{a} + \omega_b \hat{b}^\dagger \hat{b} + \omega_c \hat{c}^\dagger \hat{c} + E_J \varphi(t) \frac{\tilde{\varphi}^3}{3}, \quad \text{with} \quad (4.55)$$

$$\tilde{\varphi} = \varphi_a (\hat{a} + \xi_a) + \varphi_b (\hat{b} + \xi_b) + \varphi_c (\hat{c} + \xi_c). \quad (4.56)$$

We can now apply the frequency matching conditions for the target interaction Hamiltonian in Eq. (4.49):

$$\omega_1 = 2\omega_a - \omega_b, \quad \omega_2 = 2\omega_a + \omega_b, \quad \omega_3 = \omega_b. \quad (4.57)$$

Furthermore, to match the right coefficients ($\cosh(r)$ and $-\sinh(r)$), we can choose the flux-pump amplitudes as

$$\epsilon_1(r) = \epsilon \cosh^2(r), \quad \epsilon_2(r) = \epsilon \sinh^2(r), \quad \epsilon_3(r) = \epsilon \sinh(2r), \quad (4.58)$$

with the driving strength of the drive tones $|\epsilon| \ll 1$. Choosing $\omega_3 = \omega_b$ creates a single-photon drive in the buffer mode:

$$\hat{H}_{\text{drive}} = \tilde{F}^* \hat{b} + \tilde{F} \hat{b}^\dagger, \quad \text{with} \quad \tilde{F} \approx \frac{iE_J \epsilon_3(r) \varphi_b^2}{\kappa_b/2}, \quad (4.59)$$

where here we have assumed that $\kappa_b \gg \kappa_a, \kappa_c$. As the strength of the drive \tilde{F} is given by the microscopic properties of the system, we can add a resonant single-photon drive on the buffer mode, to reach stabilized cat states with arbitrary displacement α . We absorb the microscopic Hamiltonian in Eq. (4.59) into an effective single photon drive with effective drive amplitude $F = -g\alpha^2 e^{2r}$.

To obtain an effective description in the buffer mode, we can further assume $\kappa_b \gg g \cosh(r)$ to adiabatically eliminate buffer mode, to finally obtain the squeezed two-photon dissipator

$$\kappa_2 \mathcal{D}[b^2 - \xi^2], \quad \text{with} \quad \kappa_2 = \frac{4g^2}{\kappa_b}. \quad (4.60)$$

IV.3 Dissipation Engineering with bit-flip suppression

As the phase flip error rate induced by dephasing is already exponentially suppressed in ζ , the main error is the bit-flip induced by photon loss, which we address below.

In the approach detailed above, single-photon loss events that flip the parity of code-words, remain uncorrected, as the jump operator $\hat{L}' = \hat{b}^2 - \zeta^2$ in Eq. (4.44) remains invariant under change of parity $\hat{b} \rightarrow -\hat{b}$ that defines the logical \hat{Z}_L eigenstates of the squeezed cat code. To counteract the action of \hat{a} , an operator performing \hat{X}_L while at the same time driving excitations in the gauge mode to the ground state, has to be engineered. To address this, let us detail the second approach that autonomously corrects loss errors using a conditional dissipation, proposed in Ref. [83].

An intuitive picture gives the action of \hat{a} on one of the code-words in the subsystem decomposition:

$$\hat{a} \left(\left| \mathcal{C}_{\alpha,\xi}^+ \right\rangle_L \otimes |0\rangle_g \right) = \left| \mathcal{C}_{\alpha,\xi}^- \right\rangle_L \otimes \sqrt{\bar{n}} (\sqrt{\eta} |0\rangle_g - \sqrt{1-\eta} |1\rangle_g), \quad (4.61)$$

with $\eta \equiv (\bar{n} - \sinh^2(r))/\bar{n}$, and \bar{n} describing the average photon number of the code-words. To make use of the loss correction, we can define the jump operator

$$\hat{L} = (\hat{X}_L \otimes \tilde{I})(\hat{b}^2 - \zeta^2) \approx \hat{X}_L \otimes 2\zeta \tilde{a}. \quad (4.62)$$

We can construct the term $\hat{X}_L \otimes \tilde{I}$ from squeezing a linear combination of operators $c_1 \hat{a} + c_2 \hat{a}^\dagger$, with $c_1 + c_2 = 1$:

$$\frac{1}{\zeta} \hat{S}(\xi) (c_1 \hat{a} + c_2 \hat{a}^\dagger) \hat{S}^\dagger(\xi) = \hat{X}_L \otimes \left[\tilde{I} + \frac{1}{\zeta} (c_1 \tilde{a} + c_2 \tilde{a}^\dagger) \right] + \mathcal{O}(e^{-2\zeta^2}) \approx \hat{X}_L \otimes \tilde{I}, \quad (4.63)$$

where the last approximation holds when $\zeta \gg 1$. As a result, we can engineer a dissipator

$$\hat{L} = \frac{1}{\zeta} \hat{S}(\xi) (c_1 \hat{a} + c_2 \hat{a}^\dagger) (\hat{a}^2 - \zeta^2) \hat{S}^\dagger(\xi) \approx \hat{X}_L \otimes 2\zeta \tilde{a}, \quad (4.64)$$

that engineers the target jump operator in the limit of $\zeta \gg 1$ [83]. In [83], a proposal to realize such a conditional dissipator was explored using trapped ion setups. It remains an active question, how to engineer such dissipation on superconducting circuit devices.

V Discussion and Outlook

In this chapter, we have explored the error correction capabilities of the *squeezed cat code*. In Sec. I, we have introduced squeezed states and defined the logical code-words $|\mathcal{C}_{\alpha,\xi}^\pm\rangle$. We have shown that in the limit of large squeezing, the squeezed cat code admits discrete translation invariance in the direction of the squeezing quadrature, thus showing an interesting relation to the translation-symmetric GKP code which admits discrete translation invariance in both quadratures. The code-words of the squeezed cat code can be engineered in various ways and have been experimentally realized on various platforms [94, 348, 351, 390], with results showcasing the enhanced robustness against dephasing [94]. Notably, since our proposal of the squeezed cat for quantum error correction, different schemes have been proposed to dissipatively stabilize the squeezed cat code in superconducting circuits [392] and trapped ion systems [83]. We have analyzed quantum error correction conditions in terms of the Knill-Laflamme conditions for discrete errors in Sec. II, where we have analytically shown that the squeezed cat code possesses a double-exponential suppression with respect to dephasing in the squeezing parameter while at the same time being able to correct for loss errors by reducing the displacement. In the limit of large squeezing and small displacement, we have shown that single-photon loss and dephasing errors become perfectly correctable. This is a major advantage over the standard two-component cat code, for which the error rate associated to photon loss grows linearly with the displacement α . While this theoretical regime is typically constrained by hardware devices, we analyzed the correctability of errors of the squeezed cat code subject to the full continuous loss-dephasing channel for finite squeezing in Sec. III. For

this, we proposed a periodic recovery that aims to optimally correct the errors incurred by noise channel. By using a *semidefinite program*, we have numerically optimized the recovery operation to maximize the channel fidelity of the combined noise channel and recovery channel by finding optimal recovery operations transforming first-order error sub-spaces of the noise channel back to the code space. We also optimized the encoding parameters of the squeezed cat code to reach the optimal squeezed cat encoding for different regimes of loss and dephasing rates. Our results reveal that even for experimentally reachable values of the squeezing parameter, the correctability against loss and dephasing can be significantly increased, when compared to the standard cat code. In our analysis, we have shown that the squeezed cat shows promising properties as a strongly noise-biased bosonic qubit in which the phase-flip error rate is double-exponentially suppressed in the squeezing parameter, and hence we expect the implementation of autonomously stabilized squeezed cat qubits and concatenation with discrete-variable encodings in the near future.

5

Variational Simulation of Bosonic Open Quantum Systems

Simulating the dynamics and steady-state properties of interacting bosonic systems coupled to an environment has been a matter of active research for several decades. As the size of a quantum system increases, the full Hilbert space grows exponentially, making direct classical simulation of a large closed many-body system generally impossible. Furthermore, in open quantum systems, states are characterized by the system's density matrix, an element of linear operators acting on the Hilbert space \mathcal{H} . Describing a density matrix thus requires $\dim(\mathcal{H})^2$ elements, making simulations of large systems even more challenging compared to closed quantum systems, in which only $\dim(\mathcal{H})$ elements are needed to describe the quantum state.

Variational methods provide one of many promising frameworks to simulate the dynamics of closed and open quantum systems, which we will consider in more detail in this chapter. These methods for simulating quantum systems use a restricted subspace of the Hilbert space to avoid the computational challenges associated with a prohibitively large Hilbert space. These restricted subspaces are often motivated physically, as the dynamics of most quantum systems are naturally bounded to a narrow corner of the Hilbert space [144, 394].

In bosonic systems, the Hilbert space is infinite-dimensional, and hence, the need to capture the *relevant* part of the Hilbert space that contributes to the time evolution or steady-state of a system in consideration becomes even more apparent. Simulating the time evolution of bosonic systems is a crucial task for understanding the behavior of dynamical systems, such as bosonic quantum gates for quantum information processing, dynamical phase transitions, and quench dynamics. Simulating the dynamical behavior of bosonic systems in the context of quantum information processing, in particular, is an essential task to understand how quantum gates affect the encoded quantum state as quantum states may temporarily depart from the original manifold that encodes the quantum bit. Hence, simulating the dynamics of bosonic quantum gates gives important insight into code-subspace leakage, code-deformation, and sources of errors that might occur

along the dynamics. It further provides means to optimize quantum gates for higher-fidelity and faster quantum gates.

In the following, therefore, we will focus on the simulation of the dynamics of open many-boson quantum systems.

In Sec. I, we introduce different variational principles for open quantum systems that are equivalent under some assumptions. In Sec. II, we specifically consider a time-dependent and non-orthonormal parametrization of the basis and derive the general equations of motion. We propose the *coherent-state ladder* [β] in Sec. III that uses a parametrized basis of photon-added unnormalized coherent states and derive the resulting equations of motion using a time-dependent variational principle in Sec. IV. In Sec. V, we detail its numerical implementation and provide an analytical approach to calculate the Fidelity and Wigner function in Sec. VI. We showcase the method on various examples in Sec. VII. We further extend our developed method to include discrete rotational symmetries and propose the *cat-state ladder* time-dependent variational principle in Sec. VIII and give some examples for the simulation of single and multiple cat-qubit dynamics in Sec. IX. Finally, we formulate approaches that go beyond the coherent-state and cat-state ladder variational methods in Sec. X and conclude this chapter in Sec. XI.

I Variational Principles for Open Quantum Systems

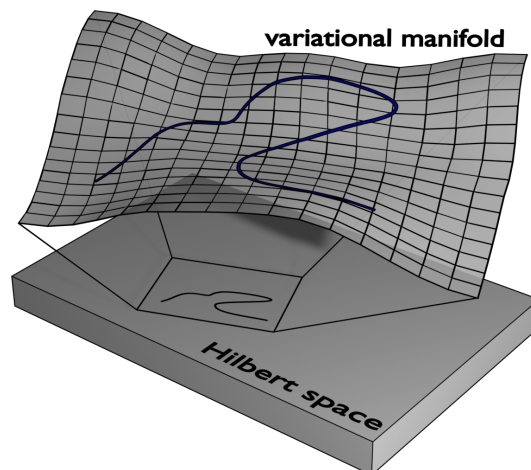


Figure 5.1: Schematic representation of the variational principle: The state-space is restricted to a variational manifold – subspace of the full Hilbert space. The evolution of the parameters in the variational manifold represents an evolution within the variational subspace.

In the following, we detail three different variational principles; the Dirac-Frenkel variational principle, McLachlan's variational principle, and the time-dependent variational principle (TDVP). Despite the different approaches of these variational principles, they can be shown to yield the same equations of motion for the variational parameters under certain conditions [100].

We suppose that the system's density matrix $\hat{\rho}$ is parametrized by a set of variational parameters $\vec{\theta}$, i.e. $\hat{\rho}(t) = \hat{\rho}(\vec{\theta}(t))$. We then want to describe the (real or imaginary) time evolution through the time-evolution of the parameters $\vec{\theta}$.

Dirac-Frenkel variational principle

The Liouvillian action on $\hat{\rho}$ can be expressed in terms of the variational parameters $\vec{\theta}$,

$$\mathcal{L}(\hat{\rho}) \approx \sum_i \frac{\partial \hat{\rho}(\vec{\theta}(t))}{\partial \theta_i} \frac{\partial \theta_i}{\partial t}. \quad (5.1)$$

The derivative $\frac{\partial \hat{\rho}(\vec{\theta}(t))}{\partial t} = \sum_i \frac{\partial \hat{\rho}(\vec{\theta}(t))}{\partial \theta_i} \frac{\partial \theta_i}{\partial t}$ lies in the tangent subspace of $\{\frac{\partial \hat{\rho}(\vec{\theta}(t))}{\partial \theta_i}\}$. But $\mathcal{L}(\hat{\rho})$ may not lie in this subspace. Therefore, we can project the left-hand side of Eq. (5.1) onto the subspace spanned by $\{\frac{\partial \hat{\rho}(\vec{\theta}(t))}{\partial \theta_i}\}$, yielding the Dirac and Frenkel variational principle [395, 396],

$$\text{Tr} \left[(\delta \hat{\rho}(\vec{\theta}(t)))^\dagger \left(\frac{d\hat{\rho}}{dt} - \mathcal{L}(\hat{\rho}) \right) \right] = 0. \quad (5.2)$$

Here, the infinitesimal variation $\delta \hat{\rho}$ is given by

$$\delta \hat{\rho} = \sum_i \frac{\partial \hat{\rho}}{\partial \theta_i} \delta \theta_i. \quad (5.3)$$

The evolution of the parameters $\vec{\theta}$ can be solved to be

$$\sum_j M_{i,j} \dot{\theta}_j = V_i, \quad (5.4)$$

with matrix \mathbf{M} and vector \vec{V} defined as

$$\begin{aligned} M_{i,j} &= \text{Tr} \left[\left(\frac{\partial \hat{\rho}(\vec{\theta}(t))}{\partial \theta_i} \right)^\dagger \frac{\partial \hat{\rho}(\vec{\theta}(t))}{\partial \theta_j} \right], \\ V_i &= \text{Tr} \left[\left(\frac{\partial \hat{\rho}(\vec{\theta}(t))}{\partial \theta_i} \right)^\dagger \mathcal{L}(\hat{\rho}) \right]. \end{aligned} \quad (5.5)$$

In general, $\vec{\theta}$ can be complex, so that $\frac{\partial \hat{\rho}(\vec{\theta}(t))}{\partial \theta_j} \neq \left(\frac{\partial \hat{\rho}(\vec{\theta}(t))}{\partial \theta_i} \right)^\dagger$, in which case \mathbf{M} , \vec{V} , and $\dot{\vec{\theta}}$ are in general also complex.

McLachlan's variational principle

The variational principle by McLachlan [397] aims to minimize the distance between the evolution of the parametrized state and the true evolution by the Liouvilian, yielding

$$\delta \left\| \frac{\partial \hat{\rho}(\theta)(t)}{\partial t} - \mathcal{L}(\hat{\rho}) \right\| = 0, \quad (5.6)$$

with the Frobenius norm of matrices $\|\hat{O}\| = \sqrt{\text{Tr}[\hat{O}^\dagger \hat{O}]}$.

Using a distance measure as in Eq. (5.6), we can obtain the distance between the parametrized state and the true evolution,

$$\|d\hat{\rho}/dt - \mathcal{L}(\hat{\rho})\|^2 = \sum_{i,j} M_{i,j} \dot{\theta}_i \dot{\theta}_j - 2 \sum_i V_i \dot{\theta}_i + \text{Tr} [\mathcal{L}(\hat{\rho})^2]. \quad (5.7)$$

The resulting equation of motion for $\vec{\theta}$ can be shown to be equivalent to the Dirac-Frenkel variational principle.

Time-dependent variational principle

In the time-dependent variational principle [398] (TDVP), we can define a Lagrangian by

$$L = \text{Tr} \left[\hat{\rho}(\vec{\theta}(t))^\dagger (d\hat{\rho}(\vec{\theta}(t))/dt - \mathcal{L}(\hat{\rho})) \right] \quad (5.8)$$

Applying the Euler-Lagrange equations, we recover the time-evolution for $\hat{\rho}$, $d\hat{\rho}/dt = \mathcal{L}(\hat{\rho})$. Assuming that $\vec{\theta}$ is complex, $\hat{\rho}$ and $\hat{\rho}^\dagger$ can be considered independent. Applying the Euler-Lagrange equation to $\vec{\theta}^*$ yields again the same evolution as for the Dirac-Frenkel variational principle. If $\vec{\theta}$ is real however, the Euler-Lagrange equation cannot lead to an equation of motion for $\vec{\theta}$.

II Time-dependent Basis

There are many different possibilities of parametrizing the density matrix $\hat{\rho}(t) = \hat{\rho}(\vec{\theta}(t))$, that are typically tailored to the specific problem or the ease of implementation. In a pure-state context e.g., a quantum state $|\psi\rangle$ can be parametrized using a set of unitaries $\{\hat{U}_i(\vec{\theta})\}$. For two-level systems, such approaches can be implemented on a quantum computer [100]. These approaches use a fixed computa-

tional basis, where variations in the state correspond to variations in parametrized operators acting on it.

An alternative approach – that we will explore in more detail here – is to introduce a time-dependent basis, where the basis itself is parametrized by variational parameters. We define the subspace $\text{Span}(\mathcal{S}) \subset \mathcal{H}$, parametrized by $\vec{\theta}$, as

$$\mathcal{S} = \{ |\varphi_k(\vec{\theta})\rangle; k = 1, \dots, N_{\text{basis}} \}, \quad (5.9)$$

where $|\varphi_k(\vec{\theta})\rangle$ are the basis states of \mathcal{S} and $N_{\text{basis}} < \dim(\mathcal{H})$ is the number of basis states. It is important to note that the basis states $|\varphi_k(\vec{\theta})\rangle$ are not assumed to be mutually orthogonal, and hence the overlap matrix \mathbf{S} defined by

$$S_{i,j} = \langle \varphi_i(\vec{\theta}) | \varphi_j(\vec{\theta}) \rangle \quad (5.10)$$

is in general non-diagonal. We now detail some important properties resulting from non-orthogonality \mathcal{S} and requirements for a variational principle. To facilitate the notation, we omit the explicit dependence of $\vec{\theta}$ from now on, except where it is crucial.

Projector and conversion of operators

One can construct an orthonormal basis from \mathcal{S} by setting

$$|\psi_k\rangle \equiv \sum_{i=1}^{N_{\text{basis}}} [\mathbf{S}^{-\frac{1}{2}}]_{k,i} |\varphi_i\rangle. \quad (5.11)$$

It can be straightforwardly verified that $\langle \psi_i | \psi_j \rangle = \delta_{i,j}$ by using the above equation. The inverse square-root of the overlap matrix \mathbf{S} above can be directly related to the Gram-Schmidt orthonormalization procedure by means of a Cholesky decomposition of \mathbf{S} .

Projecting onto the basis \mathcal{S} involves inversion of the overlap-matrix \mathbf{S} , with the projector $\hat{P}_{\mathcal{S}}$, defined as

$$\hat{P}_{\mathcal{S}} \equiv \sum_{k=1}^{N_{\text{basis}}} |\psi_k\rangle \langle \psi_k| = \sum_{i,j=1}^{N_{\text{basis}}} |\varphi_i\rangle [\mathbf{S}^{-1}]_{i,j} \langle \varphi_j|. \quad (5.12)$$

The definition above satisfies $\hat{P}_{\mathcal{S}}^2 = \hat{P}_{\mathcal{S}}$. We can thus project an arbitrary operator $\hat{O} = \sum_{m,n} |\chi_m\rangle O_{m,n} \langle \chi_n| \in \text{Op}(\mathcal{H})$, with an arbitrary orthonormal basis $\{|\chi_m\rangle\}$

onto \mathcal{S} ,

$$\hat{O}_{\mathcal{S}} \equiv \hat{P}_{\mathcal{S}} \hat{O} \hat{P}_{\mathcal{S}} = \sum_{m,n=1}^{\dim(\mathcal{H})} \sum_{i,j,k,l=1}^{N_{\text{basis}}} |\varphi_i\rangle [\mathbf{S}^{-1}]_{i,k} \langle \varphi_k | \chi_m \rangle O_{m,n} \langle \chi_n | \varphi_l \rangle [\mathbf{S}^{-1}]_{l,j} \langle \varphi_j |, \quad (5.13)$$

such that

$$\begin{aligned} \hat{O}_{\mathcal{S}i,j} &= \langle \varphi_i | \hat{O}_{\mathcal{S}} | \varphi_j \rangle = \sum_{m,n=1}^{\dim(\mathcal{H})} \sum_{k,l=1}^{N_{\text{basis}}} [\mathbf{S}^{-1}]_{i,k} A_{k,m} O_{m,n} A_{l,n}^* [\mathbf{S}^{-1}]_{l,j} \\ &= [\mathbf{S}^{-1} \mathbf{A} \mathbf{O} \mathbf{A}^\dagger \mathbf{S}^{-1}]_{i,j}, \end{aligned} \quad (5.14)$$

where we have defined $A_{k,l} = \langle \varphi_k | \chi_l \rangle$.

Consequently, projecting an operator $\hat{O}_{\mathcal{S}}$ defined in the basis \mathcal{S} onto the full Hilbert space \mathcal{H} yields

$$\hat{O}_{i,j} = \langle \chi_i | \hat{O} | \chi_j \rangle = \langle \chi_i | \hat{P} \hat{O}_{\mathcal{S}} \hat{P} | \chi_j \rangle = \sum_{m,n=1}^{\dim(\mathcal{H})} \langle \chi_i | \varphi_m \rangle O_{\mathcal{S}m,n} \langle \varphi_n | \chi_j \rangle = [\mathbf{A}^\dagger \mathbf{O}_{\mathcal{S}} \mathbf{A}]_{i,j}. \quad (5.15)$$

It is important to note that since $\mathcal{S} \subset \mathcal{H}$, an operator $\hat{O} \in \mathcal{H}$ might have support that lies outside of \mathcal{S} and hence $\hat{P} \hat{P}_{\mathcal{S}} \hat{P} \neq \hat{P}$.

Trace

Using Eq. (5.11), calculating the trace in the basis \mathcal{S} yields:

$$\text{Tr}\{\hat{O}_{\mathcal{S}}\} = \sum_{i=1}^{N_{\text{basis}}} \langle \psi_i | \hat{O}_{\mathcal{S}} | \psi_i \rangle = \dots = \text{Tr}\{\mathbf{S} \mathbf{O}_{\mathcal{S}}\}. \quad (5.16)$$

Analyticity

If the parametrization $\vec{\theta}$ is complex, a sufficient condition for the equivalence of McLachlan's variational principle and the TDVP is the analyticity in the variational parameters $\vec{\theta}$ [399]:

$$\frac{\partial |\varphi_k\rangle}{\partial \theta_i^*} = 0; \quad \forall k, i \quad (5.17)$$

This requirement ensures energy preservation in the limiting case of an isolated system in a pure state [400].

II.1 Parametrization of the Density Matrix

We now define a variational *ansatz* for the parametrized density matrix $\hat{\rho}$, by parametrizing both the basis \mathcal{S} as well as the coefficients of the density matrix itself:

$$\hat{\rho}(\vec{\theta}, \mathbf{B}) = \sum_{i,j=1}^{N_{\text{basis}}} |\varphi_i(\vec{\theta})\rangle B_{i,j} \langle \varphi_j(\vec{\theta})|. \quad (5.18)$$

Here, $\vec{\theta}$ and the density matrix coefficients \mathbf{B} constitute variational parameters. It proves useful to think of $\vec{\theta}$ as an *internal* parametrization for which the equations of motion provide the evolution of the subspace \mathcal{S} in which the density matrix resides. The *external* parametrization is given by the density matrix coefficients \mathbf{B} , for which the equations of motion provide the evolution of the density matrix *within* the co-moving manifold \mathcal{S} .

II.2 TDVP Equations of Motion

We now outline the resulting TDVP equations of motion for a variational ansatz of the density matrix defined in Eq. (5.18). The method relies on a recent formalism developed by *Joubert-Doriol et al.* [400, 401] in the context of simulating the dynamics of dissipative quantum chemistry problems. It was introduced to apply the time-dependent variational principle to open quantum systems with a density matrix ansatz as in Eq. (5.18) subject to a Lindblad master equation.

We assume that the analyticity condition, $\frac{\partial |\varphi_k\rangle}{\partial \theta_i^*} = 0$, (See Eq. (5.17)) for the basis parametrization is satisfied. As a result, the Dirac-Frenkel and McLachlan variational principles as well as the TDVP are ensured to be equivalent. We can thus impose the Dirac-Frenkel stationary condition [402] (See Sec. I)

$$\text{Tr}\{(\delta\hat{\rho})^\dagger(\dot{\hat{\rho}} - \mathcal{L}[\hat{\rho}])\} = 0, \quad (5.19)$$

with an infinitesimal variation in the density matrix $\delta\hat{\rho}$.

We can express $\delta\hat{\rho}$ in terms of its variational parameters:

$$\delta\hat{\rho} = \sum_{ij} \frac{\partial \hat{\rho}}{\partial B_{ij}} \delta B_{ij} + \sum_i \frac{\partial \hat{\rho}}{\partial \theta_i} \delta \theta_i + \sum_i \frac{\partial \hat{\rho}}{\partial \theta_i^*} \delta \theta_i^*. \quad (5.20)$$

We can insert the above expression in Eq. (5.19), and, due to the independent nature of the derivatives, we arrive at three stationary conditions:

$$\text{Tr} \left\{ \frac{\partial \hat{\rho}}{\partial B_{ij}} (\dot{\hat{\rho}} - \mathcal{L}[\hat{\rho}]) \right\} = 0 \quad (5.21)$$

$$\text{Tr} \left\{ \frac{\partial \hat{\rho}}{\partial \theta_i} (\dot{\hat{\rho}} - \mathcal{L}[\hat{\rho}]) \right\} = 0 \quad (5.22)$$

$$\text{Tr} \left\{ \frac{\partial \hat{\rho}}{\partial \theta_i^*} (\dot{\hat{\rho}} - \mathcal{L}[\hat{\rho}]) \right\} = 0 \quad (5.23)$$

We can rewrite Eq. (5.20) as

$$\frac{d\hat{\rho}}{dt} = \sum_{ij} \dot{B}_{ij} |\varphi_i\rangle\langle\varphi_j| + B_{ij} |\dot{\varphi}_i\rangle\langle\varphi_j| + B_{ij} |\varphi_i\rangle\langle\dot{\varphi}_j| \quad (5.24)$$

We replace this expression into Eq. 5.21, yielding:

$$\text{Tr} \left\{ \frac{\partial \hat{\rho}}{\partial B_{ij}} (\dot{\hat{\rho}} - \mathcal{L}[\hat{\rho}]) \right\} = 0 \quad (5.25)$$

$$= \sum_{kl} \langle\varphi_l| \mathbf{S}_{kl}^{-1} \left[|\varphi_i\rangle\langle\varphi_j| \left(\sum_{cd} \dot{B}_{cd} |\varphi_c\rangle\langle\varphi_d| \right. \right. \quad (5.26)$$

$$\left. \left. + B_{cd} |\dot{\varphi}_c\rangle\langle\varphi_d| + B_{cd} |\varphi_c\rangle\langle\dot{\varphi}_d| - \mathcal{L}[\hat{\rho}] \right) \right] |\varphi_k\rangle$$

$$= \sum_{cd} S_{jc} \dot{B}_{cd} S_{di} + \tau_{jc} B_{cd} S_{di} + S_{jc} B_{cd} \tau_{id}^* - L_{ji}. \quad (5.27)$$

In the last line, we have introduced

$$[\boldsymbol{\tau}]_{mn} = \sum_i \left\langle \varphi_m \left| \frac{\partial \varphi_n}{\partial \theta_i} \right. \right\rangle \dot{\theta}_i, \quad (5.28)$$

$$[\mathbf{L}]_{ij} = \langle\varphi_i| \mathcal{L}[\hat{\rho}] |\varphi_j\rangle. \quad (5.29)$$

We thus have the condition

$$\mathbf{S} \dot{\mathbf{B}} \mathbf{S} + \boldsymbol{\tau} \mathbf{B} \mathbf{S} + \mathbf{S} \mathbf{B} \boldsymbol{\tau}^\dagger - \mathbf{L} = 0, \quad (5.30)$$

which gives the equation of motion for the density matrix coefficients,

$$\dot{\mathbf{B}} = \mathbf{S}^{-1} \mathbf{L} \mathbf{S}^{-1} - \mathbf{S}^{-1} \boldsymbol{\tau} \mathbf{B} - \mathbf{B} \boldsymbol{\tau}^\dagger \mathbf{S}^{-1}. \quad (5.31)$$

For the equation of motion for $\dot{\theta}_i$, we have by inserting the definition of $\hat{\rho}$ from Eq. (5.24),

$$\text{Tr} \left\{ \frac{\partial \hat{\rho}}{\partial \theta_i^*} (\dot{\rho} - \mathcal{L}[\hat{\rho}]) \right\} = 0 \quad (5.32)$$

$$\begin{aligned} &= \sum_{ab} \langle \partial_{\theta_i} \varphi_b | \left\{ \sum_{cd} \left(\dot{B}_{cd} |\varphi_c\rangle \langle \varphi_d| \right. \right. \\ &\quad \left. \left. + B_{cd} |\dot{\varphi}_c\rangle \langle \varphi_d| + B_{cd} |\varphi_c\rangle \langle \dot{\varphi}_d| \right) - \mathcal{L}[\hat{\rho}] \right\} | \varphi_a \rangle B_{ab}. \end{aligned} \quad (5.33)$$

Inserting the definition of $\dot{\mathbf{B}}$ from Eq. (5.31), we obtain

$$\text{Tr} \left\{ \frac{\partial \hat{\rho}}{\partial \theta_i^*} (\dot{\rho} - \mathcal{L}[\hat{\rho}]) \right\} \quad (5.34)$$

$$\begin{aligned} &= \sum_{ab} \langle \partial_{\theta_i} \varphi_b | \left\{ \sum_{cd} \left([\mathbf{S}^{-1} \mathbf{L} \mathbf{S}^{-1} \right. \right. \\ &\quad \left. \left. - \mathbf{S}^{-1} \boldsymbol{\tau} \mathbf{B} - \mathbf{B} \boldsymbol{\tau}^\dagger \mathbf{S}^{-1}]_{cd} |\varphi_c\rangle \langle \varphi_d| \right. \right. \\ &\quad \left. \left. + B_{cd} |\dot{\varphi}_c\rangle \langle \varphi_d| + B_{cd} |\varphi_c\rangle \langle \dot{\varphi}_d| \right) - \mathcal{L}[\hat{\rho}] \right\} | \varphi_a \rangle B_{ab} \end{aligned} \quad (5.35)$$

By using the definition of the projector \hat{P} in Eq. (5.12), we have

$$\text{Tr} \left\{ \frac{\partial \hat{\rho}}{\partial \theta_i^*} (\dot{\rho} - \mathcal{L}[\hat{\rho}]) \right\} \quad (5.36)$$

$$\begin{aligned} &= \sum_{ab} \langle \partial_{\theta_i} \varphi_b | \left\{ \sum_{cd} (\hat{\mathbf{1}} - \hat{P}) |\dot{\varphi}_c\rangle B_{cd} S_{da} \right. \\ &\quad \left. + (\hat{P} - \hat{\mathbf{1}}) \mathcal{L}[\hat{\rho}] | \varphi_a \rangle \right\} B_{ab} \end{aligned} \quad (5.37)$$

$$\begin{aligned} &= \sum_{abcl} \langle \partial_{\theta_i} \varphi_b | [\hat{\mathbf{1}} - \hat{P}_S] |\partial_{\theta_l} \varphi_c\rangle [\mathbf{B} \mathbf{S} \mathbf{B}]_{cb} \dot{\theta}_l \\ &\quad - \langle \partial_{\theta_i} \varphi_b | [\hat{\mathbf{1}} - \hat{P}_S] \mathcal{L}[\hat{\rho}] | \varphi_a \rangle B_{ab}, \end{aligned} \quad (5.38)$$

where in the last step we have inserted the definition of $|\dot{\varphi}_c\rangle$.

We can finally cast the above expression into a matrix equation form:

$$\sum_{bcl} [\mathbf{C}_0]_{bc}^{il} [\mathbf{B} \mathbf{S} \mathbf{B}]_{cb} \dot{\theta}_l - \sum_{ab} [\mathbf{Y}_0]_{ba}^i B_{ab} = 0, \quad (5.39)$$

where we have defined

$$[\mathbf{C}_0]_{bc}^{kl} \equiv \langle \partial_{\theta_k} \varphi_b | [\hat{\mathbf{1}} - \hat{P}_S] |\partial_{\theta_l} \varphi_c\rangle, \quad (5.40)$$

$$[\mathbf{Y}_0]_{ba}^k \equiv \langle \partial_{\theta_k} \varphi_b | [\hat{\mathbf{1}} - \hat{P}_S] \mathcal{L}[\hat{\rho}] | \varphi_a \rangle. \quad (5.41)$$

The tensor \mathbf{C}_0 can be interpreted as a *quantum-geometric tensor* [403–407], that relates changes of the variational parameters $\vec{\theta}$ to changes in the basis states of the ansatz. \mathbf{Y}_0 , on the other hand, relates the action of the Liouvillian \mathcal{L} on the basis to variational changes of the basis with respect to the variational parameters $\vec{\theta}$.

II.3 Remarks

Non-conservation of the density matrix trace

It is important to note that by construction of the variational principle in Eq. (5.19), the trace of the density matrix is not conserved in general. This can be seen by computing

$$\mathrm{Tr}\{\dot{\hat{\rho}}\} = \mathrm{Tr}\{\dot{\mathbf{B}} + (\boldsymbol{\tau} + \boldsymbol{\tau}^\dagger)\mathbf{B}\} \quad (5.42)$$

$$= \mathrm{Tr}\{\mathbf{S}^{-1}\mathbf{L} - \mathbf{S}^{-1}\boldsymbol{\tau}\mathbf{B}\mathbf{S} - \mathbf{B}\boldsymbol{\tau}^\dagger + (\boldsymbol{\tau} + \boldsymbol{\tau}^\dagger)\mathbf{B}\} = \mathrm{Tr}\{\mathbf{S}^{-1}\mathbf{L}\}. \quad (5.43)$$

We can constrain the variational principle by applying a Lagrange multiplier to ensure the conservation of the density matrix trace:

$$\mathrm{Tr}\{(\delta\hat{\rho})^\dagger(\dot{\hat{\rho}} - \mathcal{L}[\hat{\rho}] + \lambda\hat{\rho})\} = 0 \quad (5.44)$$

$$\frac{\partial}{\partial t}\mathrm{Tr}\{\hat{\rho}\} = 0 \quad (5.45)$$

This leads to the following trace-preserving equation of motion for $\dot{\mathbf{B}}$:

$$\dot{\mathbf{B}} = \mathbf{S}^{-1}\mathbf{L}\mathbf{S}^{-1} - \mathbf{S}^{-1}\boldsymbol{\tau}\mathbf{B} - \mathbf{B}\boldsymbol{\tau}^\dagger\mathbf{S}^{-1} - \mathrm{Tr}\{\mathbf{S}^{-1}\mathbf{L}\}\mathbf{B} \quad (5.46)$$

For a detailed derivation of this result, see Ref. [400].

Non-conservation of energy for isolated systems

An important remark is that even for isolated systems, the resulting equations of motion from the employed variational principle in Eq. (5.19) do not conserve the energy during time-evolution. Assuming an isolated system, this can be seen by computing

$$\mathrm{Tr}\{\dot{\hat{\rho}}\hat{H}\} = -2\mathrm{Im}[\mathrm{Tr}\{\dot{\boldsymbol{\theta}}^\dagger\mathbf{Y}\}] \quad (5.47)$$

See Ref. [400] for a detailed numerical derivation. This property of non-conservation of energy in isolated systems enters as a result of the density matrix entering quadratically in the variational principle. As a result, the variational principle conserves $\mathrm{Tr}\{\hat{\rho}(t)^2\hat{H}\}$, rather than $\mathrm{Tr}\{\hat{\rho}(t)\hat{H}\}$. In special cases, such as time-independent bases, complete bases, pure states, and in a linear parametrization

of the basis, energy is still preserved in isolated systems [400]. In Ref. [400], a *problem-free* time-dependent variational principle is established based on a variational principle for the square root of the density matrix, such that the density matrix enters linearly in the equation of motion.

In the following, we neglect this property as we consider only dissipative systems in which the energy is in general not a conserved quantity.

III Coherent-state Ladder Time-dependent Variational Principle

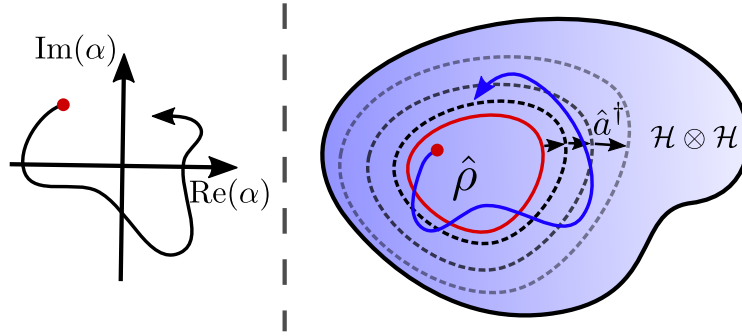


Figure 5.2: Schematic representation of the coherent-state ladder time-dependent variational principle. The basis is parametrized by the coherent-state amplitude α that displaces the Fock-space. The density matrix is parametrized by its density matrix coefficients. By including higher moments of \hat{a}^\dagger in the basis, the density matrix covers a broader subspace of the total Hilbert space. In the equations of motion, both time evolutions (indicated as paths) are coupled to each other.

This section outlines a variational method based on a coherent-state ladder basis to simulate the dynamics of bosonic systems classically. A large part of this work was published in [β].

III.1 Motivation

In a large class of quantum device setups, the quantum state of a bosonic system can be accurately described by coherent states and small quantum fluctuations thereof. As an example, a dissipative Kerr-resonator [408] in the regime of small non-linearity can be well described by coherent-like states, i.e. a coherent state and its excitations.

As outlined in Chap. 2, Sec. IV, several methods have been developed to model systems that are close to their classical limit, such as the Gross-Pitaevskii equa-

tion [131–133] and the Gutzwiller mean-field approximation [409–413]. However, quantum correlations induced by interactions cannot be captured by mean-field approaches, the truncated Wigner approximation, or low-order cumulant expansion [414, 415].

In most modern-day bosonic hardware platforms, systems can acquire a large degree of coherence from engineered driving fields, leading to long-lived quantum correlations that evolve over time. Important examples of such systems are autonomously stabilized bosonic quantum codes in which a carefully engineered environment can stabilize quantum superposition of coherent states [61, 74, 76, 78].

On the other side of the spectrum of numerical simulation techniques reside full-quantum simulations that aim to incorporate the full-quantum nature of the system’s state, e.g. by using a Fock-space representation or wave-function representation of the basis states [416, 417]. The Fock-space method is the most prominent, which relies on photon number states as its computational basis in second quantization. The Fock basis is typically truncated to include a finite number of computational basis states up to a certain photon number state to represent a quantum state in finite memory. Such a truncation is sufficient if the time-evolving quantum state can be well approximated in terms of the computational basis, such that contributions from Fock-states not included in the basis are negligible.

Representing a coherent state $|\alpha\rangle$ – characterized by its complex amplitude α (See Chap. 2, Sec. III) – using a Fock-space representation requires $\mathcal{O}(|\alpha|^2)$ Fock states. In particular, in situations when α grows large, accurately representing a coherent state in Fock-space comes with a quadratic overhead in α . This does not include excitations of a coherent state to represent, e.g., non-linear effects, such as the Kerr effect or squeezing [116, 123, 418, 419], which would further increase the number of Fock-states needed to describe the state. Due to the exponential scaling of the computational basis with respect to the number of bosonic modes when considering many-body bosonic systems, numerical simulation of the dynamics of multi-mode dissipative systems quickly becomes intractable for systems with large occupation numbers in Fock-space.

Hence, one can identify a clear need in the scientific community for an efficient numerical method that bridges the gap between a fully classical and fully quantum treatment of the underlying quantum system. Controlling the degree of quantum fluctuations included in such a method is crucial for simulating the dynamics of quantum systems that are bounded by the entropy that the system develops over time and enables the simulation of the dynamics of bosonic systems for a wide range of quantum states.

In the following, we detail the *coherent-state ladder time-dependent variational principle* that aims to bridge this gap in numerical simulation methods of multi-boson open quantum systems.

III.2 Bargmann States and the Coherent-State Ladder

To construct an efficient simulation method with the requirements detailed above, we aim to construct a *parametrized* basis that can efficiently represent coherent-like states, i.e. a state that can be described by a basis of a coherent state and few excitations thereof. To ensure the equivalence of the variational principles detailed in Sec. I, we require the parametrization of the basis states to be analytic with respect to their variational parameter (See Eq. (5.17)). Normalized coherent states, $|\alpha\rangle = e^{-\frac{|\alpha|^2}{2}} \sum_{n=0}^{\infty} \frac{\alpha^n}{\sqrt{n!}} |n\rangle$, do not satisfy the analyticity condition due to the normalization factor $e^{-\frac{|\alpha|^2}{2}}$ in front, for which it is easy to check that $\frac{\partial|\alpha\rangle}{\partial\alpha^*} \neq 0$.

Bargmann states

For a parametrization that is analytic in the variational parameter, we consider the so-called *Bargmann* states [420–422], which are un-normalized coherent states:

$$||\alpha\rangle \equiv e^{\alpha\hat{a}^\dagger} |0\rangle = \sum_{n=0}^{\infty} \frac{\alpha^n}{\sqrt{n!}} |n\rangle = e^{\frac{|\alpha|^2}{2}} |\alpha\rangle. \quad (5.48)$$

They obey the following properties:

$$\langle\beta||\alpha\rangle = e^{\beta^*\alpha}, \quad (5.49)$$

$$\hat{a}||\alpha\rangle = \alpha||\alpha\rangle, \quad (5.50)$$

$$\frac{\partial}{\partial\alpha} ||\alpha\rangle = \hat{a}^\dagger ||\alpha\rangle, \quad (5.51)$$

$$\frac{\partial}{\partial\alpha^*} ||\alpha\rangle = 0. \quad (5.52)$$

As can be seen from Eq. (5.51), the derivative of a Bargmann state $||\alpha\rangle$ is identical to the application of the creation operator to the state, $\hat{a}^\dagger ||\alpha\rangle$, admitting a very simple form (in contrast to normalized coherent states, in which $\frac{\partial|\alpha\rangle}{\partial\alpha}$ depends both on α and \hat{a}^\dagger).

Coherent-state Ladder

With the definition of the Bargmann state, we can now construct a basis to be used in a variational principle by excited Bargmann states. For this, we define

photon-added (or excited) Bargmann states [297, 298, 423]:

$$\|\alpha, n\rangle \equiv \hat{a}^{\dagger n} \|\alpha\rangle, \quad (5.53)$$

such that $\|\alpha, 0\rangle = \|\alpha\rangle$. The states $\|\alpha, n\rangle$ obey the following properties:

$$\|\alpha, n\rangle = e^{\alpha \hat{a}^\dagger} \sqrt{n!} |n\rangle, \quad (5.54)$$

$$\begin{aligned} \hat{a} \|\alpha, n\rangle &= \hat{a} \hat{a}^{\dagger n} \|\alpha\rangle = (\hat{a}^{\dagger n} \hat{a} + n \hat{a}^{\dagger n-1}) \|\alpha\rangle \\ &= \alpha \|\alpha, n\rangle + n \|\alpha, n-1\rangle, \end{aligned} \quad (5.55)$$

$$\frac{\partial}{\partial \alpha} \|\alpha, n\rangle = \hat{a}^{\dagger n+1} \|\alpha\rangle = \|\alpha, n+1\rangle. \quad (5.56)$$

Note in particular the last equation relating the derivative with respect to α of a photon-added Bargmann state $\|\alpha, n\rangle$ to a photon-added Bargmann state *with an additional* added photon $\|\alpha, n+1\rangle$. From this, we can now define a *coherent-state ladder*, which we define as the basis of n photon-added Bargmann states:

$$\mathcal{S} \equiv \{\hat{a}^{\dagger k} \|\alpha\rangle, k = 0, \dots, n\} \quad (5.57)$$

$$= \{\|\alpha, k\rangle, k = 0, \dots, n\} \quad (5.58)$$

From the above definition of the coherent-state ladder it is straightforward to show that for $\alpha < \infty$ and $n \rightarrow \infty$, \mathcal{S} spans the entire Hilbert space.

Overlap matrix

It is important to note that the coherent-state ladder basis \mathcal{S} , defined in Eq. (5.57), is non-orthonormal. We can compute the overlap of different photon-added Bargmann with the same coherent field amplitude α as

$$S_{mn} = \langle \alpha, m | \alpha, n \rangle \quad (5.59)$$

We can obtain a recursion relation for S_{ij} by computing:

$$S_{mn} = \langle \alpha, m-1 | \hat{a} \hat{a}^\dagger | \alpha, n-1 \rangle \quad (5.60)$$

$$\begin{aligned} &= S_{m-1, n-1} + (m-1)(n-1) S_{m-2, n-2} \\ &\quad + |\alpha|^2 S_{m-1, n-1} + \alpha(m-1) S_{m-2, n-1} \\ &\quad + \alpha^*(n-1) S_{m-1, n-2}. \end{aligned} \quad (5.61)$$

Furthermore, we can obtain an explicit analytical expression for the lower triangle of the overlap matrix through normal ordering of operators [424–428]:

$$S_{mn} = e^{|\alpha|^2} \alpha^{m-n} \sum_{p=0}^m \binom{m}{p} n^p |\alpha|^{2(n-p)}, \quad \text{for } m \geq n \quad (5.62)$$

where $x^n = x(x-1)\dots(x-n+1) = \prod_{k=0}^{n-1} (x-k)$ is the falling factorial [429, 430] and $\binom{n}{m} = \frac{n!}{m!(n-m)!}$ is the binomial coefficient. Using the fact that the overlap matrix \mathbf{S} is Hermitian, i.e. $\mathbf{S} = \mathbf{S}^\dagger$, the upper triangle of \mathbf{S} follows immediately.

For the inverse of the \mathbf{S} -matrix, we can similarly obtain an analytic expression:

$$[\mathbf{S}^{-1}]_{mn} = e^{-|\alpha|^2} \frac{(-\alpha)^{m-n}}{(1+m)!} \sum_{p=m}^{N-1} \binom{p}{m} \frac{|\alpha|^{2(p-m)}}{(p+1-n)!}, \quad \text{for } m \geq n. \quad (5.63)$$

Operator representation

We can represent operators of the form $\hat{a}^{\dagger r} \hat{a}^s$ in the basis of \mathcal{S} and express them in terms the overlap matrix \mathbf{S} . For example, by using Eq. 5.55, we have:

$$[\mathbf{a}]_{m,n} = \langle \alpha, m | \hat{a} | \alpha, n \rangle = \langle \alpha, m | (\alpha | \alpha, n \rangle + n | \alpha, n-1 \rangle) = \alpha S_{m,n} + n S_{m,n-1}. \quad (5.64)$$

Other operators can be calculated similarly (See appendix B for a representation of more operators).

For multiple bosonic modes, we have for an operator \hat{O}_k acting only on mode k ,

$$\mathbf{O}_k = \mathbf{S}_1 \otimes \dots \otimes \mathbf{S}_{k-1} \otimes \mathbf{O} \otimes \mathbf{S}_{k+1} \otimes \dots \otimes \mathbf{S}_N. \quad (5.65)$$

Left and right derivatives

An important property of the coherent-state ladder \mathcal{S} is that the tangent space of \mathcal{S}_n (where here the subscript n denotes the number of basis states) lies in \mathcal{S}_{n+1} , which can be shown by directly applying Eq. (5.56) to the basis states in \mathcal{S} . We can thus relate derivatives of the basis \mathcal{S} to block shifts in the matrix representation of operators. Let $[\mathbf{O}]_{m,n}$ be the matrix representation of an operator \hat{O} in the basis of \mathcal{S} . Then, by denoting \mathbf{O}^{\rightarrow} , the right derivative, we have

$$\mathbf{O}_{m,n}^{\rightarrow} \equiv \langle \alpha, m | \hat{O} \left(\frac{\partial | \alpha, n \rangle}{\partial \alpha} \right) = \langle \alpha, m | \hat{O} \hat{a}^\dagger | \alpha, n \rangle = \langle \alpha, m | \hat{O} | \alpha, n+1 \rangle = [\mathbf{O}]_{m,n+1}. \quad (5.66)$$

And similarly, for the left and left-right derivatives,

$$\mathbf{O}_{m,n}^{\leftarrow} \equiv \left(\frac{\partial \langle \alpha, m |}{\partial \alpha} \right) \hat{O} | \alpha, n \rangle = [\mathbf{O}]_{m+1,n}, \quad (5.67)$$

$$\mathbf{O}_{m,n}^{\leftrightarrow} \equiv \left(\frac{\partial \langle \alpha, m |}{\partial \alpha} \right) \hat{O} \left(\frac{\partial | \alpha, n \rangle}{\partial \alpha} \right) = [\mathbf{O}]_{m+1,n+1}. \quad (5.68)$$

Hence, derivatives with respect to the variational parameter α of the matrix representation of an operator in the basis of \mathcal{S} are directly given by its row and/or column shifts. As a result, in order to calculate first derivatives with respect to α of an operator requires to include one additional basis state in \mathcal{S} .

IV Coherent-state Ladder Equations of Motion

Single bosonic mode

We can now derive the equations of motion for a density matrix $\hat{\rho} = \hat{\rho}(\alpha, \mathbf{B})$ in a coherent-state ladder basis. Compared to the general case in Sec. II.2, here, the basis of a bosonic mode is solely characterized by a single variational parameter, α . Hence, Eq. (5.39), simplifies to

$$\sum_{bc} [\mathbf{C}_0]_{bc} [\mathbf{BSB}]_{cb} \dot{\alpha} - \sum_a [\mathbf{Y}_0]_{ba} B_{ab} = 0 \quad (5.69)$$

$$= \text{Tr}\{\mathbf{C}_0 \mathbf{BSB}\} \dot{\alpha} - \text{Tr}\{\mathbf{Y}_0 \mathbf{B}\}, \quad (5.70)$$

with \mathbf{C}_0 and \mathbf{Y}_0 in this particular basis:

$$[\mathbf{C}_0]_{bc} = \langle \partial_\alpha \varphi_b | [\hat{\mathbf{1}} - \hat{P}_S] | \partial_\alpha \varphi_c \rangle, \quad (5.71)$$

$$[\mathbf{Y}_0]_{ba} = \langle \partial_\alpha \varphi_b | [\hat{\mathbf{1}} - \hat{P}_S] \mathcal{L}[\hat{\rho}] | \varphi_a \rangle. \quad (5.72)$$

We thus have the following set of equations of motion for the parameters α and the matrix \mathbf{B} :

$$\begin{aligned} \dot{\mathbf{B}} &= \mathbf{S}^{-1} \mathbf{L} \mathbf{S}^{-1} - \mathbf{S}^{-1} \boldsymbol{\tau} \mathbf{B} - \mathbf{B} \boldsymbol{\tau}^\dagger \mathbf{S}^{-1}, \\ \dot{\alpha} &= \frac{\text{Tr}\{\mathbf{Y}_0 \mathbf{B}\}}{\text{Tr}\{\mathbf{C}_0 \mathbf{BSB}\}} \end{aligned} \quad (5.73)$$

The above set of equations presents an implicit coupled ordinary differential equation where the equation of motion of α is directly coupled to \mathbf{B} and where the

equation of motion of \mathbf{B} is coupled to α through $\boldsymbol{\tau}$, which contains $\dot{\alpha}$, and implicitly through the matrix-representation of \mathbf{S} and \mathbf{L} , which change upon a change in α .

Multiple bosonic modes

We can straightforwardly extend the equations of motion for \mathbf{B} and α , given in Eqs. (5.73), to multiple bosonic modes. To do so, we parametrize each bosonic mode k with a different coherent-state amplitude α_k , so that the basis \mathcal{S} of the density matrix is simply given by the bases of each individual modes, $\mathcal{S} = \mathcal{S}_1 \otimes \mathcal{S}_2 \otimes \cdots \otimes \mathcal{S}_N$, where N is the number of bosonic modes. Thus, the parametrization of the density matrix $\hat{\rho} = \hat{\rho}(\vec{\alpha}, \mathbf{B})$ is given by the density matrix coefficients \mathbf{B} and the basis parametrization, in which each mode k is parametrized by α_k .

As a result of the independent parametrization of the basis of each individual bosonic mode, we have

$$\langle \partial_{\alpha_k} \varphi_b | [\hat{\mathbb{1}} - \hat{P}_S] | \partial_{\alpha_{k'}} \varphi_c \rangle = 0, \quad \text{for } k \neq k'. \quad (5.74)$$

Hence, changes in the variational parameter α_k of a basis state are uncorrelated to changes in the variational $\alpha_{k'}$ of another basis state for different modes k, k' . We thus arrive at the following set of equations of motion for the parameters $\vec{\alpha}$ and the matrix \mathbf{B} in the case of multiple bosonic modes:

$$\begin{aligned} \dot{\mathbf{B}} &= \mathbf{S}^{-1} \mathbf{L} \mathbf{S}^{-1} - \mathbf{S}^{-1} \boldsymbol{\tau} \mathbf{B} - \mathbf{B} \boldsymbol{\tau}^\dagger \mathbf{S}^{-1}, \\ \dot{\alpha}_k &= \frac{\text{Tr}\{\mathbf{Y}_0^{(k)} \mathbf{B}\}}{\text{Tr}\{\mathbf{C}_0^{(k)} \mathbf{B} \mathbf{S} \mathbf{B}\}}, \end{aligned} \quad (5.75)$$

where here, we have an additional index for \mathbf{C}_0 and \mathbf{Y}_0 specifying the index of the bosonic mode,

$$[\mathbf{C}_0]_{bc}^k = \langle \partial_{\alpha_k} \varphi_b | [\hat{\mathbb{1}} - \hat{P}_S] | \partial_{\alpha_k} \varphi_c \rangle, \quad (5.76)$$

$$[\mathbf{Y}_0]_{ba}^k = \langle \partial_{\alpha_k} \varphi_b | [\hat{\mathbb{1}} - \hat{P}_S] \mathcal{L}[\hat{\rho}] | \varphi_a \rangle. \quad (5.77)$$

V Numerical implementation

We now sketch how the equations of motions Eqs. (5.73) and Eqs. (5.75) are implemented numerically.

V.1 Quantum-geometric tensor \mathbf{C}_0

The quantum-geometric tensor \mathbf{C}_0 in Eq. (5.71) can be drastically simplified by relating it to left and right derivatives of the overlap matrix \mathbf{S} :

$$[\mathbf{C}_0]_{bc} = \langle \partial_\alpha \varphi_b | [\hat{\mathbf{1}} - \hat{P}_S] | \partial_\alpha \varphi_c \rangle = \mathbf{S}^{\leftarrow} - \mathbf{S}^{\leftarrow} \mathbf{S}^{-1} \mathbf{S}^{\rightarrow}, \quad (5.78)$$

where in the last step, we have used the definitions of left- and right derivatives. By using the analytical expressions of \mathbf{S} in Eq. (5.62) and \mathbf{S}^{-1} in Eq. (5.63), we arrive with a simple analytic expression for \mathbf{C}_0 :

$$[\mathbf{C}_0]_{bc} = \begin{cases} (N-1)! & \text{for } b = c = N-1, \\ 0 & \text{otherwise.} \end{cases} \quad (5.79)$$

Hence, \mathbf{C}_0 has only one non-vanishing and α -independent matrix element for $[\mathbf{C}_0]_{N-1, N-1} = (N-1)!$. This surprisingly simple expression reveals one of the important characteristics of Bargmann states: Since the derivative in α of a photon-added Bargmann state $|\alpha, n\rangle$ is identical to the same Bargmann state with an additionally added photon, $|\alpha, n+1\rangle$ (See Eq. (5.56)), all infinitesimal variations of the basis \mathcal{S} with respect to α are described by \mathcal{S} itself, *except* for the highest excited state included in \mathcal{S} , as the derivative lies outside of \mathcal{S} . As a result, only the highest excited state in \mathcal{S} can induce a change in the variational parameter α . This makes variational changes in α susceptible to the *corner* of the basis \mathcal{S} . Consequently, the term $\text{Tr}\{\mathbf{C}_0 \mathbf{B} \mathbf{S} \mathbf{B}\}$ in Eq. (5.73) is zero if the corner of the basis, i.e. $|\alpha, N-1\rangle$, remains unpopulated. We thus have

$$\text{Tr}\{\mathbf{C}_0 \mathbf{B} \mathbf{S} \mathbf{B}\} = (N-1)! \sum_{k,l=0}^{N-1} B_{N-1,k} S_{k,l} B_{l,N-1}. \quad (5.80)$$

The multi-mode case for \mathbf{C}_0 can be calculated straightforwardly:

$$\mathbf{C}_0^{(k)} = \mathbf{S}_1 \otimes \cdots \otimes \mathbf{S}_{k-1} \otimes \mathbf{C}_0 \otimes \mathbf{S}_{k+1} \otimes \cdots \otimes \mathbf{S}_L \quad (5.81)$$

V.2 Calculation of \mathbf{L} and \mathbf{Y}_0

We can rewrite \mathbf{Y}_0 (See Eq. (5.72)) in terms of \mathbf{S} and \mathbf{L} ,

$$\mathbf{Y}_0 = \mathbf{L}^{\leftarrow} - \mathbf{S}^{\leftarrow} \mathbf{S}^{-1} \mathbf{L}. \quad (5.82)$$

We notice that, as left or right derivatives of an operator \hat{O} with respect to α can be expressed in terms of row or column shifts of the respective matrix representation

of \hat{O} in the Bargmann basis \mathcal{S} , we can directly compute \mathbf{L}^\leftarrow from \mathbf{L} , in the following way: We can expand \mathbf{L} in terms of its operator-sum representation $\mathbf{L} = \sum_p \mathbf{A}_p \mathbf{B} \mathbf{D}_p$ with left and right Kraus operator matrices \mathbf{A}_p and \mathbf{D}_p . We have $\mathbf{L}^\leftarrow = \sum_p \mathbf{A}_p^\leftarrow \mathbf{B} \mathbf{D}_p$ through linearity. Hence, we can store both \mathbf{L} and \mathbf{L}^\leftarrow in a single matrix of shape $(N+1) \times N$:

$$\mathbb{L}^{(N+1) \times N} = \sum_p \mathbf{A}_p^{(N+1) \times N} \mathbf{B}^{N \times N} \mathbf{D}_p^{N \times N}, \quad (5.83)$$

such that

$$\mathbf{L} = \mathbb{L}_{0:N-1, 0:N-1}, \quad (5.84)$$

$$\mathbf{L}^\leftarrow = \mathbb{L}_{1:N, 0:N-1}, \quad (5.85)$$

where $a : b$ denotes the index range from a to b .

We can explicitly calculate the Liouvillian \mathbf{L} from Hamiltonian \hat{H} , and jump operators \hat{L}_μ and their associated dissipation rates γ_μ :

$$L_{ij} = \langle \varphi_i | \mathcal{L}[\hat{\rho}] | \varphi_j \rangle \quad (5.86)$$

$$= \sum_{kl} -i B_{kl} \langle \varphi_i | \left[\hat{H} |\varphi_k\rangle\langle\varphi_l| - |\varphi_k\rangle\langle\varphi_l| \hat{H} \right] | \varphi_j \rangle \quad (5.87)$$

$$+ B_{kl} \sum_\mu \gamma_\mu \langle \varphi_i | \left[\hat{L}_\mu |\varphi_k\rangle\langle\varphi_l| \hat{L}_\mu^\dagger - \frac{1}{2} \hat{L}_\mu^\dagger \hat{L}_\mu |\varphi_k\rangle\langle\varphi_l| - \frac{1}{2} |\varphi_k\rangle\langle\varphi_l| \hat{L}_\mu^\dagger \hat{L}_\mu \right] | \varphi_j \rangle \quad (5.88)$$

$$= -i [H_{ik} B_{kl} S_{lj} - S_{ik} B_{kl} H_{lj}] + \sum_\mu \gamma_\mu \left[L_{\mu ik} B_{kl} L_{\mu lj}^\dagger - \frac{1}{2} (L_\mu^\dagger L_\mu)_{ik} B_{kl} S_{lj} - \frac{1}{2} S_{ik} B_{kl} (L_\mu^\dagger L_\mu)_{lj} \right], \quad (5.89)$$

leaving in matrix notation,

$$\mathbf{L} = -i [\mathbf{H} \mathbf{B} \mathbf{S} - \mathbf{S} \mathbf{B} \mathbf{H}] + \sum_\mu \gamma_\mu \left[\mathbf{L}_\mu \mathbf{B} \mathbf{L}_\mu^\dagger - \frac{1}{2} (\mathbf{L}_\mu^\dagger \mathbf{L}_\mu) \mathbf{B} \mathbf{S} - \frac{1}{2} \mathbf{S} \mathbf{B} (\mathbf{L}_\mu^\dagger \mathbf{L}_\mu) \right]. \quad (5.90)$$

Here, \mathbf{L}_μ , \mathbf{L}_μ^\dagger , and $(\mathbf{L}_\mu^\dagger \mathbf{L}_\mu)$ are the jump-operator expressions in the basis of the ansatz. From the above expression of \mathbf{L} , one can straightforwardly identify the operator-sum representation in Eq. (5.83).

To calculate $\mathbf{S}^\leftarrow \mathbf{S}^{-1}$, we can employ the analytical expressions of \mathbf{S} in Eq. (5.62) and \mathbf{S}^{-1} in Eq. (5.63) to leave again a simple analytic expression:

$$\mathbf{S}^\leftarrow \mathbf{S}^{-1} = \begin{pmatrix} 0 & 1 & \cdots & 0 \\ 0 & 0 & \cdots & 0 \\ \vdots & \vdots & \ddots & \vdots \\ 0 & 0 & \cdots & 1 \\ \binom{N}{0} \alpha^N (-1)^{1+N} & \binom{N}{1} \alpha^{N-1} (-1)^{2+N} & \cdots & \binom{N}{N-1} \alpha (-1)^{2N} \end{pmatrix} \quad (5.91)$$

Due to the off-diagonal structure in $\mathbf{S}^\leftarrow \mathbf{S}^{-1}$ – except for the last row – and due to the fact that \mathbf{L}^\leftarrow is a shift of \mathbf{L} by one row, the two terms in Eq. (5.82) exactly cancel – except for the last row – leaving only a single non-vanishing row in the expression of \mathbf{Y}_0 :

$$[\mathbf{Y}_0]_{N-1,c} = \mathbf{L}_{N-1,c}^\leftarrow - \sum_{k=0}^{N-1} \binom{N}{k} \alpha^N (-1)^{N+1+k} \mathbf{L}_{k,c} \quad (5.92)$$

This is again a direct consequence of the tangent space of \mathcal{S}_N lying in \mathcal{S}_{N+1} . Furthermore, as \mathbf{Y}_0 appears in a trace in Eqs. (5.73), we have $\text{Tr}\{\mathbf{Y}_0 \mathbf{B}\} = \sum_k \mathbf{Y}_{0,N-1,k} B_{k,N-1}$.

V.3 Numerical Regularization

It can be deduced directly from the analytical expressions of \mathbf{C}_0 and \mathbf{Y}_0 that if the density matrix $\hat{\rho}$ has no population of the *corner* of the coherent-state ladder \mathcal{S} , i.e. $\langle \alpha, N-1 | \hat{\rho} | \alpha, N-1 \rangle = B_{N-1,N-1} = 0$, both the numerator, $\text{Tr}\{\mathbf{C}_0 \mathbf{B} \mathbf{S} \mathbf{B}\}$, as well as the denominator, $\text{Tr}\{\mathbf{Y}_0 \mathbf{B}\}$, in the equation of motion for α are zero.

This fact can be reconciled in the following way. Let us suppose that for the basis \mathcal{S}_N , $\hat{\rho}(\alpha, \mathbf{B})$ can be described by a rank-deficient coefficient matrix \mathbf{B} , such that $B_{N-1,N-1} = 0$. As a result, $\dot{\alpha}$ is undefined, and only $\dot{\mathbf{B}}$ can be non-vanishing. If the Liouvillian \mathbf{L} does not contain transitions between $|\alpha, k\rangle \leftrightarrow |\alpha, N-1\rangle$, $B_{N-1,N-1}$ can never get populated and consequently, $\dot{\alpha}$ will remain undefined. In this case, the entire density matrix can be efficiently described with the smaller basis \mathcal{S}_{N-1} . Only if \mathbf{L} induces transitions to the corner of the basis is $\dot{\alpha}$ well-defined. At the heart of this problem lies a redundancy that is intrinsic to the Bargmann basis \mathcal{S} : For certain states, we have $\hat{\rho}(\alpha, \mathbf{B}) = \hat{\rho}(\beta, \mathbf{B}')$, i.e. the same density matrix might be equally described by different Bargmann bases \mathcal{S} and \mathcal{S}' . An example of this is a coherent state $|\alpha\rangle$ expressed in the coherent-state ladder \mathcal{S} that is parametrized by α . This state can be efficiently described in another basis \mathcal{S}' that is displaced in phase space by a small amount $\delta\beta$, with different density

matrix coefficients \mathbf{B}' . As a result, the equations of motion in Eqs. (5.73) are only properly defined if the corner $B_{N-1,N-1}$ is non-zero.

Mathematically, this can be shown in the following way. Suppose $B_{N-1,N-1} = \epsilon$ and $B_{1:N,N-1} = 0$, i.e. $\hat{\rho}$ has no coherences with state $|\varphi_{N-1}\rangle$. Then, the expression of $\dot{\alpha}$ simplifies to

$$\dot{\alpha} = \frac{Y_{N-1,N-1}\epsilon}{(N-1)!\epsilon^2 S_{N-1,N-1}}. \quad (5.93)$$

We can see that for $\epsilon \rightarrow 0$, $\dot{\alpha}$ diverges. Allowing for coherences associated with the corner state, $B_{1:N,N-1} \neq 0$, we get the same result as the coherences are bounded by $B_{N-1,N-1}$ due to \mathbf{B} being Hermitian.

We can regularize the equations of motion by imposing a regularization for $\dot{\alpha}$. There are multiple options to do so, of which we discuss only a few.

Implicit regularization

A straightforward regularization for $\dot{\alpha}$ is to set $\dot{\alpha} = 0$ for $B_{N-1,N-1} < \epsilon$ for a small value of ϵ . In this implicit regularization scheme, if the initial state is a rank-deficient density matrix in the basis of \mathcal{S} , the initial basis \mathcal{S} is allowed to change in its variational parameter if the time-evolution of \mathbf{B} causes a population of the corner of \mathbf{B} . A drawback of this regularization is the introduction of discontinuities in the evolution of α , which can make numerical integration schemes more demanding. Furthermore, ϵ has to be chosen carefully to be large enough to allow sufficient sensitivity in the computation of $\dot{\alpha}$ and small enough to avoid larger deviations from leakage outside of the basis \mathcal{S} leading to errors in the time-evolution.

Tikhonov regularization

We can also regularize the equation of motion for $\dot{\alpha}$, by using Tikhonov regularization [431–433] in Eqs. (5.73):

$$\dot{\alpha} = \frac{\text{Tr}\{\mathbf{C}\}\text{Tr}\{\mathbf{Y}\}}{\text{Tr}\{\mathbf{C}\}^2 + \epsilon}, \quad (5.94)$$

such that $\dot{\alpha} = 0$ if the corner of \mathbf{B} is unpopulated. This regularization has the advantage of being continuous and favoring solutions of small absolute values of $\dot{\alpha}$. Here, ϵ also has to be chosen such as to balance the artificially induced numerical error with the efficiency of integrating the regularized equations of motion.

Regularization of \mathbf{B}

Another way of regularizing the equations of motion is to artificially impose $B_{N-1,N-1} \geq \epsilon$ throughout the dynamics, e.g. by either setting $B_{N-1,N-1} = \epsilon$ in the initial state, such that $\dot{\alpha}$ is well-defined. While this regularization scheme

is numerically efficient, it directly manipulates the coefficient matrix \mathbf{B} , leading to inaccurate results that can lead to an accumulation of the error to the true variational evolution, in particular when the number of basis states N is large.

V.4 Sketch of the Implementation

We now sketch a numerical implementation for the simulation of a single bosonic mode. A schematic pseudocode for the function `RHS`, computing the right-hand-side of Eqs. (5.73), is given in algorithm 2.

Algorithm 2 Schematic pseudocode for computing the derivatives $\dot{\alpha}$ and $\dot{\mathbf{B}}$ in Eqs. (5.73).

```

1: function RHS( $\alpha$ ,  $\mathbf{B}$ )
2:    $\mathbf{S}$ ,  $\mathbf{S}^{-1} \leftarrow \mathbf{S}(\alpha)$ ,  $\mathbf{S}^{-1}(\alpha) \triangleright$  Compute  $\mathbf{S}$  using Eq. (5.61) or Eq. (5.62) and
    $\mathbf{S}^{-1}$  by numerical inversion or analytically using Eq. (5.63)
3:    $\{\mathbf{A}_p\} \leftarrow \{\mathbf{A}_p\}(\alpha, \mathbf{S}) \triangleright$  compute all other elementary operators involved in
    $\mathbb{L}$ 
4:    $\mathbb{L} \leftarrow \mathbb{L}(\mathbf{B}, \mathbf{S}, \{\mathbf{A}_p\}) \triangleright$  compute the Liouvillian action on  $\mathbf{B}$  (See
   Eq. (5.90))
5:    $\text{Tr}\{\mathbf{Y}\} \leftarrow \text{Tr}\{\mathbf{Y}(\alpha, \mathbf{B}, \mathbb{L})\} \triangleright$  compute  $\text{Tr}\{\mathbf{Y}\} = \text{Tr}\{\mathbf{Y}_0\mathbf{B}\}$ 
6:    $\text{Tr}\{\mathbf{C}\} \leftarrow \text{Tr}\{\mathbf{C}(\mathbf{B}, \mathbf{S})\} \triangleright$  compute  $\text{Tr}\{\mathbf{C}\} = \text{Tr}\{\mathbf{C}_0\mathbf{B}\mathbf{S}\mathbf{B}\}$ 
7:    $\dot{\alpha} \leftarrow \text{Tr}\{\mathbf{C}\}\text{Tr}\{\mathbf{Y}\}/(\text{Tr}\{\mathbf{C}\}^2 + \epsilon) \triangleright$  Compute regularized expression for  $\dot{\alpha}$ 
8:    $\text{drift} \leftarrow \text{drift}(\alpha, \dot{\alpha}, \mathbf{B}) \triangleright$  compute drift term  $\mathbf{B}\boldsymbol{\tau}^\dagger\mathbf{S}^{-1}$  using Eq. (5.91)
9:    $\dot{\mathbf{B}} \leftarrow \mathbf{S}^{-1}\mathbb{L}\mathbf{S}^{-1} - \text{drift} - \text{drift}^\dagger \triangleright$  compute rhs of  $\dot{\mathbf{B}}$ 
10:  return  $\dot{\alpha}$ ,  $\dot{\mathbf{B}}$ 
11: end function

```

An important remark is that when explicit numerical integration schemes are used, we can substitute the right-hand-side of $\dot{\alpha}$ into the expression of the right-hand-side of $\dot{\mathbf{B}}$, without loss of numerical accuracy, and hence we can treat implicit ordinary differential Eqs. (5.73) as explicit ones due to $\dot{\alpha}$ entering linearly in the expression of $\dot{\mathbf{B}}$.

As detailed in Sec. V.2, we can obtain \mathbf{L}^\leftarrow and \mathbf{L} directly from a single matrix \mathbb{L} . Computing \mathbb{L} requires computing operators in the Hamiltonian and jump operators with an additional basis state, such that the matrix representation of the operators is of dimension $(N + 1) \times N$.

Solving the differential equation numerically is straightforward, and a workflow sketch of integrating the equations of motion is schematically depicted in algorithm 3.

Algorithm 3 Schematic pseudocode for integrating the equations of motion

- 1: Initialize matrices \mathbf{S} , \mathbf{S}^{-1} , $\{\mathbf{A}_p\}$, and \mathbb{L} .
 - 2: Define problem-specific function $\mathbb{L}(\mathbf{B}, \mathbf{S}, \{\mathbf{A}_p\})$
 - 3: Define initial state $\alpha(t_0)$, $\mathbf{B}(t_0)$
 - 4: Set integration time T
 - 5: Set solver algorithm and its numerical accuracy
 - 6: **Solve** differential equation defined by $\text{RHS}(\alpha, \mathbf{B})$
-

Computational Resource Estimate

It is crucial to assess the scaling of the computational resources needed for the developed coherent-state ladder TDVP method with respect to the to be able to compare the method to others.

To assess the scaling of the number of computations with the basis size N and the number of modes L , we consider the resources in a single time-step, i.e. in a single evaluation of the right-hand side of the derivatives for $\dot{\alpha}$ and $\dot{\mathbf{B}}$. For a single bosonic mode with basis size N , calculating the right-hand side for $\dot{\mathbf{B}}$ and $\dot{\alpha}$ involves $\mathcal{O}(N^3)$ operations, arising from a constant number of matrix-matrix multiplications, thus leaving $\mathcal{O}(N^3)$ operations for a single mode.

For a number of L bosonic modes, with each mode having a basis size N , the computational cost can be estimated in the following way. Matrix-matrix multiplications then involve $\mathcal{O}(N^{3L})$ operations, as the Hilbert space has dimension $\dim(\mathcal{H}_S) = N^L$. Computing the L different derivatives $\dot{\alpha}_k$ for each mode k thus yields the overall scaling of $\mathcal{O}(LN^{3L})$ for this method. In comparison, a standard Fock-space method with truncated Hilbert space of dimension $\dim(\mathcal{H}_{\text{Fock}}) = N_{\text{Fock}}^L$ involves $\mathcal{O}(N_{\text{Fock}}^{3L})$ operations per time-step, where N_{Fock} is the number of Fock states in each mode. Notice that the optimal operating regime of our method is when $N_{\text{Fock}} \gg N$, which is the regime of small quantum fluctuations in the system, corresponding to low entropy.

VI Fidelity and Wigner function

Fidelity

To gauge the performance of the time-evolved density matrix of the coherent-state ladder ansatz $\hat{\rho}(\alpha(t), \mathbf{B}(t))$ with a standard Fock-space approach $\hat{\sigma}(t)$, we compute the fidelity between these two states [47, 434]:

$$\mathcal{F} \equiv \text{Tr}\{\sqrt{\sqrt{\hat{\rho}}\hat{\sigma}\sqrt{\hat{\rho}}}\}^2 \quad (5.95)$$

To do so, we compute the square root of $\hat{\rho}$ by expressing it in an orthogonal basis (See Eq. (5.11))

$$\hat{\rho} = \sum_{i,j} B_{i,j} |\varphi_i\rangle\langle\varphi_j| = \sum_{i,j} \mathcal{B}_{i,j} |\psi_i\rangle\langle\psi_j|, \quad (5.96)$$

with

$$\mathcal{B} = \mathbf{S}^{-\frac{1}{2}} \mathbf{B} \mathbf{S}^{-\frac{1}{2}}, \quad (5.97)$$

such that $\langle\psi_i|\psi_j\rangle = \delta_{i,j}$. Then, we have for the fidelity

$$\mathcal{F} = \text{Tr}\{\sqrt{\sqrt{\mathcal{B}}\mathcal{C}\sqrt{\mathcal{B}}}\}^2, \quad (5.98)$$

with $\mathcal{C}_{m,n} = \langle\psi_m|\hat{\sigma}|\psi_n\rangle$.

Wigner Function

We can calculate the Wigner function directly from $\hat{\rho}$ *without* having to transform $\hat{\rho}$ into a Fock-space representation.

$$W[\beta] \equiv \text{Tr}\{\hat{\rho}\hat{D}(\beta)\hat{\Pi}\hat{D}^\dagger(\beta)\} \quad (5.99)$$

$$= \sum_{k,l} \langle\varphi_k|[\mathbf{S}^{-1}]_{kl}\hat{\rho}\hat{D}(\beta)\hat{\Pi}\hat{D}^\dagger(\beta)|\varphi_l\rangle \quad (5.100)$$

$$= \sum_{m,n} B_{m,n} \langle\varphi_n|\hat{D}(\beta)\hat{\Pi}\hat{D}^\dagger(\beta)|\varphi_m\rangle = \text{Tr}\{\mathbf{B}\mathbf{A}\}, \quad (5.101)$$

where in the last step we have defined $A_{n,m} \equiv \langle\varphi_n|\hat{D}(\beta)\hat{\Pi}\hat{D}^\dagger(\beta)|\varphi_m\rangle$. We calculate the matrix elements A_{nm} :

$$\begin{aligned} A_{n,m} &= (-1)^m e^{|\alpha|^2} \sum_{k_1=0}^n \sum_{k_2=0}^m \sum_{k=0}^{\min(k_1,k_2)} k! \binom{n}{k_1} \binom{k_1}{k} \binom{m}{k_2} \binom{k_2}{k} \\ &\quad \times \beta^{n-k_1} (-\beta^*)^{m-k_2} (\alpha^* - \beta^*)^{k_2-k} (\beta - \alpha)^{k_1-k} e^{-2|\alpha-\beta|^2}. \end{aligned} \quad (5.102)$$

VII Applications

We now turn to applying the coherent-state ladder time-dependent variational principle, developed in the previous sections, to various systems to gauge the method's performance.

Application I: Driven-dissipative Kerr resonator

We consider as a first proof of principle a single bosonic mode consisting of a single-photon drive and Kerr-nonlinearity with Hamiltonian:

$$\hat{H} = \frac{U}{2}\hat{a}^{\dagger 2}\hat{a}^2 + F(\hat{a} + \hat{a}^\dagger), \quad (5.103)$$

where F is the single-photon driving amplitude, and U is the strength of the Kerr-nonlinearity. Furthermore, the system is subjected to single-photon loss, with dissipator $\gamma\mathcal{D}[\hat{a}]$, where γ is the photon-loss rate. In the classical limit of vanishing non-linearity and infinite driving amplitude with $F\sqrt{U}$ constant, the required number of Fock states to describe the system's dynamics accurately increases as $\mathcal{O}(F/U)^{2/3}$ [408].

In Fig. 5.3(a), we show the number of basis states N required to reach a fidelity $\mathcal{F} > 0.99$ for both the TDVP method and the Fock-space method for reference throughout the time-evolution of an initial coherent state. We observe that while the number of required Fock states needed to accurately describe the entire dynamics increases by lowering U , the number of required basis states in the coherent-state ladder \mathcal{S} remains nearly constant. Furthermore, we show in Fig. 5.3(b) the infidelity $1 - \mathcal{F}$ as a function of time for different basis sizes N in the coherent-state ladder used to describe the density matrix. We observe – as expected – a monotonous improvement in the fidelity \mathcal{F} with increasing the basis size N . The initial increase in the infidelity is due to the fact that the state departs from a coherent state, leading to leakage outside of the basis \mathcal{S} . In Fig. 5.3(c), we show the Wigner functions in the steady state for different values of U , highlighting departure from a coherent state.

Application IIb: Asymmetrically driven nonlinear photonic dimer

Next, we consider a system of two coupled dissipative bosonic modes, in which only one of the two modes is driven. The Hamiltonian of the system reads

$$\begin{aligned} \hat{H} = \sum_{i=1,2} -\Delta\hat{a}_i^\dagger\hat{a}_i + \frac{U}{2}\hat{a}_i^{\dagger 2}\hat{a}_i^2 \\ - J(\hat{a}_1^\dagger\hat{a}_2 + \hat{a}_1\hat{a}_2^\dagger) + F(\hat{a}_1^\dagger + \hat{a}_1). \end{aligned} \quad (5.104)$$

The two modes are subject to single-photon loss with dissipators $\gamma\mathcal{D}[\hat{a}_1]$ and $\gamma\mathcal{D}[\hat{a}_2]$. Here, Δ represents the detuning between the two modes with respect to the drive frequency, J is the hopping interaction, and F is the driving amplitude of mode the first mode. In a semiclassical approximation using the Gross-Pitaevskii equation, we predict multiple parametrically unstable regions for different param-

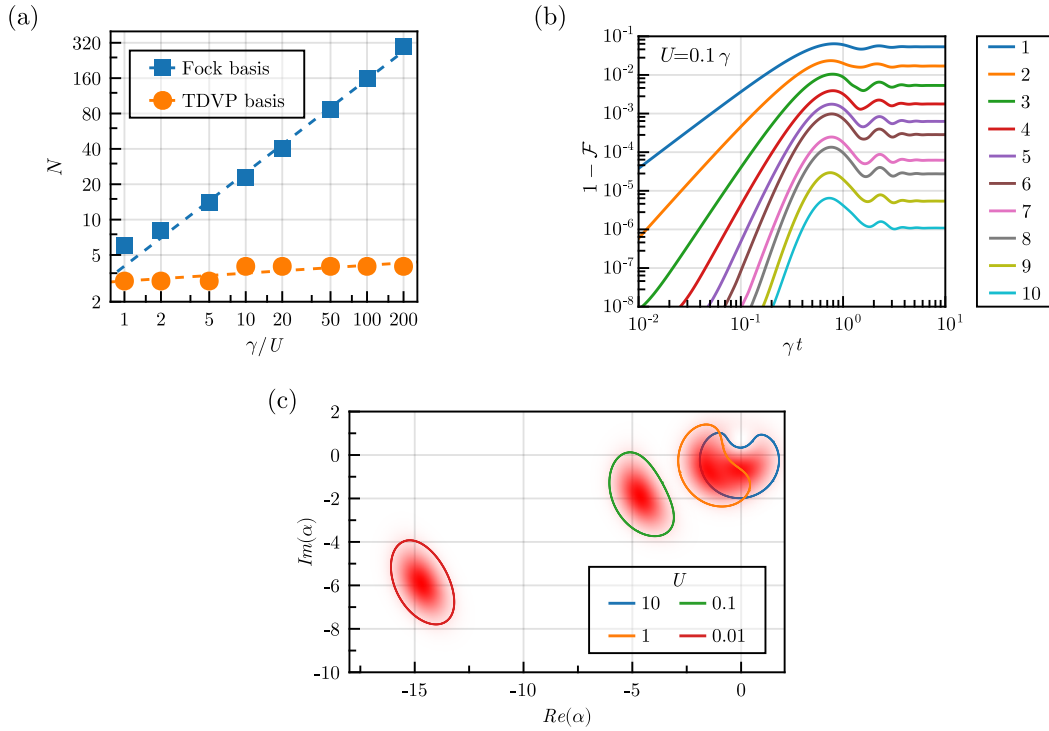


Figure 5.3: (a) Number of basis states N needed to reach a fidelity above $\mathcal{F} = 0.99$ throughout the dynamics of the dissipative Kerr resonator for the Fock-basis (blue) and the coherent-state ladder basis (orange). (b) Infidelity $1 - \mathcal{F}$ as a function time γt for different numbers of basis states N in the dissipative Kerr resonator. (c) Wigner function of the steady state for different values of U . System parameters for (a-c) are $F = 1.5\sqrt{\gamma^3/U}$ and the initial state is a coherent state with $\alpha = -1.0 - 1.84i$.

eter regimes [435, 436]. Similar to the previous application, in the classical limit of $F \rightarrow \infty$ and $U \rightarrow 0$, with $F\sqrt{U}$ constant, describing the effect of quantum fluctuations accurately becomes increasingly challenging as $|\alpha|^2 \rightarrow \infty$, and hence the average number of photons diverges as $(F/U)^{2/3}$ [408]. In this system, the field amplitudes describing the coherent states in the GPE approximation change periodically along the dynamics in the thermodynamic limit [436] as depicted in Fig.5.4(a) and thus cannot be well-described using a stationary ansatz in which the basis is time-independent, as, for example, using the shifted Fock basis [238]. This system, therefore, provides an ideal study case for the coherent-state ladder TDVP method. In Fig. 5.4(b), we show the number of basis states N needed to reach $\mathcal{F} > 0.99$ as a function of inverse non-linearity $U^{-1}\kappa$. We observe that, while scaling similarly, the coherent-state ladder basis requires a lower number of basis states N to accurately describe the dynamics of the system. In Fig. 5.4(c), we show the infidelity $1 - \mathcal{F}$ as a function of time κt for different basis sizes N . It is important to note that while in the classical limit, the system can exhibit

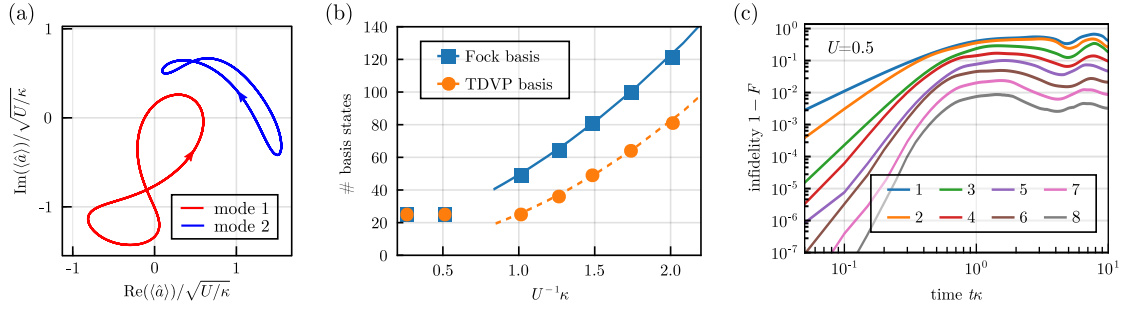


Figure 5.4: For the asymmetrically driven nonlinear photonic dimer, we show in (a) the limit cycles of the mean-field trajectories in the coherent field amplitudes $\alpha_{1,2}$ of the respective modes using the Gross-Pitaevskii equation. (b) Number of basis size required to reach a fidelity $\mathcal{F} > 0.99$ throughout the time-evolution with $t\kappa \in [0, 10]$ for the coherent-state ladder TDVP method and the Fock-space method. (c) Infidelity $1 - \mathcal{F}$ as a function of time $t\kappa$ for different basis states N per mode for an initial product state of coherent states with coherent-field amplitudes on the meanfield limit cycles in (a). System parameters: $J = 1.2\gamma$, $\Delta_{1,2} = 2\gamma$, $\alpha_1(t=0) = -1.0 - 1.84i$, $\alpha_2(t=0) = 1.36 + 0.8i$.

limit cycles (See Fig. 5.4(a)), the steady state for finite but small U can be highly entropic, leading to a large number of basis states needed to describe the state.

Application IIa: Driven-dissipative Bose-Hubbard chain

As a third example of multiple interacting bosonic driven-dissipative systems, we consider a one-dimensional Bose-Hubbard chain with periodic boundary conditions. The driven-dissipative Bose-Hubbard model has been intensively investigated theoretically [131, 413, 415, 437–441] and experimentally in semiconductor microcavities [442] and superconducting microwave resonators [443–445] in particular and can show rich physical phenomena, such as phase-transitions and critically slowing down [415]. Studying this system in a regime that can no longer be described in a mean-field approach therefore provides an ideal testbed for our developed variational method.

In the frame rotating with the frequency of the drives, the Hamiltonian reads:

$$\hat{H}_{BH} = -J \sum_{\langle i,j \rangle} (\hat{a}_i^\dagger \hat{a}_j + \text{h.c.}) + \sum_{i=1}^L F (\hat{a}_i^\dagger + \hat{a}_i) + \Delta \hat{a}_i^\dagger \hat{a}_i + \frac{U}{2} \hat{a}_i^\dagger \hat{a}_i^\dagger \hat{a}_i \hat{a}_i. \quad (5.105)$$

Each bosonic mode is subject to single-photon loss with rate γ . Here, every site is driven homogeneously. We study the system at a driving amplitude F that corresponds to a steady-state that contains quantum fluctuation and thus cannot be described by coherent states alone. In this regime, a mean-field approach using the Gross-Pitaevskii equation fails to accurately describe the full quantum solution,

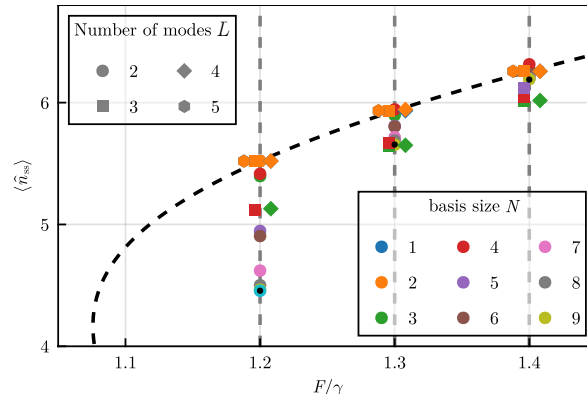


Figure 5.5: Average photon number per mode $\langle \hat{n}_{\text{ss}} \rangle$ in the steady-state of the driven-dissipative Bose-Hubbard chain as a function of driving amplitude F in units of dissipation rate γ for different basis sizes per mode N and different numbers of modes L . The dashed line represents the Gross-Pitaevskii meanfield solution. Exact results for $L = 2$ are represented in black dots. Markers of different N are offset to the driving amplitudes F corresponding to gray dashed lines for better visibility. System parameters: $U = 0.2\gamma$, $J = 0.45\gamma$, $\Delta = 0.1\gamma$.

as the steady-state solution significantly deviates from coherent states [446]. In Fig. 5.5, we show simulation results for the average number of photons $\langle \hat{n}_{\text{ss}} \rangle$ per site for different numbers of basis sizes N per mode and different numbers of modes L in the steady-state. We compare our results to a semiclassical result by means of the Gross-Pitaevskii equation [446], leading to the semi-classical equation $|\alpha|^2[2J - U - \Delta|\alpha|^2 + \gamma^2/4] = F^2$, shown as dashed lines in Fig. 5.5.

To compute the steady-state with our variational method, one can make use of a restarted procedure to facilitate the convergence towards the steady-state. For this we compute the steady-state density matrix $\hat{\rho}(\vec{\alpha}_{\text{ss}}, \mathbf{B}_{\text{ss}})$ for a basis $\otimes_{i=1}^L \mathcal{S}_N^{(i)}$. By increasing the basis size in each mode by one, we use the previously obtained state $\hat{\rho}(\vec{\alpha}_{\text{ss}}, \mathbf{B}_{\text{ss}})$ as the initial state for the larger basis $\otimes_{i=1}^L \mathcal{S}_{N+1}^{(i)}$, setting matrix elements of \mathbf{B} associated with an added basis state to zero. Due to the fact that the previous state already has a large overlap with the steady-state in the larger basis, the steady-state is reached faster compared to e.g. an initial state consisting of coherent states. Alternatively, one can directly set the right-hand side of $\vec{\alpha}$ and $\dot{\mathbf{B}}$ in Eqs. (5.75) to zero.

VIII Cat-state Ladder

An important advantage of the coherent-state ladder presented in the previous sections is that the coherent-state ladder can be straightforwardly extended to include rotational symmetries, which are ubiquitous in many physical systems that ex-

hibit weak or strong \mathbb{Z}_N symmetries. As an example, rotation-symmetric bosonic codes [341] exhibit a discrete rotational symmetry associated to the rotation operator $\hat{Z}_N = \exp\{i(\pi/N)\hat{n}\}$ which acts as the logical \hat{Z} operator on the code-space. Simulating the dynamics of physical systems implementing rotation-symmetric bosonic codes can be extremely challenging due to the involved symmetry sectors.

In the following we demonstrate the symmetry-extension of the coherent-state ladder to the simulation of cat qubit dynamics. As cat qubits have been widely studied for quantum sensing [447–451], quantum communication [452–454] and quantum computing [53, 64, 72–74, 76, 79–82, 84, 86–89, 94, 227, 233, 236, 238, 242, 290, 291, 317, 318], the need to efficiently simulate the dynamics of cat qubits is ever-present.

To this end, we make use of a subsystem decomposition, detailed in Chap. 3, Sec. III. Similar to the shifted Fock basis [238], we construct a subsystem decomposition using the coherent-state ladder, we define the unnormalized (Bargmann) cat states, characterizing the logical qubit:

$$\|\mathcal{C}_\alpha^\pm\rangle = \|\alpha\rangle \pm \|-\alpha\rangle \quad (5.106)$$

The states $\|\mathcal{C}_\alpha^\pm\rangle$ obey the relations

$$\frac{\partial}{\partial \alpha} \|\mathcal{C}_\alpha^\pm\rangle = \hat{a}^\dagger \|\mathcal{C}_\alpha^\mp\rangle, \quad (5.107)$$

$$\hat{a} \|\mathcal{C}_{\alpha,n}^\pm\rangle = \alpha \|\mathcal{C}_{\alpha,n}^\mp\rangle + n \|\mathcal{C}_{\alpha,n-1}^\mp\rangle. \quad (5.108)$$

We now define the cat-state ladder based on the coherent-state ladder by considering the two symmetry sectors:

$$\mathcal{S}_{\text{cat}} \equiv \{\hat{a}^{\dagger k} \|\mathcal{C}_\alpha^\pm\rangle, k = 0, \dots, N-1\} \quad (5.109)$$

$$= \left\{ \begin{array}{cc} \text{even :} & \text{odd :} \\ \|\mathcal{C}_\alpha^+\rangle, & \|\mathcal{C}_\alpha^-\rangle, \\ \hat{a}^\dagger \|\mathcal{C}_\alpha^-\rangle, & \hat{a}^\dagger \|\mathcal{C}_\alpha^+\rangle, \\ \vdots, & \vdots \\ \hat{a}^{\dagger N} \|\mathcal{C}_\alpha^{N\oplus 0}\rangle, & \hat{a}^{\dagger N} \|\mathcal{C}_\alpha^{N\oplus 1}\rangle \end{array} \right\} \quad (5.110)$$

$$= \{\|\mathcal{C}_{\alpha,k}^\sigma\rangle, k = 0, \dots, N-1, \sigma \in \{0(+), 1(-)\}\} \quad (5.111)$$

Here, $a \oplus b = (a + b) \bmod 2$. A basis state $\|\mathcal{C}_{\alpha,k}^\sigma\rangle$ in the cat ladder \mathcal{S}_{cat} is thus characterized by the coherent-field amplitude α , the parity $\sigma \in \{0(+), 1(-)\}$ (where $0(+)$ represents even photon number parity and $1(-)$ represents odd photon

number parity) and the order k , i.e. the number of creation operators \hat{a}^\dagger applied to the Bargmann cat $\|\mathcal{C}_\alpha^\sigma\rangle$.

Overlap matrix

Similar to the coherent-state ladder, we can compute the overlap between states in the cat-state ladder \mathcal{S}_{cat} :

$$S_{m,n}^{\mu,\nu} \equiv \langle \mathcal{C}_{\alpha,m}^\mu \| \mathcal{C}_{\alpha,n}^\nu \rangle, \quad (5.112)$$

Analogous to the coherent-state ladder in Eq. (5.61), we can compute $S_{m,n}^{\mu,\nu}$ using a recursion relation:

$$S_{mn}^{\mu\nu} = \langle \mathcal{C}_{\alpha,m-1}^{\bar{\mu}} \| \hat{a}\hat{a}^\dagger \| \mathcal{C}_{\alpha,n-1}^{\bar{\nu}} \rangle \quad (5.113)$$

$$\begin{aligned} &= S_{m-1,n-1}^{\bar{\mu}\bar{\nu}} + (m-1)(n-1)S_{m-2,n-2}^{\mu\nu} \\ &\quad + |\alpha|^2 S_{m-1,n-1}^{\mu\nu} + \alpha(m-1)S_{m-2,n-1}^{\mu\nu} \\ &\quad + \alpha^*(n-1)S_{m-1,n-2}^{\mu\nu}, \end{aligned} \quad (5.114)$$

where $\bar{\nu}$ indicates a flip of the parity index ν , i.e. $\bar{\nu} = \nu \oplus 1$. The overlap matrix for the even and odd Bargmann cat can be computed to be

$$S_{00}^{\mu\nu} = \begin{pmatrix} \mathcal{N}_\alpha^+ & 0 \\ 0 & \mathcal{N}_\alpha^- \end{pmatrix} = \begin{pmatrix} 4 \cosh(|\alpha|^2) & 0 \\ 0 & 4 \sinh(|\alpha|^2) \end{pmatrix}, \quad (5.115)$$

from which the overlap matrix \mathcal{S} with matrix elements $S_{m,n}^{\mu,\nu}$ can be computed recursively for $m, n > 0$.

Operator representation

We can compute the representation of operators in the cat-state ladder by considering their action on the two subsystems in the Hilbert-space decomposition in Eq. (3.77). For instance, we have for the annihilation operator \hat{a} , by using the relation in Eq. (5.108) [238],

$$\hat{a} = \hat{X} \otimes (\tilde{b} + \alpha). \quad (5.116)$$

In the logical subspace, \hat{a} acts as the logical \hat{X} -operator, while in the gauge mode, it acts as a displaced annihilation operator $\tilde{b} + \alpha$. Analogous to the coherent-state ladder, we can express \hat{a} in the cat ladder in terms of the overlap matrix \mathcal{S} :

$$\langle \mathcal{C}_{\alpha,m}^\mu \| \hat{a} \| \mathcal{C}_{\alpha,n}^\nu \rangle = \alpha S_{mn}^{\mu,\bar{\nu}} + n S_{m,n-1}^{\mu,\bar{\nu}}, \quad (5.117)$$

More generally, we have

$$\hat{a}^\dagger \|\mathcal{C}_{\alpha,n}^\sigma\rangle = \|\mathcal{C}_{\alpha,n+1}^{\sigma\oplus 1}\rangle \quad (5.118)$$

$$\hat{a}^{\dagger m} \|\mathcal{C}_{\alpha,n}^\sigma\rangle = \|\mathcal{C}_{\alpha,n+m}^{\sigma\oplus m}\rangle \quad (5.119)$$

We can obtain similar expressions for other operators; see appendix B for details.

Left and right derivatives

Similar to the coherent-state ladder, we can also express derivatives in terms of block shifts of matrix representations of operators in \mathcal{S}_{cat} . Specifically, we have (analogous to Eq. (5.66))

$$[\mathcal{O}^{\rightarrow}]_{m,n}^{\mu,\nu} \equiv \langle \mathcal{C}_{\alpha,m}^\mu \| \hat{\mathcal{O}} \left(\frac{\partial \|\mathcal{C}_{\alpha,n}^\nu\rangle}{\partial \alpha} \right) = \langle \mathcal{C}_{\alpha,m}^\mu \| \hat{\mathcal{O}} \hat{a}^\dagger \|\mathcal{C}_{\alpha,n}^{\nu\oplus 1}\rangle = \langle \mathcal{C}_{\alpha,m}^\mu \| \hat{\mathcal{O}} \|\mathcal{C}_{\alpha,n+1}^\nu\rangle = [\mathcal{O}]_{m,n+1}^{\mu,\nu}. \quad (5.120)$$

Analogously, we have for the right derivative and left-right derivative:

$$[\mathcal{O}^{\leftarrow}]_{m,n}^{\mu,\nu} \equiv \left(\frac{\partial \langle \mathcal{C}_{\alpha,m}^\mu \|}{\partial \alpha} \right) \hat{\mathcal{O}} \|\mathcal{C}_{\alpha,n}^\nu\rangle = [\mathcal{O}]_{m+1,n}^{\mu,\nu} \quad (5.121)$$

$$[\mathcal{O}^{\leftrightarrow}]_{m,n}^{\mu,\nu} \equiv \left(\frac{\partial \langle \mathcal{C}_{\alpha,m}^\mu \|}{\partial \alpha} \right) \hat{\mathcal{O}} \left(\frac{\partial \|\mathcal{C}_{\alpha,n}^\nu\rangle}{\partial \alpha} \right) = [\mathcal{O}]_{m+1,n+1}^{\mu,\nu}. \quad (5.122)$$

As a result, left and right derivatives are computed exactly analogous to the coherent-state ladder, except that operators carry additional indices for the parity.

By extending the variational principle detailed in Sec. IV for the coherent-state ladder \mathcal{S} to the cat-state ladder \mathcal{S}_{cat} , we obtain *exactly* the same equations of motion (Eqs. (5.73) for a single bosonic mode and Eqs. (5.75) for multiple bosonic modes), except that the matrices \mathbf{Y}_0 and \mathbf{C}_0 take a slightly different form. Importantly, as the properties of the cat-state ladder with respect to derivatives in the parametrization parameter α of \mathcal{S}_{cat} remain exactly identical to the coherent-state ladder (See Eqs. (5.120)-(5.122) above and Eqs. (5.66)-(5.68) for the coherent-state ladder \mathcal{S}), we observe the same properties of \mathbf{Y}_0 and \mathbf{C}_0 as before, with the disadvantage that analytical expressions for \mathbf{Y}_0 and \mathbf{C}_0 can no longer be obtained easily.

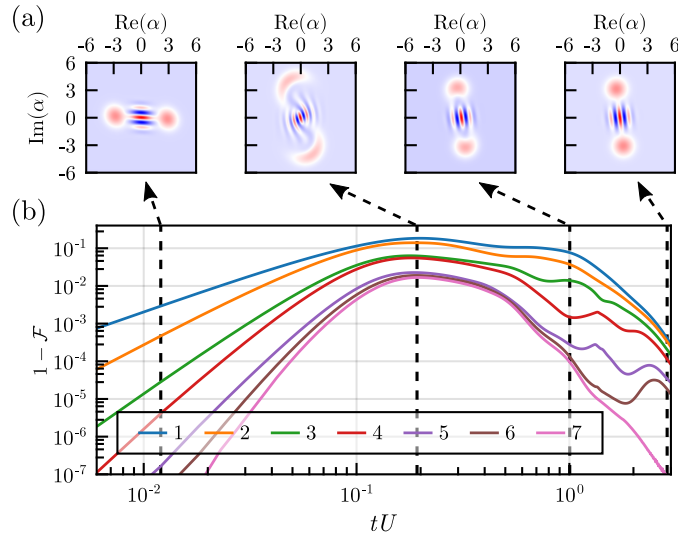


Figure 5.6: (a) Wigner functions at different times along the dynamics for an initial even cat state, highlighting the deformation of the cat state during the transient dynamics due to the present Kerr-interaction. (b) Infidelity $1 - \mathcal{F}$ as a function of time t (in units of U^{-1}) for different orders N of the basis \mathcal{S}_{cat} . System parameters: $\eta = U/4$, $G_0 = 5iU$, $G_1 = -i5U$.

IX Applications

Application Ia: Relaxation dynamics of a cat qubit.

As a first application and proof-of-principle of the cat-state ladder TDVP method, we consider a system where *both* the subspace, parametrized by α , *and* the density matrix coefficient matrix \mathbf{B} are evolving in time. To this end, we consider a quantum oscillator that is subject to a two-photon drive and Kerr-nonlinearity. In a frame rotating with the driving frequency, the system can be described with the following Hamiltonian, and Liouvillian

$$\hat{H} = \left(\frac{G}{2} \hat{a}^2 + \frac{G^*}{2} \hat{a}^{\dagger 2} \right) + \frac{U}{2} \hat{a}^{\dagger 2} \hat{a}^2, \quad (5.123)$$

$$\mathcal{L}[\hat{\rho}] = -i[\hat{H}, \hat{\rho}] + \eta \mathcal{D}[\hat{a}^2](\hat{\rho}), \quad (5.124)$$

where G is the amplitude of the two-photon drive and U is the Kerr-nonlinearity. Furthermore, the system is subject to two-photon loss with dissipation rate η . As the system admits a weak \mathbb{Z}_2 -symmetry, the steady-state manifold of the system is spanned by even and odd cat states, such that $\hat{\rho} \in \text{Span}\{|\mathcal{C}_\alpha^\mu\rangle\langle\mathcal{C}_\alpha^\nu|, \mu, \nu \in \{+, -\}\}$, with $\alpha = \sqrt{iG^2/(\eta^2 + U^2)}$ [408, 455]. We now consider an initial pure cat state $\hat{\rho}_0 = |\mathcal{C}_{\alpha'}^\sigma\rangle\langle\mathcal{C}_{\alpha'}^\sigma|$ that is not in the steady-state manifold of the system. We can, therefore, assume $\hat{\rho}_0$ to be in the steady-state manifold of the same system but

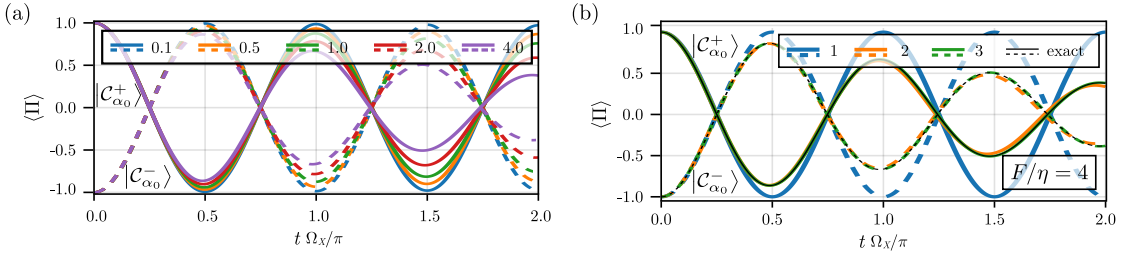


Figure 5.7: (a) For the continuous Zeno dynamics inducing a continuous \hat{X} -rotation of the cat qubit, we show the parity $\langle \hat{\Pi} \rangle$ as a function time (in units of Rabi frequency π/Ω_X) for different ratios of driving amplitude F/η for an initial even state (solid lines) and an initial odd state (dashed lines), for $G = 10\eta$. For larger values of F/η , code-space non-adiabatic effects lead to reduced gate fidelity. (b) For a non-adiabatic value of $F/\eta = 4$, we show the parity $\langle \hat{\Pi} \rangle$ as a function of time for different orders of the basis N using the cat-ladder variational method and compare the results to the exact simulation (black dashed line).

with different driving amplitude G' . Thus, evolving $\hat{\rho}_0$ with respect to Eq. (5.124), can be interpreted as a quench-dynamics, in which the system parameter G is changed from G' to G instantaneously at $t = 0$ and the system relaxes to the new steady-state. In Fig. 5.6(a), we depict snapshots of the Wigner function along selected times throughout the time evolution. We observe a significant departure from the cat-state manifold in the transient dynamics due to the Kerr interaction. This *deformation* of the cat provides an ideal test case for our variational method and allows an analysis of the performance when increasing the order of in cat-ladder ansatz. In Fig. 5.6(b), we show the infidelity $1 - \mathcal{F}$ as a function of time for different orders N in the cat-state ladder ansatz. As expected, we observe a lower fidelity in the transient regime as the density matrix significantly departs from a cat state. By increasing the order N , the dynamics of the density matrix can be described more accurately, capturing some of the quantum fluctuations in the state.

Non-adiabatic Zeno dynamics

As a second use case, our method allows for the study of time-dependent cat qubit gates and their study of leakage in particular. To this end, we now consider the case of vanishing nonlinearity, $U = 0$. We can induce a continuous \hat{X} -rotation gate through quantum Zeno dynamics [456–458] by adding a Hamiltonian evolution with a time-scale much slower than the two-photon dissipation rate (See also Chap. 3, Sec. III). A coherent rotation around the logical \hat{X} -axis can be realized by adding a single-photon drive $\hat{H}_X = F(\hat{a} + \hat{a}^\dagger)$ to the Hamiltonian in Eq. (5.123) [81], with single-photon driving amplitude F . In the adiabatic limit

$F \ll \eta$, the logical code space remains the cat qubit manifold and the qubit is adiabatically rotated an angle $\varphi = \Omega_X t$ around the \hat{X} -axis, with Rabi frequency $\Omega_X = 2F|\alpha|$ [81]. However, if the adiabatic condition is violated, the logical code space deviates from a pure cat qubit, leading to a deformation of the original cat qubit manifold. To study this effect, we show in Fig. 5.7(a) the average photon number parity $\langle \hat{\Pi} \rangle$ for different ratios of F/η as a function of time for even and odd initial cat states. We observe that for $F/\eta \gtrsim 1$, the single-photon pump induced non-adiabatic leakages outside of the original code-space manifold, reducing the fidelity of the rotation gate. To assess the efficiency of our method in capturing these non-adiabatic effects, we simulate the dynamics of the system for $F/\eta = 4$, a regime where the non-adiabatic effects are strong. In Fig. 5.7(b), we show $\langle \hat{\Pi} \rangle$ as a function of time for different orders N of the cat-state ladder basis and compare our results to the full quantum solutions. We observe that, already for $N = 3$, the variational method is able to accurately describe the time-evolution of this non-adiabatic Zeno dynamics.

Dynamics of interacting cat qubits

Simulating the dynamics of multiple interacting qubits poses an essential task. For example, studying code-space leakage and higher-order processes in cat qubit gates involving multiple cat qubits [81, 238] can lead to a significantly better understanding of these processes where analytical methods are unavailable, creating opportunities for better cat qubit device architectures and gate designs. To this end, we now consider a multi-mode bosonic system, where each mode k is described by a two-photon driven dissipative Kerr-nonlinear resonator with Hamiltonian in Eq. (5.123). Additionally, the modes interact via nearest-neighbor hopping (beam-splitter) Hamiltonian:

$$\hat{H}_{\text{int}} = \sum_{\langle k,l \rangle} J_{k,l} (\hat{a}_k \hat{a}_l^\dagger + \hat{a}_k^\dagger \hat{a}_l), \quad (5.125)$$

where $J_{k,l}$ is the hopping interaction between modes k and l . The system conserves the total photon number parity $\langle \hat{\Pi}_1 \otimes \hat{\Pi}_2 \otimes \cdots \otimes \hat{\Pi}_L \rangle$ for a system of L bosonic modes. The interaction through \hat{H}_{int} enables the coherent exchange of particles between neighboring modes, thereby creating entanglement in the system [81].

For a two-mode system, we simulate the time evolution using the cat-ladder TDVP method starting from an initial product state consisting of even-parity cat states, $|\psi(0)\rangle = |\mathcal{C}_{\alpha_1}^+\rangle \otimes |\mathcal{C}_{\alpha_2}^+\rangle$, where α_1 and α_2 differ from the coherent-state amplitudes characterizing the steady state of system. Similar to the single-mode case considered previously, this may represent a case where the two-photon drive amplitude is instantaneously changed at $t = 0$ so that the state will relax to its new steady state.

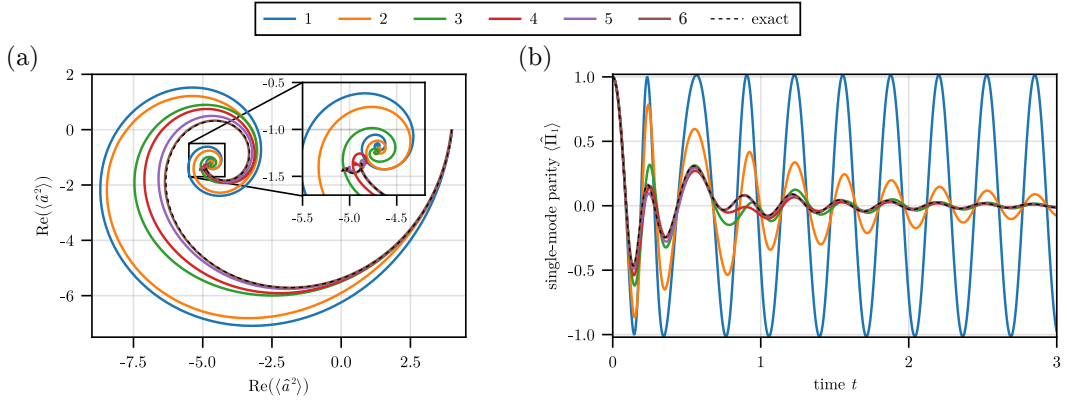


Figure 5.8: (a) Trajectories of the real and imaginary part of $\langle \hat{a}_1^2 \rangle$ along the dynamics of a system of two interacting two-photon driven-dissipative Kerr resonators for different orders N of the cat-state ladder basis. For the same system, we show in (b) the single-mode parity $\langle \hat{\Pi}_1 \rangle$ as a function of time for different values of N . System parameters: $G_i = 5U$, $\eta_i = 0.25U$, $J_{1,2} = U$, initial state: $|\psi(0)\rangle = |\mathcal{C}_{\alpha_1}^+, \mathcal{C}_{\alpha_2}^+\rangle$, with $\alpha_1 = \alpha_2 = 2$.

In Fig. 5.8, we show the real and imaginary part of $\langle \hat{a}^2 \rangle$ as the system evolves in time for different orders N of the cat-state ladder. In the setup considered, the system evolves both in the basis parameter α as well as in the density matrix coefficients \mathbf{B} , and we observe convergence to the exact dynamics for low N , showcasing the efficiency of the method in representing cat-qubit dynamics. In Fig. 5.8(b), we show the single-mode parity $\langle \hat{\Pi}_1 \rangle$ as a function of time for different values of N , where we also observe an accurate agreement with the exact dynamics for $N > 6$ for the given system parameters.

As a final example using cat-qubits, we now consider a chain of three interacting two-photon driven-dissipative Kerr resonators. Simulating these systems for large average occupation numbers $\langle \hat{n}_i \rangle$ becomes already challenging for conventional methods, such as the Fock-space method, as the required number Fock-space density matrix coefficients scale as $\langle \hat{n}_i \rangle^{2L}$. However, if the dynamics remains close to a cat qubit throughout the dynamics, the cat-state ladder TDVP method can efficiently describe the system's dynamics. The order N of the cat-ladder \mathcal{S}_{cat} required depends only on the deformation of the cat-space manifold, i.e. the amount of quantum fluctuations on top of the cat-space needed to capture the density matrix. When the dynamics remains close to a cat qubit manifold, the order N of basis states in \mathcal{S} is independent of α and thus requires significantly less memory to simulate the dynamics of the system. In Fig. 5.9(a-b), we show the single-mode parity $\langle \hat{\Pi}_1 \rangle$ and two-mode parity $\langle \hat{\Pi}_1 \hat{\Pi}_2 \rangle$ as a function of time for an initial product state of cat-qubits. For the given set of system parameters, we already observe good agreement with Fock-space simulation results for $N \geq 4$.

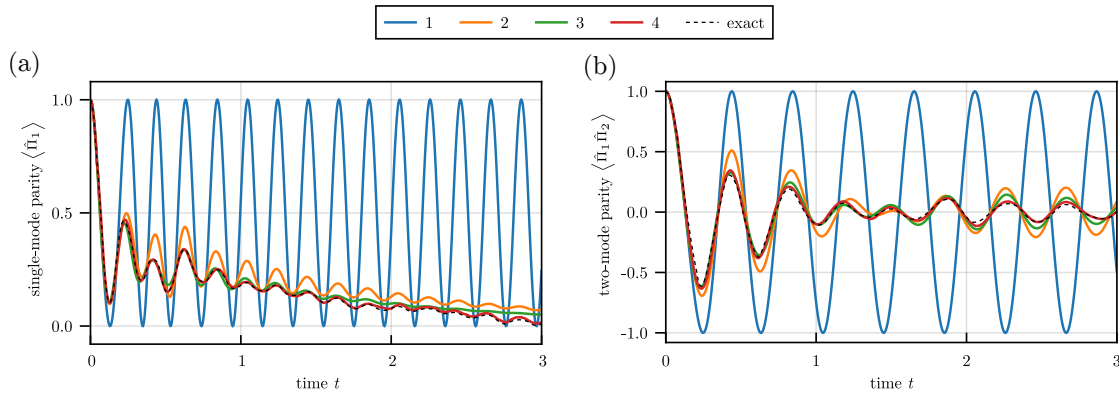


Figure 5.9: Single-mode parity $\langle \hat{\Pi}_1 \rangle$ (a) and two-mode parity $\langle \hat{\Pi}_1 \hat{\Pi}_2 \rangle$ (b) as a function of time for a system of three coupled two-photon driven-dissipative Kerr resonators. System parameters: $G_i = 5U$, $\eta_i = 0.25U$, $J_{12} = J_{23} = 0.8U$, initial state $|\psi(0)\rangle = |\mathcal{C}_{\alpha_1}^+, \mathcal{C}_{\alpha_2}^+, \mathcal{C}_{\alpha_3}^+\rangle$, with $\alpha_i = 2$.

X Beyond coherent-state and cat-state ladder TDVP

We have shown in the previous sections that the coherent-state ladder TDVP method and the cat-state ladder TDVP method can be efficient numerical variational methods to study the dynamics and steady-state properties of bosonic systems in the regime where the quantum state remains coherent-like (in the coherent-state ladder) or cat-like (in the cat-state ladder) throughout the dynamics of they system.

We can further extend the applicability of the developed methods by including higher-order photon processes in the basis-parametrization and by changing the construction of the coherent-state ladder. We will briefly discuss these aspects below.

Basis parametrization including higher-order processes

In the previous section, for both the coherent-state ladder and the cat-state ladder, the basis was parametrized by a single parameter α , characterizing the coherent-state amplitude. We can, however, include higher-order processes such as squeezing and higher-order processes in the parametrization of the basis. For a single bosonic mode, we can define the following un-normalized state that includes up to K -photon moments,

$$|\vec{\theta}\rangle \equiv \prod_{n=1}^K e^{\theta_n \hat{a}^{\dagger n}} |0\rangle. \quad (5.126)$$

We clearly identify $\theta_1 = \alpha$. Since the operators applied onto the vacuum state only contain creation operators, every operator commutes with each other. We can hence naturally relate derivatives of the state $|\vec{\theta}\rangle$ with respect to θ_n to the application of $\hat{a}^{\dagger n}$:

$$\frac{\partial}{\partial \theta_n} |\vec{\theta}\rangle = \hat{a}^{\dagger n} |\vec{\theta}\rangle. \quad (5.127)$$

We define a photon-added ladder from the basis state $|\vec{\theta}\rangle$ by $\mathcal{S}_{\vec{\theta}} \equiv \{\hat{a}^{\dagger k} |\vec{\theta}\rangle, k = 0, \dots, N\}$. We thus have the following equation of motion for the variational parameters $\vec{\theta}$ for a single bosonic mode:

$$\dot{\theta}_n = [\mathbf{C}^{-1} \mathbf{Y}]_n, \quad (5.128)$$

with

$$[\mathbf{C}]_{kl} = \text{Tr}\{\mathbf{C}_0^{k,l} [\mathbf{B} \mathbf{S} \mathbf{B}]\}, \quad (5.129)$$

$$\mathbf{Y}_k = \text{Tr}\{\mathbf{Y}_0^{(k)} \mathbf{B}\}, \quad (5.130)$$

$$[\mathbf{C}_0]_{m,n}^{k,l} \equiv \langle \partial_{\theta_k} \varphi_m | [\hat{\mathbf{1}} - \hat{P}_S] | \partial_{\theta_l} \varphi_n \rangle, \quad (5.131)$$

$$[\mathbf{Y}_0]_{m,n}^k \equiv \langle \partial_{\theta_k} \varphi_m | [\hat{\mathbf{1}} - \hat{P}_S] \mathcal{L}[\hat{\rho}] | \varphi_n \rangle. \quad (5.132)$$

Using the fact that higher-photon processes correspond to higher-order derivatives (See Eq. (5.127)), we can deduce that the equation of motion for $\vec{\theta}$ is now sensitive not only to occupations of the corner-state but also states that are of lower order. Hence, the quantum-geometric tensor \mathbf{C}_0 now contains elements not only related to the corner of the basis $\mathcal{S}_{\vec{\theta}}$, as derivatives of states in $\mathcal{S}_{\vec{\theta}}$ with respect to θ_n are identical to the application of $\hat{a}^{\dagger n}$. Consequently, if $\vec{\theta}$ and $\mathcal{S}_{\vec{\theta}}$ have the same dimensions, the quantum-geometric tensor has full rank, and the evolution of $\vec{\theta}$ is sensitive to every matrix element in \mathbf{B} . As a result, some of the numerical challenges resulting from \mathbf{C}_0 being of rank one for \mathcal{S} and rank two for \mathcal{S}_{cat} due to the two symmetry sectors, can be alleviated. For $\dim(\vec{\theta}) = \dim(\mathcal{S}_{\vec{\theta}})$, \mathbf{C}_0 is a full-rank tensor. In this case, however, from Eq. (5.128), the matrix \mathbf{C} of dimension $\dim(\vec{\theta})^2$ has to be inverted numerically – contrary to the coherent-state ladder and cat-state ladder where computing $\dot{\alpha}$ amounts to a simple division of two complex numbers (See Eqs. (5.73)).

Alternative basis constructions

A distinctive property of the coherent-state ladder \mathcal{S} is that the tangent space of \mathcal{S}_N lies in \mathcal{S}_{N+1} as outlined in Sec. III.2. Importantly, as the derivative with respect to α of a photon-added Bargmann state $|\alpha, n\rangle$ is identical to $|\alpha, n+1\rangle$

| basis | \mathcal{S} | \mathcal{S}' |
|--------------------------------------|--|--|
| | $ \alpha, n\rangle = \hat{a}^{\dagger n} \alpha\rangle$ | $ \alpha, n\rangle = (\hat{a}^\dagger + \alpha^*)^n 0\rangle$ |
| \hat{a} | $\alpha \alpha, n\rangle + n \alpha, n-1\rangle$ | $n \alpha, n-1\rangle$ |
| \hat{a}^\dagger | $ \alpha, n+1\rangle$ | $\alpha \alpha, n\rangle + \alpha, n+1\rangle$ |
| $\frac{\partial}{\partial \alpha}$ | $ \alpha, n+1\rangle$ | 0 |
| $\frac{\partial}{\partial \alpha^*}$ | 0 | $n \alpha, n-1\rangle$ |
| \mathcal{S} | recursive & analytic | recursive & analytic |
| \mathbf{C}_0 | rank-1 | rank- $(N-2)$ |

Table 5.1: Schematic comparison of the coherent-state ladder \mathcal{S} and the photon-added-displaced basis \mathcal{S}' .

(See Eq. (5.51)), the derivative of the corner state $||\alpha, N-1\rangle$ of the basis \mathcal{S}_N with respect to α does not lie in \mathcal{S}_N . As a result, the quantum-geometric tensor \mathbf{C}_0 is only non-zero corresponding to the population of the corner state, causing the equation of motion for $\dot{\alpha}$ to be well-defined only if the corner state is populated. We might seek an alternative construction of a photon-added coherent-state basis that does not result in a highly singular quantum-geometric tensor while still maintaining most of the properties of \mathcal{S} .

As a candidate basis \mathcal{S}' , we define the states

$$|\alpha, n\rangle \equiv \hat{D}(\alpha)^\dagger \hat{a}^{\dagger n} \hat{D}(\alpha) |0\rangle = (\hat{a}^\dagger + \alpha^*)^n |0\rangle. \quad (5.133)$$

Here, we apply the operator $\hat{a}^{\dagger n}$ in a frame that is displaced by α . For $n=0$, we have $|\alpha, 0\rangle = |0\rangle$. We can straightforwardly verify the following relations to derivatives with respect to α :

$$\frac{\partial}{\partial \alpha} |\alpha, n\rangle = 0, \quad (5.134)$$

$$\begin{aligned} \frac{\partial}{\partial \alpha^*} |\alpha, n\rangle &= n(\hat{a}^\dagger + \alpha^*)^{n-1} |0\rangle \\ &= n |\alpha, n-1\rangle. \end{aligned} \quad (5.135)$$

Note that here, in contrast to the basis \mathcal{S} , the derivative point *downwards* in the

basis \mathcal{S}' . Furthermore, we have the relations

$$\begin{aligned}\hat{a}|\alpha, n\rangle &= \hat{a}(\hat{a}^\dagger + \alpha^*)^n |0\rangle \\ &= [n(\hat{a}^\dagger)^{n-1} + (\hat{a}^\dagger + \alpha^*)^n \hat{a}] |0\rangle \\ &= n|\alpha, n-1\rangle = \frac{\partial}{\partial \alpha^*} |\alpha, n\rangle,\end{aligned}\tag{5.136}$$

$$\begin{aligned}\hat{a}^\dagger|\alpha, n\rangle &= \hat{a}^\dagger(\hat{a}^\dagger + \alpha^*)^n |0\rangle \\ &= (\hat{a}^\dagger - \alpha^* + \alpha^*)(\hat{a}^\dagger + \alpha^*)^n |0\rangle \\ &= [-\alpha^*(\hat{a}^\dagger + \alpha^*)^n + (\hat{a}^\dagger + \alpha^*)^{n+1}] |0\rangle \\ &= -\alpha^*|\alpha, n\rangle + |\alpha, n+1\rangle,\end{aligned}\tag{5.137}$$

where we have used the relation $[\hat{a}, f(\hat{a}^\dagger)] = \frac{\partial f}{\partial \hat{a}^\dagger}$ [459]. The overlap matrix elements $S_{m,n} = \langle \alpha, m | \alpha, n \rangle$ can be computed recursively,

$$\begin{aligned}S_{m,n} &= (|\alpha|^2 + 1)S_{m-1,n-1} + (n-1)\alpha^*S_{m-1,n-2} \\ &\quad + \alpha(m-1)S_{m-2,n-1} + (n-1)(m-1)S_{m-2,n-2},\end{aligned}\tag{5.138}$$

with $S_{0,0} = 1$ and $S_{0,n} = \alpha^{*n}$. A comparison between the coherent-state ladder \mathcal{S} and the alternative basis \mathcal{S}' is given in Tab. 5.1.

XI Discussion and Outlook

In this chapter, we have studied variational approaches of numerically simulating the dynamics of bosonic open quantum systems. In Sec. III.2, we have constructed the coherent-state ladder that lies at the heart of the ansatz for the variational method. The computational basis states of the coherent-state ladder are non-orthonormal photon-added Bargmann states. The overlap matrix and its inverse can be calculated analytically. Operators can be straightforwardly computed in this basis and derivatives with respect to the variational parameter α – parametrizing the coherent-field amplitude of the basis – can be computed as block-shifts in the matrix-representation. We have derived the resulting equations of motion and discussed the numerical implementation. We have showcased the performance of the method by applying it onto several relevant examples in Sec. VII, such as the driven-dissipative Kerr resonator, an asymmetrically driven non-linear photonic dimer, and a driven-dissipative Bose-Hubbard chain. In all these examples, and in the studied regimes, our method needed considerably fewer basis states to describe the dynamics of the system accurately.

We extended the coherent-state ladder by including rotational symmetry sectors in the variational ansatz in Sec. VIII. In particular, we introduced the *cat-state*

ladder, a computational basis based on even and odd superposition of photon-added Bargmann states. Using the cat-state ladder variational method, we numerically studied several systems of cat-qubit dynamics in Sec. IX, such as a two-photon driven-dissipative Kerr-resonator, to study quench dynamics and the non-adiabatic effect of cat-qubit rotations. These studies reveal that the cat-state ladder provides an ideal method to study cat-qubit dynamics in which the density matrix remains in a subspace that is cat-like, which is the typical working regime in many cat-qubit-based quantum devices. Furthermore, we have showcased the applicability of the cat-state TDVP method by numerically simulating two and three interacting bosonic cat-qubits, a use case in which conventional numerical methods start to become challenging.

As the tangent space of the coherent-state and cat-state ladder lie in the same space with an additional photon-added state, the quantum-geometric tensor characterizing the geometry of the variational manifold is only non-zero for the corner-state in the basis, i.e., the highest photon-added state included in the basis. As a result, the equation of motion for the evolution of the variational parameter α is well-defined only if the density matrix has non-vanishing occupation of the corner state. We discussed in Sec. V.3 different numerical regularization schemes to handle this singularity in the equations of motion. We discussed possible extensions of the coherent-state ladder ansatz in Sec. X to include higher-order photon processes in the parametrization of the basis. Additionally, we discussed an alternative construction of a coherent-state ladder that admits a similar structure to the coherent-state ladder defined previously but has a dense rank of the quantum-geometric tensor, thereby presenting a viable alternative variational basis ansatz.

The methods developed in this chapter can be extended to a wide range of applications. At the heart of the variational ansatz lies the assumption that the quantum state can be described in a basis of coherent states and quantum fluctuations thereof. In some scenarios, this assumption breaks down, for example, in the presence of bistability [131, 439, 460, 461]. It remains an interesting question how these systems can be described efficiently using a variational ansatz in the presence of dissipation.

General Conclusion and Outlook

Stepping back, we conclude this thesis by reviewing our main findings, and putting this work into a broader picture in the scientific community.

In Chap. 2, we have reviewed the theory of open bosonic systems that provided a basis for this thesis in which the systems considered were fundamentally *open*. In Chap. 3, we introduced *quantum error correction*, with a specific focus on *bosonic quantum error correction*, where we have analyzed the most common noise models encountered in bosonic systems and characterized under what conditions bosonic quantum codes are *exactly* and *approximately* correctable. Much of the discussion focused on the cat qubit – a promising candidate for fault-tolerant quantum computing.

These two introductory chapters provided the foundation for the results presented in Chap. 4 and Chap. 5.

Bosonic Quantum Error Correction

One of our guiding questions throughout this thesis was how we can efficiently encode quantum information redundantly in the state-space of a quantum harmonic oscillator with a low hardware overhead. Bosonic systems in particular, have proven to be promising candidates for fault-tolerant quantum devices, as they can be universally controlled and can be efficiently implemented on various hardware platforms.

The cat qubit is a noteworthy bosonic quantum code to which we devoted much attention in this thesis. As a *biased-noise* qubit, it is a promising solution for fault-tolerant quantum computing as an element of higher-level quantum error correction schemes.

In Chap. 4, we have proposed the *squeezed cat code* and thoroughly analyzed its error correction properties, both analytically and numerically. Surprisingly, in the limit of small displacement and large squeezing, the squeezed cat code enables the correction of *both* photon loss and dephasing errors. Furthermore, we observe a double-exponential suppression of dephasing errors with respect to the squeezing parameter, making it an even stronger noise-biased qubit. Even in experimentally

relevant regimes the squeezed cat qubit outperforms the cat qubit, in some regimes even up to an order of magnitude.

This bosonic qubit has gained interest in the scientific community [83, 94, 255, 268, 392, 462–474], and we foresee its application as a biased-noise qubit in quantum information processing, but also its use in quantum communication [469] and quantum sensing.

Although its error-correction capabilities have been studied in this thesis, some questions still remain unanswered or still need more research: How can the squeezed cat code manifold be autonomously stabilized in a circuit QED implementation? How can fault-tolerant gates be performed on the squeezed cat qubit? How can photon loss be corrected using dissipation engineering in practice? In particular, engineering quantum gates should ideally preserve the enhanced noise bias provided by the squeezed cat code [85, 89]. As the additional protection induced by a finite amount of squeezing is *not* of the same kind as provided by the displacement, finding bias-preserving gates is crucial to foster the capabilities of the squeezed cat code. We see that this is just the start and much work still needs to be done to fully understand quantum computing using the squeezed cat code.

Ultimately, it is a matter of active research to find *optimal* bosonic code, depending on the noise regime of the hardware platform. Many hardware implementations of theoretically proposed quantum error correction codes [64, 76, 78, 85, 86, 239–241, 475] have so far not taken fully into account the hardware-specific characteristics of noise and the respective noisy gate operations, and this work is no exception. Recent theoretical results, however, indicate an intricate interplay between the specific nature of the noise channel and the optimal bosonic quantum code [234, 256, 268, 476]. Investigating how the lifetime of quantum information can be increased using quantum error correction protocols *given the underlying noise of the system*, as well as the *inherently noisy gate operations* necessary for state preparation and recovery operations, is an essential step toward efficient quantum error correction.

An important remaining practical and relevant question therefore is:

What are optimal bosonic quantum codes that can be achieved on noisy quantum devices?

Making headway in answering this question requires investigating and employing analytical and numerical optimization techniques that take into account noisy hardware operations to optimize *hardware-tailored* bosonic quantum codes. More specifically, this also amounts to studying noise and noisy operations encountered at specific hardware platforms. We leave this as a fundamental open problem to the community.

Another question directly related to bosonic quantum codes that we have addressed in this thesis is: *How can we efficiently simulate these systems?*

Simulation of Open Bosonic Systems

Fully understanding processes in driven-dissipative bosonic systems requires going beyond analytical methods, which often are restricted by approximations. Simulating dynamical open multi-boson systems can be challenging due to the fact that a single bosonic mode already has an infinitely large Hilbert space. Luckily, in many physically relevant systems, the state space is restricted to a narrow – but moving – corner of the Hilbert space.

In Chap. 5, we have tackled a new simulation method to simulate the dynamics of open bosonic systems using a variational parametrization of a so-called *coherent-state ladder*. We have seen that such a variational approach is capable of simulating the dynamics of low-entropic systems which can be efficiently described by coherent states and fluctuations thereof. As such, our method goes beyond a standard mean-field description and is able to include quantum fluctuations.

Furthermore, we have extended this method and introduced the *cat-state ladder*, which includes the rotational symmetry sectors of the cat qubit. With this variational method, we were able to simulate dynamical processes in cat qubit systems in an ideal basis, requiring much fewer basis states as in, e.g., a standard Fock basis. This method allows for the simulation of many interacting cat qubits, which is an essential tool for studying the effects of many-qubit quantum circuits based on the cat code. We foresee that this method or variations of it will be applied to efficiently simulate the dynamical effects of interacting cat qubits and other bosonic codes in the future.

Let us note that this developed method is not perfect, as it includes some numerical challenges discussed in Chap. 5, Sec. X. It is an interesting question in itself to find an *ideal* variational parametrization that is not only efficient in the representation of the relevant part of the Hilbert space but also computationally efficient in computing the resulting equations of motion, and we leave this as an open question to be explored in the future.

Furthermore, when simulating many-boson systems, in the current formulation of the technique, the number of density matrix coefficients still grows exponentially with the number of bosonic modes. If the entanglement between bosonic systems is locally bounded, efficient tensor-network representations within the *cat-state ladder*, such as *matrix-product density matrix* approaches, might further increase the efficiency of this method [143, 149, 477].

As it stands, simulating the dynamics of open bosonic systems efficiently in which the quantum states admit a specific structure throughout their evolution is

an active area of research. With this work, we have contributed to an approach to efficiently simulate the dynamics of coherent-state-like and cat-like systems.

With this, let me conclude this thesis. Quantum devices have made it to the point of immense control, enabling the execution of algorithms that are beyond the capabilities of classical computers. However, to reach the regime of practically *useful applications*, new approaches are needed. Quantum error correction provides such an approach, and recent research results with bosonic systems have indicated their promise of reaching this goal. Actual quantum devices, however, are intrinsically noisy. Correcting the noise of quantum hardware and efficiently simulating the resulting dynamics efficiently is hard. Nevertheless, it is the hard problems that, time and time again, prove to be the most interesting ones. And so I hope that this work presented here has provided a step in the right direction, and I remain curious as to what comes next.

A

Analytical Knill-Laflamme matrix elements for the cat code and squeezed cat code

Here, we report the analytical Knill-Laflamme matrix elements of the form

$$\langle \psi_i | \hat{E}_l^\dagger \hat{E}_{l'} | \psi_j \rangle, \quad (\text{A.1})$$

where $\{\hat{E}_l\}$ is a given set of errors and $|\psi_{i/j}\rangle$ are the logical code words.

In the following, we consider the set of errors:

$$\left\{ \hat{\mathbb{1}}, \hat{a}, \hat{a}^\dagger \hat{a}, (\hat{a}^\dagger \hat{a})^2 \right\}. \quad (\text{A.2})$$

Cat code

As we detailed in this thesis in Chap. 3, Sec. VI, the two-component cat states are defined by

$$|\mathcal{C}_\alpha^\pm\rangle = \frac{1}{N_\alpha^\pm} (|\alpha\rangle \pm |-\alpha\rangle), \quad (\text{A.3})$$

where

$$N_\alpha^\pm = \sqrt{2(1 \pm e^{-2|\alpha|^2})}. \quad (\text{A.4})$$

Thus, the following relation between normalization constants of the even and odd cat state holds

$$\left(\frac{N_\alpha^-}{N_\alpha^+} \right)^2 = \tanh(|\alpha|^2). \quad (\text{A.5})$$

For notational convenience, however, we use the normalization constants instead.

In Tab. A.1, we show the Knill-Laflamme matrix elements

$$\langle \mathcal{C}_\alpha^\pm | \hat{E}_l^\dagger \hat{E}_{l'} | \mathcal{C}_\alpha^\pm \rangle$$

| $\hat{E}_l^\dagger \setminus \hat{E}_{l'}$ | $\hat{\mathbb{1}}$ | \hat{a} | $\hat{a}^\dagger \hat{a}$ | $(\hat{a}^\dagger \hat{a})^2$ |
|--|--|--|---|---|
| $\hat{\mathbb{1}}$ | 1 | 0 | $ \alpha ^2 \frac{(N_\alpha^\mp)^2}{(N_\alpha^\pm)^2}$ | $ \alpha ^2 \left(\alpha ^2 + \frac{(N_\alpha^\mp)^2}{(N_\alpha^\pm)^2} \right)$ |
| \hat{a}^\dagger | 0 | $ \alpha ^2 \frac{(N_\alpha^\mp)^2}{(N_\alpha^\pm)^2}$ | 0 | 0 |
| $\hat{a}^\dagger \hat{a}$ | $ \alpha ^2 \frac{(N_\alpha^\mp)^2}{(N_\alpha^\pm)^2}$ | 0 | $ \alpha ^2 \left(\alpha ^2 + \frac{(N_\alpha^\mp)^2}{(N_\alpha^\pm)^2} \right)$ | $ \alpha ^2 \left(3 \alpha ^2 + \frac{(\alpha ^4+1)(N_\alpha^\mp)^2}{(N_\alpha^\pm)^2} \right)$ |
| $(\hat{a}^\dagger \hat{a})^2$ | $ \alpha ^2 \left(\alpha ^2 + \frac{(N_\alpha^\mp)^2}{(N_\alpha^\pm)^2} \right)$ | 0 | $ \alpha ^2 \left(3 \alpha ^2 + \frac{(\alpha ^4+1)(N_\alpha^\mp)^2}{(N_\alpha^\pm)^2} \right)$ | $ \alpha ^2 \left(\alpha ^2 (\alpha ^4 + 7) + \frac{6 \alpha ^4+1}{(N_\alpha^\pm)^2} (N_\alpha^\mp)^2 \right)$ |

$$\langle \mathcal{C}_\alpha^\pm | \hat{E}_l^\dagger \hat{E}_{l'} | \mathcal{C}_\alpha^\mp \rangle$$

| $\hat{E}_l^\dagger \setminus \hat{E}_{l'}$ | $\hat{\mathbb{1}}$ | \hat{a} | $\hat{a}^\dagger \hat{a}$ | $(\hat{a}^\dagger \hat{a})^2$ |
|--|--|--|---|--|
| $\hat{\mathbb{1}}$ | 0 | $\alpha \frac{N_\alpha^\pm}{N_\alpha^\mp}$ | 0 | 0 |
| \hat{a}^\dagger | $\alpha^* \frac{N_\alpha^\mp}{N_\alpha^\pm}$ | 0 | $ \alpha ^2 \frac{\alpha^* N_\alpha^\pm}{N_\alpha^\mp}$ | $ \alpha ^2 \frac{\alpha^* (\alpha ^2 (N_\alpha^\mp)^2 + (N_\alpha^\pm)^2)}{N_\alpha^\mp N_\alpha^\pm}$ |
| $\hat{a}^\dagger \hat{a}$ | 0 | $ \alpha ^2 \frac{\alpha N_\alpha^\mp}{N_\alpha^\pm}$ | 0 | 0 |
| $(\hat{a}^\dagger \hat{a})^2$ | 0 | $ \alpha ^2 \frac{\alpha (\alpha ^2 (N_\alpha^\pm)^2 + (N_\alpha^\mp)^2)}{N_\alpha^\mp N_\alpha^\pm}$ | 0 | 0 |

Table A.1: Knill-Laflamme matrix elements for the cat states $|\mathcal{C}_\alpha^\pm\rangle$.

Squeezed cat code

As detailed in Chap. 4, Sec. I, the squeezed cat code is defined as

$$|\mathcal{C}_{\alpha,\xi}^\pm\rangle = \frac{1}{N_{\alpha,\xi}^\pm} (|\alpha, \xi\rangle \pm |-\alpha, \xi\rangle) \quad (\text{A.6})$$

$$= \hat{S}(\xi) \frac{1}{N_\gamma^\pm} (|\gamma\rangle \pm |-\gamma\rangle), \quad (\text{A.7})$$

with $\gamma = \alpha e^{i\xi}$ in the case of squeezing orthogonal to the displacement (See Chap. 4, Sec. I, Eq. (4.8) for the general case). The normalization constant is hence identical to Eq. (A.4).

Due to the different photon number parity of the code words, any Wick-ordered operator $:\hat{O} := \hat{a}^{\dagger m} \hat{a}^n$ with odd $m+n$ will change the parity of the state, and conversely, for even $m+n$, the parity of the state will remain the same. Note that the initial ordering of creation and annihilation operators in \hat{O} is irrelevant for this statement.

As a result, we generally have:

$$\langle \pm | \hat{a}^{\dagger m} \hat{a}^n | \pm \rangle \begin{cases} = 0, & \text{for } m + n \text{ even} \\ \neq 0, & \text{for } m + n \text{ odd} \end{cases}, \quad (\text{A.8})$$

where \pm describes the even and odd parity of the state. As such, this relation holds true also for the standard cat-code. The cases in the above relation change place when computing $\langle \pm | \hat{a}^{\dagger m} \hat{a}^n | \mp \rangle$.

We, therefore, only look at non-trivial (i.e. non-zero) contributions to the Knill-Laflamme matrix elements.

We show in Tab. A.2 and Tab. A.3, the non-trivial Knill-Laflamme matrix elements for the squeezed cat states and the error set in Eq. (A.2). In Tab. A.2, we provide the matrix-elements of the form $\langle \mathcal{C}_{\alpha,\xi}^{\pm} | \hat{E}_l^{\dagger} \hat{E}_{l'} | \mathcal{C}_{\alpha,\xi}^{\pm} \rangle$, and in Tab. A.3, we give matrix-elements of the form $\langle \mathcal{C}_{\alpha,\xi}^{\pm} | \hat{E}_l^{\dagger} \hat{E}_{l'} | \mathcal{C}_{\alpha,\xi}^{\mp} \rangle$.

| | |
|---|---|
| $\langle \mathcal{C}_{\alpha,\xi}^{\pm} \hat{a}^{\dagger} \hat{a} \mathcal{C}_{\alpha,\xi}^{\pm} \rangle$ | $\sinh(\xi) (\sinh(\xi) - 2\gamma^2 \cosh(\xi)) + \frac{\gamma^2 \cosh(2\xi) (N_{\alpha\xi}^{\mp})^2}{(N_{\alpha\xi}^{\pm})^2}$ |
| $\langle \mathcal{C}_{\alpha,\xi}^{\pm} (\hat{a}^{\dagger} \hat{a})^2 \mathcal{C}_{\alpha,\xi}^{\pm} \rangle$ | $\frac{1}{4} \left((4\gamma^4 + 1) \cosh(4\xi) + 4\gamma^2 \sinh(2\xi) - 6\gamma^2 \sinh(4\xi) - 2 \cosh(2\xi) + \frac{2\gamma^2 (-2\gamma^2 \sinh(4\xi) - 2 \cosh(2\xi) + 3 \cosh(4\xi) + 1) (N_{\alpha\xi}^{\mp})^2}{(N_{\alpha\xi}^{\pm})^2} + 1 \right)$ |
| $\langle \mathcal{C}_{\alpha,\xi}^{\pm} (\hat{a}^{\dagger} \hat{a})^3 \mathcal{C}_{\alpha,\xi}^{\pm} \rangle$ | $\frac{1}{32} \left[(24\gamma^4 + 11) \cosh(2\xi) - 2(24\gamma^4 + 5) \cosh(4\xi) - 2\gamma^2 [(16\gamma^4 + 45) \sinh(6\xi) - 60\gamma^2 \cosh(6\xi) + \sinh(2\xi) - 36 \sinh(4\xi)] + 5 \cosh(6\xi) - 6 + 2\gamma^2 \left(\frac{N_{\alpha\xi}^{\mp}}{N_{\alpha\xi}^{\pm}} \right)^2 \left((16\gamma^4 + 45) \cosh(6\xi) - 12(\gamma^2 (\sinh(2\xi) - 2 \sinh(4\xi) + 5 \sinh(6\xi)) + 1) + 19 \cosh(2\xi) - 36 \cosh(4\xi) \right) \right]$ |
| $\langle \mathcal{C}_{\alpha,\xi}^{\pm} (\hat{a}^{\dagger} \hat{a})^4 \mathcal{C}_{\alpha,\xi}^{\pm} \rangle$ | $\frac{1}{64} \left[-6(16\gamma^4 + 3) \cosh(2\xi) + 16(7\gamma^4 + 1) \cosh(4\xi) - 2(240\gamma^4 + 7) \cosh(6\xi) + 72\gamma^4 - 56\gamma^2 \sinh(2\xi) + (64\gamma^8 + 840\gamma^4 + 7) \cosh(8\xi) + 8(9 - 8\gamma^4) \gamma^2 \sinh(4\xi) + 8(16\gamma^4 + 45) \gamma^2 \sinh(6\xi) - 28(16\gamma^4 + 15) \gamma^2 \sinh(8\xi) + 9 + 4\gamma^2 \left(\frac{N_{\alpha\xi}^{\mp}}{N_{\alpha\xi}^{\pm}} \right)^2 \left(4(4\gamma^4 + 3) \cosh(4\xi) - 2(16\gamma^4 + 45) \cosh(6\xi) - 22 \cosh(2\xi) + 105 \cosh(8\xi) + 11 + 2\gamma^2 [56\gamma^2 \cosh(8\xi) - (8\gamma^4 + 105) \sinh(8\xi) + 12 \sinh(2\xi) - 14 \sinh(4\xi) + 60 \sinh(6\xi)] \right) \right]$ |

Table A.2: Non-trivial Knill-Laflamme matrix elements for the squeezed cat code of the form $\langle \mathcal{C}_{\alpha,\xi}^{\pm} | \hat{E}_l^{\dagger} \hat{E}_{l'} | \mathcal{C}_{\alpha,\xi}^{\pm} \rangle$.

| | |
|---|---|
| $\langle \mathcal{C}_{\alpha,\xi}^{\pm} \hat{a} \mathcal{C}_{\alpha,\xi}^{\mp} \rangle$ | $\frac{\gamma \cosh(\xi) N_{\alpha\xi}^{\pm}}{N_{\alpha\xi}^{\mp}} - \frac{\gamma \sinh(\xi) N_{\alpha\xi}^{\mp}}{N_{\alpha\xi}^{\pm}}$ |
| $\langle \mathcal{C}_{\alpha,\xi}^{\pm} \hat{a}^{\dagger} \mathcal{C}_{\alpha,\xi}^{\mp} \rangle$ | $\frac{\gamma \cosh(\xi) N_{\alpha\xi}^{\mp}}{N_{\alpha\xi}^{\pm}} - \frac{\gamma \sinh(\xi) N_{\alpha\xi}^{\pm}}{N_{\alpha\xi}^{\mp}}$ |
| $\langle \mathcal{C}_{\alpha,\xi}^{\pm} (\hat{a}^{\dagger})^2 \hat{a} \mathcal{C}_{\alpha,\xi}^{\mp} \rangle$ | $\frac{\gamma(4\gamma^2 \cosh(3\xi) + 5 \sinh(\xi) - 3 \sinh(3\xi)) N_{\alpha\xi}^{\pm}}{4N_{\alpha\xi}^{\mp}} - \frac{\gamma(4\gamma^2 \sinh(3\xi) + 3 \cosh(\xi) - 3 \cosh(3\xi)) N_{\alpha\xi}^{\mp}}{4N_{\alpha\xi}^{\pm}}$ |
| $\langle \mathcal{C}_{\alpha,\xi}^{\pm} (\hat{a}^{\dagger})^2 \hat{a} \hat{a}^{\dagger} \hat{a} \mathcal{C}_{\alpha,\xi}^{\mp} \rangle$ | $\frac{\gamma N_{\alpha\xi}^{\pm}}{16N_{\alpha\xi}^{\mp}} \left[8\gamma^2 \left(-2\gamma^2 \sinh(5\xi) + \cosh(\xi) - 4 \cosh(3\xi) + 5 \cosh(5\xi) \right) - 22 \sinh(\xi) + 27 \sinh(3\xi) - 15 \sinh(5\xi) \right] + \frac{\gamma N_{\alpha\xi}^{\mp}}{16N_{\alpha\xi}^{\pm}} \left[(16\gamma^4 + 15) \cosh(5\xi) - 8\gamma^2 (\sinh(\xi) - 4 \sinh(3\xi) + 5 \sinh(5\xi)) + 6 \cosh(\xi) - 21 \cosh(3\xi) \right]$ |
| $\langle \mathcal{C}_{\alpha,\xi}^{\pm} \hat{a}^{\dagger} \hat{a}^2 \mathcal{C}_{\alpha,\xi}^{\mp} \rangle$ | $\frac{\gamma(4\gamma^2 \cosh(3\xi) + 5 \sinh(\xi) - 3 \sinh(3\xi)) N_{\alpha\xi}^{\mp}}{4N_{\alpha\xi}^{\pm}} - \frac{\gamma(4\gamma^2 \sinh(3\xi) + 3 \cosh(\xi) - 3 \cosh(3\xi)) N_{\alpha\xi}^{\pm}}{4N_{\alpha\xi}^{\mp}}$ |
| $\langle \mathcal{C}_{\alpha,\xi}^{\pm} \hat{a}^{\dagger} \hat{a} \hat{a}^{\dagger} \hat{a}^2 \mathcal{C}_{\alpha,\xi}^{\mp} \rangle$ | $\frac{\gamma N_{\alpha\xi}^{\mp}}{16N_{\alpha\xi}^{\pm}} \left[8\gamma^2 \left(-2\gamma^2 \sinh(5\xi) + \cosh(\xi) - 4 \cosh(3\xi) + 5 \cosh(5\xi) \right) - 22 \sinh(\xi) + 27 \sinh(3\xi) - 15 \sinh(5\xi) \right] + \frac{\gamma N_{\alpha\xi}^{\pm}}{16N_{\alpha\xi}^{\mp}} \left[(16\gamma^4 + 15) \cosh(5\xi) - 8\gamma^2 (\sinh(\xi) - 4 \sinh(3\xi) + 5 \sinh(5\xi)) + 6 \cosh(\xi) - 21 \cosh(3\xi) \right]$ |

Table A.3: Non-trivial Knill-Laflamme matrix elements for the squeezed cat code of the form $\langle \mathcal{C}_{\alpha,\xi}^{\pm} | \hat{E}_l^{\dagger} \hat{E}_{l'} | \mathcal{C}_{\alpha,\xi}^{\mp} \rangle$.

B

Expressions in the coherent- and cat-state ladder

Here, we give the representation of operators in the coherent-state ladder \mathcal{S} and cat-state ladder \mathcal{S}_{cat} , detailed in Chap. 5.

I Operators in the coherent-state ladder

As detailed in the main text, we have for the operator \hat{a} :

$$[\mathbf{a}]_{m,n} = \langle \alpha, m | \hat{a} | \alpha, n \rangle = \langle \alpha, m | (\alpha | \alpha, n \rangle + n | \alpha, n-1 \rangle) = \alpha S_{m,n} + n S_{m,n-1}, \quad (\text{B.1})$$

where \mathbf{S} is the overlap matrix, with elements

$$S_{m,n} = \langle \alpha, m | \alpha, n \rangle \quad (\text{B.2})$$

From this \hat{a}^\dagger is straightforwardly computed as

$$[\mathbf{a}^\dagger]_{m,n} = \alpha^* S_{m,n} + m S_{m-1,n} \quad (\text{B.3})$$

For $\hat{a}^\dagger \hat{a}$, we have

$$\begin{aligned} [\mathbf{a}^\dagger \mathbf{a}]_{m,n} &= \left(m \langle \alpha, m-1 | + \alpha^* \langle \alpha, m | \right) \left(\alpha | \alpha, n \rangle + n | \alpha, n-1 \rangle \right) \\ &= |\alpha|^2 S_{m,n} + mn S_{m-1,n-1} + \alpha m S_{m-1,n} + \alpha^* n S_{m,n-1} \end{aligned} \quad (\text{B.4})$$

Here, it becomes evident that $[\mathbf{a}^\dagger] \cdot [\mathbf{a}] \neq [\mathbf{a}^\dagger \mathbf{a}]$.

We have for \hat{a}^2 :

$$[\mathbf{a}^2]_{m,n} = \alpha^2 S_{m,n} + 2\alpha n S_{m,n-1} + n(n-1) S_{m,n-2}. \quad (\text{B.5})$$

Furthermore, we have for the non-linear term $\mathbf{a}^\dagger^2 \mathbf{a}^2$:

$$\begin{aligned}
[\mathbf{a}^\dagger^2 \mathbf{a}^2]_{m,n} = & |\alpha|^4 S_{m,n} + 2|\alpha|^2 \alpha m S_{m-1,n} + \alpha^2 m(m-1) S_{m-2,n} \\
& + 2|\alpha|^2 \alpha^* n S_{m,n-1} + 4|\alpha|^2 mn S_{m-1,n-1} \\
& + 2\alpha m(m-1)n S_{m-2,n-1} + \alpha^{*2} n(n-1) S_{m,n-2} \\
& + 2\alpha^* mn(n-1) S_{m-1,n-2} + mn(m-1)(n-1) S_{m-2,n-2}.
\end{aligned} \tag{B.6}$$

II Operators in the cat-state ladder

For the cat-state ladder \mathcal{S}_{cat} , we have two additional parity sectors and it is convenient to use a tensor notation $O_{m,n}^{\mu,\nu}$, where the indices μ, ν carry the parity.

Let us simplify the notation by setting

$$||n, \sigma\rangle \equiv ||\mathcal{C}_{\alpha,n}^\sigma\rangle, \tag{B.7}$$

where now the dependence on α is only stated implicitly. The overlap matrix is given by

$$S_{m,n}^{\mu,\nu} = \langle m, \mu || n, \nu \rangle. \tag{B.8}$$

We note that the action of any even power of \hat{a}^n or $\hat{a}^{\dagger n}$ onto $||n, \sigma\rangle$ will not change the parity index σ , however, any odd power will flip the parity index $\sigma \rightarrow \bar{\sigma}$.

As a result, we compute the following operator representations:

$$[\mathbf{a}]_{m,n}^{\mu,\nu} = \alpha S_{m,n}^{\mu,\bar{\nu}} + n S_{m,n-1}^{\mu,\bar{\nu}} \tag{B.9}$$

$$[\mathbf{a}^\dagger]_{m,n}^{\mu,\nu} = \alpha^* S_{m,n}^{\bar{\mu},\nu} + m S_{m-1,n}^{\bar{\mu},\nu} \tag{B.10}$$

$$[\mathbf{a}^\dagger \mathbf{a}]_{m,n}^{\mu,\nu} = \alpha S_{m,n}^{\bar{\mu},\bar{\nu}} + mn S_{m-1,n-1}^{\bar{\mu},\bar{\nu}} + \alpha m S_{m-1,n}^{\bar{\mu},\bar{\nu}} + \alpha^* n S_{m,n-1}^{\bar{\mu},\bar{\nu}} \tag{B.11}$$

$$[\mathbf{a}^2]_{m,n}^{\mu,\nu} = \alpha^2 S_{m,n}^{\mu,\nu} + 2\alpha n S_{m,n-1}^{\mu,\nu} + n(n-1) S_{m,n-2}^{\mu,\nu} \tag{B.12}$$

$$[\mathbf{a}^\dagger^2]_{m,n}^{\mu,\nu} = \alpha^{*2} S_{m,n}^{\mu,\nu} + 2\alpha^* m S_{m-1,n}^{\mu,\nu} + m(m-1) S_{m-2,n}^{\mu,\nu} \tag{B.13}$$

$$\begin{aligned}
[\mathbf{a}^\dagger^2 \mathbf{a}^2]_{m,n}^{\mu,\nu} = & |\alpha|^4 S_{m,n}^{\mu,\nu} + 2|\alpha|^2 \alpha m S_{m-1,n}^{\mu,\nu} + \alpha^2 m(m-1) S_{m-2,n}^{\mu,\nu} \\
& + 2|\alpha|^2 \alpha^* n S_{m,n-1}^{\mu,\nu} + 4|\alpha|^2 mn S_{m-1,n-1}^{\mu,\nu} \\
& + 2\alpha m(m-1)n S_{m-2,n-1}^{\mu,\nu} + \alpha^{*2} n(n-1) S_{m,n-2}^{\mu,\nu} \\
& + 2\alpha^* mn(n-1) S_{m-1,n-2}^{\mu,\nu} + mn(m-1)(n-1) S_{m-2,n-2}^{\mu,\nu}.
\end{aligned} \tag{B.14}$$

Bibliography

- [α] D. S. Schlegel, F. Minganti, and V. Savona, *Quantum error correction using squeezed schrödinger cat states*, *Phys. Rev. A* **106**, 022431 (2022).
- [β] D. S. Schlegel, F. Minganti, and V. Savona, *Coherent-state ladder time-dependent variational principle for open quantum systems*, *arXiv*, 2306.13708 (2023).
- [γ] D. S. Schlegel and S. Kehrein, *Measurement-induced clock in a lattice ring of non-interacting electrons*, *arXiv*, 2312.17672 (2023).
- [1] M. Planck, *Ueber das Gesetz der Energieverteilung im Normalspectrum*, *Ann. Phys.* **309**, 553–563 (1901).
- [2] H. Kragh, *Max Planck: the reluctant revolutionary*, Physics World (2000).
- [3] A. Einstein, *Über einen die Erzeugung und Verwandlung des Lichtes betreffenden heuristischen Gesichtspunkt*, *Ann. Phys.* **322**, 132–148 (1905).
- [4] E. Rutherford, *LXXIX. The scattering of α and β particles by matter and the structure of the atom*, *Lond. Edinb. Dublin Philos. Mag. J. Sci.* **21**, 669–688 (1911).
- [5] N. Bohr, *I. On the constitution of atoms and molecules*, *Lond. Edinb. Dublin Philos. Mag. J. Sci.* **26**, 1–25 (1913).
- [6] N. Bohr, *XXXVII. On the constitution of atoms and molecules*, *Lond. Edinb. Dublin Philos. Mag. J. Sci.* **26**, 476–502 (1913).
- [7] N. Bohr, *LXXIII. On the constitution of atoms and molecules*, *Lond. Edinb. Dublin Philos. Mag. J. Sci.* **26**, 857–875 (1913).
- [8] W. Heisenberg, *Über quantentheoretische Umdeutung kinematischer und mechanischer Beziehungen*. *Z. Physik* **33**, 879–893 (1925).
- [9] E. Schrödinger, *An Undulatory Theory of the Mechanics of Atoms and Molecules*, *Phys. Rev.* **28**, 1049–1070 (1926).
- [10] E. Schrödinger, *Quantisierung als Eigenwertproblem*, *Ann. Phys.* **384**, 361–376 (1926).
- [11] P. A. M. Dirac, *The quantum theory of the electron*, *Proc. R. Soc. Lond. Ser. Contain. Pap. Math. Phys. Character* **117**, 610–624 (1927).
- [12] P. A. M. Dirac, *A theory of electrons and protons*, *Proc. R. Soc. Lond. Ser. Contain. Pap. Math. Phys. Character* **126**, 360–365 (1927).
- [13] C. Jönsson, *Elektroneninterferenzen an mehreren künstlich hergestellten Feinspalten*, *Z. Physik* **161**, 454–474 (1961).
- [14] C. Jönsson, *Electron Diffraction at Multiple Slits*, *American Journal of Physics* **42**, 4–11 (1974).
- [15] S. J. Freedman and J. F. Clauser, *Experimental Test of Local Hidden-Variable Theories*, *Phys. Rev. Lett.* **28**, 938–941 (1972).

- [16] C. L. Degen, F. Reinhard, and P. Cappellaro, *Quantum sensing*, *Rev. Mod. Phys.* **89**, 035002 (2017).
- [17] R. Landauer, *Information is Physical*, *Physics Today* **44**, 23–29 (1991).
- [18] Y. I. Manin, *Computable and Non-Computable*, Kibernetika (Sovetskoe Radio, Moscow, 1980).
- [19] P. Benioff, *The computer as a physical system: A microscopic quantum mechanical Hamiltonian model of computers as represented by Turing machines*, *J Stat Phys* **22**, 563–591 (1980).
- [20] P. A. Benioff, *Quantum mechanical Hamiltonian models of discrete processes that erase their own histories: Application to Turing machines*, *Int J Theor Phys* **21**, 177–201 (1982).
- [21] R. P. Feynman, *Simulating physics with computers*, *Int J Theor Phys* **21**, 467–488 (1982).
- [22] D. Deutsch and R. Penrose, *Quantum theory, the Church–Turing principle and the universal quantum computer*, *Proc. R. Soc. Lond. Math. Phys. Sci.* **400**, 97–117 (1997).
- [23] L. K. Grover, *A fast quantum mechanical algorithm for database search*, in *Proc. Twenty-Eighth Annu. ACM Symp. Theory Comput.* STOC '96 (July 1996), pp. 212–219.
- [24] D. Deutsch and R. Jozsa, *Rapid solution of problems by quantum computation*, *Proc. R. Soc. Lond. Ser. Math. Phys. Sci.* **439**, 553–558 (1992).
- [25] P. Shor, *Algorithms for quantum computation: discrete logarithms and factoring*, in *Proc. 35th Annu. Symp. Found. Comput. Sci.* (Nov. 1994), pp. 124–134.
- [26] P. W. Shor, *Polynomial-Time Algorithms for Prime Factorization and Discrete Logarithms on a Quantum Computer*, *SIAM J. Comput.* **26**, 1484–1509 (1997).
- [27] R. Landauer, *Is Quantum Mechanics Useful?*, *Philos. Trans. Phys. Sci. Eng.* **353**, 367–376 (1995).
- [28] W. G. Unruh, *Maintaining coherence in quantum computers*, *Phys. Rev. A* **51**, 992–997 (1995).
- [29] S. Haroche and J.-M. Raimond, *Quantum Computing: Dream or Nightmare?*, *Physics Today* **49**, 51–52 (1996).
- [30] D. Loss and D. P. DiVincenzo, *Quantum computation with quantum dots*, *Phys. Rev. A* **57**, 120–126 (1998).
- [31] I. L. Chuang and Y. Yamamoto, *Simple quantum computer*, *Phys. Rev. A* **52**, 3489–3496 (1995).
- [32] E. Knill, R. Laflamme, and G. J. Milburn, *A scheme for efficient quantum computation with linear optics*, *Nature* **409**, 46–52 (2001).
- [33] J. I. Cirac and P. Zoller, *Quantum Computations with Cold Trapped Ions*, *Phys. Rev. Lett.* **74**, 4091–4094 (1995).
- [34] Y. Nakamura, Y. A. Pashkin, and J. S. Tsai, *Coherent control of macroscopic quantum states in a single-Cooper-pair box*, *Nature* **398**, 786–788 (1999).
- [35] A. Wallraff, D. I. Schuster, A. Blais, L. Frunzio, R.-S. Huang, J. Majer, S. Kumar, S. M. Girvin, and R. J. Schoelkopf, *Strong coupling of a single photon to a superconducting qubit using circuit quantum electrodynamics*, *Nature* **431**, 162–167 (2004).
- [36] A. Blais, R.-S. Huang, A. Wallraff, S. M. Girvin, and R. J. Schoelkopf, *Cavity quantum electrodynamics for superconducting electrical circuits: An architecture for quantum computation*, *Phys. Rev. A* **69**, 062320 (2004).

- [37] F. Arute, K. Arya, R. Babbush, D. Bacon, J. C. Bardin, R. Barends, R. Biswas, S. Boixo, F. G. S. L. Brandao, D. A. Buell, B. Burkett, Y. Chen, Z. Chen, B. Chiaro, R. Collins, W. Courtney, A. Dunsworth, E. Farhi, B. Foxen, A. Fowler, C. Gidney, M. Giustina, R. Graff, K. Guerin, S. Habegger, M. P. Harrigan, M. J. Hartmann, A. Ho, M. Hoffmann, T. Huang, T. S. Humble, S. V. Isakov, E. Jeffrey, Z. Jiang, D. Kafri, K. Kechedzhi, J. Kelly, P. V. Klimov, S. Knysh, A. Korotkov, F. Kostritsa, D. Landhuis, M. Lindmark, E. Lucero, D. Lyakh, S. Mandrà, J. R. McClean, M. McEwen, A. Megrant, X. Mi, K. Michielsen, M. Mohseni, J. Mutus, O. Naaman, M. Neeley, C. Neill, M. Y. Niu, E. Ostby, A. Petukhov, J. C. Platt, C. Quintana, E. G. Rieffel, P. Roushan, N. C. Rubin, D. Sank, K. J. Satzinger, V. Smelyanskiy, K. J. Sung, M. D. Trevithick, A. Vainsencher, B. Villalonga, T. White, Z. J. Yao, P. Yeh, A. Zalcman, H. Neven, and J. M. Martinis, *Quantum supremacy using a programmable superconducting processor*, [Nature](#) **574**, 505–510 (2019).
- [38] S. Flannigan, N. Pearson, G. H. Low, A. Buyskikh, I. Bloch, P. Zoller, M. Troyer, and A. J. Daley, *Propagation of errors and quantitative quantum simulation with quantum advantage*, [Quantum Sci. Technol.](#) **7**, 045025 (2022).
- [39] G. González-García, R. Trivedi, and J. I. Cirac, *Error Propagation in NISQ Devices for Solving Classical Optimization Problems*, [PRX Quantum](#) **3**, 040326 (2022).
- [40] C. E. Shannon, *A Mathematical Theory of Communication*, [Bell Syst. Tech. J.](#) **27**, 379–423 (1948).
- [41] A. Peres, *Reversible logic and quantum computers*, [Phys. Rev. A](#) **32**, 3266–3276 (1985).
- [42] P. W. Shor, *Scheme for reducing decoherence in quantum computer memory*, [Phys. Rev. A](#) **52**, R2493–R2496 (1995).
- [43] A. Steane, *Multiple-particle interference and quantum error correction*, [Proc. R. Soc. Lond. Ser. Math. Phys. Eng. Sci.](#) **452**, 2551–2577 (1997).
- [44] A. Y. Kitaev, *Fault-tolerant quantum computation by anyons*, [Annals of Physics](#) **303**, 2–30 (2003).
- [45] E. Knill and R. Laflamme, *Theory of quantum error-correcting codes*, [Phys. Rev. A](#) **55**, 900–911 (1997).
- [46] J. L. Park, *The concept of transition in quantum mechanics*, [Found Phys](#) **1**, 23–33 (1970).
- [47] M. A. Nielsen and I. L. Chuang, *Quantum computation and quantum information: 10th anniversary edition* (Cambridge University Press, Cambridge, 2010).
- [48] S. Krinner, N. Lacroix, A. Remm, A. Di Paolo, E. Genois, C. Leroux, C. Hellings, S. Lazar, F. Swiadek, J. Herrmann, G. J. Norris, C. K. Andersen, M. Müller, A. Blais, C. Eichler, and A. Wallraff, *Realizing repeated quantum error correction in a distance-three surface code*, [Nature](#) **605**, 669–674 (2022).
- [49] S. J. Lomonaco and American Mathematical Society, eds., *Quantum computation: a grand mathematical challenge for the twenty-first century and the millennium ; American Mathematical Society, Short Course, January 17 - 18, 2000, Washington, DC*, Proceedings of Symposia in Applied Mathematics AMS Short Course Lecture Notes 58 (American Mathematical Society, Providence, RI, 2002).
- [50] A. G. Fowler, M. Mariantoni, J. M. Martinis, and A. N. Cleland, *Surface codes: Towards practical large-scale quantum computation*, [Phys. Rev. A](#) **86**, 032324 (2012).
- [51] S. J. Devitt, W. J. Munro, and K. Nemoto, *Quantum error correction for beginners*, [Rep. Prog. Phys.](#) **76**, 076001 (2013).
- [52] J. Roffe, *Quantum error correction: an introductory guide*, [Contemp. Phys.](#) **60**, 226–245 (2019).

- [53] W. Cai, Y. Ma, W. Wang, C.-L. Zou, and L. Sun, *Bosonic quantum error correction codes in superconducting quantum circuits*, [Fundamental Research](#) **1**, 50–67 (2021).
- [54] B. M. Escher, R. L. de Matos Filho, and L. Davidovich, *General framework for estimating the ultimate precision limit in noisy quantum-enhanced metrology*, [Nature Phys](#) **7**, 406–411 (2011).
- [55] W. Wang, Y. Wu, Y. Ma, W. Cai, L. Hu, X. Mu, Y. Xu, Z.-J. Chen, H. Wang, Y. P. Song, H. Yuan, C.-L. Zou, L.-M. Duan, and L. Sun, *Heisenberg-limited single-mode quantum metrology in a superconducting circuit*, [Nat Commun](#) **10**, 4382 (2019).
- [56] K. S. Chou, J. Z. Blumoff, C. S. Wang, P. C. Reinhold, C. J. Axline, Y. Y. Gao, L. Frunzio, M. H. Devoret, L. Jiang, and R. J. Schoelkopf, *Deterministic teleportation of a quantum gate between two logical qubits*, [Nature](#) **561**, 368–373 (2018).
- [57] L. D. Burkhardt, J. D. Teoh, Y. Zhang, C. J. Axline, L. Frunzio, M. Devoret, L. Jiang, S. Girvin, and R. Schoelkopf, *Error-Detected State Transfer and Entanglement in a Superconducting Quantum Network*, [PRX Quantum](#) **2**, 030321 (2021).
- [58] E. Flurin, V. V. Ramasesh, S. Hacothen-Gourgy, L. S. Martin, N. Y. Yao, and I. Siddiqi, *Observing Topological Invariants Using Quantum Walks in Superconducting Circuits*, [Phys. Rev. X](#) **7**, 031023 (2017).
- [59] L. Hu, Y.-C. Ma, Y. Xu, W.-T. Wang, Y.-W. Ma, K. Liu, H.-Y. Wang, Y.-P. Song, M.-H. Yung, and L.-Y. Sun, *Simulation of molecular spectroscopy with circuit quantum electrodynamics*, [Science Bulletin](#) **63**, 293–299 (2018).
- [60] C. S. Wang, J. C. Curtis, B. J. Lester, Y. Zhang, Y. Y. Gao, J. Freeze, V. S. Batista, P. H. Vaccaro, I. L. Chuang, L. Frunzio, L. Jiang, S. M. Girvin, and R. J. Schoelkopf, *Efficient Multiphoton Sampling of Molecular Vibronic Spectra on a Superconducting Bosonic Processor*, [Phys. Rev. X](#) **10**, 021060 (2020).
- [61] S. Rosenblum, P. Reinhold, M. Mirrahimi, L. Jiang, L. Frunzio, and R. J. Schoelkopf, *Fault-tolerant detection of a quantum error*, [Science](#) **361**, 266–270 (2018).
- [62] P. Reinhold, S. Rosenblum, W.-L. Ma, L. Frunzio, L. Jiang, and R. J. Schoelkopf, *Error-corrected gates on an encoded qubit*, [Nat. Phys.](#) **16**, 822–826 (2020).
- [63] Y. Ma, Y. Xu, X. Mu, W. Cai, L. Hu, W. Wang, X. Pan, H. Wang, Y. P. Song, C.-L. Zou, and L. Sun, *Error-transparent operations on a logical qubit protected by quantum error correction*, [Nat. Phys.](#) **16**, 827–831 (2020).
- [64] J. M. Gertler, B. Baker, J. Li, S. Shirol, J. Koch, and C. Wang, *Protecting a bosonic qubit with autonomous quantum error correction*, [Nature](#) **590**, 243–248 (2021).
- [65] C. Flühmann, T. L. Nguyen, M. Marinelli, V. Negnevitsky, K. Mehta, and J. P. Home, *Encoding a qubit in a trapped-ion mechanical oscillator*, [Nature](#) **566**, 513–517 (2019).
- [66] W. Chen, J. Gan, J.-N. Zhang, D. Matuskevich, and K. Kim, *Quantum computation and simulation with vibrational modes of trapped ions*, [Chinese Phys. B](#) **30**, 060311 (2021).
- [67] O. Katz and C. Monroe, *Programmable Quantum Simulations of Bosonic Systems with Trapped Ions*, [Phys. Rev. Lett.](#) **131**, 033604 (2023).
- [68] J. E. Bourassa, R. N. Alexander, M. Vasmer, A. Patil, I. Tzitrin, T. Matsuura, D. Su, B. Q. Baragiola, S. Guha, G. Dauphinais, K. K. Sabapathy, N. C. Menicucci, and I. Dhand, *Blueprint for a Scalable Photonic Fault-Tolerant Quantum Computer*, [Quantum](#) **5**, 392 (2021).
- [69] S. Slussarenko and G. J. Pryde, *Photonic quantum information processing: A concise review*, [Applied Physics Reviews](#) **6**, 041303 (2019).

- [70] S. Takeda and A. Furusawa, *Toward large-scale fault-tolerant universal photonic quantum computing*, [APL Photonics](#) **4**, 060902 (2019).
- [71] A. Blais, S. M. Girvin, and W. D. Oliver, *Quantum information processing and quantum optics with circuit quantum electrodynamics*, [Nat. Phys.](#) **16**, 247–256 (2020).
- [72] R. Lescanne, M. Villiers, T. Peronnin, A. Sarlette, M. Delbecq, B. Huard, T. Kontos, M. Mirrahimi, and Z. Leghtas, *Exponential suppression of bit-flips in a qubit encoded in an oscillator*, [Nat. Phys.](#) **16**, 509–513 (2020).
- [73] B. M. Terhal, J. Conrad, and C. Vuillot, *Towards scalable bosonic quantum error correction*, [Quantum Sci. Technol.](#) **5**, 043001 (2020).
- [74] A. Joshi, K. Noh, and Y. Y. Gao, *Quantum information processing with bosonic qubits in circuit QED*, [Quantum Sci. Technol.](#) **6**, 033001 (2021).
- [75] W.-L. Ma, S. Puri, R. J. Schoelkopf, M. H. Devoret, S. M. Girvin, and L. Jiang, *Quantum control of bosonic modes with superconducting circuits*, [Science Bulletin](#) **66**, 1789–1805 (2021).
- [76] N. Ofek, A. Petrenko, R. Heeres, P. Reinhold, Z. Leghtas, B. Vlastakis, Y. Liu, L. Frunzio, S. M. Girvin, L. Jiang, M. Mirrahimi, M. H. Devoret, and R. J. Schoelkopf, *Extending the lifetime of a quantum bit with error correction in superconducting circuits*, [Nature](#) **536**, 441–445 (2016).
- [77] P. Campagne-Ibarcq, A. Eickbusch, S. Touzard, E. Zalys-Geller, N. E. Frattini, V. V. Sivak, P. Reinhold, S. Puri, S. Shankar, R. J. Schoelkopf, L. Frunzio, M. Mirrahimi, and M. H. Devoret, *Quantum error correction of a qubit encoded in grid states of an oscillator*, [Nature](#) **584**, 368–372 (2020).
- [78] V. V. Sivak, A. Eickbusch, B. Royer, S. Singh, I. Tsioutsios, S. Ganjam, A. Miano, B. L. Brock, A. Z. Ding, L. Frunzio, S. M. Girvin, R. J. Schoelkopf, and M. H. Devoret, *Real-time quantum error correction beyond break-even*, [Nature](#) **616**, 50–55 (2023).
- [79] P. T. Cochrane, G. J. Milburn, and W. J. Munro, *Macroscopically distinct quantum-superposition states as a bosonic code for amplitude damping*, [Phys. Rev. A](#) **59**, 2631–2634 (1999).
- [80] T. C. Ralph, A. J. F. Hayes, and A. Gilchrist, *Loss-Tolerant Optical Qubits*, [Phys. Rev. Lett.](#) **95**, 100501 (2005).
- [81] M. Mirrahimi, Z. Leghtas, V. V. Albert, S. Touzard, R. J. Schoelkopf, L. Jiang, and M. H. Devoret, *Dynamically protected cat-qubits: a new paradigm for universal quantum computation*, [New J. Phys.](#) **16**, 045014 (2014).
- [82] S. Touzard, A. Grimm, Z. Leghtas, S. O. Mundhada, P. Reinhold, C. Axline, M. Reagor, K. Chou, J. Blumoff, K. M. Sliwa, S. Shankar, L. Frunzio, R. J. Schoelkopf, M. Mirrahimi, and M. H. Devoret, *Coherent Oscillations inside a Quantum Manifold Stabilized by Dissipation*, [Phys. Rev. X](#) **8**, 021005 (2018).
- [83] Q. Xu, G. Zheng, Y.-X. Wang, P. Zoller, A. A. Clerk, and L. Jiang, *Autonomous quantum error correction and fault-tolerant quantum computation with squeezed cat qubits*, [npj Quantum Inf](#) **9**, 1–11 (2023).
- [84] S. Puri, S. Boutin, and A. Blais, *Engineering the quantum states of light in a Kerr-nonlinear resonator by two-photon driving*, [npj Quantum Inf](#) **3**, 1–7 (2017).
- [85] S. Puri, L. St-Jean, J. A. Gross, A. Grimm, N. E. Frattini, P. S. Iyer, A. Krishna, S. Touzard, L. Jiang, A. Blais, S. T. Flammia, and S. M. Girvin, *Bias-preserving gates with stabilized cat qubits*, [Sci. Adv.](#) **6**, eaay5901 (2020).

- [86] A. Grimm, N. E. Frattini, S. Puri, S. O. Mundhada, S. Touzard, M. Mirrahimi, S. M. Girvin, S. Shankar, and M. H. Devoret, *Stabilization and operation of a Kerr-cat qubit*, *Nature* **584**, 205–209 (2020).
- [87] J. Guillaud and M. Mirrahimi, *Repetition Cat Qubits for Fault-Tolerant Quantum Computation*, *Phys. Rev. X* **9**, 041053 (2019).
- [88] J. Guillaud and M. Mirrahimi, *Error rates and resource overheads of repetition cat qubits*, *Phys. Rev. A* **103**, 042413 (2021).
- [89] J. Guillaud, J. Cohen, and M. Mirrahimi, *Quantum computation with cat qubits*, (2023).
- [90] The LIGO Scientific Collaboration, *A gravitational wave observatory operating beyond the quantum shot-noise limit*, *Nature Phys* **7**, 962–965 (2011).
- [91] The LIGO Scientific Collaboration, *Enhanced sensitivity of the LIGO gravitational wave detector by using squeezed states of light*, *Nature Photon* **7**, 613–619 (2013).
- [92] V. Giovannetti, S. Lloyd, and L. Maccone, *Quantum-Enhanced Measurements: Beating the Standard Quantum Limit*, *Science* **306**, 1330–1336 (2004).
- [93] B. J. Lawrie, P. D. Lett, A. M. Marino, and R. C. Pooser, *Quantum Sensing with Squeezed Light*, *ACS Photonics* **6**, 1307–1318 (2019).
- [94] X. Pan, J. Schwinger, N.-N. Huang, P. Song, W. Chua, F. Hanamura, A. Joshi, F. Valadares, R. Filip, and Y. Y. Gao, *Protecting the Quantum Interference of Cat States by Phase-Space Compression*, *Phys. Rev. X* **13**, 021004 (2023).
- [95] V. Fock, *Konfigurationsraum und zweite Quantelung*, *Z. Physik* **75**, 622–647 (1932).
- [96] S. Finazzi, A. Le Boité, F. Storme, A. Baksic, and C. Ciuti, *Corner-Space Renormalization Method for Driven-Dissipative Two-Dimensional Correlated Systems*, *Phys. Rev. Lett.* **115**, 080604 (2015).
- [97] A. Polkovnikov, *Phase space representation of quantum dynamics*, *Annals of Physics* **325**, 1790–1852 (2010).
- [98] A. Polkovnikov, *Quantum corrections to the dynamics of interacting bosons: Beyond the truncated Wigner approximation*, *Phys. Rev. A* **68**, 053604 (2003).
- [99] E. Wigner, *On the Quantum Correction For Thermodynamic Equilibrium*, *Phys. Rev.* **40**, 749–759 (1932).
- [100] X. Yuan, S. Endo, Q. Zhao, Y. Li, and S. C. Benjamin, *Theory of variational quantum simulation*, *Quantum* **3**, 191 (2019).
- [101] H.-P. Breuer and F. Petruccione, *The Theory of Open Quantum Systems* (Oxford University Press, Jan. 2007).
- [102] D. C. Marinescu and G. M. Marinescu, “CHAPTER 2 - Measurements and Quantum Information”, in *Classical and Quantum Information*, edited by D. C. Marinescu and G. M. Marinescu (Academic Press, Boston, Jan. 2012), pp. 133–220.
- [103] G. Schaller, *Open Quantum Systems Far from Equilibrium*, Vol. 881, Lecture Notes in Physics (Springer International Publishing, Cham, 2014).
- [104] M.-D. Choi, *Completely positive linear maps on complex matrices*, *Linear Algebra and its Applications* **10**, 285–290 (1975).
- [105] K. Kraus, A. Böhm, J. D. Dollard, and W. H. Wootters, eds., *States, Effects, and Operations Fundamental Notions of Quantum Theory*, Vol. 190, Lecture Notes in Physics (Springer, Berlin, Heidelberg, 1983).

- [106] S. Banerjee, *Open Quantum Systems: Dynamics of Nonclassical Evolution*, Vol. 20, Texts and Readings in Physical Sciences (Springer, Singapore, 2018).
- [107] G. Lindblad, *On the generators of quantum dynamical semigroups*, *Commun.Math. Phys.* **48**, 119–130 (1976).
- [108] G. Schaller and G. Schaller, *Dynamics of Open Quantum Systems*, in *Open Quantum Systems Far from Equilibrium*, Vol. 881 (2014), pp. 1–26.
- [109] A. Jamiolkowski, *Linear transformations which preserve trace and positive semidefiniteness of operators*, *Reports on Mathematical Physics* **3**, 275–278 (1972).
- [110] M. Am-Shallem, A. Levy, I. Schaefer, and R. Kosloff, *Three approaches for representing Lindblad dynamics by a matrix-vector notation*, [10.48550/arXiv.1510.08634](https://arxiv.org/abs/1510.08634) (2015).
- [111] W. H. Press, ed., *Numerical recipes: the art of scientific computing*, 3rd ed (Cambridge University Press, Cambridge, UK ; New York, 2007).
- [112] F. Minganti, A. Biella, N. Bartolo, and C. Ciuti, *Spectral theory of Liouvillians for dissipative phase transitions*, *Phys. Rev. A* **98**, 042118 (2018).
- [113] V. V. Albert and L. Jiang, *Symmetries and conserved quantities in Lindblad master equations*, *Phys. Rev. A* **89**, 022118 (2014).
- [114] D. Nigro, *On the uniqueness of the steady-state solution of the Lindblad–Gorini–Kossakowski–Sudarshan equation*, *J. Stat. Mech.* **2019**, 043202 (2019).
- [115] E. M. Kessler, G. Giedke, A. Imamoglu, S. F. Yelin, M. D. Lukin, and J. I. Cirac, *Dissipative phase transition in a central spin system*, *Phys. Rev. A* **86**, 012116 (2012).
- [116] S. Haroche and J.-M. Raimond, *Exploring the Quantum: Atoms, Cavities, and Photons* (Oxford University Press, Aug. 2006).
- [117] C. Cohen-Tannoudji, B. Diu, F. Laloë, S. R. Hemley, N. Ostrowsky, and D. B. Ostrowsky, *Quantum mechanics*, Second edition (Wiley-VCH Verlag GmbH & Co, Weinheim, Germany, 2020).
- [118] M. Hillery, R. F. O’Connell, M. O. Scully, and E. P. Wigner, *Distribution functions in physics: Fundamentals*, *Physics Reports* **106**, 121–167 (1984).
- [119] R. L. Stratonovich, *On a Method of Calculating Quantum Distribution Functions*, *Sov. Phys. Dokl.* **2**, 416 (1957).
- [120] B.-G. Englert, *On the operator bases underlying Wigner’s, Kirkwood’s and Glauber’s phase space functions*, *J. Phys. A: Math. Gen.* **22**, 625 (1989).
- [121] C. Brif and A. Mann, *Phase-space formulation of quantum mechanics and quantum-state reconstruction for physical systems with Lie-group symmetries*, *Phys. Rev. A* **59**, 971–987 (1999).
- [122] U. Leonhardt, *Essential Quantum Optics: From Quantum Measurements to Black Holes* (Cambridge University Press, Cambridge, 2010).
- [123] C. Gerry and P. Knight, *Introductory Quantum Optics* (Cambridge University Press, Cambridge, 2004).
- [124] H. Weimer, A. Kshetrimayum, and R. Orús, *Simulation methods for open quantum many-body systems*, *Rev. Mod. Phys.* **93**, 015008 (2021).
- [125] A. J. Daley, *Quantum trajectories and open many-body quantum systems*, *Adv. Phys.* **63**, 77–149 (2014).
- [126] K. Mølmer, Y. Castin, and J. Dalibard, *Monte Carlo wave-function method in quantum optics*, *J. Opt. Soc. Am. B, JOSAB* **10**, 524–538 (1993).

- [127] J. Dalibard, Y. Castin, and K. Mølmer, *Wave-function approach to dissipative processes in quantum optics*, *Phys. Rev. Lett.* **68**, 580–583 (1992).
- [128] R. Dum, P. Zoller, and H. Ritsch, *Monte Carlo simulation of the atomic master equation for spontaneous emission*, *Phys. Rev. A* **45**, 4879–4887 (1992).
- [129] H. J. Carmichael, *Stochastic Schrödinger Equations: What They Mean and What They Can Do*, in *Coherence Quantum Opt. VII*, edited by J. H. Eberly, L. Mandel, and E. Wolf (1996), pp. 177–192.
- [130] S. Diehl, A. Tomadin, A. Micheli, R. Fazio, and P. Zoller, *Dynamical Phase Transitions and Instabilities in Open Atomic Many-Body Systems*, *Phys. Rev. Lett.* **105**, 015702 (2010).
- [131] I. Carusotto and C. Ciuti, *Quantum fluids of light*, *Rev. Mod. Phys.* **85**, 299–366 (2013).
- [132] E. P. Gross, *Structure of a quantized vortex in boson systems*, *Nuovo Cim* **20**, 454–477 (1961).
- [133] L. P. Pitaevskii, *Vortex lines in an imperfect Bose gas*, *Sov. Phys. JETP*. **13**, 451–454 (1961).
- [134] K. Vogel and H. Risken, *Quasiprobability distributions in dispersive optical bistability*, *Phys. Rev. A* **39**, 4675–4683 (1989).
- [135] I. Carusotto and C. Ciuti, *Spontaneous microcavity-polariton coherence across the parametric threshold: Quantum Monte Carlo studies*, *Phys. Rev. B* **72**, 125335 (2005).
- [136] H. J. Carmichael, *Statistical Methods in Quantum Optics 2*, Theoretical and Mathematical Physics (Springer, Berlin, Heidelberg, 2008).
- [137] R. Cabrera, D. I. Bondar, K. Jacobs, and H. A. Rabitz, *Efficient method to generate time evolution of the Wigner function for open quantum systems*, *Phys. Rev. A* **92**, 042122 (2015).
- [138] M. Roda-Llordes, D. Candoli, P. T. Grochowski, A. Riera-Campeny, T. Agrenius, J. J. García-Ripoll, C. Gonzalez-Ballester, and O. Romero-Isart, *Numerical Simulation of Large-Scale Nonlinear Open Quantum Mechanics*, [10.48550/arXiv.2306.09083](https://arxiv.org/abs/10.48550/arXiv.2306.09083) (2023).
- [139] J. E. Bourassa, N. Quesada, I. Tzitrin, A. Száva, T. Isacsson, J. Izaac, K. K. Sabapathy, G. Dauphinais, and I. Dhand, *Fast Simulation of Bosonic Qubits via Gaussian Functions in Phase Space*, *PRX Quantum* **2**, 040315 (2021).
- [140] D. Eeltink, F. Vicentini, and V. Savona, *Variational dynamics of open quantum systems in phase space*, [10.48550/arXiv.2307.07429](https://arxiv.org/abs/10.48550/arXiv.2307.07429) (2023).
- [141] K. Donatella, Z. Denis, A. Le Boité, and C. Ciuti, *Continuous-time dynamics and error scaling of noisy highly entangling quantum circuits*, *Phys. Rev. A* **104**, 062407 (2021).
- [142] G. Vidal, *Efficient Classical Simulation of Slightly Entangled Quantum Computations*, *Phys. Rev. Lett.* **91**, 147902 (2003).
- [143] F. Verstraete, J. J. García-Ripoll, and J. I. Cirac, *Matrix Product Density Operators: Simulation of Finite-Temperature and Dissipative Systems*, *Phys. Rev. Lett.* **93**, 207204 (2004).
- [144] F. Verstraete, V. Murg, and J. Cirac, *Matrix product states, projected entangled pair states, and variational renormalization group methods for quantum spin systems*, *Adv. Phys.* **57**, 143–224 (2008).
- [145] N. Schuch, M. M. Wolf, F. Verstraete, and J. I. Cirac, *Computational Complexity of Projected Entangled Pair States*, *Phys. Rev. Lett.* **98**, 140506 (2007).

- [146] U. Schollwöck, *The density-matrix renormalization group*, *Rev. Mod. Phys.* **77**, 259–315 (2005).
- [147] G. D. las Cuevas, N. Schuch, D. Pérez-García, and J. I. Cirac, *Purifications of multipartite states: limitations and constructive methods*, *New J. Phys.* **15**, 123021 (2013).
- [148] M. Zwolak and G. Vidal, *Mixed-State Dynamics in One-Dimensional Quantum Lattice Systems: A Time-Dependent Superoperator Renormalization Algorithm*, *Phys. Rev. Lett.* **93**, 207205 (2004).
- [149] E. Mascarenhas, H. Flayac, and V. Savona, *Matrix-product-operator approach to the nonequilibrium steady state of driven-dissipative quantum arrays*, *Phys. Rev. A* **92**, 022116 (2015).
- [150] A. Nagy and V. Savona, *Variational Quantum Monte Carlo Method with a Neural-Network Ansatz for Open Quantum Systems*, *Phys. Rev. Lett.* **122**, 250501 (2019).
- [151] S. Endo, J. Sun, Y. Li, S. C. Benjamin, and X. Yuan, *Variational Quantum Simulation of General Processes*, *Phys. Rev. Lett.* **125**, 010501 (2020).
- [152] M. J. Hartmann and G. Carleo, *Neural-Network Approach to Dissipative Quantum Many-Body Dynamics*, *Phys. Rev. Lett.* **122**, 250502 (2019).
- [153] F. Vicentini, A. Biella, N. Regnault, and C. Ciuti, *Variational Neural-Network Ansatz for Steady States in Open Quantum Systems*, *Phys. Rev. Lett.* **122**, 250503 (2019).
- [154] H.-J. Briegel, T. Calarco, D. Jaksch, J. I. Cirac, and P. Zoller, *Quantum computing with neutral atoms*, *J. Mod. Opt.* **47**, 415–451 (2000).
- [155] M. Saffman, T. G. Walker, and K. Mølmer, *Quantum information with Rydberg atoms*, *Rev. Mod. Phys.* **82**, 2313–2363 (2010).
- [156] C. S. Adams, J. D. Pritchard, and J. P. Shaffer, *Rydberg atom quantum technologies*, *J. Phys. B: At. Mol. Opt. Phys.* **53**, 012002 (2019).
- [157] L. Henriët, L. Beguin, A. Signoles, T. Lahaye, A. Browaeys, G.-O. Reymond, and C. Jurczak, *Quantum computing with neutral atoms*, *Quantum* **4**, 327 (2020).
- [158] S. R. Cohen and J. D. Thompson, *Quantum Computing with Circular Rydberg Atoms*, *PRX Quantum* **2**, 030322 (2021).
- [159] M. Morgado and S. Whitlock, *Quantum simulation and computing with Rydberg-interacting qubits*, *AVS Quantum Science* **3**, 023501 (2021).
- [160] I. Cong, H. Levine, A. Keesling, D. Bluvstein, S.-T. Wang, and M. D. Lukin, *Hardware-Efficient, Fault-Tolerant Quantum Computation with Rydberg Atoms*, *Phys. Rev. X* **12**, 021049 (2022).
- [161] T. M. Graham, Y. Song, J. Scott, C. Poole, L. Phuttitarn, K. Jooya, P. Eichler, X. Jiang, A. Marra, B. Grinkemeyer, M. Kwon, M. Ebert, J. Cherek, M. T. Lichtman, M. Gillette, J. Gilbert, D. Bowman, T. Ballance, C. Campbell, E. D. Dahl, O. Crawford, N. S. Blunt, B. Rogers, T. Noel, and M. Saffman, *Multi-qubit entanglement and algorithms on a neutral-atom quantum computer*, *Nature* **604**, 457–462 (2022).
- [162] J. Wurtz, A. Bylinskii, B. Braverman, J. Amato-Grill, S. H. Cantu, F. Huber, A. Lukin, F. Liu, P. Weinberg, J. Long, S.-T. Wang, N. Gemelke, and A. Keesling, *Aquila: QuEra’s 256-qubit neutral-atom quantum computer*, [10.48550/arXiv.2306.11727](https://arxiv.org/abs/10.48550/arXiv.2306.11727) (2023).
- [163] J. Benhelm, G. Kirchmair, C. F. Roos, and R. Blatt, *Towards fault-tolerant quantum computing with trapped ions*, *Nature Phys* **4**, 463–466 (2008).

- [164] J. W. Britton, B. C. Sawyer, A. C. Keith, C.-C. J. Wang, J. K. Freericks, H. Uys, M. J. Biercuk, and J. J. Bollinger, *Engineered two-dimensional Ising interactions in a trapped-ion quantum simulator with hundreds of spins*, [*Nature* **484**, 489–492 \(2012\)](#).
- [165] R. Blatt and C. F. Roos, *Quantum simulations with trapped ions*, [*Nature Phys* **8**, 277–284 \(2012\)](#).
- [166] S. Weidt, J. Randall, S. C. Webster, K. Lake, A. E. Webb, I. Cohen, T. Navickas, B. Lekitsch, A. Retzker, and W. K. Hensinger, *Trapped-Ion Quantum Logic with Global Radiation Fields*, [*Phys. Rev. Lett.* **117**, 220501 \(2016\)](#).
- [167] B. Lekitsch, S. Weidt, A. G. Fowler, K. Mølmer, S. J. Devitt, C. Wunderlich, and W. K. Hensinger, *Blueprint for a microwave trapped ion quantum computer*, [*Sci. Adv.* **3**, e1601540 \(2017\)](#).
- [168] C. Hempel, C. Maier, J. Romero, J. McClean, T. Monz, H. Shen, P. Jurcevic, B. P. Lanyon, P. Love, R. Babbush, A. Aspuru-Guzik, R. Blatt, and C. F. Roos, *Quantum Chemistry Calculations on a Trapped-Ion Quantum Simulator*, [*Phys. Rev. X* **8**, 031022 \(2018\)](#).
- [169] C. D. Bruzewicz, J. Chiaverini, R. McConnell, and J. M. Sage, *Trapped-ion quantum computing: Progress and challenges*, [*Applied Physics Reviews* **6**, 021314 \(2019\)](#).
- [170] P. J. Low, B. M. White, A. A. Cox, M. L. Day, and C. Senko, *Practical trapped-ion protocols for universal qudit-based quantum computing*, [*Phys. Rev. Res.* **2**, 033128 \(2020\)](#).
- [171] Y. Nam, J.-S. Chen, N. C. Pimenti, K. Wright, C. Delaney, D. Maslov, K. R. Brown, S. Allen, J. M. Amini, J. Apisdorf, K. M. Beck, A. Blinov, V. Chaplin, M. Chmielewski, C. Collins, S. Debnath, K. M. Hudek, A. M. Ducore, M. Keesan, S. M. Kreikemeier, J. Mizrahi, P. Solomon, M. Williams, J. D. Wong-Campos, D. Moehring, C. Monroe, and J. Kim, *Ground-state energy estimation of the water molecule on a trapped-ion quantum computer*, [*npj Quantum Inf* **6**, 1–6 \(2020\)](#).
- [172] K. R. Brown, J. Chiaverini, J. M. Sage, and H. Häffner, *Materials challenges for trapped-ion quantum computers*, [*Nat Rev Mater* **6**, 892–905 \(2021\)](#).
- [173] J. M. Pino, J. M. Dreiling, C. Figgatt, J. P. Gaebler, S. A. Moses, M. S. Allman, C. H. Baldwin, M. Foss-Feig, D. Hayes, K. Mayer, C. Ryan-Anderson, and B. Neyenhuis, *Demonstration of the trapped-ion quantum CCD computer architecture*, [*Nature* **592**, 209–213 \(2021\)](#).
- [174] S. A. Moses, C. H. Baldwin, M. S. Allman, R. Ancona, L. Ascarrunz, C. Barnes, J. Bartolotta, B. Bjork, P. Blanchard, M. Bohn, J. G. Bohnet, N. C. Brown, N. Q. Burdick, W. C. Burton, S. L. Campbell, J. P. Campora, C. Carron, J. Chambers, J. W. Chan, Y. H. Chen, A. Chernoguzov, E. Chertkov, J. Colina, J. P. Curtis, R. Daniel, M. DeCross, D. Deen, C. Delaney, J. M. Dreiling, C. T. Ertsgaard, J. Esposito, B. Estey, M. Fabrikant, C. Figgatt, C. Foltz, M. Foss-Feig, D. Francois, J. P. Gaebler, T. M. Gatterman, C. N. Gilbreth, J. Giles, E. Glynn, A. Hall, A. M. Hankin, A. Hansen, D. Hayes, B. Higashi, I. M. Hoffman, B. Horning, J. J. Hout, R. Jacobs, J. Johansen, L. Jones, J. Karcz, T. Klein, P. Lauria, P. Lee, D. Liefer, S. T. Lu, D. Lucchetti, C. Lytle, A. Malm, M. Matheny, B. Mathewson, K. Mayer, D. B. Miller, M. Mills, B. Neyenhuis, L. Nugent, S. Olson, J. Parks, G. N. Price, Z. Price, M. Pugh, A. Ransford, A. P. Reed, C. Roman, M. Rowe, C. Ryan-Anderson, S. Sanders, J. Sedlacek, P. Shevchuk, P. Siegfried, T. Skripka, B. Spaun, R. T. Sprenkle, R. P. Stutz, M. Swallows, R. I. Tobey, A. Tran, T. Tran, E. Vogt, C. Volin, J. Walker, A. M. Zolot, and J. M. Pino, *A Race-Track Trapped-Ion Quantum Processor*, [*Phys. Rev. X* **13**, 041052 \(2023\)](#).
- [175] A. Blais, J. Gambetta, A. Wallraff, D. I. Schuster, S. M. Girvin, M. H. Devoret, and R. J. Schoelkopf, *Quantum-information processing with circuit quantum electrodynamics*, [*Phys. Rev. A* **75**, 032329 \(2007\)](#).

- [176] J. Clarke and F. K. Wilhelm, *Superconducting quantum bits*, *Nature* **453**, 1031–1042 (2008).
- [177] M. H. Devoret and R. J. Schoelkopf, *Superconducting Circuits for Quantum Information: An Outlook*, *Science* **339**, 1169–1174 (2013).
- [178] G. Wendin, *Quantum information processing with superconducting circuits: a review*, *Rep. Prog. Phys.* **80**, 106001 (2017).
- [179] P. Krantz, M. Kjaergaard, F. Yan, T. P. Orlando, S. Gustavsson, and W. D. Oliver, *A quantum engineer’s guide to superconducting qubits*, *Applied Physics Reviews* **6**, 021318 (2019).
- [180] M. Kjaergaard, M. E. Schwartz, J. Braumüller, P. Krantz, J. I.-J. Wang, S. Gustavsson, and W. D. Oliver, *Superconducting Qubits: Current State of Play*, *Annu. Rev. Condens. Matter Phys.* **11**, 369–395 (2020).
- [181] A. Blais, A. L. Grimsmo, S. M. Girvin, and A. Wallraff, *Circuit quantum electrodynamics*, *Rev. Mod. Phys.* **93**, 025005 (2021).
- [182] N. Goss, A. Morvan, B. Marinelli, B. K. Mitchell, L. B. Nguyen, R. K. Naik, L. Chen, C. Jünger, J. M. Kreikebaum, D. I. Santiago, J. J. Wallman, and I. Siddiqi, *High-fidelity qutrit entangling gates for superconducting circuits*, *Nat Commun* **13**, 7481 (2022).
- [183] A. Somoroff, Q. Ficheux, R. A. Mencia, H. Xiong, R. Kuzmin, and V. E. Manucharyan, *Millisecond Coherence in a Superconducting Qubit*, *Phys. Rev. Lett.* **130**, 267001 (2023).
- [184] L.-M. Duan and H. J. Kimble, *Scalable Photonic Quantum Computation through Cavity-Assisted Interactions*, *Phys. Rev. Lett.* **92**, 127902 (2004).
- [185] S. Tanzilli, W. Tittel, M. Halder, O. Alibart, P. Baldi, N. Gisin, and H. Zbinden, *A photonic quantum information interface*, *Nature* **437**, 116–120 (2005).
- [186] J. L. O’Brien, A. Furusawa, and J. Vučković, *Photonic quantum technologies*, *Nature Photon* **3**, 687–695 (2009).
- [187] A. Aspuru-Guzik and P. Walther, *Photonic quantum simulators*, *Nature Phys* **8**, 285–291 (2012).
- [188] H. Zheng, D. J. Gauthier, and H. U. Baranger, *Waveguide-QED-Based Photonic Quantum Computation*, *Phys. Rev. Lett.* **111**, 090502 (2013).
- [189] A. Peruzzo, J. McClean, P. Shadbolt, M.-H. Yung, X.-Q. Zhou, P. J. Love, A. Aspuru-Guzik, and J. L. O’Brien, *A variational eigenvalue solver on a photonic quantum processor*, *Nat Commun* **5**, 4213 (2014).
- [190] F. Flamini, N. Spagnolo, and F. Sciarrino, *Photonic quantum information processing: a review*, *Rep. Prog. Phys.* **82**, 016001 (2018).
- [191] S. Pirandola, B. R. Bardhan, T. Gehring, C. Weedbrook, and S. Lloyd, *Advances in photonic quantum sensing*, *Nature Photon* **12**, 724–733 (2018).
- [192] A. W. Elshaari, W. Pernice, K. Srinivasan, O. Benson, and V. Zwiller, *Hybrid integrated quantum photonic circuits*, *Nat. Photonics* **14**, 285–298 (2020).
- [193] J. Wang, F. Sciarrino, A. Laing, and M. G. Thompson, *Integrated photonic quantum technologies*, *Nat. Photonics* **14**, 273–284 (2020).
- [194] M. V. Larsen, X. Guo, C. R. Breum, J. S. Neergaard-Nielsen, and U. L. Andersen, *Deterministic multi-mode gates on a scalable photonic quantum computing platform*, *Nat. Phys.* **17**, 1018–1023 (2021).

- [195] G. Moody, V. J. Sorger, D. J. Blumenthal, P. W. Juodawlkis, W. Loh, C. Sorace-Agaskar, A. E. Jones, K. C. Balram, J. C. F. Matthews, A. Laing, M. Davanco, L. Chang, J. E. Bow-ers, N. Quack, C. Galland, I. Aharonovich, M. A. Wolff, C. Schuck, N. Sinclair, M. Lončar, T. Komljenovic, D. Weld, S. Mookherjea, S. Buckley, M. Radulaski, S. Reitzenstein, B. Pingault, B. Machielse, D. Mukhopadhyay, A. Akimov, A. Zheltikov, G. S. Agarwal, K. Srinivasan, J. Lu, H. X. Tang, W. Jiang, T. P. McKenna, A. H. Safavi-Naeini, S. Steinhauer, A. W. Elshaari, V. Zwiller, P. S. Davids, N. Martinez, M. Gehl, J. Chiaverini, K. K. Mehta, J. Romero, N. B. Lingaraju, A. M. Weiner, D. Peace, R. Cernansky, M. Lobino, E. Diamanti, L. T. Vidarte, and R. M. Camacho, *2022 Roadmap on integrated quantum photonics*, *J. Phys. Photonics* **4**, 012501 (2022).
- [196] E. Pelucchi, G. Fagas, I. Aharonovich, D. Englund, E. Figueroa, Q. Gong, H. Hannes, J. Liu, C.-Y. Lu, N. Matsuda, J.-W. Pan, F. Schreck, F. Sciarrino, C. Silberhorn, J. Wang, and K. D. Jöns, *The potential and global outlook of integrated photonics for quantum technologies*, *Nat Rev Phys* **4**, 194–208 (2022).
- [197] C. Taballione, M. C. Anguita, M. de Goede, P. Venderbosch, B. Kassenberg, H. Snijders, N. Kannan, W. L. Vleeshouwers, D. Smith, J. P. Epping, R. van der Meer, P. W. H. Pinkse, H. van den Vlekkert, and J. J. Renema, *20-Mode Universal Quantum Photonic Processor*, *Quantum* **7**, 1071 (2023).
- [198] M. Aspelmeyer, T. J. Kippenberg, and F. Marquardt, *Cavity optomechanics*, *Rev. Mod. Phys.* **86**, 1391–1452 (2014).
- [199] S. Barzanjeh, A. Xuereb, S. Gröblacher, M. Paternostro, C. A. Regal, and E. M. Weig, *Optomechanics for quantum technologies*, *Nat. Phys.* **18**, 15–24 (2022).
- [200] N. Fiaschi, B. Hensen, A. Wallucks, R. Benevides, J. Li, T. P. M. Alegre, and S. Gröblacher, *Optomechanical quantum teleportation*, *Nat. Photon.* **15**, 817–821 (2021).
- [201] I. Marinković, A. Wallucks, R. Riedinger, S. Hong, M. Aspelmeyer, and S. Gröblacher, *Optomechanical Bell Test*, *Phys. Rev. Lett.* **121**, 220404 (2018).
- [202] K. Stannigel, P. Rabl, A. S. Sørensen, M. D. Lukin, and P. Zoller, *Optomechanical transducers for quantum-information processing*, *Phys. Rev. A* **84**, 042341 (2011).
- [203] K. Stannigel, P. Komar, S. J. M. Habraken, S. D. Bennett, M. D. Lukin, P. Zoller, and P. Rabl, *Optomechanical Quantum Information Processing with Photons and Phonons*, *Phys. Rev. Lett.* **109**, 013603 (2012).
- [204] E. Joos and H. D. Zeh, *The emergence of classical properties through interaction with the environment*, *Z. Physik B - Condensed Matter* **59**, 223–243 (1985).
- [205] H. E. Brandt, *Qubit devices and the issue of quantum decoherence*, *Progress in Quantum Electronics* **22**, 257–370 (1999).
- [206] W. H. Zurek, *Decoherence, einselection, and the quantum origins of the classical*, *Rev. Mod. Phys.* **75**, 715–775 (2003).
- [207] M. A. Schlosshauer, *Decoherence: and the Quantum-To-Classical Transition* (Springer Science & Business Media, July 2007).
- [208] M. Schlosshauer, *Quantum Decoherence*, *Physics Reports* **831**, 1–57 (2019).
- [209] G. Bacciagaluppi, “The role of decoherence in quantum mechanics”, in *The Stanford encyclopedia of philosophy*, edited by E. N. Zalta, Fall 2020 (Metaphysics Research Lab, Stanford University, 2020).
- [210] D. Gottesman, *Class of quantum error-correcting codes saturating the quantum Hamming bound*, *Phys. Rev. A* **54**, 1862–1868 (1996).
- [211] A. M. Steane, *Simple quantum error-correcting codes*, *Phys. Rev. A* **54**, 4741–4751 (1996).

- [212] A. Calderbank, E. Rains, P. Shor, and N. Sloane, *Quantum error correction via codes over $GF(4)$* , *IEEE Trans. Inf. Theory* **44**, 1369–1387 (1998).
- [213] A. Steane, *Enlargement of Calderbank-Shor-Steane quantum codes*, *IEEE Trans. Inf. Theory* **45**, 2492–2495 (1999).
- [214] D. A. Lidar and T. A. Brun, eds., *Quantum Error Correction* (Cambridge University Press, Cambridge, 2013).
- [215] G. G. La Guardia, *Quantum Error Correction: Symmetric, Asymmetric, Synchronizable, and Convolutional Codes*, Quantum Science and Technology (Springer International Publishing, Cham, 2020).
- [216] D. G. Cory, M. D. Price, W. Maas, E. Knill, R. Laflamme, W. H. Zurek, T. F. Havel, and S. S. Somaroo, *Experimental Quantum Error Correction*, *Phys. Rev. Lett.* **81**, 2152–2155 (1998).
- [217] J. Chiaverini, D. Leibfried, T. Schaetz, M. D. Barrett, R. B. Blakestad, J. Britton, W. M. Itano, J. D. Jost, E. Knill, C. Langer, R. Ozeri, and D. J. Wineland, *Realization of quantum error correction*, *Nature* **432**, 602–605 (2004).
- [218] T. B. Pittman, B. C. Jacobs, and J. D. Franson, *Demonstration of quantum error correction using linear optics*, *Phys. Rev. A* **71**, 052332 (2005).
- [219] P. Schindler, J. T. Barreiro, T. Monz, V. Nebendahl, D. Nigg, M. Chwalla, M. Hennrich, and R. Blatt, *Experimental Repetitive Quantum Error Correction*, *Science* **332**, 1059–1061 (2011).
- [220] M. D. Reed, L. DiCarlo, S. E. Nigg, L. Sun, L. Frunzio, S. M. Girvin, and R. J. Schoelkopf, *Realization of three-qubit quantum error correction with superconducting circuits*, *Nature* **482**, 382–385 (2012).
- [221] I. L. Chuang, D. W. Leung, and Y. Yamamoto, *Bosonic quantum codes for amplitude damping*, *Phys. Rev. A* **56**, 1114–1125 (1997).
- [222] S. L. Braunstein, *Error Correction for Continuous Quantum Variables*, *Phys. Rev. Lett.* **80**, 4084–4087 (1998).
- [223] S. Lloyd and J.-J. E. Slotine, *Analog Quantum Error Correction*, *Phys. Rev. Lett.* **80**, 4088–4091 (1998).
- [224] D. Gottesman, A. Kitaev, and J. Preskill, *Encoding a qubit in an oscillator*, *Phys. Rev. A* **64**, 012310 (2001).
- [225] W. Wasilewski and K. Banaszek, *Protecting an optical qubit against photon loss*, *Phys. Rev. A* **75**, 042316 (2007).
- [226] J. Niset, U. L. Andersen, and N. J. Cerf, *Experimentally Feasible Quantum Erasure-Correcting Code for Continuous Variables*, *Phys. Rev. Lett.* **101**, 130503 (2008).
- [227] Z. Leghtas, G. Kirchmair, B. Vlastakis, R. J. Schoelkopf, M. H. Devoret, and M. Mirrahimi, *Hardware-Efficient Autonomous Quantum Memory Protection*, *Phys. Rev. Lett.* **111**, 120501 (2013).
- [228] N. C. Menicucci, *Fault-Tolerant Measurement-Based Quantum Computing with Continuous-Variable Cluster States*, *Phys. Rev. Lett.* **112**, 120504 (2014).
- [229] P. Hayden, S. Nezami, G. Salton, and B. C. Sanders, *Spacetime replication of continuous variable quantum information*, *New J. Phys.* **18**, 083043 (2016).
- [230] A. Ketterer, A. Keller, S. P. Walborn, T. Coudreau, and P. Milman, *Quantum information processing in phase space: A modular variables approach*, *Phys. Rev. A* **94**, 022325 (2016).

- [231] F. Lacerda, J. M. Renes, and V. B. Scholz, *Coherent state constellations for Bosonic Gaussian channels*, in [2016 IEEE Int. Symp. Inf. Theory ISIT](#) (July 2016), pp. 2499–2503.
- [232] M. H. Michael, M. Silveri, R. T. Brierley, V. V. Albert, J. Salmilehto, L. Jiang, and S. M. Girvin, *New Class of Quantum Error-Correcting Codes for a Bosonic Mode*, [Phys. Rev. X](#) **6**, 031006 (2016).
- [233] M. Bergmann and P. van Loock, *Quantum error correction against photon loss using NOON states*, [Phys. Rev. A](#) **94**, 012311 (2016).
- [234] M. Y. Niu, I. L. Chuang, and J. H. Shapiro, *Hardware-efficient bosonic quantum error-correcting codes based on symmetry operators*, [Phys. Rev. A](#) **97**, 032323 (2018).
- [235] V. V. Albert, S. O. Mundhada, A. Grimm, S. Touzard, M. H. Devoret, and L. Jiang, *Pair-cat codes: autonomous error-correction with low-order nonlinearity*, [Quantum Sci. Technol.](#) **4**, 035007 (2019).
- [236] V. V. Albert, K. Noh, K. Duivenvoorden, D. J. Young, R. T. Brierley, P. Reinhold, C. Vuillot, L. Li, C. Shen, S. M. Girvin, B. M. Terhal, and L. Jiang, *Performance and structure of single-mode bosonic codes*, [Phys. Rev. A](#) **97**, 032346 (2018).
- [237] A. L. Grimsmo and S. Puri, *Quantum Error Correction with the Gottesman-Kitaev-Preskill Code*, [PRX Quantum](#) **2**, 020101 (2021).
- [238] C. Chamberland, K. Noh, P. Arrangoiz-Arriola, E. T. Campbell, C. T. Hann, J. Iverson, H. Putterman, T. C. Bohdanowicz, S. T. Flammia, A. Keller, G. Refael, J. Preskill, L. Jiang, A. H. Safavi-Naeini, O. Painter, and F. G. Brandão, *Building a Fault-Tolerant Quantum Computer Using Concatenated Cat Codes*, [PRX Quantum](#) **3**, 010329 (2022).
- [239] L. Hu, Y. Ma, W. Cai, X. Mu, Y. Xu, W. Wang, Y. Wu, H. Wang, Y. P. Song, C.-L. Zou, S. M. Girvin, L.-M. Duan, and L. Sun, *Quantum error correction and universal gate set operation on a binomial bosonic logical qubit*, [Nat. Phys.](#) **15**, 503–508 (2019).
- [240] B. de Neeve, T.-L. Nguyen, T. Behrle, and J. P. Home, *Error correction of a logical grid state qubit by dissipative pumping*, [Nat. Phys.](#) **18**, 296–300 (2022).
- [241] C. Berdou, A. Murani, U. Réglade, W. Smith, M. Villiers, J. Palomo, M. Rosticher, A. Denis, P. Morfin, M. Delbecq, T. Kontos, N. Pankratova, F. Rautschke, T. Peronnin, L.-A. Sellem, P. Rouchon, A. Sarlette, M. Mirrahimi, P. Campagne-Ibarcq, S. Jezouin, R. Lescanne, and Z. Leghtas, *One Hundred Second Bit-Flip Time in a Two-Photon Dissipative Oscillator*, [PRX Quantum](#) **4**, 020350 (2023).
- [242] U. Réglade, A. Bocquet, R. Gautier, A. Marquet, E. Albertinale, N. Pankratova, M. Hallén, F. Rautschke, L.-A. Sellem, P. Rouchon, A. Sarlette, M. Mirrahimi, P. Campagne-Ibarcq, R. Lescanne, S. Jezouin, and Z. Leghtas, *Quantum control of a cat-qubit with bit-flip times exceeding ten seconds*, [10.48550/arXiv.2307.06617](#) (2023).
- [243] D. Huffman, *A Method for the Construction of Minimum-Redundancy Codes*, [Proc. IRE](#) **40**, 1098–1101 (1952).
- [244] F. J. MacWilliams and N. J. A. Sloane, *The theory of error correcting codes*, North-Holland Mathematical Library v. 16 (North-Holland Pub. Co. Sole distributors for the U.S.A. and Canada, Elsevier/North-Holland, Amsterdam New York, 1977).
- [245] R. W. Hamming, *Coding and Information Theory* (Prentice-Hall, 1980).
- [246] T. M. Cover and J. A. Thomas, *Elements of Information Theory*, 1st ed. (Wiley, 1991).
- [247] M. Grassl, “Classical Information Theory and Classical Error Correction”, in [Quantum Information](#) (John Wiley & Sons, Ltd, 2016) Chap. 1, pp. 1–17.

- [248] W. K. Wootters and W. H. Zurek, *A single quantum cannot be cloned*, *Nature* **299**, 802–803 (1982).
- [249] C. H. Bennett, D. P. DiVincenzo, J. A. Smolin, and W. K. Wootters, *Mixed-state entanglement and quantum error correction*, *Phys. Rev. A* **54**, 3824–3851 (1996).
- [250] S. L. Braunstein, *Quantum error correction for communication with linear optics*, *Nature* **394**, 47–49 (1998).
- [251] S. Lloyd and S. L. Braunstein, *Quantum Computation over Continuous Variables*, *Phys. Rev. Lett.* **82**, 1784–1787 (1999).
- [252] S. D. Bartlett and B. C. Sanders, *Universal continuous-variable quantum computation: Requirement of optical nonlinearity for photon counting*, *Phys. Rev. A* **65**, 042304 (2002).
- [253] S. D. Bartlett, H. de Guise, and B. C. Sanders, *Quantum encodings in spin systems and harmonic oscillators*, *Phys. Rev. A* **65**, 052316 (2002).
- [254] C. Weedbrook, S. Pirandola, R. García-Patrón, N. J. Cerf, T. C. Ralph, J. H. Shapiro, and S. Lloyd, *Gaussian quantum information*, *Rev. Mod. Phys.* **84**, 621–669 (2012).
- [255] F. A. Mele, F. Salek, V. Giovannetti, and L. Lami, *Quantum communication on the bosonic loss-dephasing channel*, [10.48550/arXiv.2401.15634](https://arxiv.org/abs/10.48550/arXiv.2401.15634) (2024).
- [256] P. Leviant, Q. Xu, L. Jiang, and S. Rosenblum, *Quantum capacity and codes for the bosonic loss-dephasing channel*, *Quantum* **6**, 821 (2022).
- [257] H. Risken, *The Fokker-Planck Equation: Methods of Solution and Applications*, edited by H. Haken, Vol. 18, Springer Series in Synergetics (Springer, Berlin, Heidelberg, 1996).
- [258] K. H. Wanser, *Fundamental phase noise limit in optical fibres due to temperature fluctuations*, *Electron. Lett.* **28**, 53–54 (1992).
- [259] J. P. Gordon and L. F. Mollenauer, *Phase noise in photonic communications systems using linear amplifiers*, *Opt. Lett.*, **OL 15**, 1351–1353 (1990).
- [260] D. Derickson, *Fiber optic test and measurement* (Prentice Hall PTR, Upper Saddle River, N.J., 1998).
- [261] S. D. Bartlett, T. Rudolph, and R. W. Spekkens, *Reference frames, superselection rules, and quantum information*, *Rev. Mod. Phys.* **79**, 555–609 (2007).
- [262] A. Arqand, L. Memarzadeh, and S. Mancini, *Quantum capacity of a bosonic dephasing channel*, *Phys. Rev. A* **102**, 042413 (2020).
- [263] M. Rexiti, L. Memarzadeh, and S. Mancini, *Discrimination of dephasing channels*, *J. Phys. A: Math. Theor.* **55**, 245301 (2022).
- [264] S. Dehdashti, J. Notzel, and P. van Loock, *Quantum capacity of a deformed bosonic dephasing channel*, [10.48550/arXiv.2211.09012](https://arxiv.org/abs/10.48550/arXiv.2211.09012) (2022).
- [265] B. Schumacher, *Sending entanglement through noisy quantum channels*, *Phys. Rev. A* **54**, 2614–2628 (1996).
- [266] M. Reimpell and R. F. Werner, *Iterative Optimization of Quantum Error Correcting Codes*, *Phys. Rev. Lett.* **94**, 080501 (2005).
- [267] B. Schumacher and M. D. Westmoreland, *Quantum processes, systems, and information*, 1. publ (Cambridge Univ. Press, Cambridge, 2010).
- [268] G. Zheng, W. He, G. Lee, and L. Jiang, *The Near-optimal Performance of Quantum Error Correction Codes*, [10.48550/arXiv.2401.02022](https://arxiv.org/abs/10.48550/arXiv.2401.02022) (2024).
- [269] P. Reinhold, “Controlling Error-Correctable and Bosonic Qubits”, PhD thesis (Yale University, New Haven, 2019).

- [270] R. Kosut, I. A. Walmsley, and H. Rabitz, *Optimal Experiment Design for Quantum State and Process Tomography and Hamiltonian Parameter Estimation*, [10.48550/arXiv.quant-ph/0411093](#) (2004).
- [271] R. L. Kosut and D. A. Lidar, *Quantum error correction via convex optimization*, *Quantum Inf Process* **8**, 443–459 (2009).
- [272] A. S. Fletcher, P. W. Shor, and M. Z. Win, *Optimum quantum error recovery using semidefinite programming*, *Phys. Rev. A* **75**, 012338 (2007).
- [273] L. Vandenberghe and S. Boyd, *Semidefinite Programming*, *SIAM Rev.* **38**, 49–95 (1996).
- [274] S. Boyd and L. Vandenberghe, *Convex Optimization* (Cambridge University Press, Cambridge, 2004).
- [275] Y. Nesterov and A. Nemirovskii, *Interior-Point Polynomial Algorithms in Convex Programming*, Studies in Applied and Numerical Mathematics (Society for Industrial and Applied Mathematics, Jan. 1994).
- [276] S. J. Wright, *Primal-Dual Interior-Point Methods*, Other Titles in Applied Mathematics (Society for Industrial and Applied Mathematics, Jan. 1997).
- [277] H. Wolkowicz, R. Saigal, L. Vandenberghe, and F. S. Hillier, eds., *Handbook of Semidefinite Programming*, Vol. 27, International Series in Operations Research & Management Science (Springer US, Boston, MA, 2000).
- [278] A. Ben-Tal and A. Nemirovski, *Lectures on Modern Convex Optimization*, MOS-SIAM Series on Optimization (Society for Industrial and Applied Mathematics, Jan. 2001).
- [279] J. Renegar, *A Mathematical View of Interior-Point Methods in Convex Optimization*, MOS-SIAM Series on Optimization (Society for Industrial and Applied Mathematics, Jan. 2001).
- [280] M. J. Todd, *Semidefinite optimization*, *Acta Numer.* **10**, 515–560 (2001).
- [281] R. D. C. Monteiro, *First- and second-order methods for semidefinite programming*, *Math. Program., Ser. B* **97**, 209–244 (2003).
- [282] B. Gärtner and J. Matoušek, “Semidefinite Programming”, in *Approximation Algorithms and Semidefinite Programming*, edited by B. Gärtner and J. Matousek (Springer, Berlin, Heidelberg, 2012), pp. 15–25.
- [283] E. W. Cheney and D. R. Kincaid, *Linear Algebra: Theory and Applications* (Jones & Bartlett Learning, 2009).
- [284] D. K. Tuckett, S. D. Bartlett, and S. T. Flammia, *Ultra-high Error Threshold for Surface Codes with Biased Noise*, *Phys. Rev. Lett.* **120**, 050505 (2018).
- [285] D. K. Tuckett, S. D. Bartlett, S. T. Flammia, and B. J. Brown, *Fault-Tolerant Thresholds for the Surface Code in Excess of 5% under Biased Noise*, *Phys. Rev. Lett.* **124**, 130501 (2020).
- [286] D. K. Tuckett, A. S. Darmawan, C. T. Chubb, S. Bravyi, S. D. Bartlett, and S. T. Flammia, *Tailoring Surface Codes for Highly Biased Noise*, *Phys. Rev. X* **9**, 041031 (2019).
- [287] P. Aliferis and J. Preskill, *Fault-tolerant quantum computation against biased noise*, *Phys. Rev. A* **78**, 052331 (2008).
- [288] D. Ruiz, J. Guillaud, A. Leverrier, M. Mirrahimi, and C. Vuillot, *LDPC-cat codes for low-overhead quantum computing in 2D*, [10.48550/arXiv.2401.09541](#) (2024).
- [289] T. C. Ralph, A. Gilchrist, G. J. Milburn, W. J. Munro, and S. Glancy, *Quantum computation with optical coherent states*, *Phys. Rev. A* **68**, 042319 (2003).

- [290] Z. Leghtas, S. Touzard, I. M. Pop, A. Kou, B. Vlastakis, A. Petrenko, K. M. Sliwa, A. Narla, S. Shankar, M. J. Hatridge, M. Reagor, L. Frunzio, R. J. Schoelkopf, M. Mirrahimi, and M. H. Devoret, *Confining the state of light to a quantum manifold by engineered two-photon loss*, *Science* **347**, 853–857 (2015).
- [291] M. Bild, M. Fadel, Y. Yang, U. von Lüpke, P. Martin, A. Bruno, and Y. Chu, *Schrödinger cat states of a 16-microgram mechanical oscillator*, *Science* **380**, 274–278 (2023).
- [292] W. Rossmann, *Lie groups: an introduction through linear groups*, Reprinted, Oxford Graduate Texts in Mathematics 5 (Oxford Univ. Press, Oxford, 2009).
- [293] B. C. Hall, *Lie groups, Lie algebras, and representations: an elementary introduction*, Second edition, Graduate Texts in Mathematics 222 (Springer, Cham Heidelberg New York Dordrecht London, 2015).
- [294] G. Pantaleoni, B. Q. Baragiola, and N. C. Menicucci, *Modular Bosonic Subsystem Codes*, *Phys. Rev. Lett.* **125**, 040501 (2020).
- [295] G. Pantaleoni, B. Q. Baragiola, and N. C. Menicucci, *Subsystem analysis of continuous-variable resource states*, *Phys. Rev. A* **104**, 012430 (2021).
- [296] H. Putterman, J. Iverson, Q. Xu, L. Jiang, O. Painter, F. G. S. L. Brandão, and K. Noh, *Stabilizing a Bosonic Qubit Using Colored Dissipation*, *Phys. Rev. Lett.* **128**, 110502 (2022).
- [297] G. S. Agarwal and K. Tara, *Nonclassical properties of states generated by the excitations on a coherent state*, *Phys. Rev. A* **43**, 492–497 (1991).
- [298] G. S. Agarwal and K. Tara, *Nonclassical character of states exhibiting no squeezing or sub-Poissonian statistics*, *Phys. Rev. A* **46**, 485–488 (1992).
- [299] D. J. Reilly, *Challenges in Scaling-up the Control Interface of a Quantum Computer*, in *2019 IEEE Int. Electron Devices Meet. IEDM* (Dec. 2019), pp. 31.7.1–31.7.6.
- [300] A. M. Steane, *Overhead and noise threshold of fault-tolerant quantum error correction*, *Phys. Rev. A* **68**, 042322 (2003).
- [301] B. M. Terhal, *Quantum error correction for quantum memories*, *Rev. Mod. Phys.* **87**, 307–346 (2015).
- [302] J. P. Paz and W. H. Zurek, *Continuous error correction*, *Proc. R. Soc. Lond. Ser. Math. Phys. Eng. Sci.* **454**, 355–364 (1998).
- [303] O. Oreshkov, “Continuous-time quantum error correction”, in *Quantum Error Correction*, edited by T. A. Brun and D. A. Lidar (Cambridge University Press, Cambridge, 2013), pp. 201–228.
- [304] K.-C. Hsu and T. A. Brun, *Method for quantum-jump continuous-time quantum error correction*, *Phys. Rev. A* **93**, 022321 (2016).
- [305] J.-M. Lihm, K. Noh, and U. R. Fischer, *Implementation-independent sufficient condition of the Knill-Laflamme type for the autonomous protection of logical qudits by strong engineered dissipation*, *Phys. Rev. A* **98**, 012317 (2018).
- [306] E. Kapit, *Hardware-Efficient and Fully Autonomous Quantum Error Correction in Superconducting Circuits*, *Phys. Rev. Lett.* **116**, 150501 (2016).
- [307] J. Lebreuilly, K. Noh, C.-H. Wang, S. M. Girvin, and L. Jiang, *Autonomous quantum error correction and quantum computation*, [10.48550/arXiv.2103.05007](https://arxiv.org/abs/10.48550/arXiv.2103.05007) (2021).
- [308] V. V. Albert, “Lindbladians with multiple steady states: theory and applications”, PhD thesis (Yale University, New Haven, 2017).

- [309] H. D. Simaan and R. Loudon, *Off-diagonal density matrix for single-beam two-photon absorbed light*, *J. Phys. A: Math. Gen.* **11**, 435 (1978).
- [310] R. Gautier, M. Mirrahimi, and A. Sarlette, *Designing High-Fidelity Zeno Gates for Dissipative Cat Qubits*, *PRX Quantum* **4**, 040316 (2023).
- [311] R. Azouit, F. Chittaro, A. Sarlette, and P. Rouchon, *Towards generic adiabatic elimination for bipartite open quantum systems*, *Quantum Sci. Technol.* **2**, 044011 (2017).
- [312] P. Forni, A. Sarlette, T. Capelle, E. Flurin, S. Deléglise, and P. Rouchon, *Adiabatic elimination for multi-partite open quantum systems with non-trivial zero-order dynamics*, [10.48550/arXiv.1803.07810](https://arxiv.org/abs/1803.07810) (2018).
- [313] R. Lescanne, L. Verney, Q. Ficheux, M. H. Devoret, B. Huard, M. Mirrahimi, and Z. Leghtas, *Escape of a Driven Quantum Josephson Circuit into Unconfined States*, *Phys. Rev. Appl.* **11**, 014030 (2019).
- [314] L. Verney, R. Lescanne, M. H. Devoret, Z. Leghtas, and M. Mirrahimi, *Structural Instability of Driven Josephson Circuits Prevented by an Inductive Shunt*, *Phys. Rev. Appl.* **11**, 024003 (2019).
- [315] R. Gautier, A. Sarlette, and M. Mirrahimi, *Combined Dissipative and Hamiltonian Confinement of Cat Qubits*, *PRX Quantum* **3**, 020339 (2022).
- [316] D. Ruiz, R. Gautier, J. Guillaud, and M. Mirrahimi, *Two-photon driven Kerr quantum oscillator with multiple spectral degeneracies*, *Phys. Rev. A* **107**, 042407 (2023).
- [317] L. Gravina, F. Minganti, and V. Savona, *Critical Schrödinger Cat Qubit*, *PRX Quantum* **4**, 020337 (2023).
- [318] S. M. Girvin, *Introduction to quantum error correction and fault tolerance*, *SciPost Phys. Lect. Notes*, 070 (2023).
- [319] D. Gottesman, “Stabilizer Codes and Quantum Error Correction”, PhD thesis (California Institute of Technology, Pasadena, California, 1997).
- [320] B. M. Terhal and D. Weigand, *Encoding a qubit into a cavity mode in circuit QED using phase estimation*, *Phys. Rev. A* **93**, 012315 (2016).
- [321] K. Noh, V. V. Albert, and L. Jiang, *Quantum Capacity Bounds of Gaussian Thermal Loss Channels and Achievable Rates With Gottesman-Kitaev-Preskill Codes*, *IEEE Trans. Inf. Theory* **65**, 2563–2582 (2019).
- [322] J. M. Arrazola, T. R. Bromley, J. Izaac, C. R. Myers, K. Brádler, and N. Killoran, *Machine learning method for state preparation and gate synthesis on photonic quantum computers*, *Quantum Sci. Technol.* **4**, 024004 (2019).
- [323] M. Eaton, R. Nehra, and O. Pfister, *Non-Gaussian and Gottesman–Kitaev–Preskill state preparation by photon catalysis*, *New J. Phys.* **21**, 113034 (2019).
- [324] J. Hastrup, K. Park, J. B. Brask, R. Filip, and U. L. Andersen, *Measurement-free preparation of grid states*, *npj Quantum Inf* **7**, 1–8 (2021).
- [325] J. Hastrup and U. L. Andersen, *Improved readout of qubit-coupled Gottesman-Kitaev-Preskill states*, *Quantum Sci. Technol.* **6**, 035016 (2021).
- [326] K. R. Motes, B. Q. Baragiola, A. Gilchrist, and N. C. Menicucci, *Encoding qubits into oscillators with atomic ensembles and squeezed light*, *Phys. Rev. A* **95**, 053819 (2017).
- [327] S. Pirandola, S. Mancini, D. Vitali, and P. Tombesi, *Constructing finite-dimensional codes with optical continuous variables*, *EPL* **68**, 323 (2004).

- [328] S. Pirandola, S. Mancini, D. Vitali, and P. Tombesi, *Generating continuous variable quantum codewords in the near-field atomic lithography*, *J. Phys. B: At. Mol. Opt. Phys.* **39**, 997 (2006).
- [329] B. Royer, S. Singh, and S. M. Girvin, *Stabilization of Finite-Energy Gottesman-Kitaev-Preskill States*, *Phys. Rev. Lett.* **125**, 260509 (2020).
- [330] Y. Shi, C. Chamberland, and A. Cross, *Fault-tolerant preparation of approximate GKP states*, *New J. Phys.* **21**, 093007 (2019).
- [331] D. Su, C. R. Myers, and K. K. Sabapathy, *Conversion of Gaussian states to non-Gaussian states using photon-number-resolving detectors*, *Phys. Rev. A* **100**, 052301 (2019).
- [332] B. C. Travaglione and G. J. Milburn, *Preparing encoded states in an oscillator*, *Phys. Rev. A* **66**, 052322 (2002).
- [333] H. M. Vasconcelos, L. Sanz, and S. Glancy, *All-optical generation of states for “Encoding a qubit in an oscillator”*, *Opt. Lett.*, **OL 35**, 3261–3263 (2010).
- [334] D. J. Weigand and B. M. Terhal, *Generating grid states from Schrödinger-cat states without postselection*, *Phys. Rev. A* **97**, 022341 (2018).
- [335] D. J. Weigand and B. M. Terhal, *Realizing modular quadrature measurements via a tunable photon-pressure coupling in circuit QED*, *Phys. Rev. A* **101**, 053840 (2020).
- [336] L. J. Mensen, B. Q. Baragiola, and N. C. Menicucci, *Phase-space methods for representing, manipulating, and correcting Gottesman-Kitaev-Preskill qubits*, *Phys. Rev. A* **104**, 022408 (2021).
- [337] I. Tzitrin, J. E. Bourassa, N. C. Menicucci, and K. K. Sabapathy, *Progress towards practical qubit computation using approximate Gottesman-Kitaev-Preskill codes*, *Phys. Rev. A* **101**, 032315 (2020).
- [338] B. W. Walshe, B. Q. Baragiola, R. N. Alexander, and N. C. Menicucci, *Continuous-variable gate teleportation and bosonic-code error correction*, *Phys. Rev. A* **102**, 062411 (2020).
- [339] K. H. Wan, A. Neville, and S. Kolthammer, *Memory-assisted decoder for approximate Gottesman-Kitaev-Preskill codes*, *Phys. Rev. Res.* **2**, 043280 (2020).
- [340] B. de Neeve, T. L. Nguyen, T. Behrle, and J. Home, *Error correction of a logical grid state qubit by dissipative pumping*, [10.48550/arXiv.2010.09681](https://arxiv.org/abs/10.48550/arXiv.2010.09681) (2020).
- [341] A. L. Grimsmo, J. Combes, and B. Q. Baragiola, *Quantum Computing with Rotation-Symmetric Bosonic Codes*, *Phys. Rev. X* **10**, 011058 (2020).
- [342] J. Hastrup, J. S. Neergaard-Nielsen, and U. L. Andersen, *Deterministic generation of a four-component optical cat state*, *Opt. Lett.*, **OL 45**, 640–643 (2020).
- [343] D. Su, I. Dhand, and T. C. Ralph, *Universal quantum computation with optical four-component cat qubits*, *Phys. Rev. A* **106**, 042614 (2022).
- [344] R. Schnabel, N. Mavalvala, D. E. McClelland, and P. K. Lam, *Quantum metrology for gravitational wave astronomy*, *Nat Commun* **1**, 121 (2010).
- [345] C. Xu, L. Zhang, S. Huang, T. Ma, F. Liu, H. Yonezawa, Y. Zhang, and M. Xiao, *Sensing and tracking enhanced by quantum squeezing*, *Photon. Res.*, **PRJ 7**, A14–A26 (2019).
- [346] G. Frascella, S. Agne, F. Y. Khalili, and M. V. Chekhova, *Overcoming detection loss and noise in squeezing-based optical sensing*, *npj Quantum Inf* **7**, 1–6 (2021).
- [347] J.-H. Lü, W. Ning, X. Zhu, F. Wu, L.-T. Shen, Z.-B. Yang, and S.-B. Zheng, *Critical quantum sensing based on the Jaynes-Cummings model with a squeezing drive*, *Phys. Rev. A* **106**, 062616 (2022).

- [348] J. Etesse, M. Bouillard, B. Kanseri, and R. Tualle-Brouri, *Experimental Generation of Squeezed Cat States with an Operation Allowing Iterative Growth*, *Phys. Rev. Lett.* **114**, 193602 (2015).
- [349] R. Filip, *Amplification of Schrödinger-cat state in a degenerate optical parametric amplifier*, *J. Opt. B: Quantum Semiclass. Opt.* **3**, S1 (2001).
- [350] R. Filip, *Gaussian quantum adaptation of non-Gaussian states for a lossy channel*, *Phys. Rev. A* **87**, 042308 (2013).
- [351] H. Le Jeannic, A. Cavaillès, K. Huang, R. Filip, and J. Laurat, *Slowing Quantum Decoherence by Squeezing in Phase Space*, *Phys. Rev. Lett.* **120**, 073603 (2018).
- [352] H.-Y. Lo, D. Kienzler, L. de Clercq, M. Marinelli, V. Negnevitsky, B. C. Keitch, and J. P. Home, *Spin-motion entanglement and state diagnosis with squeezed oscillator wavepackets*, *Nature* **521**, 336–339 (2015).
- [353] D. Menzies and R. Filip, *Gaussian-optimized preparation of non-Gaussian pure states*, *Phys. Rev. A* **79**, 012313 (2009).
- [354] K. Park, J. Hastrup, J. S. Neergaard-Nielsen, J. B. Brask, R. Filip, and U. L. Andersen, *Slowing quantum decoherence of oscillators by hybrid processing*, *npj Quantum Inf* **8**, 1–8 (2022).
- [355] A. Serafini, S. D. Siena, F. Illuminati, and M. G. A. Paris, *Minimum decoherence cat-like states in Gaussian noisy channels*, *J. Opt. B: Quantum Semiclass. Opt.* **6**, S591 (2004).
- [356] R. Y. Teh, P. D. Drummond, and M. D. Reid, *Overcoming decoherence of Schrödinger cat states formed in a cavity using squeezed-state inputs*, *Phys. Rev. Res.* **2**, 043387 (2020).
- [357] B. R. Mollow and R. J. Glauber, *Quantum Theory of Parametric Amplification. I*, *Phys. Rev.* **160**, 1076–1096 (1967).
- [358] B. R. Mollow and R. J. Glauber, *Quantum Theory of Parametric Amplification. II*, *Phys. Rev.* **160**, 1097–1108 (1967).
- [359] D. Stoler, *Equivalence Classes of Minimum Uncertainty Packets*, *Phys. Rev. D* **1**, 3217–3219 (1970).
- [360] D. Stoler, *Equivalence Classes of Minimum-Uncertainty Packets. II*, *Phys. Rev. D* **4**, 1925–1926 (1971).
- [361] E. Y. C. Lu, *New coherent states of the electromagnetic field*, *Lett. Nuovo Cimento* **2**, 1241–1244 (1971).
- [362] E. Y. C. Lu, *Quantum correlations in two-photon amplification*, *Lett. Nuovo Cimento* **3**, 585–589 (1972).
- [363] H. P. Yuen, *Generalized coherent states and the statistics of two-photon lasers*, *Physics Letters A* **51**, 1–2 (1975).
- [364] H. P. Yuen, *Two-photon coherent states of the radiation field*, *Phys. Rev. A* **13**, 2226–2243 (1976).
- [365] J. N. Hollenhorst, *Quantum limits on resonant-mass gravitational-radiation detectors*, *Phys. Rev. D* **19**, 1669–1679 (1979).
- [366] C. M. Caves, *Quantum-mechanical noise in an interferometer*, *Phys. Rev. D* **23**, 1693–1708 (1981).
- [367] K. B. Moeller, T. G. Jørgensen, and J. P. Dahl, *Displaced squeezed number states: Position space representation, inner product, and some applications*, *Phys. Rev. A* **54**, 5378–5385 (1996).

- [368] W. Schleich and J. A. Wheeler, *Oscillations in photon distribution of squeezed states*, *J. Opt. Soc. Am. B*, JOSAB **4**, 1715–1722 (1987).
- [369] W. Schleich and J. A. Wheeler, *Oscillations in photon distribution of squeezed states and interference in phase space*, *Nature* **326**, 574–577 (1987).
- [370] W. Schleich, *Quantum optics in phase space*, 1. ed (Wiley-VCH, Berlin Weinheim, 2001).
- [371] R. L. Hudson, *When is the wigner quasi-probability density non-negative?*, *Reports on Mathematical Physics* **6**, 249–252 (1974).
- [372] M. Göppl, A. Fragner, M. Baur, R. Bianchetti, S. Filipp, J. M. Fink, P. J. Leek, G. Puebla, L. Steffen, and A. Wallraff, *Coplanar waveguide resonators for circuit quantum electrodynamics*, *Journal of Applied Physics* **104**, 113904 (2008).
- [373] B. Yurke, *Squeezed-state generation using a Josephson parametric amplifier*, *J. Opt. Soc. Am. B*, JOSAB **4**, 1551–1557 (1987).
- [374] C. J. Myatt, B. E. King, Q. A. Turchette, C. A. Sackett, D. Kielpinski, W. M. Itano, C. Monroe, and D. J. Wineland, *Decoherence of quantum superpositions through coupling to engineered reservoirs*, *Nature* **403**, 269–273 (2000).
- [375] A. Ourjoumtsev, R. Tualle-Brouiri, J. Laurat, and P. Grangier, *Generating Optical Schrödinger Kittens for Quantum Information Processing*, *Science* **312**, 83–86 (2006).
- [376] J. S. Neergaard-Nielsen, B. M. Nielsen, C. Hettich, K. Mølmer, and E. S. Polzik, *Generation of a Superposition of Odd Photon Number States for Quantum Information Networks*, *Phys. Rev. Lett.* **97**, 083604 (2006).
- [377] A. Ourjoumtsev, H. Jeong, R. Tualle-Brouiri, and P. Grangier, *Generation of optical ‘Schrödinger cats’ from photon number states*, *Nature* **448**, 784–786 (2007).
- [378] H. Takahashi, K. Wakui, S. Suzuki, M. Takeoka, K. Hayasaka, A. Furusawa, and M. Sasaki, *Generation of Large-Amplitude Coherent-State Superposition via Ancilla-Assisted Photon Subtraction*, *Phys. Rev. Lett.* **101**, 233605 (2008).
- [379] L. Gilles, B. M. Garraway, and P. L. Knight, *Generation of nonclassical light by dissipative two-photon processes*, *Phys. Rev. A* **49**, 2785–2799 (1994).
- [380] N. Shukla, S. Nimmrichter, and B. C. Sanders, *Squeezed comb states*, *Phys. Rev. A* **103**, 012408 (2021).
- [381] N. Khaneja, T. Reiss, C. Kehlet, T. Schulte-Herbrüggen, and S. J. Glaser, *Optimal control of coupled spin dynamics: design of NMR pulse sequences by gradient ascent algorithms*, *Journal of Magnetic Resonance* **172**, 296–305 (2005).
- [382] R. Wu, R. Chakrabarti, and H. Rabitz, *Optimal control theory for continuous-variable quantum gates*, *Phys. Rev. A* **77**, 052303 (2008).
- [383] S. J. Glaser, U. Boscain, T. Calarco, C. P. Koch, W. Köckenberger, R. Kosloff, I. Kuprov, B. Luy, S. Schirmer, T. Schulte-Herbrüggen, D. Sugny, and F. K. Wilhelm, *Training Schrödinger’s cat: quantum optimal control*, *Eur. Phys. J. D* **69**, 279 (2015).
- [384] M. H. Goerz, F. Motzoi, K. B. Whaley, and C. P. Koch, *Charting the circuit QED design landscape using optimal control theory*, *npj Quantum Inf* **3**, 1–10 (2017).
- [385] Y. Chen, Y. Hao, Z. Wu, B.-Y. Wang, R. Liu, Y. Hou, J. Cui, M.-H. Yung, and X. Peng, *Accelerating quantum optimal control through iterative gradient-ascent pulse engineering*, *Phys. Rev. A* **108**, 052603 (2023).
- [386] A. R. Conn, K. Scheinberg, and L. N. Vicente, *Introduction to derivative-free optimization*, MPS-SIAM Series on Optimization 8 (Society for Industrial and Applied Mathematics/Mathematical Programming Society, Philadelphia, 2009).

- [387] N. Hansen, S. Finck, R. Ros, and A. Auger, “Real-Parameter Black-Box Optimization Benchmarking 2009: Noiseless Functions Definitions”, Report (INRIA, 2009).
- [388] H. D. Hegerfeldt and T. S. Wilser, “Ensemble or Individual System, Collapse or no Collapse: A Description of a Single Radiating Atom”, in *Classical and Quantum Systems - Foundations and Symmetries*, Proceedings of the Second International Wigner Symposium (World Scientific, Singapore, July 1991), pp. 104–115.
- [389] H. Carmichael, *An Open Systems Approach to Quantum Optics: Lectures Presented at the Université Libre de Bruxelles October 28 to November 4, 1991*, edited by H. Araki, E. Brézin, J. Ehlers, U. Frisch, K. Hepp, R. L. Jaffe, R. Kippenhahn, H. A. Weidenmüller, J. Wess, J. Zittartz, and W. Beiglböck, Vol. 18, Lecture Notes in Physics Monographs (Springer, Berlin, Heidelberg, 1993).
- [390] K. Huang, H. Le Jeannic, J. Ruauadel, V. B. Verma, M. D. Shaw, F. Marsili, S. W. Nam, E. Wu, H. Zeng, Y.-C. Jeong, R. Filip, O. Morin, and J. Laurat, *Optical Synthesis of Large-Amplitude Squeezed Coherent-State Superpositions with Minimal Resources*, *Phys. Rev. Lett.* **115**, 023602 (2015).
- [391] C. Flühmann and J. P. Home, *Direct Characteristic-Function Tomography of Quantum States of the Trapped-Ion Motional Oscillator*, *Phys. Rev. Lett.* **125**, 043602 (2020).
- [392] T. Hillmann and F. Quijandria, *Quantum error correction with dissipatively stabilized squeezed-cat qubits*, *Phys. Rev. A* **107**, 032423 (2023).
- [393] E. E. Hach III and C. C. Gerry, *Generation of mixtures of Schrödinger-cat states from a competitive two-photon process*, *Phys. Rev. A* **49**, 490–498 (1994).
- [394] Y. Ashida, T. Shi, M. C. Bañuls, J. I. Cirac, and E. Demler, *Variational principle for quantum impurity systems in and out of equilibrium: Application to Kondo problems*, *Phys. Rev. B* **98**, 024103 (2018).
- [395] P. A. M. Dirac, *Note on Exchange Phenomena in the Thomas Atom*, *Proc. Camb. Philos. Soc.* **26**, 376 (1930).
- [396] J. Frenkel, *Wave Mechanics: Advanced General Theory* (Oxford University Press, Oxford, 1934).
- [397] A. McLachlan, *A variational solution of the time-dependent Schrödinger equation*, *Mol. Phys.* **8**, 39–44 (1964).
- [398] P. Kramer and M. Saraceno, *Geometry of the time-dependent variational principle in quantum mechanics*, Lecture Notes in Physics (Springer Berlin Heidelberg, 1981).
- [399] J. Broeckhove, L. Lathouwers, E. Kesteloot, and P. Van Leuven, *On the equivalence of time-dependent variational principles*, *Chemical Physics Letters* **149**, 547–550 (1988).
- [400] L. Joubert-Doriol and A. F. Izmaylov, *Problem-free time-dependent variational principle for open quantum systems*, *The Journal of Chemical Physics* **142**, 134107 (2015).
- [401] L. Joubert-Doriol and A. F. Izmaylov, *Nonadiabatic Quantum Dynamics with Frozen-Width Gaussians*, *J. Phys. Chem. A* **122**, 6031–6042 (2018).
- [402] A. Raab and H.-D. Meyer, *Multiconfigurational expansions of density operators: equations of motion and their properties*, *Theor Chem Acc* **104**, 358–369 (2000).
- [403] A. Connes and M. Marcolli, *Noncommutative geometry, quantum fields and motives*, Colloquium Publications / American Mathematical Society 55 (American Mathematical Society, Providence, RI, 2008).
- [404] R. Cheng, *Quantum Geometric Tensor (Fubini-Study Metric) in Simple Quantum System: A pedagogical Introduction*, [10.48550/arXiv.1012.1337](https://arxiv.org/abs/10.48550/arXiv.1012.1337) (2013).

- [405] S.-i. Amari, *Information Geometry and Its Applications*, Vol. 194, Applied Mathematical Sciences (Springer Japan, Tokyo, 2016).
- [406] X.-Y. Hou, Z. Zhou, X. Wang, H. Guo, and C.-C. Chien, *Local geometry and quantum geometric tensor of mixed states*, [10.48550/arXiv.2305.07597](https://arxiv.org/abs/2305.07597) (2023).
- [407] E. Ercolessi, R. Fioresi, and T. Weber, *The geometry of quantum computing*, *Int. J. Geom. Methods Mod. Phys.*, **2440011** (2024).
- [408] N. Bartolo, F. Minganti, W. Casteels, and C. Ciuti, *Exact steady state of a Kerr resonator with one- and two-photon driving and dissipation: Controllable Wigner-function multimodality and dissipative phase transitions*, *Phys. Rev. A* **94**, 033841 (2016).
- [409] A. Le Boité, G. Orso, and C. Ciuti, *Steady-State Phases and Tunneling-Induced Instabilities in the Driven Dissipative Bose-Hubbard Model*, *Phys. Rev. Lett.* **110**, 233601 (2013).
- [410] T. E. Lee, S. Gopalakrishnan, and M. D. Lukin, *Unconventional Magnetism via Optical Pumping of Interacting Spin Systems*, *Phys. Rev. Lett.* **110**, 257204 (2013).
- [411] J. Jin, A. Biella, O. Viyuela, L. Mazza, J. Keeling, R. Fazio, and D. Rossini, *Cluster Mean-Field Approach to the Steady-State Phase Diagram of Dissipative Spin Systems*, *Phys. Rev. X* **6**, 031011 (2016).
- [412] W. Casteels, R. M. Wilson, and M. Wouters, *Gutzwiller Monte Carlo approach for a critical dissipative spin model*, *Phys. Rev. A* **97**, 062107 (2018).
- [413] D. Huybrechts and M. Wouters, *Dynamical hysteresis properties of the driven-dissipative Bose-Hubbard model with a Gutzwiller Monte Carlo approach*, *Phys. Rev. A* **102**, 053706 (2020).
- [414] M. Sánchez-Barquilla, R. E. F. Silva, and J. Feist, *Cumulant expansion for the treatment of light-matter interactions in arbitrary material structures*, *The Journal of Chemical Physics* **152**, 034108 (2020).
- [415] F. Vicentini, F. Minganti, R. Rota, G. Orso, and C. Ciuti, *Critical slowing down in driven-dissipative Bose-Hubbard lattices*, *Phys. Rev. A* **97**, 013853 (2018).
- [416] J. R. Johansson, P. D. Nation, and F. Nori, *QuTiP 2: A Python framework for the dynamics of open quantum systems*, *Computer Physics Communications* **184**, 1234–1240 (2013).
- [417] S. Krämer, D. Plankensteiner, L. Ostermann, and H. Ritsch, *QuantumOptics.jl: A Julia framework for simulating open quantum systems*, *Computer Physics Communications* **227**, 109–116 (2018).
- [418] R. Loudon, *The quantum theory of light*, 3rd ed, Oxford Science Publications (Oxford University Press, Oxford ; New York, 2000).
- [419] G. Kirchmair, B. Vlastakis, Z. Leghtas, S. E. Nigg, H. Paik, E. Ginossar, M. Mirrahimi, L. Frunzio, S. M. Girvin, and R. J. Schoelkopf, *Observation of quantum state collapse and revival due to the single-photon Kerr effect*, *Nature* **495**, 205–209 (2013).
- [420] V. Bargmann, *On a Hilbert space of analytic functions and an associated integral transform part I*, *Commun. Pure Appl. Math.* **14**, 187–214 (1961).
- [421] I. Segal, *Mathematical problems of relativistic physics: With an appendix on group representations in hilbert space*, Lectures in Applied Mathematics; Proceedings of the Summer Seminar, Boulder, Colorado, 1960, 2 (American Mathematical Society, 1967).
- [422] S. Pérez-Esteva and C. Villegas-Blas, *First summer school in analysis and mathematical physics: quantization, the segal-bargmann transform, and semiclassical analysis* (American Mathematical Society, 2000).

- [423] H. B. Monir, N. Amir, and S. Iqbal, *Photon-Added $SU(1, 1)$ Coherent States and their Non-Classical Properties*, *Int J Theor Phys* **58**, 1776–1790 (2019).
- [424] L. Cohen, *Expansion Theorem for Functions of Operators*, *Journal of Mathematical Physics* **7**, 244–245 (1966).
- [425] R. M. Wilcox, *Exponential Operators and Parameter Differentiation in Quantum Physics*, *Journal of Mathematical Physics* **8**, 962–982 (1967).
- [426] W. Witschel, *Ordered operator expansions by comparison*, *J. Phys. A: Math. Gen.* **8**, 143 (1975).
- [427] P. Blasiak, A. Horzela, K. A. Penson, A. I. Solomon, and G. H. E. Duchamp, *Combinatorics and Boson normal ordering: A gentle introduction*, *American Journal of Physics* **75**, 639–646 (2007).
- [428] P. Blasiak, “Combinatorics of boson normal ordering and some applications”, PhD thesis (Institute of Nuclear Physics of Polish Academy of Sciences, Krakow and Universite Pierre et Marie Curie, Paris, 2005).
- [429] L. Pochhammer, *Ueber die Differentialgleichung der allgemeineren hypergeometrischen Reihe mit zwei endlichen singulären Punkten*. *J. Für Reine Angew. Math. Crelles J.* **1888**, 76–159 (1888).
- [430] J. F. Steffensen, *Interpolation: Second Edition* (Courier Corporation, Nov. 2013).
- [431] A. N. Tikhonov and V. Y. Arsenin, *Solutions of ill-posed problems* (V. H. Winston & Sons, Washington, D.C.: John Wiley & Sons, New York, 1977), pp. xiii+258.
- [432] A. N. Tikhonov, A. V. Goncharsky, V. V. Stepanov, and A. G. Yagola, *Numerical Methods for the Solution of Ill-Posed Problems* (Springer Netherlands, Dordrecht, 1995).
- [433] R. Kress, *Numerical analysis* (New York, NY : Springer New York, 1998).
- [434] R. Jozsa, *Fidelity for Mixed Quantum States*, *J. Mod. Opt.* **41**, 2315–2323 (1994).
- [435] D. Sarchi, I. Carusotto, M. Wouters, and V. Savona, *Coherent dynamics and parametric instabilities of microcavity polaritons in double-well systems*, *Phys. Rev. B* **77**, 125324 (2008).
- [436] K. Seibold, R. Rota, and V. Savona, *Dissipative time crystal in an asymmetric nonlinear photonic dimer*, *Phys. Rev. A* **101**, 033839 (2020).
- [437] M. J. Hartmann, *Quantum simulation with interacting photons*, *J. Opt.* **18**, 104005 (2016).
- [438] C. Noh and D. G. Angelakis, *Quantum simulations and many-body physics with light*, *Rep. Prog. Phys.* **80**, 016401 (2016).
- [439] W. Casteels, R. Fazio, and C. Ciuti, *Critical dynamical properties of a first-order dissipative phase transition*, *Phys. Rev. A* **95**, 012128 (2017).
- [440] T. Graß, *Excitations and correlations in the driven-dissipative Bose-Hubbard model*, *Phys. Rev. A* **99**, 043607 (2019).
- [441] R. Rota, F. Minganti, C. Ciuti, and V. Savona, *Quantum Critical Regime in a Quadratically Driven Nonlinear Photonic Lattice*, *Phys. Rev. Lett.* **122**, 110405 (2019).
- [442] T. Jacqmin, I. Carusotto, I. Sagnes, M. Abbarchi, D. D. Solnyshkov, G. Malpuech, E. Galopin, A. Lemaître, J. Bloch, and A. Amo, *Direct Observation of Dirac Cones and a Flatband in a Honeycomb Lattice for Polaritons*, *Phys. Rev. Lett.* **112**, 116402 (2014).
- [443] A. A. Houck, H. E. Türeci, and J. Koch, *On-chip quantum simulation with superconducting circuits*, *Nature Phys* **8**, 292–299 (2012).

- [444] M. Fitzpatrick, N. M. Sundaresan, A. C. Y. Li, J. Koch, and A. A. Houck, *Observation of a Dissipative Phase Transition in a One-Dimensional Circuit QED Lattice*, [*Phys. Rev. X* **7**, 011016 \(2017\)](#).
- [445] R. Labouvie, B. Santra, S. Heun, and H. Ott, *Bistability in a Driven-Dissipative Superfluid*, [*Phys. Rev. Lett.* **116**, 235302 \(2016\)](#).
- [446] A. Le Boité, G. Orso, and C. Ciuti, *Bose-Hubbard model: Relation between driven-dissipative steady states and equilibrium quantum phases*, [*Phys. Rev. A* **90**, 063821 \(2014\)](#).
- [447] Arman, G. Tyagi, and P. K. Panigrahi, *Sensing Single Photon in a Cat State*, [*Opt. Lett.* **46**, 1177 \(2021\)](#).
- [448] A. R. Milne, C. Hempel, L. Li, C. L. Edmunds, H. J. Slatyer, H. Ball, M. R. Hush, and M. J. Biercuk, *Quantum Oscillator Noise Spectroscopy via Displaced Cat States*, [*Phys. Rev. Lett.* **126**, 250506 \(2021\)](#).
- [449] S. Ramezanpour, *Sensitive Schrödinger Cat States*, [10.48550/arXiv.2311.05771 \(2023\)](#).
- [450] M. Tatsuta, Y. Matsuzaki, and A. Shimizu, *Quantum metrology with generalized cat states*, [*Phys. Rev. A* **100**, 032318 \(2019\)](#).
- [451] R.-H. Zheng, W. Ning, Y.-H. Chen, J.-H. Lü, L.-T. Shen, K. Xu, Y.-R. Zhang, D. Xu, H. Li, Y. Xia, F. Wu, Z.-B. Yang, A. Miranowicz, N. Lambert, D. Zheng, H. Fan, F. Nori, and S.-B. Zheng, *Observation of a Superradiant Phase Transition with Emergent Cat States*, [*Phys. Rev. Lett.* **131**, 113601 \(2023\)](#).
- [452] H. Do, R. Malaney, and J. Green, *Teleportation of a Schrödinger's-Cat State via Satellite-Based Quantum Communications*, in [2019 IEEE Globecom Workshop GC Wkshps](#) (Dec. 2019), pp. 1–5.
- [453] T. Liu, Z.-F. Zheng, Y. Zhang, Y.-L. Fang, and C.-P. Yang, *Transferring entangled states of photonic cat-state qubits in circuit QED*, [*Front. Phys.* **15**, 21603 \(2020\)](#).
- [454] B. Vlastakis, A. Petrenko, N. Ofek, L. Sun, Z. Leghtas, K. Sliwa, Y. Liu, M. Hatridge, J. Blumoff, L. Frunzio, M. Mirrahimi, L. Jiang, M. H. Devoret, and R. J. Schoelkopf, *Characterizing entanglement of an artificial atom and a cavity cat state with Bell's inequality*, [*Nat Commun* **6**, 8970 \(2015\)](#).
- [455] D. Roberts and A. A. Clerk, *Driven-Dissipative Quantum Kerr Resonators: New Exact Solutions, Photon Blockade and Quantum Bistability*, [*Phys. Rev. X* **10**, 021022 \(2020\)](#).
- [456] P. Facchi and S. Pascazio, *Quantum Zeno Subspaces*, [*Phys. Rev. Lett.* **89**, 080401 \(2002\)](#).
- [457] J. M. Raimond, C. Sayrin, S. Gleyzes, I. Dotsenko, M. Brune, S. Haroche, P. Facchi, and S. Pascazio, *Phase Space Tweezers for Tailoring Cavity Fields by Quantum Zeno Dynamics*, [*Phys. Rev. Lett.* **105**, 213601 \(2010\)](#).
- [458] J. M. Raimond, P. Facchi, B. Peaudecerf, S. Pascazio, C. Sayrin, I. Dotsenko, S. Gleyzes, M. Brune, and S. Haroche, *Quantum Zeno dynamics of a field in a cavity*, [*Phys. Rev. A* **86**, 032120 \(2012\)](#).
- [459] W. H. Louisell, *Quantum Statistical Properties of Radiation* (Wiley, 1973).
- [460] P. D. Drummond and D. F. Walls, *Quantum theory of optical bistability. I. Nonlinear polarisability model*, [*J. Phys. A: Math. Gen.* **13**, 725 \(1980\)](#).
- [461] C. Ciuti and I. Carusotto, *Quantum fluid effects and parametric instabilities in microcavities*, [*Phys. Status Solidi B* **242**, 2224–2245 \(2005\)](#).

- [462] A. V. Baeva, N. G. Veselkova, N. I. Masalaeva, and I. V. Sokolov, *Measurement-assisted non-Gaussian gate for Schrödinger cat states preparation: Fock resource state versus cubic phase state*, *Eur. Phys. J. D* **78**, 12 (2024).
- [463] E. N. Bashmakova, S. B. Korolev, and T. Y. Golubeva, *Effect of entanglement in the generalized photon subtraction scheme*, *Laser Phys. Lett.* **20**, 115203 (2023).
- [464] V. Crescimanna, A. Z. Goldberg, and K. Heshami, *Seeding Gaussian boson samplers with single photons for enhanced state generation*, *Phys. Rev. A* **109**, 023717 (2024).
- [465] D. Han, N. Wang, M. Wang, and X. Su, *Simultaneous Preparation of Two Optical Cat States Based on a Nondegenerate Optical Parametric Amplifier*, *Ann. Phys.* **535**, 2300010 (2023).
- [466] E. G. Herrera, F. Torres-Leal, and B. M. Rodríguez-Lara, *Continuous-time quantum harmonic oscillator state engineering*, *New J. Phys.* **25**, 123045 (2023).
- [467] S. B. Korolev, E. N. Bashmakova, and T. Y. Golubeva, *Error Correction Using Squeezed Fock States*, [10.48550/arXiv.2312.16000](https://arxiv.org/abs/10.48550/arXiv.2312.16000) (2023).
- [468] J. Lee, N. Kang, S.-H. Lee, H. Jeong, L. Jiang, and S.-W. Lee, *Fault-tolerant quantum computation by hybrid qubits with bosonic cat-code and single photons*, [10.48550/arXiv.2401.00450](https://arxiv.org/abs/10.48550/arXiv.2401.00450) (2023).
- [469] P.-Z. Li, J. Dias, W. J. Munro, P. van Loock, K. Nemoto, and N. L. Piparo, *Performance of Rotation-Symmetric Bosonic Codes in a Quantum Repeater Network*, [10.48550/arXiv.2308.15815](https://arxiv.org/abs/10.48550/arXiv.2308.15815) (2023).
- [470] M.-Y. Mao, Z. Cheng, Y. Xia, A. M. Oleś, and W.-L. You, *Machine-learning-inspired quantum optimal control of nonadiabatic geometric quantum computation via reverse engineering*, *Phys. Rev. A* **108**, 032616 (2023).
- [471] Y. Mori, Y. Matsuzaki, S. Endo, and S. Kawabata, *Hardware-Efficient Bosonic Quantum Computing with Detection Capability of Single Photon Loss*, [10.48550/arXiv.2403.00291](https://arxiv.org/abs/10.48550/arXiv.2403.00291) (2024).
- [472] S. U. Shringarpure, Y. S. Teo, and H. Jeong, *Error suppression in multicomponent cat codes with photon subtraction and teleamplification*, [10.48550/arXiv.2401.04439](https://arxiv.org/abs/10.48550/arXiv.2401.04439) (2024).
- [473] M. S. Winnel, J. J. Guanzon, D. Singh, and T. C. Ralph, *Deterministic preparation of optical squeezed cat and Gottesman-Kitaev-Preskill states*, [10.48550/arXiv.2311.10510](https://arxiv.org/abs/10.48550/arXiv.2311.10510) (2023).
- [474] S. Zhao, M. G. Krauss, T. Bienaime, S. Whitlock, C. P. Koch, S. Qvarfort, and A. Metelmann, *Fast and robust cat state preparation utilizing higher order nonlinearities*, [10.48550/arXiv.2312.05218](https://arxiv.org/abs/10.48550/arXiv.2312.05218) (2023).
- [475] Z. Ni, S. Li, X. Deng, Y. Cai, L. Zhang, W. Wang, Z.-B. Yang, H. Yu, F. Yan, S. Liu, C.-L. Zou, L. Sun, S.-B. Zheng, Y. Xu, and D. Yu, *Beating the break-even point with a discrete-variable-encoded logical qubit*, *Nature* **616**, 56–60 (2023).
- [476] Z. Wang, T. Rajabzadeh, N. Lee, and A. H. Safavi-Naeini, *Automated discovery of autonomous quantum error correction schemes*, [10.48550/arXiv.2108.02766](https://arxiv.org/abs/10.48550/arXiv.2108.02766) (2021).
- [477] C. Hubig, I. P. McCulloch, and U. Schollwöck, *Generic construction of efficient matrix product operators*, *Phys. Rev. B* **95**, 035129 (2017).

David Schlegel

Curriculum Vitae

EPFL SB IPHYS LTPN
PH H2 504 (Bâtiment PH)

Station 3

CH-1015 Lausanne

✉ schlegel.david.ds@gmail.com

🌐 davidschlegel.xyz

Positions

- Feb 2020 - **École Polytechnique Fédérale de Lausanne**, Switzerland,
Apr 2024 Doctoral student at the Swiss Federal Institution of Technology (EPFL),
in the Laboratory of Theoretical Physics of Nanosystems (LTPN),
Supervisor: Prof. Vincenzo Savona.
- June 2023 - **IOP Publishing Ltd**, Bristol, United Kingdom,
June 2024 PhD student contributor to PHYSICS WORLD

Education

- Sept 2016 - **University of Göttingen**, Germany,
Feb 2020 M.Sc., Physics, Feb 2020
Thesis: *Time-periodic Structure in Open Quantum Systems*
Advisor: Prof. Stefan Kehrein
- Sept 2016 - **Ghent University**, Belgium,
Mar 2017 Master studies in physics in the ERASMUS+ European Exchange
Program
- Sept 2013 - **University of Göttingen**, Germany,
Jan 2021 B.A., Physics and Philosophy, Jan 2021, Two Subjects Bachelor
- Sept 2013 - **University of Göttingen**, Germany,
Aug 2016 B.Sc., Physics, Aug 2016
Thesis: *Coherent tunneling pathways in electron transport through single-
molecule junctions*, Advisor: Dr. Rainer Härtle

Scientific Publications

- David S. Schlegel and Stefan Kehrein, *Measurement-induced Clock in a Lattice Ring of Non-interacting Electrons*, [arXiv 2312.17672](https://arxiv.org/abs/2312.17672) (2023).
- David S. Schlegel, Fabrizio Minganti, and Vincenzo Savona, *Coherent-State Ladder Time-Dependent Variational Principle for Open Quantum Systems*, [arXiv 2306.13708](https://arxiv.org/abs/2306.13708) (2023).
- David S. Schlegel, Fabrizio Minganti, and Vincenzo Savona, *Quantum error correction using squeezed Schrödinger cat states*, [Phys. Rev. A 106, 022431](https://doi.org/10.1103/PhysRevA.106.022431) (2022).

Popular Science and News Articles

- David Schlegel, *Cat qubits reach a new level of stability*, [Physics World, IOP Publishing \(2024\)](#).
- David Schlegel, *Rapidly swapping photons make a high-quality quantum gate*, [Physics World, IOP Publishing \(2023\)](#).
- David Schlegel, *Unumgänglich: Quantenfehlerkorrektur*, [iX Special 2021: Quantencomputer](#).

Reviews

- Sept 2022 Referee for Physical Review A.
 Jan 2024 Referee for Physical Review Research.

International Conferences

- March 5-10 **APS March Meeting**, Las Vegas, USA,
 2023 Contributed talk: *Efficient simulation of rotation-symmetric many-boson open quantum systems via symmetric time-dependent variational ansatz*
- Feb 5-10 **Quantum Information Processing (QIP)**, Ghent, Belgium,
 2023 Poster: *Quantum error correction using squeezed Schrödinger cat states*
- Aug 29-31 **Solvay workshop on Quantum Simulation**, Brussels, Belgium,
 2022 Poster: *Quantum error correction using squeezed Schrödinger cat states*
- March 14-18 **APS March Meeting**, Chicago, USA,
 2022 Contributed talk: *Saving the cat: Approximate quantum error correction using squeezed Schrödinger cat states*

Projects and Internships

- April 24-16 **NCCR-SPIN** PhD retreat, Engelberg, Switzerland,
 2023 **Co-organizer**. Tasks: Schedule, Scientific program
- June 13-17 **Quantum Computing Hard- and Software Summer School 2022**,
 2022 EPFL, Switzerland,
Co-organizer. Tasks: Schedule, Speaker-invitations, venue organization, session chair, reimbursement
- May 20 - 26 **IBM Quantum Challenge 2021**
 2021 Achievement: *Advanced*
- March 14-28 **CERN Internship**, Geneva, Switzerland,
 2015 Project internship: *Development of an Efficiency-based Threshold Scan at the ATLAS detector*

Research visits, Schools, and Workshops

- April 24-16 **NCCR-SPIN** PhD retreat, Engelberg, Switzerland,
 2023 Talk: *Bosonic quantum error correction*

-
- April 17-21 **TUM**, Munich, Germany,
2023 research visit in the group *Theory of Complex Quantum Systems*
Invited talk: *Efficiently Simulating Interacting Cat-Qubits in Driven-Dissipative Systems*
- Sept 1-2 **Antwerp University**, Antwerp, Belgium
2022 research visit in the group *Theory of Quantum Systems and Complex Systems*
- March 29 **Seminar Talk**, Quantum Computing Association, ETH Zürich, Switzerland,
2022
Invited Talk: *Saving the cat: From Open Quantum Systems to Bosonic Quantum Error Correction*
- Jan 31 - Feb 1 **10th NCCR QSIT Winter School**, Arosa, Switzerland,
2022 Poster: *Quantum error correction using squeezed Schrödinger cat states*
- Nov 15-19 **Lemnic Quantum Science School**, Geneva & Lausanne, Switzerland
2021
- April 12-23 **7th Les Houches School in Computational Physics**, Les Houches,
2021 France
Dynamics of Complex Quantum Systems, from Theory to Computation
- July 6-10 **Variational Methods for Quantum Many-Body Systems**, Lyon,
2020 France
- Oct 14-18 **Lemnic Quantum Science School**, Geneva & Lausanne, Switzerland
2019
- March 31 – **DPG Spring Meeting** of the Condensed Matter Section, Regensburg,
Apr 5 2019 Germany
- July 9-12 **Introductory Course on Quantum Information**,
2018 Institute for Quantum Optics and Quantum Information, Innsbruck, Austria
- Feb 19-23 **Winter School on Numerical Methods for Strongly Correlated
2018 Quantum Systems**, Marburg, Germany

Teaching Experience

EPFL

- Spring 2020 Quantum physics II – PHYS-314
Fall 2020 Quantum physics I – PHYS-313
Spring 2021 Quantum physics II – PHYS-314
Fall 2021 Quantum physics I – PHYS-313
Spring 2022 General physics: quanta – PHYS-207(a)
Fall 2022 Quantum physics I – PHYS-313
Spring 2023 General physics: quanta – PHYS-207(a)

University of Göttingen

- Oct 2015 - ○ Analytical mechanics
- Aug 2019 ○ Mathematics for physicists (2 times)
- Physics III: Electrodynamics (2 times)
- Lab Course (2 times)

Technical Skills

Programming Languages PYTHON, JULIA, C, C++, HASKELL, BASH
Software MATHEMATICA, GIT, L^AT_EX, QISKIT

Languages

German **Native**
English **Full professional proficiency**
French **Limited Working Proficiency (B2)**
Dutch **Elementary Proficiency (A2)**
Spanish **Elementary Proficiency (A1)**